

**Binding Interactions of the mRNA Regulator
CELF1**

By John Michael Edwards, MChem (Hons)

Thesis submitted to the University of Nottingham for the degree of
Doctor of Philosophy

September 2012

Abstract

CELF1 is an RNA binding protein with regulatory roles in translation, alternative splicing and mRNA degradation. This protein is of particular interest as its upregulation is believed to be involved in the pathogenesis of type 1 myotonic dystrophy. CELF1 functions by binding to a specific sequence in the 3' untranslated region of its target mRNAs. This sequence has been termed the "EDEN" motif, but the exact requirements for binding of CELF1 were not well defined. In this study we therefore aimed to determine the sequence requirements for an RNA substrate to form a high affinity interaction with CELF1, and characterise the structure of the resulting complex. The CELF1 protein is composed of three structured RNA recognition motifs separated by flexible linkers. Our strategy was to investigate the RNA binding properties of each domain in isolation, and then the requirements for tandem binding of the domains in order to build up the complete "EDEN" motif capable of forming a high affinity complex with the wild type protein.

This has been accomplished using NMR spectroscopy to map the chemical shift perturbations in each domain on binding to a range of RNA substrates. ITC was also used to investigate the binding affinities of each domain, and the enhancement of affinity when domains bind in tandem. By these methods we have refined the sequence requirements for simultaneous binding of all domains of CELF1, and designed RNA substrates which will bind with higher affinity than any previously reported. We have also shown the potential involvement of RNA secondary structure in forming the CELF1 binding site, and identified two possible examples of this in natural mRNA targets.

CELF1 binding triggers deadenylation of its target mRNAs and this is suspected to be via a mechanism involving recruitment of poly (A) ribonuclease. These two proteins have been shown to interact, but no structural information was available to show which domains were interacting, or whether CELF1 was capable of

forming a ternary complex with both RNA and poly(A) ribonuclease. Since the ribonuclease exists as a 146 kDa dimer, the complex of it with CELF1 was an ambitious target for NMR. In this study we demonstrate that high resolution NMR data can be acquired on this key regulatory complex. Using this we go on to confirm the interaction between these two proteins, and that the domains involved in binding suggest a ternary complex is possible.

Acknowledgments

Firstly I would like to thank my supervisor Professor Mark Searle for introducing me to this project, and for his constant support and encouragement throughout my PhD. Thanks also go to Dr. Jonas Emsley and Dr. Cornelia de Moor both for their earlier work on the CELF1 protein which made this project possible, and for many useful discussions from their continuing investigations into this protein system. Special thanks go to Dr. Emilie Malaurie for the original vectors containing the CELF1 and t187 constructs, and for her advice and assistance during the early stages of the project.

Special thanks go to Dr. Jed Long for his patience and time spent training me in molecular biology and biophysical techniques. Thanks also go to Dr. Huw Williams for his help with the NMR, computer systems and molecular modelling, and to Dr. Neil Oldham for help with the mass spectrometry. I would also like to thank Dr. Chan Li for his help in the collection of the SAXS data.

I thank the other members of the Searle group past and present both for their help in the lab and for their friendship, in particular Jennifer Adlington, Liz Morris, Tom Garner, Katherine Portman, Jonathon Phillips and Alex Cousins. I would also like to thank two undergraduate project students, Joanne Bailey and Zoe Le Gray-Wise, for their contributions. Thanks also go to everyone else in lab A20.

I would like to thank the BBSRC and the University of Nottingham for funding. Finally I would like to thank my family, in particular my parents, for their support throughout my PhD.

Table of Contents

Acknowledgments	iii
Abbreviations	xi
1 Introduction.....	1
1.1.1 Deadenylation	2
1.2 Structure of the CELF Proteins	4
1.2.1 RNA Recognition Motifs	4
1.2.2 Structure of CELF1	6
1.2.3 NMR and X-ray Crystallography Data Available for CELF1	7
1.3 Target RNA Sequences of CELF1.....	10
1.4 Link between CELF1 and Myotonic Dystrophy.....	15
1.5 MBNL1	19
1.6 Dimerisation of CELF1	19
1.7 Phosphorylation of CELF1.....	20
1.8 Interactions of CELF1 with Poly (A) Ribonuclease.....	20
1.9 Aims and Objectives	21
2 Biophysical Techniques	23
2.1 Protein NMR.....	23
2.1.1 Transverse Relaxation Optimized Spectroscopy (TROSY)	24
2.1.2 NMR Assignment of Proteins	25
2.1.3 Protein Backbone Assignment Using 3D Heteronuclear NMR Experiments	
27	
2.2 NMR Titrations	35
2.3 Isothermal Titration Calorimetry (ITC)	37
2.4 Small Angle X-ray Scattering.....	42

2.5	Mass Spectrometry.....	46
3	Materials and Methods	49
3.1	Protein Sequences.....	49
3.2	Sterilization.....	51
3.3	Buffers	52
3.4	Overnight Cultures	53
3.4.1	Glycerol Stocks	53
3.5	Overexpression.....	53
3.6	Sonication.....	53
3.7	Metal Affinity Chromatography	54
3.8	His-Tag Removal by Thrombin Cleave	56
3.9	Gel Filtration.....	56
3.10	Desalting.....	58
3.11	Storage and Stability.....	58
3.12	Production of Isotopically Labelled Protein	58
3.13	Test Growths	59
3.14	SDS-PAGE Gels.....	60
3.15	Molecular Biology.....	61
3.15.1	Plasmids.....	61
3.15.2	Site Directed Mutagenesis.....	62
3.15.3	Cloning.....	64
3.15.4	Restriction Digest.....	64
3.15.5	Ligation	66
3.15.6	Production of Deletion Constructs	66
3.15.7	Sequencing	68
3.15.8	Production of Calcium Competent Cells.....	68
3.15.9	Transformation.....	69

3.15.10	Agar Plates.....	69
3.15.11	Agarose Gels.....	70
3.16	NMR Acquisition.....	70
3.16.1	Data Analysis.....	71
3.16.2	Sample Preparation.....	71
3.16.3	1D experiments.....	71
3.16.4	HSQC Experiments.....	72
3.16.5	3D Experiments.....	72
3.16.6	¹⁵ N Heteronuclear NOE.....	76
3.16.7	Paramagnetic Relaxation Enhancement.....	76
3.17	X-ray Crystallography.....	77
3.18	Size Exclusion Chromatography.....	78
3.19	SAXS.....	78
3.20	ITC.....	79
3.21	Mass Spectrometry.....	80
3.22	Molecular Modelling.....	80
4	RNA Interactions of the Isolated RRM3 of CELF1.....	84
4.1.1	Purification of RRM1.....	85
4.1.2	NMR Assignment of RRM1.....	86
4.1.3	Purification of RRM2.....	89
4.1.4	NMR Assignment of RRM2.....	91
4.1.5	Purification of RRM3.....	94
4.1.6	NMR Assignment of RRM3.....	95
4.2	Interaction of CELF1 RRM3s with Guanine-Rich Elements.....	98
4.2.1	Interactions of RRM1 with Guanine-Rich Elements.....	99
4.2.2	Removal of one UGU site from the EDEN7 RNA Substrate.....	108
4.2.3	Interactions of RRM2 with Guanine-Rich Elements.....	110

4.2.4	RRM3	115
4.2.5	Summary of NMR Titrations with GRE Sequences	115
4.3	Interactions of CELF1 RRMs with CUG Repeat RNA Substrates	116
4.3.1	RRM1	117
4.3.2	Comparison of RRM1 Interaction with UGU and UGC Sites.....	118
4.3.3	Interactions of RRM2 with CUG Repeat RNAs.....	121
4.3.4	Summary of Interactions between the CELF1 domains and CUG Repeat RNAs	124
4.4	Interaction of CELF1 RRMs with Adenosine-Rich Elements	124
4.4.1	RRM1	124
4.4.2	RRM2	125
4.5	Determination of Complex Stoichiometry by ESI Mass Spectrometry.....	127
4.5.1	RRM1	127
4.5.2	RRM2	130
4.6	Conclusions.....	132
5	Tandem RNA Binding of the two N-terminal Domains of CELF1.....	134
5.1.1	Purification of a Construct of the N-terminal domains of CELF1	135
5.1.2	Comparison of the Isolated Domains and t187 Spectra.....	137
5.1.3	Assignment of the ¹⁵ N TROSY Spectrum.....	140
5.2	Interactions of the N-terminal Domains of CELF1 with Tandem UGU Sites in Guanine Rich Elements.....	140
5.2.1	Interaction of the N-terminal Domains of CELF1 with the EDEN15 GRE.	142
5.2.2	Interaction of the N-terminal Domains of CELF1 with the EDEN11 GRE.	145
5.2.3	Interaction of the N-terminal Domains of CELF1 with the EDEN7 GRE..	146
5.2.4	Systematic Investigation of Spacing Requirements for Tandem Binding of the N-terminal domains of CELF1.....	149
5.2.5	Interaction of the N-terminal Domains of CELF1 with GRE Sequences..	150

5.3	Enhanced Affinity when Binding Multiple Domains of CELF1 in Tandem	153
5.3.1	Dependence of Binding Affinity on the Separation between UGU Sites	157
5.4	Determining the Stoichiometry of Complexes with GRE Substrates by Mass Spectrometry	161
5.5	Investigation of Binding Affinity Enhancement in Tandem binding to UGC and UAU Sites	164
5.5.1	Tandem Binding to UGC Sites	165
5.5.2	Tandem Binding to Adenosine Rich Elements	168
5.6	Investigating the Involvement of Unstructured Regions Flanking RRM1 and RRM2 in RNA Binding	170
5.6.1	Evidence for Conformational Flexibility from ¹⁵ N Heteronuclear NOEs.	171
5.6.2	Investigation of Involvement of the RRM2 C-Terminus Using an Extended CELF1 Construct	173
5.7	Summary of Cooperative Binding by the N-terminal Domains of CELF1 to RNA targets	179
6	Optimal RNA Targets of Full Length CELF1	181
6.1	Introduction	181
6.2	Purification of Wild Type CELF1	182
6.2.1	Production of a Stable Construct Containing all three Domains	190
6.2.2	Production of Deletion Mutants Using a Single Step PCR	190
6.3	Expression and Purification of RRM123	193
6.3.1	NMR Characterisation of RRM123	195
6.3.2	¹⁵ N Heteronuclear NOE	197
6.4	Interactions of RRM123 with the EDEN11 GRE	199
6.4.1	ITC of the EDEN11 GRE Binding to RRM123	202
6.5	CELF1 Recognition of the EDEN15 GRE	203
6.6	Design of a High Affinity EDEN Motif	206
6.6.1	NMR Studies of the EDEN-2U/4U Complex with RRM123	207
6.6.2	Size Exclusion Chromatography	211

6.6.3	RRM123 Binding to an RNA Substrate Containing a Hairpin Loop.....	213
6.6.4	ITC of RRM123 Binding to EDEN-2U/4U and EDEN-2U/HL.....	215
6.6.5	Comparison of ITC Data shows Two Distinct Binding Schemes	218
6.7	Refining the Criteria for an EDEN Motif	219
6.7.1	EDEN4U/2U	220
6.7.2	Involvement of RNA Secondary Structure in CELF1 Binding	221
6.7.3	Determination of the Minimal Binding Sequence for CELF1.....	223
6.7.4	Investigation of a Two Domain Construct of RRM2 and RRM3.....	225
6.7.5	Summary of ITC Data for all RNA Substrates.....	229
6.8	Conclusions.....	230
7	Characterisation of a Complex of CELF1 with a High Affinity EDEN Motif	231
7.1	Arrangement of the Domains on the RNA Substrate	232
7.2	Modelling RRM123 in Complex with a High Affinity RNA Substrate	234
7.3	Paramagnetic Relaxation Enhancement	238
7.3.1	Paramagnetic Relaxation Enhancement in RRM1 on binding to MTSL Labelled UGUU	240
7.3.2	PRE on labelling of the EDEN-2U/4U substrate with MTSL.....	244
7.4	Small Angle X-ray Scattering.....	247
7.4.1	Guinier Plots	247
7.4.2	Kratky Plots.....	248
7.4.3	Predicted Envelope.....	249
7.5	Refining the Model	252
7.6	Conclusions.....	253
8	CELF1 Phosphorylation and Interactions with Poly(A) Ribonuclease.....	254
8.1	Phosphorylation	254
8.2	Dimerisation of CELF1	260
8.3	Poly(A) Ribonuclease	261
8.4	Aims	263

8.5	Expression and Purification of Poly(A) Ribonuclease	263
8.6	NMR Studies of Poly(A) Ribonuclease	266
8.7	Interactions of CELF1 with Poly(A) Ribonuclease	268
8.7.1	Isolation of the PARN RRM	274
8.7.2	Supplementary Biophysical Techniques	276
8.8	Conclusions	277
9	Conclusions	279
9.1	Future Work	284
10	References	287
11	Appendix	312
11.1	Primers	312
11.2	NMR Assignments	313
11.2.1	RRM1 Wild Type Assignment	313
11.2.2	RRM1 S28D Assignment	316
11.2.3	RRM2 Assignment	319
11.2.4	RRM3 Assignment	322

Abbreviations

A: Adenine

AFM: Atomic Force Microscopy

ARE: A/U rich elements

BMRB: Biomagnetic Resonance Bank

BSA: Bovine Serum Albumen

bp: Base pairs

C: Cytosine

CELF1: CUGBP1 and Elav-Like Factor 1

CSP: Chemical Shift Perturbation

CUG-BP1: CUG repeat binding protein 1

DAN: Deadenylating Nuclease

DM1: Type 1 Myotonic Dystrophy

DM2: Type 2 Myotonic Dystrophy

DNA: Deoxyribonucleic Acid

DTT: Dithiothreitol

EDEN: Embryonic Deadenylation Element

EDEN-BP: Embryonic Deadenylation Element Binding Protein

EDTA: Ethylene Diamine Tetraacetic Acid

elav: Embryonic Lethality and Abnormal Visual system

ESI-MS: Electrospray Ionisation Mass Spectrometry

G: Guanine

GRE: Guanine/Uridine Rich Element

HSQC: Heteronuclear Single Quantum Coherence

IMAC: Immobilised Metal Ion Affinity Chromatography

IPTG: Isopropyl thiogalactopyranoside

ITC: Isothermal Titration Calorimetry

kDa: KiloDaltons

LB: Luria Broth

M: Molar

MS: Mass Spectrometry

mRNA: Messenger RNA

MTSL: *S*-(2,2,5,5-tetramethyl-2,5-dihydro-1H-pyrrol-3-yl)methyl methanesulfonylthioate

MWCO: Molecular Weight Cutoff

NaCl: Sodium Chloride

NMR: Nuclear Magnetic Resonance

NOE: Nuclear Overhauser Effect

NOESY: Nuclear Overhauser Effect Spectroscopy

OD: Optical Density

PAGE: Polyacrylamide Gel Electrophoresis

PCR: Polymerase Chain Reaction

PDB: Protein Data Bank

PRE: Paramagnetic Relaxation Enhancement

RDC: Residual Dipolar Coupling

Rg: Radius of Gyration

RMSD: Root Mean Square Deviation

RNA: Ribonucleic Acid

RNP: Ribonucleoprotein Domain

rpm: Revolutions per minute

RRM: RNA Recognition Motif

SAXS: Small Angle X-Ray Scattering

SDS: Sodium Dodecyl Sulphate

TEMED: N,N,N,N-Tetramethylethylenediamine

Tm: Melting temperature

TOCSY: Total Correlation Spectroscopy

TROSY: Transverse Relaxation Optimized Spectroscopy

U: Uracil

UTR: Untranslated region

UV: Ultra Violet

Amino Acid Codes

Amino Acid Name	3 Letter Code	1 Letter Code	Amino Acid Name	3 Letter Code	1 Letter Code
Alanine	Ala	A	Leucine	Leu	L
Arginine	Arg	R	Lysine	Lys	K
Asparagine	Asn	N	Methionine	Met	M
Aspartic Acid	Asp	D	Phenylalanine	Phe	F
Cysteine	Cys	C	Proline	Pro	P
Glutamine	Gln	Q	Serine	Ser	S
Glutamic Acid	Glu	E	Threonine	Thr	T
Glycine	Gly	G	Tryptophan	Trp	W
Histidine	His	H	Tyrosine	Tyr	Y
Isoleucine	Ile	I	Valine	Val	V

1 Introduction

The CELF proteins are a family of RNA binding proteins with regulatory roles in translation, alternative splicing and deadenylation. The term CELF stands for CUG-BP and ETR-3-like factor, referring to earlier terms for the founder members CELF1 and CELF2. Four additional members of this protein family have been identified, based primarily on sequence similarity. Some of these proteins had previously been grouped into the “Bruno-like” family of proteins, named after a homologous protein in *Drosophila*, which was later determined to be equivalent to the CELF family^{1,2,3,4}. CELF proteins are found in most animals and plants, but not in yeast or bacteria. The CELF family of proteins is divided into two subfamilies: CELF1 - 2 and CELF3 – 6, with at least one protein from each subfamily present in all plants and animals. All six CELF proteins are found in humans. The focus of this study is on the CELF1 protein, which is of particular interest due to its involvement in type 1 myotonic dystrophy (DM1)⁵. CELF1 was originally identified as a human RNA binding protein by its ability to bind to a (CUG)₈ RNA substrate^{6,7} and hence is referred to in most earlier work as CUG binding protein 1 (CUG-BP1).

CELF1 was initially shown to be involved in the alternative splicing of mRNAs in the nucleus^{8,9,10}. It was however noted to be found in both the nucleus and the cytoplasm¹¹ and so was suspected to have additional functions to regulating alternative splicing which were dependent on its environment. These additional functions were first identified in the *Xenopus Laevis* homolog of CELF1, which was determined to cause rapid deadenylation of certain mRNAs when in the cytoplasm. This homolog of the protein was therefore originally named EDEN-BP (Embryonic Deadenylation Element – Binding Protein)¹². It was later demonstrated to bind to a U/G rich sequence termed the “Embryonic Deadenylation Element” or EDEN motif in the 3’ untranslated region of mRNAs. This triggers deadenylation and translational repression of the mRNA, by a

mechanism which is believed to involve the recruitment of poly(A) ribonuclease (PARN)¹³.

1.1.1 Deadenylation

Almost all eukaryotic protein-encoding mRNAs have a poly (A) tail at the 3' end, the structure of which is shown in Figure 1.1. When released from the nucleus mRNAs have a uniform poly (A) tail length, which is about 250 nucleotides in most mammals. Once in the cytoplasm different mRNAs are affected by a range of deadenylases and regulatory proteins, resulting in variable length poly (A) tails. The length of the poly (A) tail affects the susceptibility of the mRNA to degradation, and hence the efficiency with which it is translated. Regulation of gene expression is therefore achieved by regulation of the length of these poly (A) tails^{14, 15, 16}.

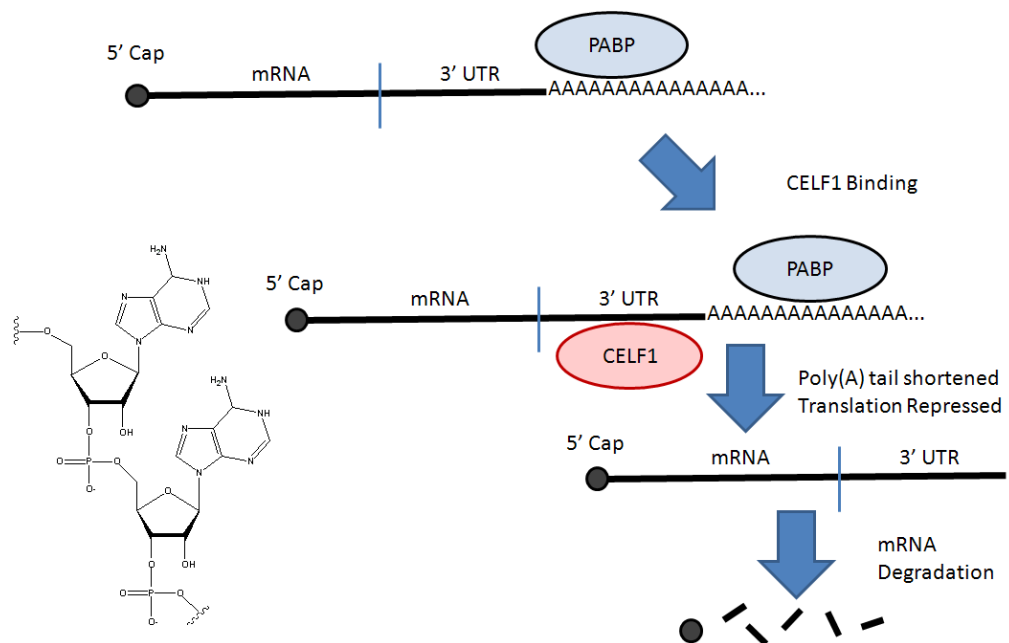


Figure 1.1: Outline of the deadenylation process and its role in mRNA regulation. Top left is shown the structure of a section of the poly(A) tail. To the right is shown the structure of a typical mRNA, with a PABP bound to the poly(A) tail. If an RNA sequence recognised by CEL F1 is present (the Embryonic Deadenylation Element or EDEN motif), CEL F1 can bind and triggers rapid shortening of the poly(A) tail. The mechanism by which CEL F1 triggers deadenylation has not been confirmed, but may involve recruitment of poly(A) ribonuclease. Shortening of the poly(A) tail reduces the efficiency of the mRNA translation, and increases its susceptibility to degradation.

The 3' ends of mRNAs are protected from degradation by exonucleases by poly (A) binding proteins (PABPs)¹⁷. Removal of these (or the 5' cap) is required for degradation to occur^{18, 19}. These PABPs have also been determined to promote recruitment of the small ribosomal subunit via an interaction with eukaryotic translation initiation factor 4F (eIF4F), encouraging translational initiation²⁰. Increasing the length of the poly (A) tail that the PABPs can bind to will therefore increase the efficiency of the mRNA's translation. Conversely shortening of the poly (A) tail reduces the efficiency of its translation, as well as making the mRNA more vulnerable to degradation.

In *Xenopus*, CELF1 was identified as a translational repressor, which functions by binding to a specific motif in the 3' untranslated regions of its target mRNAs. CELF1's target RNA motif was termed the "Embryonic Deadenylation Element" or EDEN motif^{12, 21}. This binding event triggers rapid deadenylation, and hence translational repression and degradation of the bound mRNA. Due to the uncertainties in the sequence requirements for CELF1 binding the exact criteria for an EDEN motif are not well defined, which prevents easy identification of all mRNAs regulated by this protein. While an EDEN motif alone is sufficient for deadenylation to occur, additional elements present in the 3' UTR have been reported to increase the efficiency of the process. Possible auxiliary elements include a triply repeated AUU motif in the 3' UTR of the mRNA or a repeating AUUUA motif²².

Human and *Xenopus* CELF1 have a very high degree of sequence conservation. They have an 88% sequence identity overall, with an even higher degree of conservation within the three structured domains of the protein. The two proteins have been demonstrated to be functionally interchangeable, and hence the additional role of human CELF1 as a deadenylation factor was identified²³. Based on this it is presumed that these proteins are recognising the same mRNA targets²². Clarifying the nature of the EDEN motif is of particular interest, since upregulation of CELF1 has been linked to type 1 myotonic dystrophy, and the

phenotype of this disease is believed to be at least partially due to the misregulation of CELF1's target mRNAs^{7, 24, 25, 26, 27}.

1.2 Structure of the CELF Proteins

All six members of the CELF family of proteins have the same overall domain arrangement. The proteins each contain three structured domains, all of which are RNA recognition motifs (RRMs). In the CELF proteins RRM1 and 2 are generally located relatively close to the N-terminus of the protein, with a short flexible linker between them. RRM3 is typically located near the C-terminus of the protein, with between 180 and 220 residues of unstructured protein between it and RRM2. This unstructured region has been termed the “divergent domain”, as differences in it are used to divide the CELF family into the two subfamilies.

It was unclear whether the “divergent domain” linking RRM2 and RRM3 plays any direct role in binding to the RNA, or whether it simply allows the RRMs sufficient freedom of movement relative to each other to adopt the appropriate conformation for binding. Deletion of this linker region in CELF1 has been reported to result in a loss of RNA binding in a yeast three-hybrid assay, but the construct used not only removed the linker, but also significantly truncated the adjacent RRM2 and RRM3 domains^{28, 29}. The resulting disruption to the fold of these two structured domains may therefore be responsible for the reported loss of binding, rather than the removal of the RRM2 – RRM3 linker itself.

1.2.1 RNA Recognition Motifs

RNA Recognition Motifs (RRMs) are one of the most abundant classes of protein domains in eukaryotes. They are also known as RNA binding domains (RBDs) or ribonucleoprotein domains (RNPs). RRMs are also found in prokaryotes but they are rarer, and prokaryotic proteins generally do not contain multiple RRMs³⁰. In

contrast almost half of those eukaryotic proteins containing an RRM have multiple RRM domains, with as many as six in a single protein³¹. There are around 500 human proteins which are currently known to contain at least one RRM³². The number of nucleotides that can be recognised by an individual RRM varies, with examples known that bind as few as two^{33, 34, 35}, and as many as eight³⁶. Multiple RRMs working in combination allow longer RNA sequences to be recognised, and can dramatically increase the overall binding affinity into the nanomolar range^{37, 38}.

The classic RRM protein fold consists of a four-stranded antiparallel beta-sheet packed against two alpha helices. The overall topology is $\beta 1 - \alpha 1 - \beta 2 - \beta 3 - \alpha 2 - \beta 4$. The first and third strands of the beta sheet contain highly conserved aromatic residues, which usually form key parts of the binding surface for the RNA by stacking interactions with the RNA bases^{39, 40}. There are some known variations on the classic RRM fold, such as the addition of a third alpha helix at the N or C terminus of the domain. The N and C-terminal regions of RRMs are generally unstructured, but can still play a role in binding the RNA by folding over the exposed side of the RNA strand and holding it in place against the beta sheet^{31, 41, 42, 43}.

Despite their name RRMs are not always restricted to interacting with RNA and can also be involved in binding DNA⁴⁴, and in protein - protein interactions⁴⁵. In some cases this competes with, or completely prevents conventional interactions of the RRM with RNA by obstructing the normal binding surface. There are however known examples of RRMs which can bind to both proteins and RNA simultaneously due to the interactions occurring via different binding surfaces.

1.2.2 Structure of CELF1

Human CELF1 has the same basic arrangement of three RRM s as the other CELF family members. RRM1 and 2 are located near the N-terminus of the protein, separated by approximately 8 residues of relatively unstructured linker. RRM3 is near the C-terminus of the protein, separated from RRM2 by around 215 residues, which are believed to be completely unstructured. Human CELF1 is a 486 amino acid protein with a total mass of 52.1 kDa. The *Xenopus Laevis* homolog has an additional three amino acids in the flexible linker between RRM2 and RRM3, increasing the total mass to 52.7 kDa. The exact arrangement of the RRM s is shown in Figure 1.2.

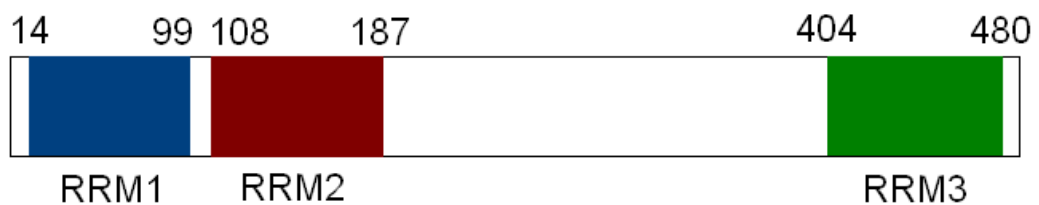


Figure 1.2: Arrangement of the RRM s in the CELF1 protein sequence. Numbers indicate the approximate limits of the structured regions.

In general RRM s have two major conserved regions, which have been termed RNP1 (in β -strand 3) and RNP2 in β -strand 1^{46, 47}. RNP1 is defined as: K/R – G – F/Y – G/A – F/Y – V/I/L – X – F/Y, where X is any amino acid. RNP2 is defined as I/V/L – F/Y – I/V/L – X – N – L. These RNP1 and 2 motifs are to some extent conserved in all three RRM s of CELF1, but there are some notable deviations from the normal pattern of residues.

RNP2: I/V/L – F/Y – I/V/L – X – N – L

RRM1: M – F – V – G – Q – V

RRM2 : L - F - I - G - M - I

RRM3 : L - F - I - Y - H - L

RNP1 : K/R - G - F/Y - G/A - F/Y -V/I/L - X - F/Y

RRM1 : K - G - C - C - F - V - T - F

RRM2 : R - G - C - A - F - V - T - F

RRM3 : K - C - F - G - F - V - S - Y

RRM1 and RRM2 in particular show significant differences in these regions, as one of the key conserved aromatic residues is missing. The first aromatic residue in RNP1 has been replaced with a cysteine, which is conserved between RRM1 and RRM2. A phenylalanine residue is however present at this position in RRM3. RRM3 also has an additional tyrosine residue in the RNP2 region, as opposed to a conserved glycine residue in RRM1 and RRM2. These additional aromatic residues permit different potential stacking interactions with the RNA bases, and so RRM3 may have distinct differences in interactions with RNA compared to the other two domains. One other deviation from the classic RNP regions is the lack of a conserved asparagine in RNP2, which is the case for all the three RRM.

1.2.3 NMR and X-ray Crystallography Data Available for CELF1

Structural data for some domains of CELF1 had already been published prior to this study, and additional NMR and x-ray crystallography data appeared during its course. In 2004, Jun *et al.* published NMR assignments and a solution structure for the N-terminal region of CELF1, specifically residues 14 - 187 of the human CELF1 protein incorporating the whole of RRM1 and RRM2⁴⁸. The

structures of these domains are shown in Figure 1.3. In 2009 Tsuda *et al.* published NMR solution structures of an isolated RRM3 construct (residues 377 - 480), both unbound and in complex with the RNA substrate UGUGUG⁴⁹. Shown in Figure 1.4 are their NMR solution structures for RRM3 in isolation, and in complex with the RNA sequence UGUGUG. (PDB ID: 2CPZ and 2RQ4)

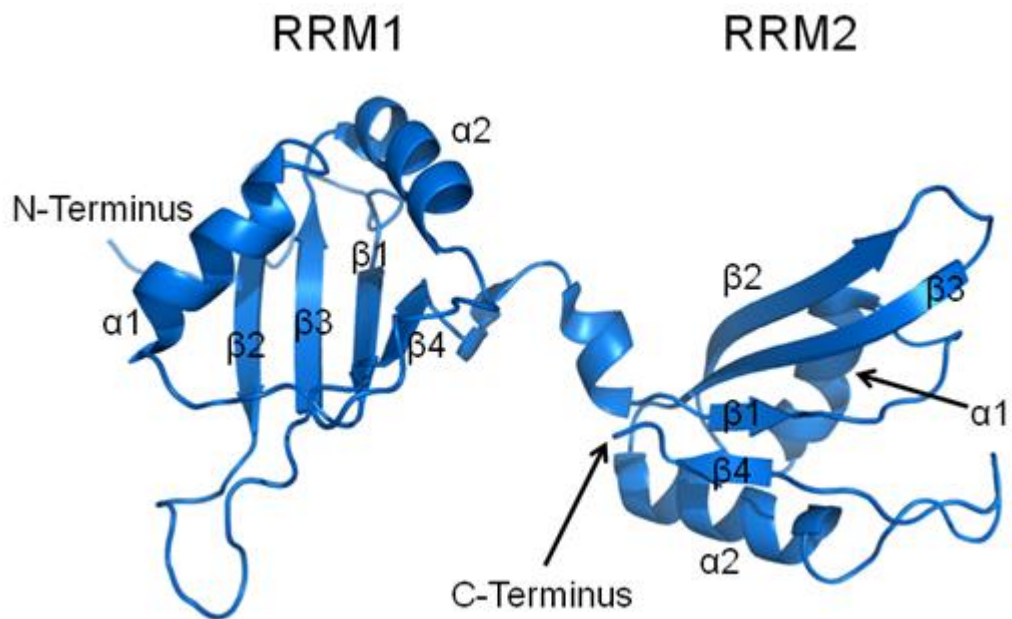


Figure 1.3: Structure of the N-terminal domains of CELF1 by Jun *et al.* (PDB ID: 2DHS). RRM1 on is on the left, RRM2 on the right. The similarities in the fold of each domain can be seen. Given the high level of sequence conservation between them it is expected that the structure of the CELF1 domains is the same in homologous proteins, such as in *Xenopus Laevis*. This image was produced using the program MOLMOL⁵⁰.

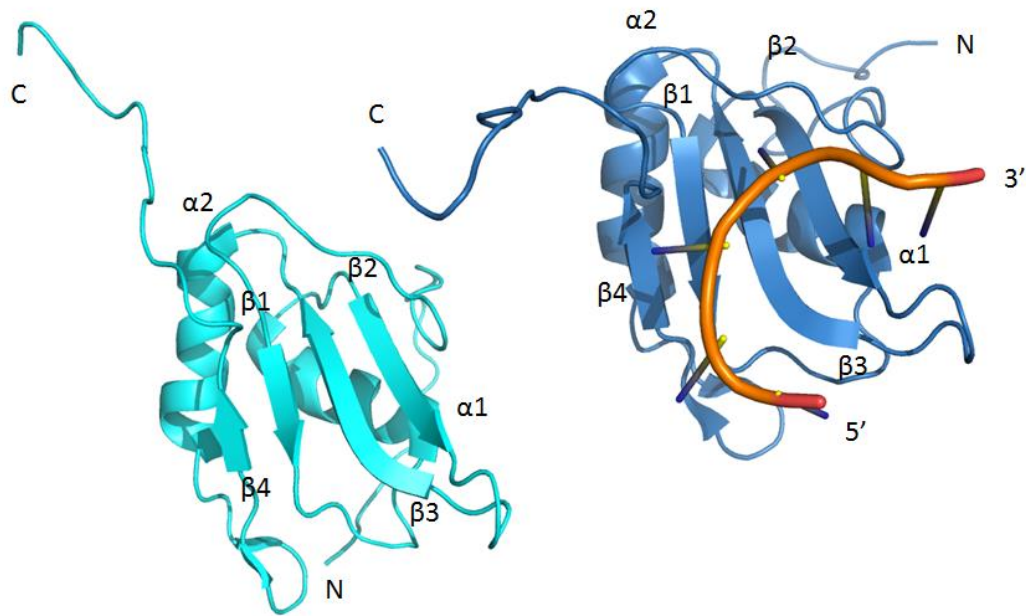


Figure 1.4: Structure of RRM3 of human CELF1, determined by Tsuda *et al.* Structures of both the protein in isolation (left), and in complex with the RNA sequence UGUGUG (right) are shown. As there is only a single residue difference in this domain between human and *Xenopus* CELF1, it can be assumed that the structure and function is conserved between the two protein homologs²⁵.

A notable feature of the RRM3 bound structure was the involvement of an unstructured N-terminal extension of the domain in binding RNA. This region folds back across the β -sheet surface, forming additional contacts with the RNA strand. Studies of the third domain of the homologous protein in *Drosophila* (usually identified as Bruno-1) had previously indicated a 40 residue N-terminal extension was required for RNA binding, which is likely due to a similar interaction. No evidence has been presented for any similar extended regions being involved in RNA binding by the other two domains.

In 2010 Teplova *et al.* produced crystal structures of an isolated RRM1 construct and a construct of the two N-terminal domains in complex with various U/G rich RNA substrates. They were however unable to observe any plausible structures for tandem binding of the N-terminal domains onto a single RNA molecule⁵¹. This was attributed to be a result of crystal packing interactions by the authors,

rather than any inherent problem with binding both domains simultaneously to the RNA substrates in solution. Teplova *et al.* also reported attempts to model the tandem binding of the two N-terminal domains by analogy to the known structures of HuD and PABP. These proteins have similar pairs of RRMs separated by comparable flexible linkers of 10 – 12 residues, but have two distinct binding modes. When PABP binds the two RRMs are arranged side by side, allowing the β -sheets to form a relatively flat surface with the RNA substrate bound across it in a linear arrangement. In contrast in HuD the RRMs are rotated with respect to each other, introducing a sharp turn into the RNA backbone. Plausible models of the N-terminal domains of CELF1 bound to the RNA substrate could be constructed for either arrangement due to the flexibility of both the linker between the domains, and the spacer between their target sites in the RNA sequence. It was concluded that more data was required on the tandem binding of the domains to distinguish between these models.

The region of the protein between residues 187 and 385 (the “divergent domain”) has no NMR or x-ray crystallography data available, but is believed to be completely unstructured. There is also no structure incorporating more than two of the three CELF1 domains, and so no information as to how RRM3 might work together with the N-terminal domains in order to recognise the RNA substrate.

1.3 Target RNA Sequences of CELF1

CELF1 has been shown to interact with three distinct types of RNA sequence: UG rich elements²⁸, CUG repeats⁵² and AU rich elements^{53, 54}. While a (CUG)₈ probe was the first RNA sequence identified to bind to CELF1, UG rich sequences, in particular those containing UGU trinucleotides, were later found to bind with a much higher affinity^{29, 55}. Isothermal titration calorimetry conducted by Tsuda *et al.* on RRM3 in isolation showed a strong preference for UG repeats

over CUG or AU repeats, the latter two showing no significant interaction⁴⁹. The reported interactions of CELF1 with CUG and AU repeats must therefore involve one or both of the N-terminal domains of the protein. The comparison of the residues in the RNA binding surfaces of each RRM of CELF1 showed that RRM3 is the most distinct of the three domains, with two additional aromatic residues. It would therefore not be surprising if its preferred target sequences were also distinct.

Some natural mRNA sequences have been empirically determined to be targets of CELF1 by observation of binding to the protein, and subsequent deadenylation and translational repression of the mRNA in a reporter assay. In 2006 Moraes *et al.* reported that sections of the RNAs TNF α and c-fos were capable both of binding to CELF1, and inducing rapid shortening of an attached poly(A) tail suggesting that these sequences contain functional EDEN motifs⁵⁶. These sequences are however 250 bases in length, and the size of the RNA binding surfaces of CELF1 means that only a small section of these sequences can possibly be being recognised. Both RNAs contain multiple UGUX sites, with eight in TNF α and nine in c-fos. This is higher than would be expected for a randomly generated RNA sequence, which would average 2.9 of these sites in 250 bases. The authors tentatively suggested the section near the start of the c-fos sequence: UGUUCAUUGUAAUGUU as a possible binding site for CELF1 as it contains three of these UGUX sites in close proximity, one for each RRM.

sequence⁵⁷. Also in 2008 Vlasova *et al.* identified the consensus sequence UGUUUGUUUGU as a possible CELF1 binding site, which was commonly present in short lived mRNAs^{58, 59}. In 2010 Rattenbacher *et al.* reported further studies of human CELF1 mRNA targets, producing a consensus sequence of UGUGUGUGUGU, with some flexibility for G -> U substitution between UGU sites⁶⁰. These three sequences are all consistent with CELF1 targeting a repeating UGU motif, with the nucleotides separating the UGU sites being of lesser importance. The 11 nucleotide sequence UGUUUGUUUGU has therefore been proposed as a functional EDEN motif, and has been termed the “Guanine Rich Element” (GRE)⁵⁷⁻⁵⁸.

A limitation of these analyses is that they only demonstrated that the GRE and similar sequences were being bound by at least some of the domains of CELF1, not that they were sufficient to trigger deadenylation and hence translational repression when present in an mRNA. Both Vlasova *et al.* and Rattenbacher *et al.* demonstrated that certain RNA sequences containing the GRE trigger deadenylation, and so represent functional EDEN motifs. However the GRE was only a small part of these sequences which in all cases were at least 50 nucleotides in length, and contained additional UGU sites outside of the GRE.

Vlasova *et al.* 2008

C-jun: UUUCUUGUUUUGUUUUGUUUUGGGUAUCCUGCCCAGUGUUGUUUUGUAAAUAAGAGAUUU

Jun B: CUAAGAGUUUAUUUUUAAGACGUGUUUUGUUUUGUGUGUGUUUUGUUUU

TNFRSF1B: CUUCUGGAGCCCUUGGGUUUUUUUGUUUUGUUUUGUUUUGUUUUGUUUUGUUUU

Rattenbacher *et al.* 2010

NDUFS2: CCUGUUCCUCACUGGAAAUUGGCCUCUGUGUGUGUGUGUGUGUGUGUGUGUGU
GUGUGUAUGUUCAUGUACACUUGGCUGUCAGGC

GSN-GU: AAGAGGCCUUAGAGCGAGCCGAGCAGAGCAGCUCUGCUAUGAGUGUGUGUGUGUGUGU
UGUGUGUUGUUUCUUUUUUUUUUUUUUUACAGUAUC

PPIC-GU: GAAAACAAGGAUAUGCUUUGGCAGGGGUGUGUGUGUGUGUGUGUGUGUGUGUGUGUGUGUGUGU
UGUGUUGUGUUGUCUUUCAUUUUUUGCUUUUUU

Figure 1.6: These are the RNA sequences which were shown to trigger deadenylation in these two studies, and so must contain functional EDEN motifs. All of them contain a GRE and/or an extended UG

repeating region. Mutation of the central G in all UGU trinucleotides to C was demonstrated to render the EDEN motif non-functional for all of the sequences except PPIC-GU, where these mutations were not conducted.

In Figure 1.6 are shown the complete sequences which were demonstrated to contain functional EDEN motifs in these two studies. While each does contain either the GRE or a lengthy UG repeat, there are a minimum of six possible UGU sites in each sequence. There is also a wide range of possible spacing between UGU sites, and no indication which sites are being occupied by the three domains of CELF1. There was therefore insufficient evidence to conclude that the GRE alone was sufficient for binding of all three domains of CELF1, or to serve as a functional EDEN motif capable of triggering deadenylation. An extended version of the c-jun sequence had previously been shown to be a functional EDEN motif in *Xenopus*²².

During the course of this study Teplova *et al.* reported crystal structures showing that both RRM1 and RRM2 were capable of recognising the RNA sequence UGUU. If the EDEN11 GRE sequence is capable of binding all three domains of CELF1 simultaneously, then at least one of the three domains would have to be binding to a UGU site rather than a UGUU site. Their model of the tandem interaction of the N-terminal domains also highlighted the importance of the spacing between the binding sites of each domain. Depending on whether a domain was recognising a UGU or a UGU(U/G) site, it would have only a single nucleotide, or no spacer at all between it and the neighbouring binding site on the GRE substrate. These short or non-existent spacers between the binding sites seemed likely to result in steric clashes between the RRMs. To predict whether any given sequence can bind CELF1 it was therefore important to clarify not only the minimum site required for each domain to bind, but also the spacing between the sites that would permit the domains to bind in tandem.

Proposed EDEN Motif	RNA Sequence
----------------------------	---------------------

c-fos ARE ⁵⁶	<u>UGUU</u> CAU <u>UGUA</u> A <u>UGUU</u>
EDEN15 ⁵⁷	<u>UGUU</u> <u>UGUU</u> <u>UGUU</u> <u>UGU</u>
EDEN11 GRE ⁵⁸	<u>UGUU</u> <u>UGUU</u> <u>UGU</u>
UG Repeat ⁶⁰	<u>UGUG</u> <u>UGUG</u> <u>UGU</u>

Table 1-1: This table shows short RNA sequences which have been proposed as EDEN motifs. The underlined nucleotides are suggested to be critical to binding, with the nucleotides separating them being less conserved. While longer sequences containing these motifs have been demonstrated to trigger deadenylation, it has not been shown that any of these alone are sufficient to function as an EDEN motif. They may therefore represent only part of the minimum EDEN motif. While all have been demonstrated to bind CELF1, no structural data has been published to show whether this is involving simultaneous binding of all three RRMs, or only a subset of them.

1.4 Link between CELF1 and Myotonic Dystrophy

Myotonic dystrophy type 1 (DM1), also known as Steinert's disease, is the most common form of muscular dystrophy, affecting around 1 in 8000 people. The major symptoms are progressive muscle atrophy, myotonia (an inability to relax a contracted muscle) and cardiac conduction defects⁶¹. At a molecular level misregulation of alternative splicing of some mRNAs has been observed in cases of DM1. Incorrect splicing patterns have been found in more than 20 different mRNAs in DM1 tissues, mostly in skeletal muscle and the brain. These include the mRNAs for the insulin receptor, the tau protein and the CLC-1 muscle chloride channel. Not all of these mis-spliced mRNAs have been correlated with the symptoms of DM1, though the mis-splicing of the CLC-1 mRNA is associated with myotonia. In CLC-1 exon 7a is inappropriately incorporated, which results in a truncated and non-functional form of the CLC protein^{62, 63}. Overexpression of CELF1 in mouse models reproduces these splicing defects, as well as the other features of the DM1 phenotype^{64, 65, 66}. Correction of the CLC-1 splicing defect in a mouse model with a myotonic phenotype restored normal chloride transport and hence normal function⁶⁷.

DM1 is an inherited disorder, caused by an expanded region of CUG repeats in the 3' UTR of the dystrophin-myotonia protein kinase gene (DMPK) of chromosome 19^{68, 69, 70, 71, 72, 73}. Healthy individuals have been observed to have up to 38 repeats of CUG at this position. Symptoms of DM1 have been observed in individuals with as few as 50 repeats, and cases with more than 4000 CUG repeats are known. There is a strong correlation between the number of repeats and the severity of the DM1 symptoms^{74, 75}. The age of onset of DM1 is also strongly correlated to the number of repeats⁷⁶. The most severe and early onset form of the disease is associated with a minimum of 1500 repeats. The number of these repeats is unstable, and can increase through generations⁷⁷. Type 2 myotonic dystrophy (DM2) has similar symptoms to DM1, but is caused by an expanded CCUG repeating motif in the unrelated ZNF9 gene^{78, 79}. Between 100 and 11000 CCUG repeats have been observed in DM2 cases.

In both DM1 and DM2 these expanded RNAs form aggregates in the nucleus, and it has been concluded that the symptoms of the disease are a result of the presence of these mutant RNAs, rather than effects directly related to the DMPK and ZNF9 genes^{80, 81}.

Antisense transcripts, consisting of a CAG repeating sequence may also be expressed in DM1 cells. Expression of long CAG repeating RNAs has been shown to induce toxicity in animal models^{82, 83}. Both the sense and antisense transcripts also have the potential to undergo non-ATG initiated transcription, resulting in the production of long chains of a single amino acid type (polyglutamine and poly-leucine)⁸⁴. These would be expected to aggregate, giving another possible source of cellular toxicity^{85, 86}. Polyglutamine aggregates have been observed in DM1 tissues, so may play some role in the disease pathogenesis.

The expanded RNAs are not exported from the nucleus to the cytoplasm, instead aggregating into insoluble foci. Electron microscopy and crystallography have shown that the extended CUG repeats of DM1 form stable hairpin structures. These are composed of normal Watson-Crick base pairing between C and G bases separated by mismatched U-U pairs^{87,88}. While CELF1 is known to bind at least with a low affinity to long CUG repeating sequences, it has not been detected in these foci. The RNA splicing protein muscle blind-like (MBNL1) has been found to bind to the double stranded sections of these RNAs, and is sequestered into the foci^{89,90}. This has led to the hypothesis that CELF1 is not involved in binding to these CUG repeat RNAs *in vivo* at all and so is not directly involved in DM1 pathogenesis, but this is inconsistent with the observed effects of CELF1 upregulation in mouse models. It has however been found that very short CUG RNAs do not form foci but still result in the DM1 phenotype, suggesting the foci are a symptom rather than a direct cause of DM1. The possibility that the foci only contain a fraction of the CUG RNAs has been raised to explain this observation⁹¹. If this is the case then direct binding of CELF1 to extended CUG RNAs may be occurring, and playing a role in DM1 pathogenesis.

This theory is supported by size exclusion chromatography of CELF1 extracts from DM1 cells, which give an apparent molecular weight for the protein in excess of 150 kDa. This is in contrast to the protein from wild type cells with a mass of just over 50 kDa, and was found to be sensitive to the presence of RNases indicating this shift is due to binding to a long RNA sequence⁹¹. Almost all of the CELF1 protein in DM1 cells was found to be in the form of this RNA complex. CELF1 has been shown to be incapable of binding to double stranded RNA *in vitro*. Electron microscopy of CUG RNA hairpins showed CELF1 would only bind to single stranded sections at the ends of the hairpin, not to the double stranded stem⁹². It can be hypothesized that binding to MBNL1 encourages formation of double stranded RNA, displacing CELF1. This would account for the complete absence of CELF1 in the insoluble foci, despite it being almost saturated by soluble non-focus CUG RNA.

CELF1 and MBNL1 appear to be antagonistic proteins. Sequestering of MBNL1 in the insoluble foci effectively results in increased CELF1 activity. The half-life of CELF1 is normally quite short (estimated at 3 hours *in vivo*), but is likely to be increased by up to a factor of five by binding to the longer lived single stranded CUG RNA⁹³. It has been suggested that CELF1 upregulation in DM1 is due to the protein being hyperphosphorylated by protein kinase C (PKC) and hence stabilized⁹⁴. The mechanism of this PKC activation is unknown, and it is possible that PKC upregulation is an effect of CELF1 upregulation rather than a cause.

A recent paper by Masuda *et al.* (2012) suggests a more direct mechanism for CELF1 upregulation in DM1 cells. In cross-linked immunoprecipitation assays with CELF1 and MBNL1, they note that the CELF1 mRNA appears to have an MBNL1 target site in its 3' untranslated region (UTR). They also noted a possible CELF1 target (or EDEN motif) in the 3' UTR of the MBNL1 mRNA. Since both of these proteins ultimately trigger the degradation, and hence repression of their target mRNAs, this implies that CELF1 and MBNL1 directly regulate each other. When MBNL1 is sequestered by the expanded CUG repeat RNA in DM1 cells, this will reduce its repression of its target mRNAs, including CELF1. CELF1 will therefore be upregulated, even without any extension of its half life via phosphorylation, or binding to soluble CUG RNAs. Hyperphosphorylation by PKC may be exacerbating the condition by stabilizing the already elevated levels of CELF1, but this may not be the direct cause it was originally thought to be. This has implications for the treatment of DM1. Potential therapies for DM1 have so far focused on disruption of the MBNL1/CUG repeat RNA interaction^{95, 96, 97}. This mutual regulation suggests that if CELF1 could be sequestered or otherwise inactivated, it should not only restore normal splicing patterns, but also upregulate MBNL1 directly. CELF1 therefore represents a potential drug target for treatment of DM1.

1.5 MBNL1

Muscle Blind-Like 1 (MBNL1) is an RNA binding protein known to regulate alternative splicing of mRNA. It has recently been reported to also be involved in translational repression, similar to CELF1. The interplay of these two regulatory proteins, particularly in the context of type 1 myotonic dystrophy is of interest. The MBNL1 protein has 388 amino acid residues, and a total mass of 41.8 kDa. It is composed of four small CCCH - type zinc finger domains, arranged in pairs. Domains 1 and 2 are located near the N-terminus, while 3 and 4 are roughly in the middle of the protein chain. X-ray crystal structures of all four domains are available (Teplova *et al.* 2008), and the rest of the protein is believed to have no significant secondary structure⁹⁸.

These four zinc finger motifs recognize a YGCY motif, where Y is either of the pyrimidine bases^{99, 100}. Immunoprecipitation assays by Masuda *et al.* identified a somewhat different MBNL1 target motif of CU(G/C)C, consistent with earlier reports¹⁰¹. The extended CUG RNA sequences in DM1 satisfy both sets of criteria, and have been shown to sequester MBNL1 along the double stranded sections of the resulting CUG hairpins. Both MBNL1 and CELF1 are regulators of alternative splicing, but analysis of the distribution of their target motifs around introns and exons shows distinct patterns for the two proteins. EDEN motifs were found to be concentrated immediately before and after alternative exons. MBNL1 motifs in contrast are less common in these regions, and more enriched in the exon regions themselves¹⁰².

1.6 Dimerisation of CELF1

Xenopus CELF1 has been reported to undergo dimerisation in a yeast two-hybrid assay, and it has been suggested that this might have a role in recognition of RNA^{54, 103}. No evidence of dimerisation has been reported in the literature for

human CELF1. It is not clear if the yeast two-hybrid observation is due to the formation of a true dimer, or if it could be the result of two CELF1 proteins binding onto a single RNA molecule of the RNA substrate.

1.7 Phosphorylation of CELF1

Shortly after its discovery CELF1 was shown to be a phosphoprotein^{11, 104}. Protein kinase C (PKC), as mentioned previously, can stabilise CELF1 by hyperphosphorylating the protein in DM1 cells. However the protein is also predicted to have phosphorylation sites for several other phosphatases¹⁰⁵. It has been suggested that phosphorylation of CELF1 may therefore play an important role in regulating its RNA binding preferences, and interactions with other proteins^{106, 107, 108}. Phosphorylation has been demonstrated to occur at Ser28 and Ser302, with some reported effects on the RNA binding properties of CELF1^{106, 109}. It has been proposed that phosphorylation at Ser28 may serve as a “switch” altering CELF1’s preferred target from the U/G rich sequences so far identified to a C/G rich sequence. A specific example is a reported increase binding affinity to the cyclin D1 mRNA sequence shown below when the phosphomimetic mutation S28D is made to CELF1¹⁰⁹.

Cyclin D1:

```
5'-CCCAGCCAGGACCCACAGCCCUCCCCAGCUGCCCAGGAAGAGCCCCAGCC-3'
```

This sequence is very distinct from any other CELF1 consensus sequence in the literature, as it is G/C rich and with very few uracils. If this concept of a Ser28 switch is correct, it is possible that the “EDEN motif” may actually vary depending on the phosphorylation state of CELF1.

1.8 Interactions of CELF1 with Poly (A) Ribonuclease

CELF1 has been reported to interact with poly(A) ribonuclease (PARN), also known as DAN (deadenylating nuclease)⁵⁶. This interaction was observed even in the absence of RNA, suggesting the two proteins bind directly to each other. Since the function of PARN is to shorten the poly(A) tail of mRNAs, it presents a possible mechanism for how CELF1 triggers deadenylation of its mRNAs. If CELF1 can interact with both PARN and its mRNA targets simultaneously, it can therefore recruit the deadenylase to the mRNA. PARN has been successfully purified¹¹⁰, and the structures of all of its domains are known from x-ray crystallography^{111, 112}. So far no structural data has been reported to indicate which regions of the proteins are involved in the interaction with CELF1. NMR data has previously been collected on an isolated construct of the RRM (residues 430 – 516), but not on any larger sections of the protein.

1.9 Aims and Objectives

The primary aim of this study was to determine the sequence requirements for high affinity CELF1 binding. While a few potential high affinity CELF1 targets had been identified (e.g. the GRE and EDEN15 consensus sequences), the criteria for an “EDEN motif” were still not well defined. It was also unknown what role each domain of CELF1 played in recognising RNA. Our aims were therefore:

- 1) Express and purify constructs of each domain of CELF1 in isolation. Using these, determine the minimum RNA sequence requirements for each domain to bind. NMR and ITC can be used to investigate whether each domain requires a UGU(U/G) site, or if the shorter UGU site is sufficient. Also we aimed to investigate which domains are involved in the reported interactions of CELF1 with CUG repeats and AREs.
- 2) Using a construct containing the two N-terminal domains of CELF1, determine the spacing required between UGU or UGU(U/G) sites in a sequence for tandem binding of the two domains onto a single RNA

molecule. Confirm by ITC that this tandem interaction results in an enhanced binding affinity compared to the isolated RRMs. Investigate whether a similar enhancement in binding affinity is seen for tandem interactions with CUG repeats and AREs. We also aimed to check for any involvement of N- and C-terminal extensions of RRM1 and RRM2 in RNA binding, similar to that seen for RRM3.

- 3) Express and purify a construct containing all three RRMs of CELF1, ideally the full length wild type protein. NMR titrations can then be used to determine whether all three RRMs are capable of binding onto the EDEN15 and GRE sequences, and so whether these represent complete and functional EDEN motifs. If these sequences are not capable of simultaneous interaction with all three domains, we aimed to design sequences that can form a high affinity complex. By investigating the minimum sequence that will still bind all three RRMs, we can determine the criteria for a functional EDEN motif. We also aimed to determine by ITC whether binding affinity is enhanced for simultaneous binding of all three domains.
- 4) Using the criteria determined for the EDEN motif, rationalise those sequences already reported to be functional EDEN motifs, and show which regions of these long sequences are actually recognised by CELF1.
- 5) Characterise the structure of CELF1 in complex with a high affinity EDEN motif, ideally using a combination of NMR and x-ray crystallography.
- 6) Investigate whether phosphorylation at Ser28 is serving as a “switch”, altering the RNA binding preferences of CELF1. Using NMR and ITC on a phosphomimetic mutant (S28D) we will determine if phosphorylation does change the target from UG rich sequences to CG rich sequences as suggested.
- 7) Investigate the reported interaction between poly(A) ribonuclease and CELF1. To this end we aimed to express and purify full length wild type

PARN, and conduct preliminary NMR studies of the protein in isolation, and in the presence of wild type CELF1. PARN forms a homodimer with a mass of 146 kDa, and so a complex with CELF1 could be as large as 200 kDa. This system is therefore a challenging target for NMR, and our first aim was to determine whether high resolution NMR data could be collected on this key regulatory complex. If it proved possible to acquire high resolution NMR data, we aimed to observe chemical shift perturbations from interaction of the proteins, and so determine which domains of both the CELF1 and PARN proteins are involved in their interaction.

2 Biophysical Techniques

2.1 Protein NMR

NMR spectroscopy is an established technique for both structural determination of proteins, and observing their interactions with other molecules. It has a major advantage over techniques such as ITC and mass spectrometry in that it can provide information on a residue by residue basis, rather than just the overall properties of the protein. NMR can also provide detailed structural data of proteins in biologically relevant aqueous solutions, without the need for crystallization. This allows dynamic aspects of protein systems to be investigated, which would not necessarily be evident from crystal structures^{113, 114}. Over 8000 structures derived from NMR data are present in the protein data bank, representing a significant fraction of all protein structures so far solved. Large proteins (with masses of greater than ~35 kDa) have historically been challenging for NMR, but the development of techniques such as TROSY, selective isotopic labelling of amino acid types, and improvements in spectrometer field strength have greatly increased the size of the systems that can be investigated by this technique^{115, 116}. Proteins of several hundred amino acids have been successfully

assigned, and high resolution spectra have been collected for proteins in complexes in excess of 800 kDa in mass^{117, 118}.

In protein NMR the ^1H - ^{15}N HSQC, which correlates ^1H and ^{15}N chemical shifts, is a particularly useful experiment since it shows a single peak for each residue in the protein¹¹⁹. Each amino acid gives a single peak from the backbone NH, with the exception of proline where the nitrogen has no hydrogen bonded to it. Some additional peaks are also produced by NH and NH_2 groups in the side chains of amino acids (specifically tryptophan, arginine, asparagine, glutamine and lysine). The ^1H - ^{15}N HSQC can therefore serve as a “fingerprint” for the protein, with each peak providing information on the environment of each residue. If the environment of a residue changes, for example when a ligand binds to the protein or if the protein conformation is altered, then the chemical shifts will change and the peak for the residue will move in the ^1H - ^{15}N HSQC.

2.1.1 Transverse Relaxation Optimized Spectroscopy (TROSY)

The size of the proteins and other macromolecules that could be studied by NMR was initially quite limited. Prior to the development of the TROSY technique by Pervushin *et al.* in 1997 very few solution NMR structures for proteins larger than 20 kDa were produced¹²⁰. NMR of larger proteins has two inherent problems. Firstly larger proteins inevitably result in more signals on any given spectrum, leading to spectral crowding and overlapping peaks. Secondly larger proteins have lower transverse relaxation times (T_2). The rapid loss of magnetization therefore results in very low intensity signals for large proteins.

In the case of amide protons there are two major relaxation mechanisms: the chemical shift anisotropy of the protons (CSA), and dipole-dipole interactions between the proton and nitrogen spins (DD). CSA relaxation is proportional to B_0^2 , while DD relaxation is independent of magnetic field strength. At high

magnetic fields, such as in the 600 and 800 MHz spectrometers used in this study, these effects are of comparable magnitude. In a ^1H - ^{15}N HSQC spectrum with no decoupling a peak from an amide proton is split into four by coupling between the ^1H and ^{15}N nuclei, as shown in Error! Reference source not found. , with each of the four components having different relaxation rates and linewidths. These differences are the result of constructive and destructive interference between the CSA and DD relaxation mechanisms. The normal decoupling process for an HSQC collapses these four components into a single peak, averaging the relaxation rates. The TROSY experiment instead selects for the component (DD-CSA), which has the slowest relaxation rate and hence the narrowest linewidth^{121, 122, 123},¹¹⁵

The TROSY experiment has only 50% of the inherent sensitivity of the HSQC since the signal from the faster relaxing components is discarded. However in proteins larger than ~20 kDa, this is more than compensated for by the narrower line widths. The effect is dependent on the field strength (as CSA relaxation is proportional to B_0^2), with optimal results for ^{15}N amide groups at 1 GHz. Use of this technique has allowed NMR studies of much larger proteins and complexes than was previously possible¹¹⁵.

2.1.2 NMR Assignment of Proteins

In order to extract most of the useful information from an NMR spectrum such as a ^1H - ^{15}N HSQC it is necessary to know which peak corresponds to which residue in the protein. Without this only the general properties of the whole protein such as its size and whether it is folded into a rigid structure can be determined. Matching each peak to a specific residue is known as “assigning” the spectrum, and there are a number of possible methods for accomplishing this.

The simplest method is to use 2D homonuclear experiments, specifically the Total Correlation Spectroscopy (TOCSY) and Nuclear Overhauser Effect Spectroscopy (NOESY) experiments. The TOCSY experiment shows correlations from magnetisation transfer through bonds by scalar coupling of spins. The NOESY experiment shows through-space magnetisation transfer rather than directly through bonds. By observing cross-peaks between the backbone NH of a residue and its neighbouring residues it is possible to “walk” along the protein backbone. Different amino acids give different patterns of side chain proton peaks, and once the type of each amino acid in a chain is known, it is then possible to match the chain to a specific section of the protein sequence¹²⁴.

This method has the advantage that it does not require any expensive isotopic labelling of the protein, but it is generally unsuitable for large proteins (larger than ~10 - 15 kDa) as signals from each residue are only separated by their proton chemical shift. As the size of the protein increases the odds of it containing multiple residues with the same proton chemical shift also increases. Overlapped signals can make connectivities extremely difficult to determine, and this problem is exacerbated by the tendency to broader linewidths for larger proteins. With ¹⁵N labelled protein the signals can be separated by their ¹⁵N chemical shift as well as the proton shift in 3D experiments such as the HSQC-NOESY and HSQC-TOCSY. This reduces the issue of overlapping signals to some extent^{125, 126}.

To assign larger proteins a different strategy using 3D heteronuclear NMR experiments is preferred, in which peaks are separated in the carbon and nitrogen dimensions as well as the proton dimension, reducing spectral crowding and overlap even further¹²⁷. These experiments require the protein to be isotopically labelled with both ¹³C and ¹⁵N. The more abundant ¹²C is not detectable by NMR as it has a spin of zero. ¹⁴N is detectable by NMR as it has a net spin of 1, but quadrupolar interactions result in extreme broadening of its signals in large molecules making it impractical to acquire high resolution data. The ¹³C and ¹⁵N

nuclei both have spins of $\frac{1}{2}$ and so are suitable for high resolution NMR studies. The natural abundance of these isotopes is low (1.11% for ^{13}C and 0.37% for ^{15}N), and their sensitivity is lower than for ^1H , so it is necessary to produce proteins enriched with these isotopes. This is usually accomplished by recombinant expression in a medium where only suitably labelled carbon and nitrogen sources are present¹²⁸.

Once isotopically labelled material is available 3D heteronuclear experiments such as the HNCACB¹²⁹, HNCO¹³⁰, HNCA¹³¹, HN(CA)CO¹³² and HN(CO)CACB^{130, 133} can be carried out. The name of each experiment refers to which of the nearby carbon nuclei are correlated to each backbone amide group. The exact magnetization transfer pathways and how the experiments can be used to assign the ^1H - ^{15}N HSQC spectrum of a protein are explained in the following sections. TROSY versions of all of these 3D heteronuclear experiments exist, and allow high quality spectra to be collected for large proteins^{134, 135}. All of the protein assignments in this study were determined using this strategy of 3D heteronuclear NMR experiments on proteins labelled with both ^{13}C and ^{15}N .

2.1.3 Protein Backbone Assignment Using 3D Heteronuclear NMR Experiments

In the HNCACB experiment magnetization is transferred from the NH proton to the ^{15}N and then to the $\text{C}\alpha$ and $\text{C}\beta$ of both the i and $i-1$ residues. It is then transferred back to the ^{15}N and the NH proton in order to be detected, as shown in Figure 2.1¹²⁹. The spectrum therefore usually shows four peaks correlated to each NH. The $\text{C}\alpha$ and $\text{C}\beta$ of the same residue as the NH (residue i) usually result in high intensity peaks, and are of opposite phases. There are also peaks for the $\text{C}\alpha$ and $\text{C}\beta$ of the preceding residue (residue $i-1$) which are generally of weaker intensity and may not be visible in experiments with a poor signal to noise ratio. An alternative experiment exists (CBCANH) in which the magnetization is transferred from the $\text{H}\alpha$ and $\text{H}\beta$ of both the i and $i-1$ residues to the corresponding $\text{C}\alpha$ and $\text{C}\beta$, and then to the NH¹³⁶. The same set of peaks is observed as in the

HNCACB experiment, but the sensitivity is generally inferior for proteins with short T_2 relaxation times¹²⁷.

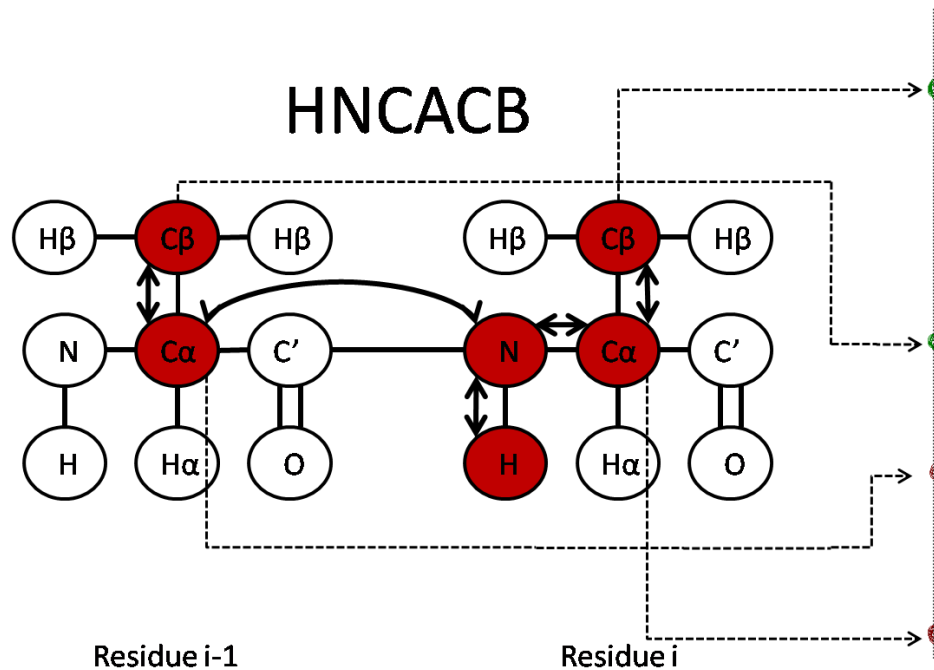


Figure 2.1: Magnetisation transfer during an HNCACB experiment. Atoms highlighted in red indicate those observed in the spectrum. On the right is shown an example of the resulting pattern of peaks seen in this experiment for each atom in the amino acid. The signals from the $C\alpha$ and $C\beta$ of residue $i-1$ are generally less intense than those from residue i due to the lower efficiency of the transfer from the nitrogen to the $C\alpha$.

The HNCACB experiment can be paired with the HN(CO)CACB experiment, in which the magnetization is transferred to the carbonyl before being transferred to the $C\alpha$ (see Figure 2.2). This results in a spectrum which shows only the $C\alpha$ and $C\beta$ of the preceding residue ($i-1$) to that containing the NH^{133} . Overlaying these spectra removes any ambiguity in the HNCACB experiment as to which peaks correspond to the i and $i-1$ residues. The only exception to these patterns is if either the i or $i-1$ residue is a glycine, in which case there will be no $C\beta$ signal for that residue.

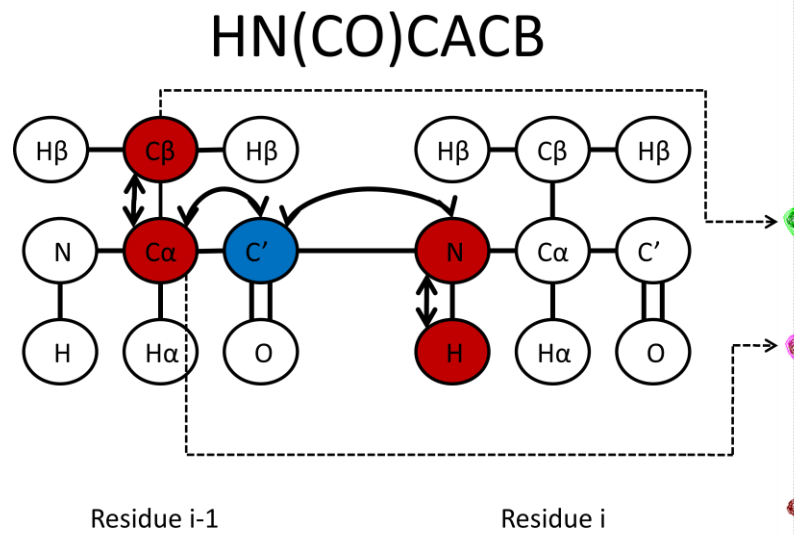


Figure 2.2: Transfer of magnetization in the HN(CO)CACB experiment. Atoms in red are observed in the spectrum. Atoms in blue have magnetization transferred through them, but are not observed in the spectrum.

Locating a different residue which has $C\alpha$ and $C\beta$ chemical shifts in the HNCACB spectrum matching those seen in the HN(CO)CACB spectrum for the first residue allows it to be assigned as the preceding residue in the protein chain. In this manner the correlations can be tracked from residue i to $i-1$ along the backbone of the protein. Alternatively the protein backbone can be traced in the opposite direction (from residue i to $i+1$) by identifying the $C\alpha$ and $C\beta$ shifts of residue i from the HNCACB spectrum, and matching those to $C\alpha$ and $C\beta$ shifts in the HN(CO)CACB spectrum for a different residue, which can then be confirmed as residue $i+1$ in the chain. An example of this assignment method is shown in Figure 2.3.

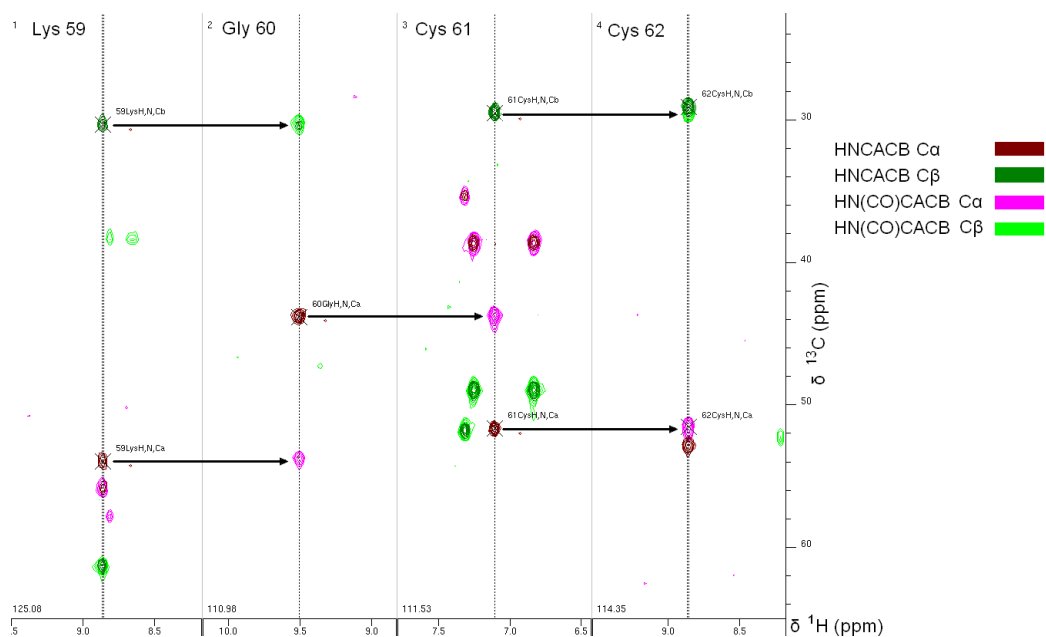


Figure 2.3: An example of assignment of the protein backbone using the HNCACB and HN(CO)CACB 3D experiments. From left to right are shown four strips through the 3D spectra at the ^1H and ^{15}N chemical shifts of four peaks in the ^1H - ^{15}N HSQC. For each residue the peak for the $\text{C}\alpha$ of the current residue is shown in pink, while the peak for the $\text{C}\alpha$ of the preceding residue is shown in maroon. Similarly $\text{C}\beta$ of the current residue is shown in light green, while the $\text{C}\beta$ of the preceding residue is shown in dark green. The arrows show matching ^{13}C chemical shifts for peaks in the HNCACB spectrum of residue i and peaks in the HN(CO)CACB spectrum of residue $i+1$. For example, correlated to the amide proton of Lys59 are two peaks unique to the HNCACB spectrum, from the $\text{C}\alpha$ and $\text{C}\beta$ of Lys59. Their ^{13}C chemical shifts match those of two peaks correlated to the amide proton of Gly60 in the HN(CO)CACB spectrum, which are known to be from the $\text{C}\alpha$ and $\text{C}\beta$ of the preceding residue to Gly60. This therefore confirms that Lys59 is the preceding residue to Gly60. Gly60 has only a $\text{C}\alpha$ signal, with a ^{13}C chemical shift that matches a signal in the HN(CO)CACB spectrum that is correlated to the amide proton of Cys61, again showing these residues are connected. Similarly matching $\text{C}\alpha$ and $\text{C}\beta$ chemical shifts are highlighted for Cys61 and Cys62. This example shows data from residues 59 – 62 of the RRM1 construct of CELF1.

The HNC(O) and HN(CA)CO spectra also allow backbone connectivities to be determined by a similar method, and so can be used to corroborate the assignments made based on the HNCACB and HN(CO)CACB pair of experiments. In the HNC(O) experiment the magnetization is passed from the proton to ^{15}N , and then to the directly bonded carbonyl. This experiment therefore shows only a single peak, which is from the carbonyl of the $i-1$ residue (see Figure 2.4)¹³³.

HNCO

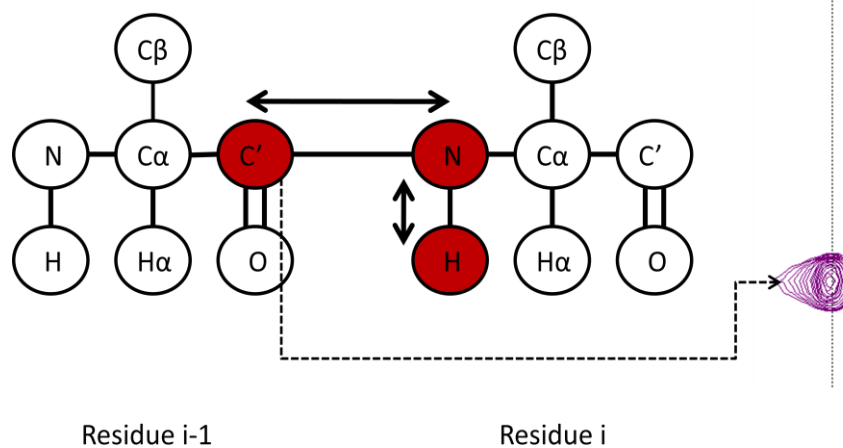


Figure 2.4: Magnetization transfer in the HNCO experiment. The short pathway results in this experiment having the highest sensitivity of this set.

In the HN(CA)CO experiment the magnetization is passed from ^{15}N to both the i and $i-1$ $C\alpha$ instead, and from there onto the directly bonded carbonyls. The spectrum therefore has two peaks, one from the carbonyl of residue i , and one from $i-1$ (see Figure 2.5)¹³².

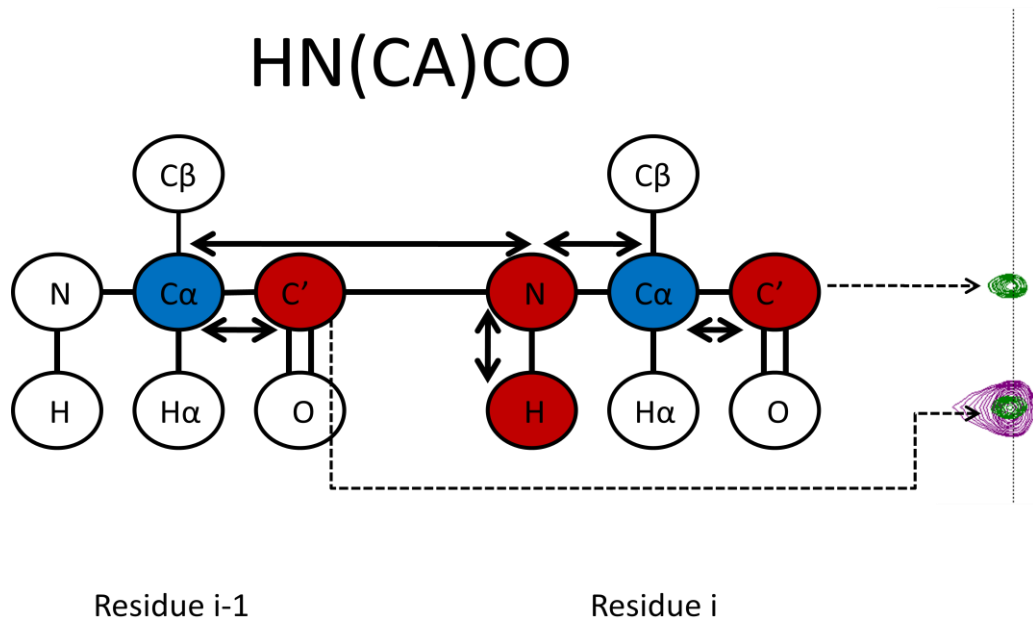


Figure 2.5: Magnetization transfer pathway in the HN(CA)CO experiment. While the magnetization is transferred via the $C\alpha$, only the carbonyls are observed in the spectrum. The transfer from the nitrogen to the directly bonded $C\alpha$ in residue i is generally more efficient than to the $i-1$ $C\alpha$, so the residue i carbonyl usually gives a more intense signal.

The carbonyl chemical shifts cannot be used to identify the residue type since no amino acids have particularly distinctive shifts, but can help resolve situations where multiple residues have very similar $C\alpha$ and $C\beta$ shifts. An example of this is shown in Figure 2.6.

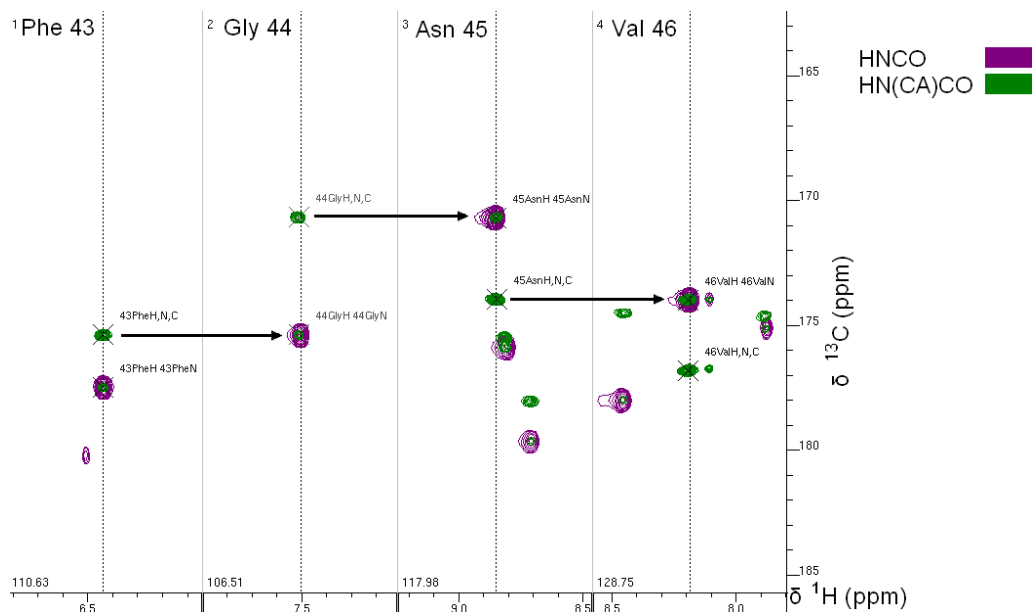


Figure 2.6: An example of using the HNCO and HN(CA)CO spectra for backbone assignment. As the HN(CA)CO spectrum shows peaks for both the *i* and *i-1* residue, while the HNCO spectrum only shows the *i-1*, it is again possible to find matching ^{13}C chemical shifts and track the connectivity along the protein backbone. A strip through the 3D spectra is shown for each residue at the ^1H and ^{15}N chemical shifts corresponding to their signal in the ^1H - ^{15}N HSQC. Phe43 shows a single peak correlated to the amide proton in the HNCO spectrum, and two in the HN(CA)CO spectrum. The peak that only appears in the HN(CA)CO spectrum is from the carbonyl of Phe43. The peak appearing on both spectra is from the carbonyl of the preceding residue. An arrow indicates the matching ^{13}C chemical shifts of the Phe43 carbonyl and the peaks known to be from the carbonyl of the previous residue to Gly44. This confirms the residues are connected, and similarly matching chemical shifts are highlighted for Gly44, Asn45 and Val46. This example shows data from residues 43 – 46 of the RRM3 construct of CELF1.

Since they have no amide proton and so are not visible in the ^1H - ^{15}N HSQC, prolines in the sequence create breaks in the chain of connected residues. Weak or missing signals from other residues in the ^1H - ^{15}N HSQC will also cause breaks, so normally the connectivity cannot be tracked all the way from the C-terminus to N-terminus. Instead a series of shorter sections are assigned and combined to give the complete assignment of the protein.

This method has so far produced a set of short chains of connected residues, but as yet the position of each chain in the protein sequence, and hence the exact assignment of each NH signal in the ^1H - ^{15}N HSQC has not been determined. To

unambiguously assign a signal to a specific residue requires examination of the exact $C\alpha$ and $C\beta$ chemical shifts seen in the HNCACB spectrum. Certain amino acid residues have distinctive shifts which allow the amino acid type for a specific residue to be determined. For example, glycine is unique in that it has no $C\beta$ and so has fewer peaks than other residues in the HNCACB spectrum. The $C\alpha$ also has a distinctive shift of 45 ± 2 ppm allowing glycine residues to be immediately recognised (such as Gly60 in Figure 2.3). Other distinctive residue types are alanine (which has a uniquely low $C\beta$ chemical shift of 18 ± 3 ppm) as well as serine and threonine (which are the only residues with larger $C\beta$ shifts than $C\alpha$ shifts).

Unique patterns of these distinctive residues can then be identified in the sequential chains so far produced, and matched to the sequence of the protein. For example, the t187 construct of CELF1 contains the sequence TFFT from residues 154 - 157. This is the only instance of two adjacent threonine residues in the protein sequence. When two residues adjacent in the chain were determined to be threonines by their unusual $C\beta$ shifts they could therefore be specifically assigned as Thr156 and Thr157. This “locked in” this particular chain section allowing all the other residues in it to be assigned as well. The assignment could then be confirmed by the presence of another threonine two residues before Thr156, and by checking the other residues in the chain had plausible $C\alpha$ and $C\beta$ shifts for their assigned amino acid type. These were verified using the reference chemical shifts in CCPNMR Analysis version 2.0.¹³⁷

The assignment could be extended out from these known residues, but not beyond the proline residues at positions 143 and 180 which have no NH signal, and hence no known chemical shift information. Other distinctive residues, such as the adjacent alanine residues at positions 71 and 72 were therefore necessary to build up the full assignment of the protein. Use of this strategy can provide assignments for the HN, NH, CO, $H\alpha$, $C\alpha$ and $C\beta$ (if present) atoms of each amino acid in the protein. Assignment of any additional side chain atoms can be assisted by 3D experiments such as the HCCH-TOCSY if required¹³⁸.

2.2 NMR Titrations

The exact chemical shifts observed for an amide group in the protein are sensitive to the surrounding environment. If that environment changes, for example when a ligand binds to the surface of the protein, then the chemical shifts of nearby residues will change significantly. Movement of peaks in the NMR spectra therefore can be used to confirm whether a given ligand does or does not bind to the protein. From the ^1H - ^{15}N HSQC information can also be collected on a per-residue basis, identifying which residues are most disrupted upon binding to the ligand. This method can be used to map the binding surfaces of the protein¹³⁹. Depending whether the exchange between free and bound forms is fast or slow on the NMR timescale, two different effects may be seen. If the rate constant k is greater than the frequency difference between the exchanging sites ($\delta\nu$) then the process is said to be in fast exchange. In fast exchange the peak for each backbone NH appears with chemical shifts that are a population weighted average of the shifts for the bound and unbound states. These peaks therefore move gradually over the course of the titration as shown in Figure 2.7.

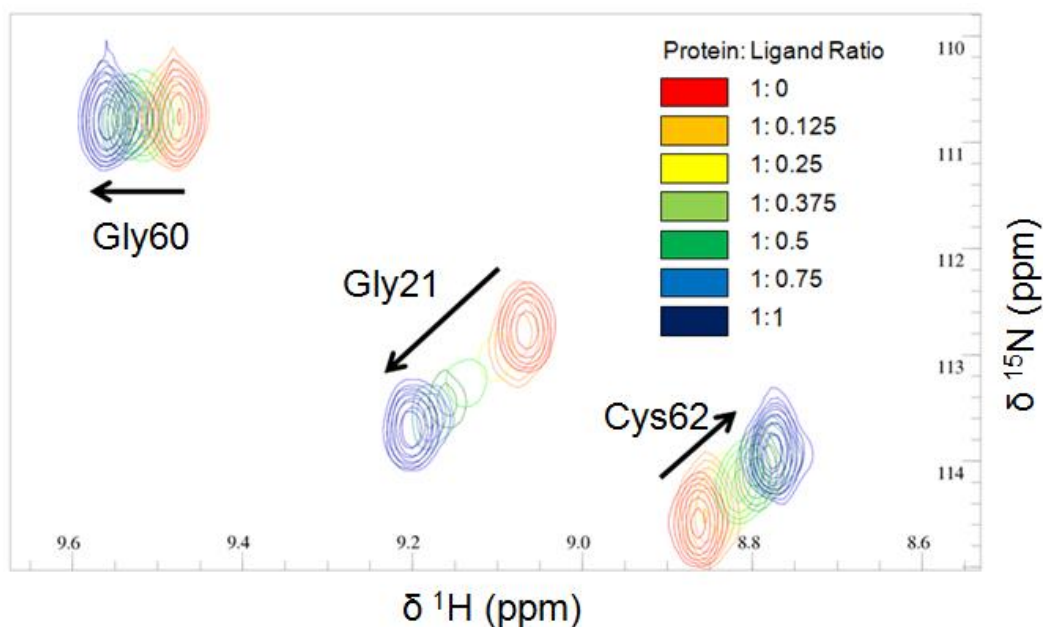


Figure 2.7: Example of a titration with signals in fast exchange. The peaks gradually move over the course of the titration allowing their assignments to be tracked from point to point. Data is from a titration of a

construct of RRM1 of CELF1 with the RNA substrate UGUUUGU, and shows a region of the ^1H - ^{15}N HSQC containing three peaks. Gly60 and Cys62 are in fast exchange. Gly21 is in intermediate exchange with very weak signals for some of the intermediate points.

An alternative is slow exchange, where $k < \delta\nu$, in which case the intensity of affected peaks from the unbound protein will decrease over the course of the titration, and a new set of peaks from these residues in the bound protein will appear. An example of this is shown in Figure 2.8. A disadvantage of titrations in slow exchange is that the assignments cannot simply be tracked from the free form to the bound form throughout the titration. In crowded regions of the spectrum it is often unclear which residues new peaks from the bound form correspond to without collecting additional 3D heteronuclear data and reassigning them. While it can be stated that the residues for which the peaks from the free form are lost on titration are involved in the binding, this cannot be quantified without assignment of the bound form. An intermediate situation where k is comparable to $\delta\nu$ can occur, in which case the peak will both lose intensity and move, as can be seen for Gly21 in Figure 2.7.

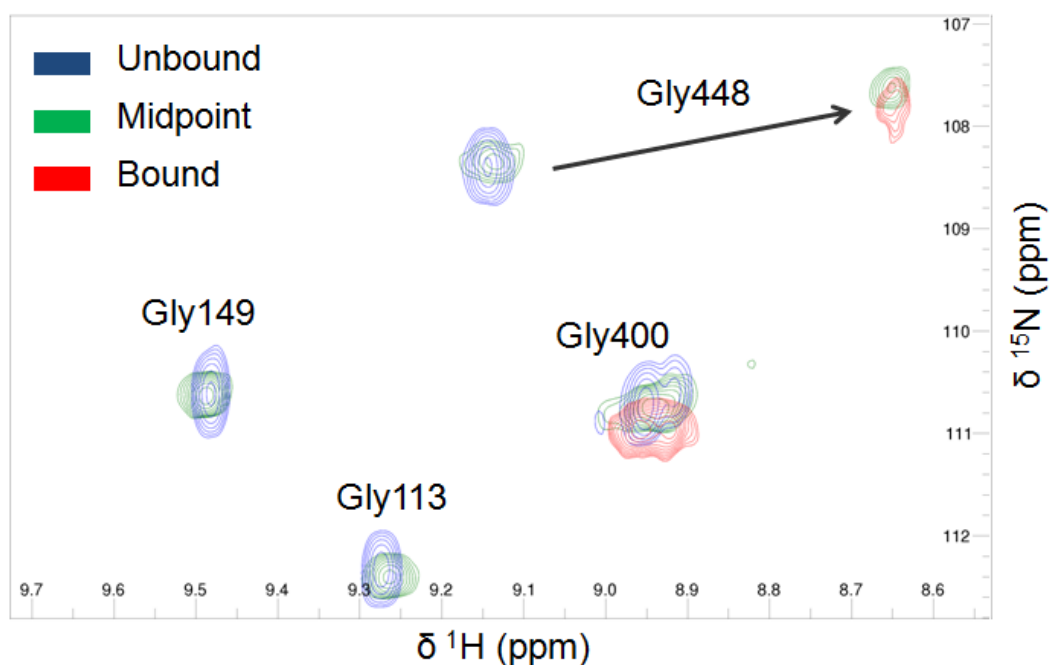


Figure 2.8: An example of an NMR titration with some residues in slow exchange. In blue is shown the spectrum of the unbound protein. In red is the spectrum when the titration with RNA is at saturation

point. In green is the spectrum at a 0.5:1 RNA to protein ratio (the midpoint of the titration). The peaks from Gly113, Gly149 and Gly448 do not move gradually as in fast exchange, but instead disappear over the course of the titration. New peaks from the bound form appear, as can be seen for Gly448. It is possible to see both the free and bound peaks for this residue at the midpoint. Some of the less affected residues in this titration are still in fast exchange, such as Gly400. Data is from a titration of the RRM23 construct of CELF1 with UGUUUGU, collected on an 800 MHz Bruker Avance III spectrometer.

It is possible to have a mixture of residues in fast exchange and slow exchange in a single titration, as $\delta\nu$ between the resonances of the free and bound forms will be different for each affected residue. The effects on each residue can be quantified as the “chemical shift perturbation” (CSP) to highlight the most affected regions of the protein. Since the ^{15}N chemical shifts have a larger dispersion than the ^1H chemical shifts it is necessary to apply a scaling factor to them. Without this scaling the overall CSP value will be almost entirely dependent on the ^{15}N component. The chemical shift perturbation is calculated as:

$$\text{CSP} = \left(\left(\frac{\Delta\delta\text{N}^2}{10} \right) + \Delta\delta\text{H}^2 \right)^{0.5}$$

In this study ^{15}N labelled protein was titrated with RNA to identify the affinity and binding sites of different RNA substrates for each RRM. A ^1H - ^{15}N HSQC/TROSY spectrum was collected at each titration point so that binding curves could be produced and the saturation point of each titration identified.

2.3 Isothermal Titration Calorimetry (ITC)

Isothermal titration calorimetry is a powerful technique for directly measuring the affinity of interactions between biomacromolecules¹⁴⁰. It can be used to investigate protein-protein interactions¹⁴¹, protein-nucleic acid interactions^{142, 143}, and interactions between proteins and small molecules¹⁴⁴. In this study ITC was carried out using a VP-ITC microcalorimeter containing two cells, as shown in Figure 2.9. One is a sealed reference cell containing water, while the other is the

sample cell containing 1.424 ml of a dilute solution of one of the two molecules to be studied (usually a protein). 300 μl of the second molecule (such as a small ligand molecule or another protein) is injected into the sample cell from the syringe in small aliquots (typically 5 or 10 μl), stirring constantly to ensure mixing of the solutions. The syringe concentration is generally a minimum of 10 times the cell concentration to ensure the titration reaches saturation point. The experiment can also be run reversed with the protein in the syringe and ligand in the cell which may be necessary if one of the components has a limited solubility.

Processes such as binding or dissociation result in release or uptake of heat from the sample cell. This is compensated by a highly sensitive thermostat which maintains the reference and sample cells at the same constant temperature. The difference in power required to maintain the sample cell at the same temperature as the reference cell is directly dependent on the enthalpy change of the reaction. By plotting the enthalpy change for each injection against the molar ratio of the two components, and fitting a suitable model to the resulting curve, the stoichiometry (n), K_d , ΔH and ΔS for the interaction can be determined.

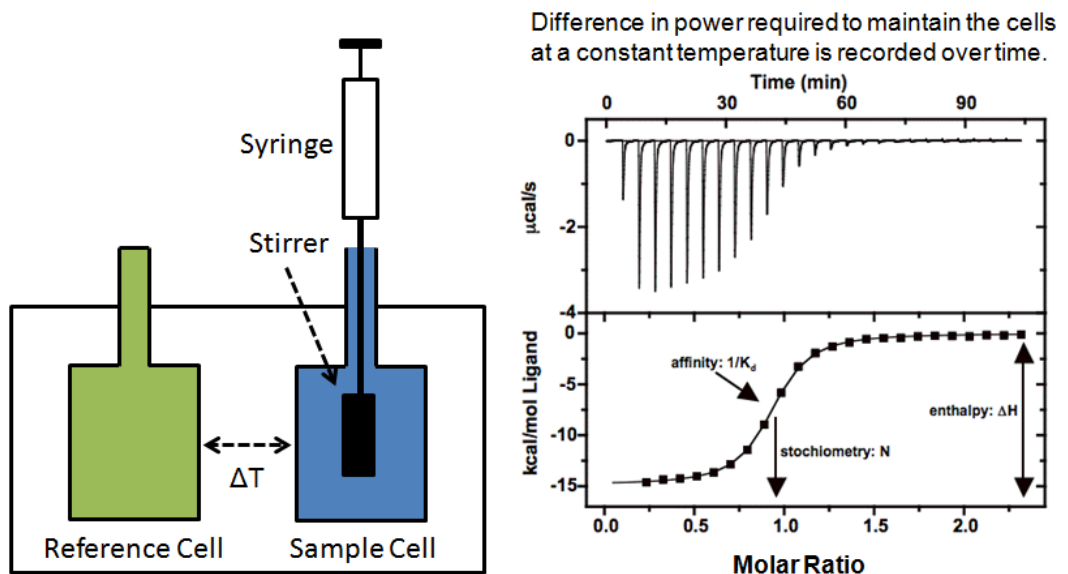


Figure 2.9: Left is a diagram showing the basic layout of an isothermal titration calorimeter. On the right is shown an example of a typical ITC trace for a 1:1 binding interaction with the relationships to the parameters n , K_d and ΔH for the process highlighted.

Also in Figure 2.9 is shown an example of raw ITC data for a simple 1:1 binding case. This particular example shows an exothermic reaction, so each injection results in a release of heat, and hence a brief reduction in the power required to maintain the sample cell at a constant temperature. This appears as a negative peak on the ITC trace. As more of the ligand is injected the protein in the cell will approach saturation. Fewer protein molecules are unoccupied and free to bind ligands and release heat with each injection, so the magnitude of the peaks declines to zero. Eventually the protein is completely saturated, no further interaction can occur, and so no significant change is seen from further ligand injections. Integration of each peak with respect to time gives the area under it which is equal to $n\Delta H$ for the injection, and can be plotted against the molar ratio of the two components.

For a simple 1:1 binding case, the enthalpy of the reaction is the difference between the magnitudes of the initial and final injections. Ideally the final injections will result in no significant enthalpy change, though buffer mismatches can result in the baseline of the trace reaching a plateau above or below zero. The stoichiometry of the reaction is the ligand/protein ratio at the inflection point of the curve, and the gradient of the curve at that point is equal to $1/K_d$. In the event of a buffer mismatch the experiment can be repeated without the protein in the cell to produce a ligand into buffer trace which can be subtracted from the main titration trace as a baseline correction¹⁴⁵.

In a reaction at equilibrium the rate of formation of the complex is defined as k_1 and the rate of dissociation of the complex is defined as k_{-1} . The dissociation constant K_d is a useful measure of the affinity of an interaction, and can be calculated as:

$$K_d = k_{-1}/k_1$$

ITC can accurately determine K_d values between several hundred micromolar and 10 nanomolar^{146, 147}. For higher affinity binding the curve becomes a step function, with very few points defining the shape around the inflection point. This prevents accurate determination of the gradient at the inflection point, and hence K_d . Reducing the concentration of both protein and ligand will result in a shallower curve, but this also reduces the absolute magnitude of each peak and hence the signal to noise ratio for the experiment. This renders ITC unsuitable for direct measurement of K_d values less than ~10 nM. In some cases it is possible to calculate K_d values for very high affinity ligands from competition experiments with lower affinity ligands. Very low affinity binding cannot be measured because the concentration of the ligand would have to be impractically high in order for the titration to reach saturation point. ITC has the disadvantage of requiring a relatively large amount of material compared to techniques such as surface plasmon resonance (SPR). For the titrations in this study concentrations of 125 – 250 μ M were required for the component in the syringe. From the K_d values, the binding stoichiometry (n) and ΔH it is possible to calculate ΔG and ΔS for the interaction using the equations:

$$\Delta G = -RT \ln K_a \text{ (where } K_a = 1/K_d)$$

$$\Delta G = \Delta H - T\Delta S.$$

Where $R = 8.314 \text{ JK}^{-1}\text{mol}^{-1}$ (the gas constant) and T is the temperature in kelvin¹⁴⁸.

The software package Origin 7.0 was used to fit binding curves to the ITC data collected throughout this study. Since the volume of solution in the cell changes over the course of the titration the concentration of the macromolecule in the cell is not a constant. The model adjusts for this change in concentration at each point in the titration using the equation:

$$M_t = M_{t0} \frac{\left(1 - \frac{\Delta V}{2V_0}\right)}{\left(1 + \frac{\Delta V}{2V_0}\right)}$$

Where M_t is the current concentration of macromolecule in the cell, M_{t0} is the initial concentration macromolecule in the cell, V_0 is the initial cell volume and ΔV is the volume added from the syringe. Similarly the adjusted concentration of the ligand at each point (X_t) can be calculated from hypothetical concentration of the ligand if there was no volume change (X_{t0}) using the equation:

$$X_t = X_{t0} \left(1 - \frac{\Delta V}{2V_0}\right)$$

These adjusted values are then used in Origin's binding model for a simple 1:1 interaction to calculate the total heat content of the solution (Q) at each point as follows:

K_a = Binding constant

n = Number of binding sites on each macromolecule in the cell.

V_0 = Cell volume

ΔH = molar enthalpy change for ligand binding

$$Q = \left(\frac{nM_t\Delta HV_0}{2}\right) \left(1 + \left(\frac{X_t}{nM_t}\right) + \left(\frac{1}{nK_aM_t}\right) - \left(\left(1 + \frac{X_t}{nM_t} + \frac{1}{nK_aM_t}\right)^2 - \frac{4X_t}{nM_t}\right)^{0.5}\right)$$

From this equation the model can calculate Q at each point in the experiment for specified values of n , K_a and ΔH . The experimental data however is measuring the change in Q for each injection. The heat released by the i th injection is:

$$\Delta Q_i = Q_i + \left(\frac{dV_i}{V_0}\right) \left(Q_i + \frac{Q_{i-1}}{2}\right) - Q_{i-1}$$

Where V_i is the volume of the i th injection. From an initial estimate of the values of n , ΔH and K_a an iterative fitting process using a non-linear regression method is then conducted to determine the closest fitting values to the experimental data¹⁴⁴.

2.4 Small Angle X-ray Scattering

Small angle X-ray scattering (SAXS) is a technique which can be used for studying the general structure of biomacromolecules in solution. It does not allow high resolution structures to be produced but it can be used to construct a low resolution 3D model showing the average size and shape of the particles. SAXS has a resolution range of approximately 10 – 250 Å¹⁴⁹. This is usually not sufficient to resolve secondary structure elements, but it can determine the relative orientation of large structured domains. This technique can also provide the radius of gyration of the protein or complex from a Guinier plot, and general information about its overall flexibility from a Kratky plot¹⁵⁰.

In a SAXS experiment a monochromatic beam of x-rays is directed through the sample. These x-rays are scattered by the particles in the sample, typically through a very small angle. A large fraction of the x-rays are not scattered, and simply pass straight through the sample to the detector, so a tightly focused (or collimated) x-ray beam is required. Since the buffer will also cause some scattering, it is usual to repeat the experiment with a blank sample containing only the buffer solution. This scattering curve can then be subtracted from the curve for the real sample, leaving only the SAXS profile of the macromolecules in the solution. As the properties measured are averaged over all the particles in the sample SAXS requires the sample to be monodisperse (i.e. it must be ensured that all of the scattering particles are identical, and non-interacting). The presence

of aggregates, or different size oligomers in the sample is particularly problematic as the scattering intensity of a particle varies with the square of its molecular weight. A small population of high molecular weight aggregates, which would be tolerated by NMR techniques due to line broadening rendering them unobservable, can make SAXS data impossible to interpret.

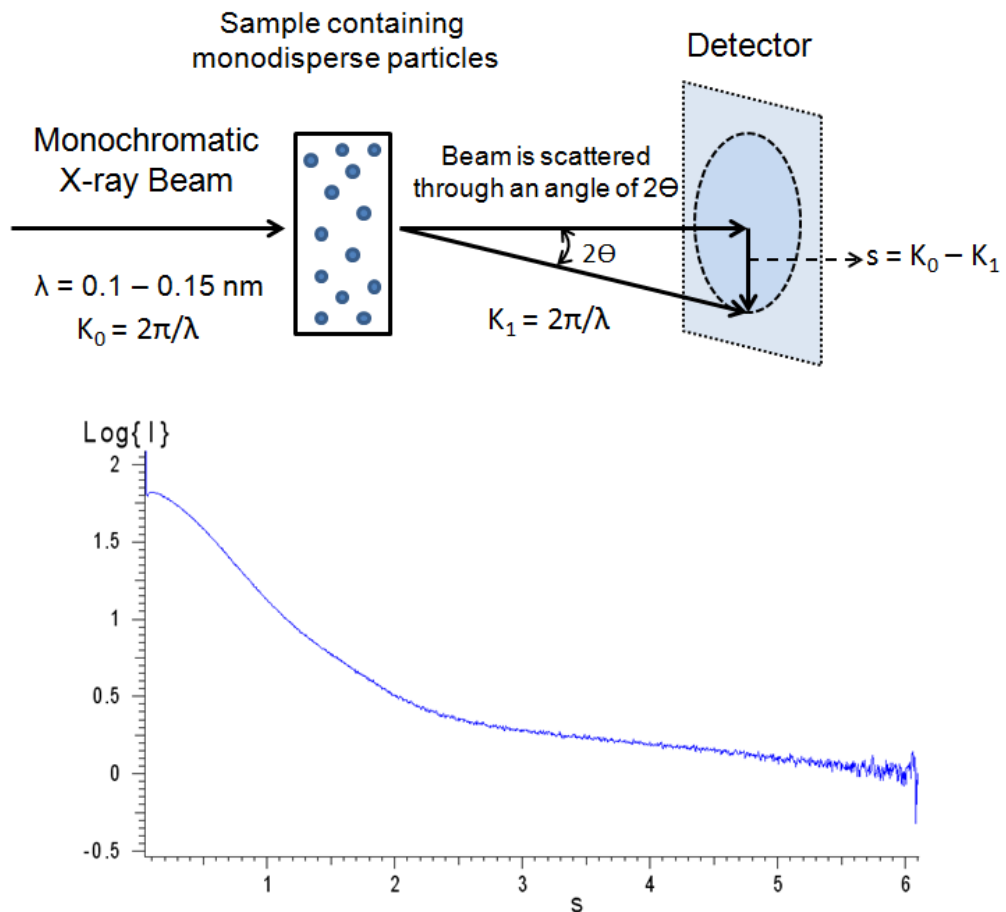


Figure 2.10: Basic scheme for a SAXS experiment. Below is shown an example of a 1D scattering curve.

A 1D SAXS trace shows a plot of intensity against $s=4\pi(\sin\theta)/\lambda$ where θ is the scattering angle and λ is the wavelength. For monodisperse particles this approximates to a Gaussian curve for small values of s . Therefore $\ln(I) = \ln(I_0) - Ks^2$ (where K is a constant). A Guinier plot of $\ln(I)$ against s^2 therefore should be linear near the origin, and this can be used as a check that a sample is monodisperse. The gradient of the line in the Guinier plot (K) is approximately

equal to $-R_g^2/3$, where R_g is the radius of gyration of the protein. Collecting this information at multiple concentrations can detect any aggregation of the protein, since the apparent radius of gyration would then vary depending on the concentration¹⁵⁰.

A Kratky plot of $I s^2$ plotted against s provides qualitative information about the overall structure and flexibility of a particle in solution¹⁵¹. In general a Kratky plot for a rigid globular protein takes the form of a Gaussian curve. An unfolded protein typically shows a plateau for high values of s , without a clearly defined peak. A protein with multiple structured domains separated by flexible linkers generally shows a mixture of these schemes, potentially with multiple peaks¹⁵².

A major advantage of SAXS is that it operates on solution samples, and does not require crystallization of the protein. Difficulties producing crystals of sufficient quality for diffraction studies can be a major barrier to x-ray crystallography. CELF1 constructs containing all three RRM domains have failed to produce diffraction quality crystals, hence the use of solution techniques such as NMR and SAXS to examine the structure of the larger complexes. SAXS also has the advantage that it can provide structural information on very large protein complexes, where NMR becomes impractical due to signal broadening from rapid relaxation, and signal overlap. Sample preparation is straightforward, and does not require isotopic labelling or large quantities of material.

A limitation of SAXS is that the scattering curves produced are one-dimensional. This can result in ambiguities when producing a 3D model of the particle, as there may be many models consistent with the 1D SAXS data. For example, SAXS is not capable of determining chirality. Enantiomers appear identical as only information on the distances between scattering centres is measured. The SAXS model of a particle inevitably is of a low resolution, typically 10 Å or larger, so this technique is generally used to complement other techniques such as NMR and X-ray crystallography¹⁵³.

2.5 Mass Spectrometry

In mass spectrometry a sample is ionised, and the resulting measurements are therefore for a sample in the gas phase. There are several possible methods for ionising a sample, the most commonly used being electrospray ionisation (ESI) and matrix-assisted laser desorption/ionisation (MALDI)¹⁵⁴. For all experiments in this study, ESI was the ionisation method used.

In electrospray ionisation the sample is pumped through an extremely narrow capillary, across the tip of which a high voltage is applied. An additional nebulising gas (nitrogen) flows around the outside of the capillary and into the mass spectrometer. This results in the formation of extremely small charged droplets, which decrease in size as the volatile solvent evaporates. As these droplets shrink they release sample ions, which pass through an intermediate vacuum region before entering the high vacuum of the mass analyser. The mass to charge ratio (m/z) of the ions determines their velocity, and hence the time required to reach the detector. In time of flight mass spectrometry this is used to calculate the m/z of the sample ions¹⁵⁵. ESI results in sample ions with a range of charge states (ions with equal mass, but different charges which appear as discrete peaks in the mass spectrum). This is in contrast with MALDI which generally results in only a single charge state for each species^{156, 157}.

The number of populated charge states, and the overall average charge provide some indication of how folded a protein is. This is because they are dependent on the solvent exposed surface area of the protein during the early stages of desolvation. This will be larger for an unfolded protein than for a structured protein of the same mass. Unfolded proteins therefore show a wider range of different charge states, and a higher average charge than structured proteins^{158, 159}.

Mass spectrometry measures the mass to charge ratio (m/z) of the ions produced

and so the mass of a protein. This makes it a rapid method to confirm the identity of a protein. This technique has the advantage that it can be used on very low sample concentrations ($< 1 \mu\text{M}$), and so requires very little material. It can also be used to investigate much larger protein complexes than techniques such as NMR, capable of observing complexes in the MDa range¹⁶⁰. Mass spectrometry data can usually be collected in a matter of minutes, making it considerably faster than ITC or multidimensional NMR. Binding stoichiometries can be determined simply based on the mass of the bound complex, if it remains intact in the gas phase.

A major limitation of ESI-MS is the need to remove NaCl and similar salts from the sample. Even in very small quantities, these lead to the formation of sodium adducts. Proteins with different numbers of attached sodium ions have slightly different masses, resulting in poorly defined broad signals from which it may not be possible to calculate an accurate mass for the protein itself. A similar problem is encountered for ESI-MS of nucleic acids.

Since it measures the mass to charge ratio rather than simply the mass of an ion, mass spectrometry can have problems distinguishing between protein oligomers and monomers. While a protein dimer has twice the mass of the monomer, it will also tend to have twice the charge resulting in the same overall m/z value. For ionisation methods such as ESI that generate a range of charge states it is however possible to determine the presence of dimers. The dimeric species will result in an extra set of peaks between those of the monomeric species with m/z values implying half-integer values of z . These are the odd numbered charge states of the dimeric species. An example of this in ESI-MS is shown in Figure 2.11.

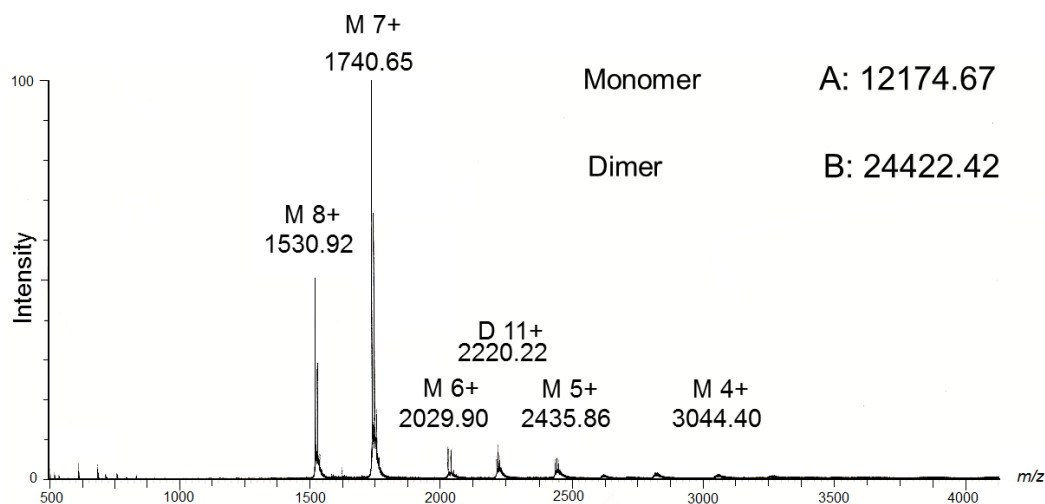


Figure 2.11: An example of an ESI mass spectrum of a mixture of a protein monomer and dimer. A range of charge states from 4+ to 8+ is seen for the monomeric form. There is an additional peak with an apparent +5.5 charge state, which is the 11+ charge state from a small population of the dimeric form. The even numbered charge states of the dimer would give peaks with the same m/z values as the monomeric species. This data is from an isolated RRM1 construct of CELF1.

There is a potential issue with ESI-MS that interactions in the gas phase may not be representative of the protein's behaviour in solution, particularly for non-covalently bound complexes. For example, binding that relies on hydrophobic interactions may be lost on entering the gas phase due to the lack of solvent molecules¹⁶¹. Clusters of proteins may also form in the gas phase which do not form in solution¹⁶¹⁻¹⁶².

3 Materials and Methods

3.1 Protein Sequences

The genes for *Xenopus Laevis* CELF1 and *Xenopus Laevis* poly (A) ribonuclease had been previously cloned into the pET28 and pET33 plasmids respectively by Dr Emilie Malaurie, who also produced the t187 and t242 constructs of CELF1 cloned into the pET28b vector (shown in Figure 3.1).

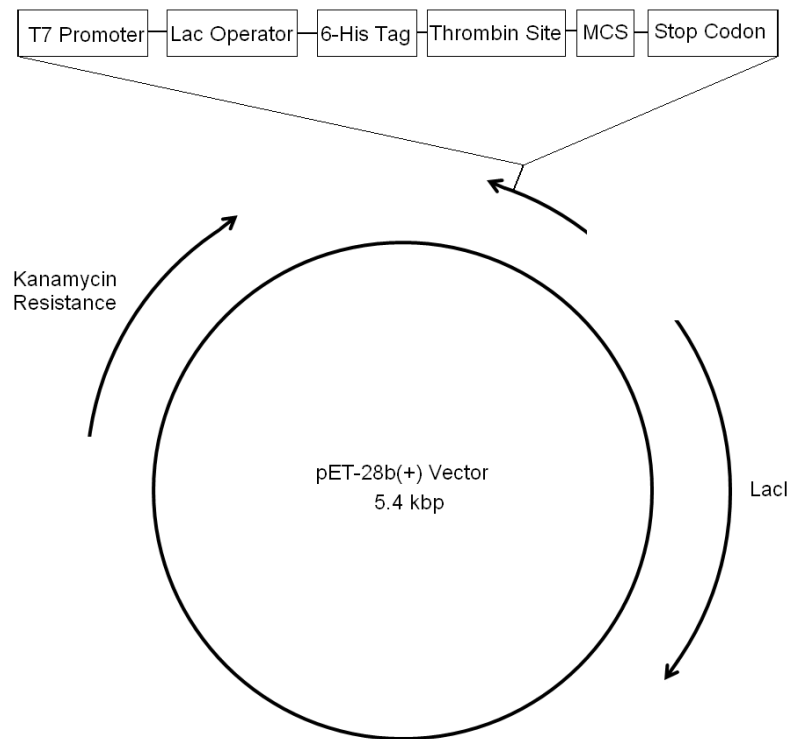


Figure 3.1: Plasmid map of the pET-28b vector.

All other constructs used in these studies were derived from these plasmids. The protein sequences are as follows:

Wild Type CELF1 (*Xenopus Laevis*)

MNGTMDHPDHPDPDSIKMFVGVPRSWSEKELRELFQYGAVYEINVLRDRSQNPPQSK
GCCFITFYTRKAALEAQNALHNMKVLPGMHHPIQMKPADSEKNNAVEDRKLFIGMVSKN
CNENDIRAMFSPFGQIEECRILRGPDGMSRGCASFVTFTRRSMAQMAIKSMHQAQTMEGC
SSPIVVKFADTQKDKEQKRMTQQLQQMQQLNAASMWGNLTGLNSLAPQYLALLQQT
SSGNLNSLSGLHPMGAEYGTGMTSGLNAIQLQNLAALAAAASAAQNTPSAGAALTSSSSPL
SILTSSGSSPSSNNSINTMASLGALQTLGATAGLNVNSLAGMAAFNGGLGSSLSNGTGST
MEALSQAYSGIQYAAAALPSLYNQSLLSQQQLGAAGSQKEGPEGANLFIYHLPQEFGDQD
LLQMFMFPGNVVSSKVFIDKQTNLSKCFGFVSYDNPVSAQAAIQSMNGFQIGMKRLKVQL
KRSKNDSKPY

Poly (A) Ribonuclease (*Xenopus Laevis*)

MEITRSNFKDTPKVVYKAIEEADFLAIDGFEFSGISDGPSVSTLTNGFDTPEERYTKLKKHSMEF
LLFQFGLCTFNVDNTEAKYLMKSFNFYIFPKPFNRNSPDKKFVCQSSSIDFLANQGDFDNKV
FRNGIPYLNQEEERVLVDQYEDRRSQSNGASTMSYISPNSKTPVSIPDEQKGFIDKVVERV
EDFLKNEQKSMNVEPCTGYQRKLIYQTLNWKYPRGIHVETVESEKKERYIVISKVDEEERKR
MEQQKQAKEREELDDAVGFSRIIQAISSSGKLVVGHNMMLLDVMHTIHQFFCQLPDELNEFK
EVTNCVFPRLVDTKLMASTNPFKEIYNTSLAELEKRLKEAPFKPPKVDSAEGFQSYNTASEQ
LHEAGYDAYITGLCFISMANYLGSFLSPPKDYVSCRKIVRPFNKLFMRIMDIPYLNLEGPD
LQPKRDNLVHVTFPKEWKTSPLYQLFSAFGNIQVSWIDDTSAFVLSQPEQVQIAVNTSKYA
ESYRIQTYAEYIEKKNDESQTKRKWAEDGWKDLERKRLKTQYNSYIPQNPVYFGNCFAPSFA
VKRSMSPIQEEAASDDTEEVHTHEENDPSNPGATEQGKKPKNHKRQKIDSAPPETSDGGSS
VLFEVPDTW

All constructs were fused to an N-terminal histidine tag (consisting of six histidine residues in a row), with a thrombin cleavage site between the tag and the

protein allowing its removal where necessary. Removal of the tag with thrombin leaves an additional six amino acids (GSHMAS) attached to the N-terminus of the protein. This allowed the proteins to be purified by metal affinity chromatography.

3.2 Sterilization

All glassware, pipette tips, media and buffers were sterilized by autoclaving for 15 minutes at 121°C (using a Phillip Harris Status Autoclave). Universals, petri dishes and other disposables were supplied in sterile condition by the manufacturers. Any reagents that could not be autoclaved due to heat sensitivity (e.g. kanamycin, IPTG) were sterilized by filtering through a 0.22 µm sterile filter immediately before use.

Workspaces were cleaned using 100% ethanol before growths or other cell work was conducted. All sterile work was carried out by a Bunsen burner flame. Glassware used in growths and other cell work was sterilised with Trigene for 20 minutes, or by autoclaving in the case of the 2 L flasks. Disposable materials were autoclaved prior to incineration.

3.3 Buffers

The following table shows the buffers which were used for cell lysis, purification and NMR experiments for each protein construct.

Buffer	Composition	Constructs
Lysis buffer A	25 mM potassium phosphate, 50 mM NaCl, pH 7.0	RRM1, RRM2, RRM3, t187, t242
Lysis buffer B	25 mM potassium phosphate, 200 mM NaCl, pH 7.0	RRM123, RRM23
Lysis Buffer C	25 mM potassium phosphate, 50 mM NaCl, 4 M Urea, pH 7.0	Wild Type CELF1
Lysis Buffer D	20 mM potassium phosphate, 500 mM NaCl, 10% v/v glycerol, 5 mM imidazole, pH 7.9.	Wild Type Poly (A) Ribonuclease
Anion Exchange A	25 mM potassium phosphate, 50 mM NaCl, 10% v/v glycerol, 200 μ M EDTA, pH 7.0	Wild Type Poly (A) Ribonuclease
Anion Exchange B	25 mM potassium phosphate, 2 M NaCl, 10% v/v glycerol, 200 μ M EDTA, pH 7.0	Wild Type Poly (A) Ribonuclease
NMR Buffer A	25 mM potassium phosphate, 50 mM NaCl, 10% v/v D ₂ O, pH 7.0	RRM1, RRM2, RRM3, t187, t242
NMR Buffer B	25 mM potassium phosphate, 200 mM NaCl, 10% v/v D ₂ O, pH 7.0	RRM123, RRM23
NMR Buffer C	25 mM potassium phosphate, 50 mM NaCl, 200 mM Urea 10% v/v D ₂ O, pH 7.0	Wild Type CELF1, Wild Type Poly (A) Ribonuclease

3.4 Overnight Cultures

15 ml of overnight cultures were grown in autoclaved Luria-Bertani broth (Sigma, 10 g/L tryptone, 5 g/L yeast extract, 10 g/l NaCl). *E. Coli*. XL1-Blue and BL21 (DE3) strains were used throughout. All constructs used in this study were in either a pET28 or pET33 vector both of which incorporate kanamycin resistance. 30 µg/ml kanamycin was therefore used as an antibiotic control. Cultures were grown for ~16 hours at 37°C and an agitation rate of 180 rpm.

3.4.1 Glycerol Stocks

Glycerol stocks were produced from overnight cultures by mixing 0.4 ml of cell culture in LB with 0.4 ml of autoclaved 30% (v/v) glycerol in sterile eppendorfs. All glycerol stocks were stored at -80°C.

3.5 Overexpression

1 L baffled flasks of LB were each inoculated using one 15 ml overnight culture, containing 30 µg/ml of kanamycin as antibiotic control. These 1 L cultures were incubated at 37°C, with an agitation rate of 180 rpm, until the OD at 595 nm was in the range 0.6 - 0.8. At this point 1 ml of 1 M IPTG was added to each flask to induce protein overexpression in *E. Coli* BL21 (DE3). The flasks were then incubated overnight (~16 hours) at 30°C, 180 rpm, unless otherwise specified. Cells were harvested by centrifugation at 3000 g for 15 minutes. The supernatant was then discarded and the pelleted cells stored at -20°C.

3.6 Sonication

For all constructs except CELF1 Wild Type and PARN deadenylase, a cell pellet from 1 litre of cell culture was resuspended in 10 ml of lysis buffer (50 mM NaCl, 25 mM phosphate, pH 7.0) from here referred to as buffer A. One EDTA-free protease inhibitor tablet (manufactured by Roche) was added to prevent protein degradation. The suspension was then sonicated at 10 microns for 10 minutes with 30 second breaks on ice every 30 seconds. Cell debris was pelleted by centrifugation at 35000 g for 30 minutes. The supernatant was then loaded onto an IMAC column.

For the purification of CELF1 wild type, cell lysis was carried out in 4 M urea, 200 mM NaCl, 25 mM phosphate, pH 7.0 buffer. Under these conditions the fragmentation of the linker between RRM2 and 3 was substantially reduced. The purification of poly (A) ribonuclease used a different lysis buffer (20 mM potassium phosphate, 500 mM NaCl, 10% v/v glycerol, 5 mM imidazole, pH 7.9) which was based on the 2006 paper by Nilsson *et al.*

3.7 Metal Affinity Chromatography

The attachment of a six histidine tag to the protein allows it to undergo a high affinity interaction with metal ions such as Ni²⁺ and Co²⁺. The His-Pur affinity column (Pierce, Thermo Scientific) uses Co²⁺ ions attached to the surface of glass beads in a resin. The His-tagged proteins in the cell lysate can therefore be selectively bound to this solid column matrix. After washing to remove non-specifically binding proteins the His-tagged protein can be eluted, usually by addition of a high concentration of imidazole to compete for the metal binding sites. The protein can also be eluted by reduction of the pH to less than 6.0, but acidic conditions may not be tolerated by some proteins.

A His-tag binding cobalt column was prepared by addition of 1 ml of His-Pur resin to a Talon PD10 column (GE Life Sciences), washing with 20 column volumes of water and finally 20 column volumes of buffer A. The supernatant from the sonication step was then added to this column, which was capped and tumbled at 4°C for 2 hours to allow binding of the protein to the beads. After two hours the supernatant was drained off the column under gravity, leaving the His-tagged protein bound to the cobalt resin.

For the t187, t242, RRM1, RRM2 and RRM3 constructs, the IMAC column stage of the purification was conducted as follows. After the supernatant was drained from the cobalt column, the beads were washed with 25 ml of a high salt buffer (25 mM phosphate, 2 M NaCl, pH 7.0) to remove any RNA or DNA bound to the protein. This was followed by a 25 ml low imidazole wash to remove non-specifically binding proteins (25mM phosphate, 100 mM NaCl, 10 mM imidazole, pH 7.0). The protein was finally eluted from the column using 750 mM imidazole, 25 mM phosphate, 100 mM NaCl pH 7.0 elution buffer. This was collected in 2 ml fractions which were tested for protein content by SDS-PAGE. The proteins were normally eluted in the first 6 ml of elution buffer. Protein containing fractions were then recombined for the thrombin cleave step. The RRM123 construct was purified by the same protocol except that the His-tag was not removed from the protein, which was immediately gel-filtered.

For CELF1 wild type, centrifugation to remove cell debris and binding to the IMAC column was carried out as for the other constructs. After allowing time for protein to bind to the column a high salt wash (25 ml 2 M NaCl, 2 M urea, 25 mM phosphate) was applied, followed by a dilute imidazole wash (25 ml of 200 mM NaCl, 2 M urea, 25 mM phosphate, 1 mM imidazole). The protein was eluted in 0.5 M Imidazole, 2 M NaCl, 1 M urea, 25 mM phosphate and collected in 2 ml aliquots. The thrombin cleave step was omitted, so EDTA was added to the elution fractions to a concentration of 5 mM, and the eluted protein was immediately gel filtered using the protocol in section 3.9.

3.8 His-Tag Removal by Thrombin Cleave

All proteins constructs incorporated a thrombin cleave site (LVPRGS) between the 6-His-tag and the protein. Elution fractions from the IMAC column were transferred to a centrifugal concentrator (3 kDa molecular weight cutoff), and diluted up to 20 ml with buffer A. This was then spun at 4000 g until the volume had been reduced by 50%, at which point it was again diluted to 20 ml with buffer A. This was repeated until the imidazole concentration of the solution was reduced to less than 0.1 M, as a higher concentration could interfere with the thrombin cleave step. The protein solution was then transferred to a universal, and 5 units of thrombin were added. The universal was agitated overnight at room temperature to cleave the His-tag from the protein. Mass spectrometry was used to confirm the tag had been successfully removed. Due to solubility and stability issues the His-tag was not removed from RRM123, wild type CELF1 or poly(A) ribonuclease. In the purification protocol for these proteins the elution fractions from the IMAC were immediately loaded onto a gel filtration column.

3.9 Gel Filtration

Gel filtration separates out any impurities left after the metal affinity chromatography stage based on their different molecular masses and also the overall shape of the proteins. It also serves to buffer exchange the protein from the high imidazole elution buffer to an imidazole-free phosphate buffer. Initial purifications of t187 and all purifications of t242, RRM123, CELF1 wild type and PARN deadenylase were carried out using a Superdex 200 gel filtration column (GE Life Sciences). RRM1, RRM2, RRM3 and later purifications of t187 were gel filtered using a Superdex 75 column due to the lower mass of these constructs.

Gel filtration columns were pre-equilibrated with 400 ml of 30 mM potassium phosphate, 100 mM NaCl, pH 7.0 buffer. Protein solutions were centrifuged at 4000 g for 10 minutes, or filtered through a 0.2 µm filter prior to loading onto the column in order to remove any insoluble material. Gel filtration columns were run at 3 ml/min unless otherwise specified. 10 ml fractions were collected, and those containing protein were identified by 280 nm absorbance except in the case of RRM2. Since the RRM2 construct contains no tryptophan or tyrosine it has no significant 280 nm absorbance, so it was necessary to locate the protein by SDS-PAGE. RRM3 also showed limited absorbance at 280 nm due to the absence of tryptophan in the construct. Normal elution fractions for all constructs are shown in the table below.

Protein Construct	Gel Filtration Column	Elution Fractions
T187	Superdex 200	260 - 270 ml
	Superdex 75	180 - 200 ml
T242	Superdex 200	240 - 260 ml
RRM1	Superdex 75	210 - 220 ml
RRM2	Superdex 75	230 - 250 ml
RRM23	Superdex 75	190 – 210 ml
RRM123	Superdex 200	220 – 240 ml

Those gel filtration fractions containing protein were frozen with liquid nitrogen and lyophilised.

3.10 Desalting

Lyophilised protein from the gel filtration step was redissolved in MilliQ water and centrifuged at 4000 g for 10 minutes to remove any insoluble material before loading onto 5x5 ml HiTrap desalting column (Amersham Biosciences). The column was pre-equilibrated with degassed and filtered MilliQ water. The salt content of the elution fractions was monitored based on conductivity, while protein content was monitored based on 280 nm absorbance. Liquid nitrogen was used to freeze the relevant desalted fractions for lyophilisation.

3.11 Storage and Stability

Lyophilised protein was stored at -20°C. Protein solutions requiring long-term storage were kept at -80°C. RNA and DNA solutions were stored dissolved in nuclease-free water at -20°C.

3.12 Production of Isotopically Labelled Protein

For the production of ¹⁵N labelled protein the growth was carried out in minimal media rather than LB. M9 Minimal media was prepared by dissolving 6 g dipotassium hydrogen phosphate, 3 g sodium dihydrogen phosphate, 0.5 g of NaCl, 0.3 g anhydrous magnesium sulphate and 0.015 g calcium chloride in 1 L of water. The media was then autoclaved to sterilise it. 1 g of ¹⁵N labelled ammonium chloride and 4 g of glucose were dissolved in 40 ml of MilliQ water and added to the media using a 0.2 µm syringe filter to sterilise the solution. These were the only nitrogen and carbon sources in the media. In addition 10 mg of biotin and 10 mg of thiamine were added.

Four 15 ml overnight cultures were prepared for each 1 litre flask. Prior to inoculating the M9 minimal media the cells were harvested by centrifugation at 1000 g for 10 minutes. The cells were then resuspended in 15 ml of M9 minimal media and incubated at 37°C 200 rpm for 30 minutes. The cells were then added to the 1 litre flasks, which were incubated at 37°C, 180 rpm until the OD at 595 nm reached 0.6 – 0.8. Protein expression was then induced by addition of 1 ml of 1 M IPTG per litre. The remainder of the expression and purification protocol was identical to that for LB growths.

To produce samples with both ¹⁵N and ¹³C labelling, the 4 g of glucose was replaced with 2 g of ¹³C labelled glucose. The growths normally required an additional 2 hours before induction (until an O.D. of approximately 0.6 was reached) to compensate for the lower glucose concentration.

3.13 Test Growths

10 ml growths were used as a small scale test for successful induction of protein expression and solubility. 10 ml of LB in a universal was inoculated with BL21 (DE3) cells containing the relevant protein construct. The appropriate antibiotic control (normally kanamycin at 30 µg/ml) was added to these. These test growths were incubated at 37°C. When the O.D. of the growths reached 0.6 a 1 ml SDS-PAGE gel sample was taken, and the growths were induced with 10 µl 1 M IPTG. Test inductions were carried out at multiple temperatures (e.g. 37°C, 30°C and 25°C) to determine the optimum conditions for overexpression of soluble protein. 1 ml SDS-PAGE samples were then taken at intervals so the levels of protein in the soluble and total fractions could be monitored.

These SDS-PAGE samples were prepared by resuspending the cells in 300 µl of buffer A and sonicating them for 10 seconds, followed by a 10 second break on ice, followed by a final 10 seconds of sonication. 20 µl gel samples were taken

from this total fraction, and the remainder was centrifuged at 13,000 g for 10 minutes to pellet all insoluble proteins. 20 µl of the supernatant was then taken from the soluble protein fraction. SDS-PAGE was carried out as specified in section 3.14 to determine the most suitable temperature and duration to maximise the yield of soluble protein.

3.14 SDS-PAGE Gels

Approximate quantities and molecular weights of proteins in samples at various stages in the purification were determined using a Min-Protean®3 SDS-PAGE system (BioRad). 15% polyacrylamide gels were used for the t242, t187 and isolated RRM constructs. 20% gels were used for RRM123, wild type CELF1 and PARN deadenylase. The 15% resolving layer was prepared from 1.7 ml 30% protogel, 0.85 ml 1.5 M Tris.HCl pH 8.8, 0.034 ml 10% m/v sodium dodecyl sulphate (SDS), 0.816 ml MilliQ water. Immediately before pouring 40 µl of 100 mg/ml ammonium persulfate and 10µl TEMED were added to start the polymerisation reaction. The stacking gel was prepared from 0.266 ml 30% protogel, 0.5 ml 0.5 M Tris.HCl pH 6.8, 0.02 ml 10% SDS, 1.21 ml MilliQ water. 30 µl of 100 mg/ml ammonium persulfate and 10 µl TEMED were added immediately prior to pouring the gel. The stacking layer was added over the resolving layer once it had set and was cast around a Teflon comb to form ten sample wells, each with a volume of approximately 12 µl.

Samples were prepared by adding 0.5 sample volumes of loading buffer (100 mM Tris, pH 6.8, 4% SDS (w/v), 0.2% bromophenol blue (w/v), 20% glycerol (v/v), 200 mM DTT), and heating for 5 minutes at 90°C. 10 µl of sample was then loaded into the sample wells. 5 µl of low molecular weight markers (either Sigma Low Range Markers or Novex Prestained Protein Standard (Invitrogen)) were run in one lane of each gel as a reference. The mass of each protein in the reference markers is listed in the table below.

Sigma Low Molecular Weight Markers:

Protein	Mass (kDa)
Albumin	66
Ovalbumin	45
Glyceraldehyde-3-Phosphate Dehydrogenase	36
Carbonic Anhydrase	29
Trypsinogen	24
Trypsin Inhibitor	20
α -lactalbumin	14.2
Apoprotinin	6.5

A Biorad SDS-PAGE kit was used to run the gel in SDS buffer (25 mM Tris, 0.25 M glycine, 0.1% v/v SDS). Gels were run at 180 V for approximately 1 hour. Coomassie Brilliant Blue protein stain was used to stain gels (0.25% w/v Brilliant Blue R-250 (Fisher) 45% v/v methanol, 10% v/v glacial acetic acid) for 1 hour. Destaining was carried out with a mix of 10% v/v glacial acetic acid and 25% v/v methanol, over the course of at least 24 hours. Images of the gels were collected using a Syngene gel documentation system.

3.15 Molecular Biology

3.15.1 Plasmids

Both the pET28 and pET33 vectors (Novagen) are based on the system developed by Studier *et al*^{163, 164, 165}. This encodes a T7 promoter sequence upstream of a multiple cloning site (MCS) into which the gene to be expressed can be cloned.

This T7 promoter is specific to the bacteriophage T7 RNA polymerase, which is not found elsewhere in prokaryotes. The plasmid also encodes the *lac* repressor protein, a *lac* operator and an antibiotic resistance gene (in both of these vectors this is kanamycin resistance). Expression of the gene of interest can only occur if the T7 RNA polymerase is present, and the *lac* operator is not being repressed.

The strain of host cells used throughout was BL21 (DE3), which incorporate the gene for T7 RNA polymerase, again after a *lac* operator. The *lac* operators therefore repress both the expression of the T7 RNA polymerase in the bacterial chromosome and the expression of the gene of interest in the pET vector. The *lac* operator only represses these genes in the absence of allolactose (a metabolite of allolactose). Expression of the proteins is induced by the addition of isopropyl-thio- β -D-galactoside (IPTG), which mimics allolactose and so activates both of the genes repressed by *lac* operators. Once the T7 polymerase is present the protein of interest is then rapidly expressed.

In both of these vectors the protein of interest is expressed as a fusion with an N-terminal 6-His-tag. This tag is separated from the protein by a thrombin cleavable site (LVPRGS) allowing it to be removed if necessary. The tag allows the protein to be purified by immobilised metal ion affinity chromatography (IMAC), as explained in section 3.7.

3.15.2 Site Directed Mutagenesis

The required primers were produced by the School of Biomedical sciences, University of Nottingham. A QuikChange site directed mutagenesis (Stratagene) was used for the process. The forward and reverse primers were designed to meet the kit's specification, which was a 25 – 45 bases in length for each primer, a minimum of 40% G/C content, a melting temperature of at least 78°C and for the primer to terminate with at least one G or C base. For the reaction the following

reagents were combined in a sterile 0.2 ml thin walled PCR tube (Starlab):

37.5 μ l Sterile MilliQ water

5 μ l 10x reaction buffer (20 mM Tris.HCl pH 8.8, 10 mM KCl, 10 mM NH₄SO₄, 2 mM MgSO₄, 0.1% Triton X-100, 0.1 mg/ml bovine serum albumen).

2.5 μ l DMSO

1 μ l template DNA (approximately 50 ng/ μ l)

1 μ l Forward primer (125 ng/ μ l)

1 μ l Reverse primer (125 ng/ μ l)

1 μ l dNTPs (10 mM for each nucleotide)

1 μ l (3 units) Pfu Turbo DNA polymerase (added last).

The PCR tube was then transferred to the PCR thermocycler block and run for 18 cycles of 30 seconds at 95°C, 30 seconds at 55°C, 30 seconds at 68°C. The 95°C step denatures the template DNA, separating the two strands. The 55°C step allows the primers to anneal to their complementary sections in the template DNA. To optimise the reaction the annealing temperature sometimes required adjusting in the 50 – 60°C range. The 72°C step is a suitable temperature for the DNA polymerase to extend the primers.

The remaining parental template DNA was digested with 1 μ l (10 units) DpnI endonuclease (New England Biolabs) at 37°C for 1 hour. DpnI selectively cleaves methylated DNA. This step is necessary as this DNA will not contain the point mutation, but will still provide antibiotic resistance when transformed into cells. In all cases the template DNA was extracted from XL1 Blue *E. Coli* cells and was therefore methylated. DNA generated by the PCR is not methylated, and so is not digested by the DpnI. The PCR product was transformed into XL1 Blues using the protocol in section 3.15.9.

3.15.3 Cloning

Template DNA containing the gene to be cloned was extracted from XL1 Blues using a Qiagen Spin Miniprep kit. The primers for production of the isolated RRM2 construct were designed so that the forward primers contained the HindIII restriction site at the 5' end of the gene, while the reverse primers contained the NheI restriction site at the 3' end of the gene. A PCR of the insert was then carried out by combining 1 µl of template DNA, 1 µl forward primer, 1 µl reverse primer, 1 µl dNTPs, 5 µl reaction buffer (New England Biolabs buffer B as the) and 40 µl sterile MilliQ water were mixed in a 0.2 ml thin walled PCR tube. 1 µl of TAQ polymerase was then added, and the tube transferred to a PCR machine. This was heated to 95°C for 2 minutes to denature the DNA, and then underwent 30 cycles of 30 seconds at 95°C, 30 seconds at 60°C and 30 seconds at 72°C to amplify the insert.

The PCR product was digested with 1 µl Dpn1 for 1 hour at 37°C. A PCR purification kit (Qiagen) was used according to the manufacturer's instructions to purify the insert, which was then purified further by running on a 1% w/v agarose gel. The section of the gel containing the insert DNA was then excised from the agarose gel using a sterile scalpel, and the DNA extracted using a Qiagen gel extraction kit. The vector DNA was prepared by growing a 15 ml overnight cell culture of XL1 Blues containing a "blank" pET28b plasmid with no gene present in the multiple cloning site. This plasmid DNA was extracted using a Qiagen Miniprep Spin kit.

3.15.4 Restriction Digest

For the restriction digest two sterile 0.2 ml thin-walled PCR tubes were used, one to prepare the insert and the other for the vector. The following reagents were combined:

Insert:

37.5 μ l Insert DNA

5 μ l 10x Reaction Buffer B

2.5 μ l Sterile MilliQ water

1 μ l 50x BSA

2 μ l HindIII restriction enzyme

2 μ l NheI restriction enzyme

Vector:

32 μ l blank pET28 vector DNA

4 μ l 10x reaction buffer B

1 μ l 50x BSA

2 μ l HindIII restriction enzyme

2 μ l NheI restriction enzyme

These PCR tubes were then incubated at 37°C for 3 hours, after which the enzymes were inactivated by heating to 65°C for 15 minutes. The vector was then treated with antarctic phosphatase, in the reaction mixture shown below. During this process the insert was stored on ice.

40 µl Vector DNA

5 µl 10x antarctic phosphatase buffer

4 µl Sterile MilliQ water

1 µl Antarctic phosphatase

The reaction mixture was heated to 37°C for 10 minutes, and then to 65°C for 15 minutes to heat inactivate the enzyme. This left the insert and vector with complementary ends which could be ligated together. The insert and vector were both visualised and purified on a 1% w/v agarose gel. A deeper gel than usual (42 ml instead of the normal 30 ml) was used to accommodate the larger volume of DNA. The DNA was extracted from the gel using a Qiagen gel extraction kit according to the manufacturer's instructions.

3.15.5 Ligation

A 4:1 ratio of insert to vector DNA was combined in a 0.2 ml thin walled PCR tube, with 2 µl of 10x ligation buffer (New England Biolabs) and 1 µl T4 ligase (Promega, 3 units). The total reaction volume was 18 µl. Ligation was carried out at 16°C overnight (~16 hours). After this the reaction mixture was heated to 65°C for 10 minutes to inactivate the ligase. The ligated product was then transformed into XL1-Blue cells (using the protocol in section 3.15.9, except that an increased volume of 5 µl of DNA was added to 100 µl of competent cells), and plated onto agar. Tetracyclin and kanamycin were used as antibiotic selections.

3.15.6 Production of Deletion Constructs

The RRM3, RRM23 and RRM123 constructs were produced by deletion of unwanted sections of the CELF1 wild type construct. This used a single step PCR

process, as outlined by Qi *et al.* and Liu *et al.*^{166, 167}. The following reagents were combined in a 0.2 ml thin-walled PCR tube.

37.5 µl sterile MilliQ water.

5 µl 10x Reaction Buffer

2.5 µl DMSO

1 µl dNTPs

1 µl Template DNA (in this case full length CELF1 wild type)

1 µl Forward Primer

1 µl Reverse Primer

1 µl (3 Units) Pfu Phusion DNA Polymerase (Promega)

The thermocycler program used was as follows:

1 Cycle:

5 minutes at 95°C (Initial denaturation of the DNA)

18 Cycles:

1 minute at 95°C (Denaturation)

2 minutes at 68°C (Annealing of the non-overlapping sections of the primers)

12 minutes at 72°C (Extension step, lasting 1 minute per 500 bases in the DNA template)

1 Cycle:

2 minutes at 60°C (Annealing of the complimentary sections of the primers)

30 minutes at 72°C (Final elongation step)

1 µl DpnI was then added, and the reaction mixture was incubated at 37°C for 2 hours to break down any remaining methylated template DNA. The PCR product

was then visualised by agarose gel to confirm amplification. As all PCRs using this method deleted several hundred bases from the construct, the size difference between the PCR product and template on the agarose gel provided an indicator of whether the deletion was successful. The PCR product was then transformed into XL1 Blue cells using the protocol in section 3.15.9. If the reaction was successful the cells had resistance to the antibiotic, and formed colonies on the LB agar plate.

3.15.7 Sequencing

PCR products and cloned plasmids were sequenced using the Sanger method¹⁶⁸ by the School of Biomedical Sciences, Queens Medical Centre, Nottingham. 5 µl DNA samples with concentrations of approximately 100 ng/µl were supplied, with 5 µl of forward and reverse primers where appropriate. The T7 promoter primer (TAA TAC GAC TCA CTA TAG GG) was used for sequencing all constructs in the pET28 vector. The program Chromas 2.21 (Technelysium) was used to view sequencing results.

3.15.8 Production of Calcium Competent Cells

15 ml of LB containing 12.5 µg/ml of tetracycline was inoculated with XL1 blues, and incubated at 37°C for 16 hours. After 16 hours 200 µl of this culture was transferred to a second universal of 10 ml LB with 12.5µg/ml of tetracycline. This was again incubated at 37°C until the OD reached approximately 0.3. The cells were then centrifuged at 1000 g for 15 minutes, and the supernatant discarded. 4 ml of sterile, chilled 50 mM CaCl₂ was then used to resuspend the cells, after which they were stored on ice for a minimum of 2 hours.

3.15.9 Transformation

After at least 2 hours on ice the cells were centrifuged at 1000 g for 15 minutes, and resuspended in 800 µl of chilled, sterile 50 mM CaCl₂ before being returned to the ice bath for another 30 minutes. These calcium competent cells were divided into 100 µl aliquots. For transformations using the product of a PCR, 5 µl of DNA was added to an aliquot of calcium competent cells. For transformations into BL21 (DE3) cells 1 µl of DNA was used. The cells were heat-shocked by transferring them to a water bath at 42°C for 30 seconds, after which they were placed back on ice for 2 minutes. 400 µl of LB was then added to each aliquot, and these were incubated at 37°C for 30 minutes. The cells were then spread onto agar plates with appropriate antibiotic selections, which were then sealed with Nesco film and incubated overnight at 37°C. A negative control plate was produced using an aliquot of cells with no added plasmid DNA, to confirm the antibiotic control was effective.

The following day colonies were picked and 10 ml overnight cultures inoculated with them. Glycerol stocks were prepared from these overnights, and DNA was extracted from the remainder of the cell culture using a QIAprep miniprep kit (Qiagen) according to the manufacturer's instructions.

3.15.10 Agar Plates

Agar plates were prepared by dissolving LB-agar (Sigma, 15 g/l agar, 10 g/l tryptone, 5 g/l yeast extract, 10 g/l NaCl) in MilliQ water at 40 g/l. After autoclaving, the agar was melted in a microwave and allowed to cool to approximately 40°C. Any required controls (kanamycin and/or tetracycline) were sterile filtered through a 0.22 µm filter before addition to the agar. The agar was then plated onto sterile petri dishes and stored at 4°C. Before use the plates were transferred to a 37°C incubator for 30 minutes to remove any excess moisture.

3.15.11 Agarose Gels

1% w/v DNA gels were prepared by dissolving 0.3 g of agarose in 30 ml Tris Acetate EDTA (TAE) buffer (40 mM Tris-acetate pH 5.0, 1 mM EDTA), and then heating the resulting mixture in a microwave until the agarose had melted. The solution was allowed to cool for 5 minutes, after which 1 μ l of ethidium bromide was added. The gel was then cast in a 7 x 10 cm gel tray (Mini Sub GT Cell – Biorad), around a comb to create eight 20 μ l sample wells. After the gel had set, it was immersed in TAE buffer (40 mM Tris.HCl, 1 mM EDTA, 20 mM acetic acid). DNA samples were prepared by adding 2 μ l of 6x DNA loading buffer (Novagen, bromophenol blue) to 10 μ l of sample. 2-log DNA ladder markers (New England Biolabs) were used as a reference, prepared from 1 μ l supplied marker stock, 1 μ l 6x loading dye and 4 μ l MilliQ water. A potential of 70 V was applied across the gel until the bands had migrated sufficiently to resolve the different masses. UV light was used to visualize the DNA bands, and gels were imaged using a Syngene gel documentation system.

When used for purification rather than visualisation of PCR products a deeper gel was prepared to accommodate the greater volume of sample. 0.42 g of agarose was dissolved in 42 ml of TAE buffer to prepare a 1% gel. DNA samples were loaded into adjacent lanes, so they could be excised in a single piece of the agarose gel.

3.16 NMR Acquisition

All NMR experiments were run on a 600 MHz Bruker Avance spectrometer with a TXI probe or an 800 MHz Bruker Avance III spectrometer with a QCI probe. Data processing was carried out using Topspin 2.3 and later 3.0. Standard Bruker

pulse sequences were used throughout. Spectra were referenced internally to trimethylsilylpropionate (TSP) at 0.00 ppm in the ^1H dimension.

3.16.1 Data Analysis

An exponential window function with 2 Hz line broadening was applied to all 1D proton spectra. For 2D spectra zero-filling of up to 2048 points was applied to the direct and indirect dimensions for data acquired on the 600 MHz spectrometer. Zero-filling of up to 4096 points was applied to data from the 800 MHz spectrometer. A sine-squared apodization function and polynomial baseline correction was applied to both dimensions. CCPNMR versions 1.1.15 and 2.1.2 were used for data analysis.

3.16.2 Sample Preparation

The composition of NMR buffer was 25 mM phosphate, 50 mM NaCl, 10% (v/v) D_2O , pH 7.0 unless otherwise specified. The buffers were prepared using RNase free water throughout. Lyophilised protein samples were dissolved in 600 μl of buffer, centrifuged at 13,000 g for 1 minute to remove any insoluble material, and then transferred to NMR tubes. Protein concentrations were between 400 μM and 1 mM for experiments using the 600 MHz spectrometer and 20 μM – 400 μM for those at 800 MHz. All RNA substrates were supplied by Dharmacon in a 2' protected form. Prior to the experiments the RNA was deprotected according to the supplier's instructions and dissolved in RNase free water to a concentration of 5 mM.

3.16.3 1D experiments

Standard Bruker pulse sequences were used in recording all 1D experiments. Appropriate decoupling was applied when necessary for isotopically labelled samples. Water suppression was applied using excitation sculpting¹⁶⁹ and WATERGATE pulse sequences¹⁷⁰. The transmitter frequency was set to the water frequency (~4.7 ppm, 2823 Hz for the 600 MHz spectrometer, 3765 Hz for the 800 MHz spectrometer).

3.16.4 HSQC Experiments

¹⁵N and ¹³C Heteronuclear single quantum coherence spectra (HSQCs) were recorded for the smallest construct (RRM2). For larger constructs ¹⁵N transverse relaxation optimised spectroscopy (TROSY) was used to compensate for loss of signal from rapid relaxation. RNA titrations used a protein concentration of 400 μM when recorded with the 600 MHz spectrometer, and 250 μM with the 800 MHz spectrometer, except where otherwise specified. RNA was titrated into the sample until saturation point was reached (determined by no further changes being observed in the ¹H-¹⁵N HSQC/TROSY of the protein over multiple titration points).

3.16.5 3D Experiments

In order to assign the NH, HN, C' Cα and Cβ of each residue, a series of standard 3D Bruker experiments were used. These included HNCO¹³⁰, HN(CA)CO¹³², HNCA¹³¹, HNCACB¹²⁹, HN(CO)CACB^{130, 133} and HCCH-TOCSY¹³⁸. These experiments were conducted on the RRM1, RRM2, RRM3 and t187 constructs, and also the S28D mutant of RRM1.

t187

Experiment	Scans	¹H	¹⁵N	¹³C	Spectral Widths (ppm) (¹H, ¹⁵N, ¹³C)	AQ Times (s) (¹H, ¹⁵N, ¹³C)
¹ H- ¹⁵ N HSQC	64	2048	64	-	F2: 16.02 F1: 32.00	F2: 0.10650, F1: 0.01644
HNCO	32	2048	64	98	F3: 11.97 F2: 32.00 F1: 25.00	F3: 0.14254, F2: 0.01644, F1: 0.01299
HN(CA)CO	256	2048	32	48	F3: 11.97 F2: 32.00 F1: 25.00	F3: 0.14254, F2: 0.00822, F1: 0.00636
HNCACB	72	2048	40	64	F3: 11.97 F2: 32.00 F1: 74.96	F3: 0.14254, F2: 0.01028, F1: 0.00250
HN(CO)CACB	48	2048	32	128	F3: 11.97 F2: 32.00 F1: 74.96	F3: 0.14254, F2: 0.00822, F1: 0.00565
HCCH- TOCSY	32	2048	64	64	F3: 11.97 F2: 74.96 F1: 12.00	F3: 0.14254, F2: 0.00283, F1: 0.00444

RRM1

Experiment	Scans	¹H	¹⁵N	¹³C	Spectral Widths (ppm) (¹H, ¹⁵N, ¹³C)	AQ Times (s) (¹H, ¹⁵N, ¹³C)
¹ H- ¹⁵ N HSQC	64	2048	64	-	F2: 16.02 F1: 32.00	F2: 0.10650, F1: 0.01644
HNCO	32	2048	64	98	F3: 14.98 F2: 32.00	F3: 0.11387, F2: 0.01644,

					F1: 25.00	F1: 0.01259
HN(CA)CO	32	2048	64	98	F3: 14.98 F2: 32.00 F1: 25.00	F3: 0.11387, F2: 0.01644, F1: 0.01299
HNCACB	72	2048	40	64	F3: 14.98 F2: 32.00 F1: 85.02	F3: 0.11387, F2: 0.01028, F1: 0.00250
HN(CO)CACB	48	2048	32	128	F3: 14.98 F2: 32.00 F1: 85.02	F3: 0.11387, F2: 0.00822, F1: 0.00472
HCCH- TOCSY	32	2048	64	64	F3: 11.97 F2: 74.96 F1: 12.00	F3: 0.14254, F2: 0.00283, F1: 0.00444

RRM2

Experiment	Scans	¹H	¹⁵N	¹³C	Spectral Widths (ppm) (¹H, ¹⁵N, ¹³C)	AQ Times (s) (¹H, ¹⁵N, ¹³C)
¹ H- ¹⁵ N HSQC	64	2048	64	-	F2: 16.02 F1: 32.00	F2: 0.10650, F1: 0.01644
HNCO	32	2048	64	80	F3: 14.98 F2: 32.00 F1: 25.00	F3: 0.14254, F2: 0.01644, F1: 0.01060
HN(CA)CO	64	2048	32	80	F3: 14.98 F2: 32.00 F1: 25.00	F3: 0.14254, F2: 0.00822, F1: 0.00808
HNCACB	48	2048	40	128	F3: 14.98 F2: 32.00 F1: 84.96	F3: 0.11387, F2: 0.01028, F1: 0.00499

HN(CO)CACB	48	2048	32	128	F3: 14.98 F2: 32.00 F1: 84.96	F3: 0.11387, F2: 0.01028, F1: 0.00499
HCCH- TOCSY	40	2048	48	64	F3: 11.97 F2: 74.96 F1: 12.00	F3: 0.14254, F2: 0.00212, F1: 0.00444

RRM3

Experiment	Scans	¹H	¹⁵N	¹³C	Spectral Widths (ppm) (¹H, ¹⁵N, ¹³C)	AQ Times (s) (¹H, ¹⁵N, ¹³C)
¹ H- ¹⁵ N HSQC	64	2048	64	-	F2: 16.02 F1: 32.00	F2: 0.10650, F1: 0.01644
HNCO	32	2048	64	80	F3: 14.03 F2: 32.00 F1: 25.00	F3: 0.12165, F2: 0.01644, F1: 0.01060
HN(CA)CO	32	2048	64	80	F3: 14.03 F2: 32.00 F1: 25.00	F3: 0.12165, F2: 0.01644, F1: 0.01060
HNCACB	40	2048	64	128	F3: 15.02 F2: 32.00 F1: 90.00	F3: 0.11360, F2: 0.01644, F1: 0.00471
HN(CO)CACB	32	2048	44	128	F3: 17.96 F2: 35.23 F1: 75.02	F3: 0.09503, F2: 0.01120, F1: 0.00499

Assignment of the structured regions of RRM123 and wild type CELF1 were carried out by comparison with the assignments of the isolated RRMs. With the exception of residues immediately adjacent to the cut sites of these constructs,

there were minimal differences in the chemical shifts, allowing assignments to be directly transferred.

3.16.6 ^{15}N Heteronuclear NOE

Pulse sequences consisting of standard ^1H - ^{15}N HSQCs with and without proton saturation during the relaxation period prior to the initial ^{15}N pulse were used to measure the heteronuclear NOE. The experiments were run as interleaved ^1H - ^{15}N HSQCs which were subsequently split into a pair of ^1H - ^{15}N HSQCs, one with proton saturation and one without. The heteronuclear NOE for each residue was calculated as intensity (with proton saturation)/ intensity (equilibrium). ^{15}N heteronuclear NOE data was collected at the start and end points of RNA titrations to compare flexibility in the free and bound states.

3.16.7 Paramagnetic Relaxation Enhancement

Dipolar interactions with unpaired electrons enhance the relaxation rate of surrounding nuclear spins. The magnitude of the relaxation enhancement is related to the distance from the paramagnetic centre. PRE can therefore be used to obtain additional distance restraints between the paramagnetic centre and the surrounding nuclei¹⁷¹. ^1H nuclei are the most sensitive to paramagnetic relaxation enhancement (PRE), with ^{13}C and ^{15}N showing only 1/16 and 1/100 of the effect respectively.

There are various methods for incorporating an unpaired electron spin into proteins and other macromolecules. One common method is the introduction of lanthanide $^{3+}$ ions coordinated to the protein, normally by substituting for a naturally occurring metal ion such as Mg^{2+} . Another method is to couple a small stable radical group, such as a nitroxide, to the protein. This is generally carried out by attaching it to a free thiol group in the protein. If no suitable cysteines are

naturally present in the protein, this requires site directed mutagenesis to add one in a suitable location. Proteins with multiple cysteines present may require all but one mutating to a similar residue (e.g. alanine or serine) in order for the paramagnetic tag to be attached to one specific site in the protein, which can present a problem if they are involved in interactions of interest¹⁷².

Similar methods can be used to attach a paramagnetic group to RNA or DNA. In RNA 4-thiouridine can be incorporated into specific positions in the sequence which allows MTSL to be attached in a similar reaction to that with cysteines in proteins. RNAs containing 4-thiouridines at specific positions are commercially available, and were purchased from Dharmacon.

CELF1 has seven endogenous cysteine residues at positions 61, 62, 119, 137, 150, 172 and 446. Of these 61, 62 and 150 are part of the RNA binding patch, and have substantially perturbed chemical shifts on binding. Attaching a large paramagnetic tag to any of these residues would likely disrupt RNA binding. Selectively attaching a paramagnetic tag to the t187 construct would require mutating five cysteines to other residues. RRM3 is the easiest construct to attach the tag to, since it has only a single cysteine residue, and it is not located in the RNA binding patch.

After completion of PRE titrations the paramagnetic tag was reduced by addition of a 5 molar excess of sodium L-ascorbate to the NMR sample. 16 hours was sufficient for full reduction of the tag attached to a cysteine in RRM3. The tag attached to 4-thiouridine RNA however was only partially reduced after this time. A final ¹H-¹⁵N HSQC was then collected on the reduced sample to confirm the magnitudes of the PRE effects.

3.17 X-ray Crystallography

Crystallization trials of the RRM1 construct unbound and in the presence of the CUGCUG RNA substrate were conducted using Qiagen crystallization screening suites. An identical set of trials were also conducted for the S28D mutant of RRM1. Trials were also run for the RRM123 construct unbound, and in the presence of the EDEN2U/4U RNA. In all cases these consisted of 96-well Intelliplate sitting drop vapour diffusion plates, which were loaded using a Matrix Hydra II micro-dispensing system. No diffraction quality crystals were produced in any of these trials.

3.18 Size Exclusion Chromatography

An analytical Superdex GF200 column (GE Life Sciences) was used for size exclusion chromatography. Since this technique was only used in order to compare the bound complex to the free protein a size calibration curve with known protein standards was not collected. Samples were dissolved in 1 ml of 50 mM potassium phosphate, 200 mM NaCl, pH 7.0 buffer and injected on the column. The elution volume of the protein and RNA was detected by the change in absorbance at 280 nm.

3.19 SAXS

SAXS samples were prepared by dissolving lyophilised protein in 30 mM potassium phosphate, 100 mM NaCl, pH 7.0 buffer. RNA was added from a 5 mM stock to a 1:1 ratio to produce the samples of the complex. The samples of the protein-RNA complex were then loaded onto a Superdex 200 gel filtration column in order to separate the complex from any remaining unbound protein or RNA. This step was essential in order to ensure the SAXS sample was monodisperse. The sample was then transferred to a 3000 MWCO centrifugal concentrator and concentrated to 5 mg/ml. The sample concentration was checked

by the 280 nm absorbance using a Nanodrop ND-100 spectrophotometer. Once at a concentration of 5 mg/ml samples were frozen using liquid nitrogen and stored at -80°C. A range of concentrations for SAXS data collection was produced by dilution of this concentrated stock.

3.20 ITC

Isothermal titration calorimetry (ITC) was carried out using a VP-ITC high sensitivity microcalorimeter (manufactured by MicroCal Inc, GE Healthcare). The instrument was controlled using VPViewer2000 version 1.4.27 (MicroCal). The ITC cell was cleaned by addition of Decon90 to the cell for 10 minutes, followed by washing through a minimum of 500 ml of MilliQ water. The syringe was also cleaned by washing through 500 ml of MilliQ water. A titration of water into water was carried out prior to each experiment to confirm the machine was free of contamination and that the baseline was stable. All solutions were degassed for 10 minutes in a Thermovac (MicroCal) before loading. For reverse titrations the cell was filled with 1.4 ml of 25 μ M RNA dissolved in RNase free water. 300 μ l of 250 μ M protein, also dissolved in RNase free water, was loaded into the syringe. In experiments involving the RRM123 construct the cell concentration was reduced to 12.5 μ M, and the syringe concentration to 125 μ M. All titrations were carried out at 25°C. After an equilibration period of 20 minutes, 30 injections of 10 μ l were added at 600 second intervals. A constant stirring speed of 300 rpm was applied throughout the titration to rapidly mix the contents of the cell.

A reference power of 5 μ cal s^{-1} was used except where otherwise specified. Fitting of the resulting data was carried out using the Origin 7.0 fitting program, assuming a single site binding model from which ΔH , ΔS , K_d and the stoichiometry for the interaction could be determined. For traces where a one site model was not appropriate, such as those showing multiple binding events, a fit to a multi-site binding model was attempted instead. Baseline correction was

necessary for some datasets.

3.21 Mass Spectrometry

All ESI mass spectra were collected on a Waters SYNAPT instrument with a quadruple time-of-flight mass analyzer calibrated using horse heart myoglobin. Data acquisition and analysis was carried out using Masslynx (Waters) software. All proteins required an additional desalting step to reduce salt to levels suitable for ESI mass spectrometry. This second desalt was carried out into 50mM ammonium acetate, in which the HiTrap desalting column had been pre-equilibrated. All proteins were run as native rather than denatured samples so that binding activity could be observed. Sample was injected at 5 μ l/minute using a Harvard Apparatus automatic syringe pump and a 100 μ l Hamilton syringe. The capillary voltage was 2.80 kV. The sample cone voltage was 30 V. Unbound protein samples were run in positive ion mode, bound protein/RNA complexes were run in both positive and negative ion mode. Data acquisition was carried out over 3 minutes at 1 scan/second and combined. Data was acquired over an m/z range of 500 – 5000.

3.22 Molecular Modelling

All hydrogen atoms for both the protein and RNA were introduced to the PDB files, using XLEAP. Na⁺ ions were also introduced to give an overall neutral charge (all protein/RNA systems modelled otherwise had an overall negative charge due to the RNA phosphate backbone). TIP3P water was used as an explicit solvent, and was added in a truncated octahedron geometry to a distance of 9 Å around the protein. Energy minimisation was carried out using the SANDER modules of the AMBER program. Energy minimisation was conducted in three stages. The first step minimised the water molecules only, by applying a restraint mask with a force constant of 200 to all other atoms in the system. The second stage minimised the water and Na⁺ ions added to achieve an overall neutral

charge for the system, by restricting the restraint mask to the atoms of the protein and RNA only. The third step minimised the entire system, with no restraint mask. Each step included an initial minimisation by the steepest descent method, lasting for 50 cycles, followed by conjugate gradient minimisation for up to a maximum of 5000 cycles. Molecular dynamics simulations consisted of an initial 10 ps step at 100 K, followed by a temperature ramp to 300 K over a further 10 ps with a restraint mask of weight 200 applied to the protein and nucleic acid. The force constant of the restraint mask was then reduced to zero in seven stages (100, 50, 25, 10, 5, 2, 1) of 10 ps each. The final step of the molecular dynamics simulation was at 300 K with no restraint mask, and allowed to run for a minimum of 1 ns. The resulting models were viewed using Pymol.

Three crystal structures were used as starting points for constructing models: the structure of RRM3 in complex with the RNA sequence UGUGUG by Tsuda *et al.* (PDB ID: 2RQC), the structure of two RRM1 proteins in complex with the sequence GUUGUUUUGUUU by Teplova *et al.* (PDB ID: 3NNH), and the structure of the two N-terminal RRMs with RRM2 bound to the RNA sequence GUUGUUUUGUUU, also by Teplova *et al.* (PDB ID: 3NMR).

The first model to be constructed was of the two N-terminal domains (the t187 construct) in complex with the RNA sequence UGUUUUGU. The RNA in the structure of bound RRM1 (3NNH) was truncated to the sequence UUGU, leaving a single RRM1 protein bound to a UGU site. The second RRM1 protein was removed. The residues of the remaining RRM1 protein were then superimposed onto the RRM1 section of the protein in structure 3NMR, minimising RMSD for the protein. Replacing the atom coordinates of the RRM1 section of the protein in structure 3NMR with those from the superimposed RRM1 from structure 3NNH combined the two structures, resulting in a single protein of residues 14 - 187 of CELF1, with a fragment of RNA containing a UGU(U) site bound to each domain. Residues 1 – 13 are not included in any crystal structure, and since they were not believed to be involved in RNA binding they were omitted. The RNA

molecule bound to RRM2 in this structure was truncated to the core UGUU sequence in contact with the protein.

The RNA fragments UGUU (bound to RRM2) and UUGU (bound to RRM1) were then connected to form the RNA UGUUUUGU. Due to the orientation of the two domains in the original 3NMR structure this required the introduction of an implausibly long bond connecting the two RNA fragments in this initial structure. The energy minimisation step detailed earlier allowed the protein domains and RNA to shift until this bond had relaxed to a normal length. Molecular dynamics simulations were then conducted from this starting point, using the temperature ramps specified earlier.

This structure served as the N-terminal fragment for later models containing all three RRMs of the protein. Since no structural data exists for the RRM2 – RRM3 linker region a section of the RRM123 protein consisting of residues 186 - 216 was constructed in the program XLEAP, and then energy minimised in AMBER. This linker was then attached to the N-terminal fragment by superimposing residues 186 and 187 of the linker onto their counterparts in RRM2 of the N-terminal fragment (minimising RMSD). The C-terminal fragment was similarly attached by superimposing residues 215 and 216 of the RRM3 structure onto the corresponding residues in the RRM2 - RRM3 linker. Combining the atom coordinates from the PDB files resulted in a complete RRM123 protein with two separate RNA fragments, UGUUUUGU bound to the N-terminal domains and UGUGUG to RRM3. This model was energy minimised, and underwent molecular dynamics simulations in AMBER for 1 ns at 300 K.

To produce the complex with the EDEN-2U/4U RNA the fragment bound to RRM3 was truncated to the UGU site. A section of RNA consisting of the sequence UUUUUU was constructed in XLEAP, energy minimised in AMBER, and attached to the RRM3 fragment by superposition of the 3' uracil with the 5'

uracil of this UGU site. The 5' uracil of this RNA spacer was then superimposed onto the 3' U of the N-terminal bound UGUUUUGU fragment, which necessitated the introduction of implausibly long bonds into the RNA backbone to make this connection. This structure, corresponding to RRM123 in complex with EDEN-2U/4U with the domains arranged in the order 2 – 1 – 3, was energy minimised over five steps, with a restraint mask applied to the protein and RNA. The force constant of this restraint mask was reduced (from 200 to 100, 50, 10 and 1) allowing all bonds to relax slowly to normal lengths. The structure was then subjected to molecular dynamics simulations in AMBER for 2 ns. A model of the same complex, but with the RRMs in the order 3 – 2 – 1 was also constructed by the same method.

Models of RRM123 in complex with the EDEN-2U/HL RNA sequence were also constructed. The RNA hairpin (consisting of the sequence *UCCCGAGGACGGGU* folded to form hydrogen bonds between the bases in italics) was constructed in XLEAP, and energy minimised. The 5' and 3' uracils were then superimposed onto U9 and U12 respectively of EDEN-2U/4U in the complex of this RNA sequence with RRM123. U10 and U11 of the EDEN-2U/4U sequence were then deleting, leaving an overall RNA sequence matching EDEN-2U/HL. The model then underwent energy minimisation and a 2 ns molecular dynamics simulation.

4 RNA Interactions of the Isolated RRMs of CELF1

Our initial aim was to produce constructs of each of the three RRMs of CELF1 in isolation, and assign their NMR spectra. The smaller size of these constructs made them more amenable to some biophysical techniques, in particular NMR. They were also far less prone to degradation than the full length CELF1 protein, and were considerably more soluble in buffers with low salt concentrations. Knowing the minimum RNA sites for binding of each RRM made it easier to design sequences to bind the full length protein, and understand the role of each RRM in recognising the EDEN motif.

Consensus sequences for CELF1 from the literature provided a starting point. UGUUUGUUUGU (the EDEN11 GRE) and UGUUUGUUUGUUUGUU (the EDEN15 GRE) have been suggested as possible targets for wild type CELF1. Long UG repeating sequences had also been suggested as possible targets. From this it has been hypothesised that each domain is recognising a UGU, UGUU or UGUG site. We therefore aimed to determine the minimum site required for binding of each of the three domains of CELF1.

CELF1 was originally noted to bind to a long repeating CUG RNA, hence its original name of CUG-BP1, before it was discovered to bind UG rich sequences such as the GRE with a higher affinity. Even though CUG sequences were known to be relatively low affinity substrates they were still of interest due to the possibility of them binding to CELF1 in DM1 cells. We therefore also aimed to identify the binding sites on the protein for CUG sequences to determine if they overlapped with the sites for UG rich sequences and so whether there would be competition between these RNAs.

4.1.1 Purification of RRM1

The RRM1 construct was produced by making a single point mutation in a plasmid of CELF1 in the pET28b(+) vector, which was supplied by Dr Emilie Malaurie (University of Nottingham). This altered the codon for Asn102 to a stop codon, truncating the protein and leaving only residues 1 - 101 attached to the N-terminal 6-His tag. The stop codon was placed at this position as it was in a flexible section of the linker between RRM1 and RRM2, and four residues after the C-terminus of the structured RRM1 domain. DNA sequencing confirmed that the point mutation was successful.

The plasmid DNA was transformed into BL21 (DE3) cells for expression. RRM1 was found to be soluble in lysis buffer A, with the vast majority of the protein remaining in the soluble fraction after a 16 hour induction at 30°C. These cells were lysed by sonication and the protein was allowed two hours to bind to an IMAC cobalt resin column. Washing and elution steps were carried out according to the protocol in section 3.7. After a thrombin cleave step to remove the N-terminal 6-His tag, the protein was gel filtered using a Superdex GF75 column to remove trace impurities. Finally the protein was desalted, frozen with liquid N₂ and lyophilised to produce pure protein. The mass and purity of the protein at each stage was checked using SDS-PAGE, an example of which is shown in Figure 4.1. The overall yield was approximately 25 mg/l of RRM1 for growths in LB, and 14 mg/l for M9 minimal media.

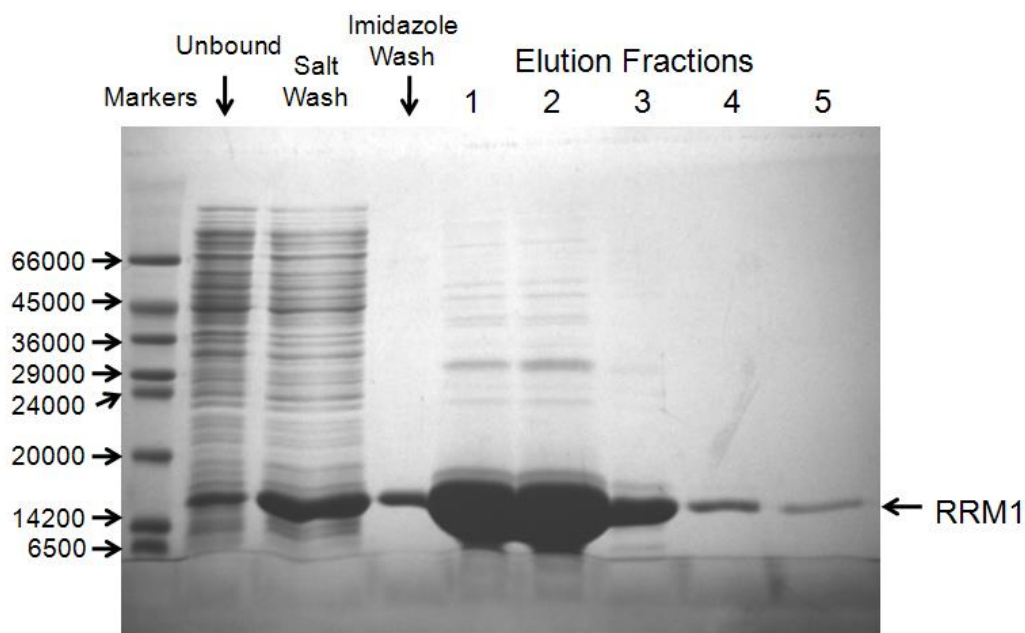


Figure 4.1: SDS-PAGE of samples from the IMAC column stage of the RRM1 purification. Standard molecular weight markers (Sigma) are shown in lane 1. Lane 2 contains a diluted sample of the cell lysate drained from the IMAC column after the His-tagged proteins had been allowed to bind. Lanes 3 and 4 contain samples from the two wash steps, both of which eluted significant quantities of RRM1 as well as non-specifically binding proteins. To reduce this loss of protein the NaCl concentration in the high salt wash was reduced to 1 M and the imidazole concentration in the low imidazole wash was reduced to 1 mM in later purifications. Lanes 5 – 9 contain samples from the high imidazole elution fractions. These five fractions were retained for gel filtration to remove the impurities visible on the gel (particularly in fractions 1 – 3).

Once the unlabelled material was confirmed to be intact and correctly folded based on the dispersion of peaks in the 1D proton NMR spectrum, ^{15}N labelled, and doubly labelled (^{15}N and ^{13}C) RRM1 was produced so the ^1H - ^{15}N HSQC of the protein could be collected and assigned.

4.1.2 NMR Assignment of RRM1

The RRM1 construct has 101 residues, of which 9 are prolines which have no backbone amide protons and hence no signals in the ^1H - ^{15}N HSQC. There are six additional residues (GSHMAS) remaining at the N-terminus from the 6-His-tag

after thrombin cleavage. A very poor signal to noise ratio was observed in the ^1H - ^{15}N HSQC for residues in this region of the protein, and in most cases no corresponding signals in the 3D spectra could be located. This can be attributed to the N-terminus of the protein being sufficiently dynamic to adopt a range of conformers in solution, each with slightly different chemical shifts for these residues, broadening the peaks. Example data from the HNCACB and HN(CO)CACB spectra used for assignment is shown below.

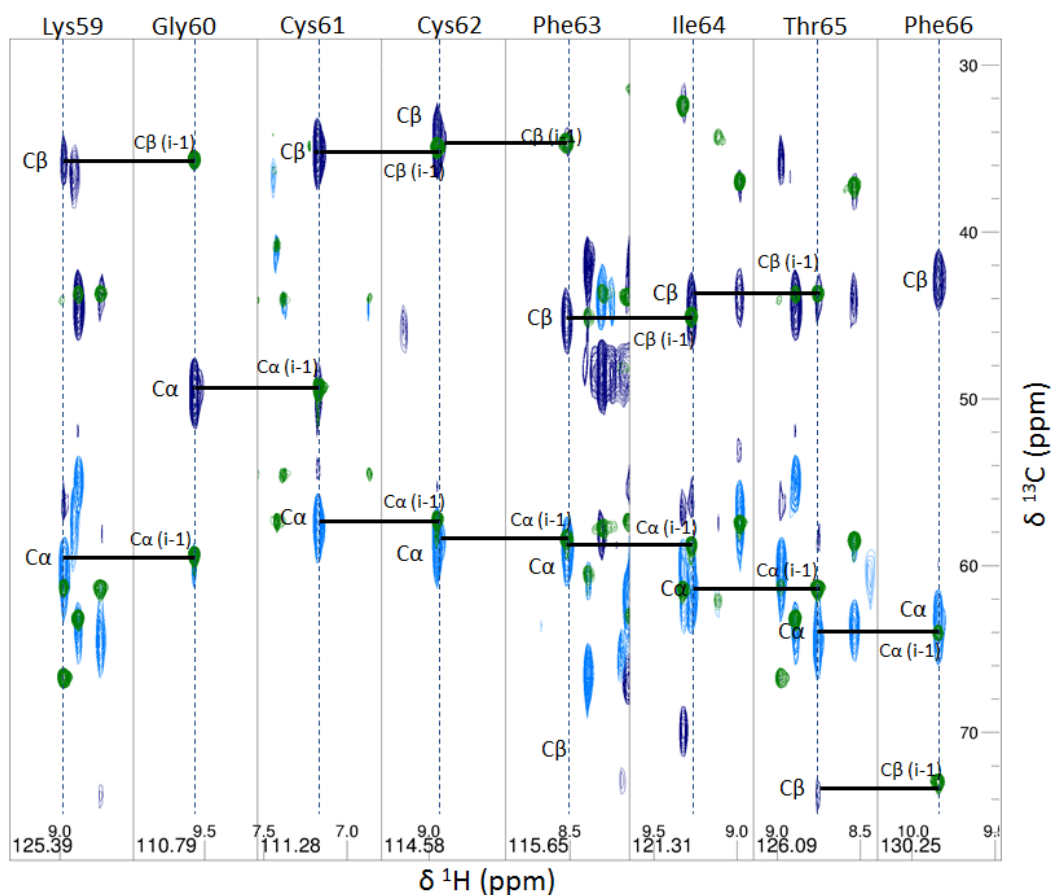


Figure 4.2: This figure shows strips through the three dimensional HNCACB and HN(CO)CACB data for residues 59 – 66 of the RRM1 construct. Peaks in the HN(CO)CACB spectra are shown in green. Peaks from the HNCACB spectra are shown in light and dark blue. Negative phase peaks, corresponding to C β s (and C α s of glycines) are in dark blue. Positive phase peaks, corresponding to the C α s of all residues except glycines are shown in light blue. In each strip the peaks are labelled, showing the matching chemical shifts between residue i and residue $i-1$. The black lines show the “backbone walk” through this section of the protein.

Of the 92 non-proline residues in RRM1 itself, 90 were assigned to peaks in the ^1H - ^{15}N HSQC. Assignments are missing for Met1 and Asp12, as well as the

remaining residues from the 6-His tag. Asp12 is situated between prolines 11 and 13, preventing the normal 3D heteronuclear assignment strategy from being used. The assignment of RRM1 is shown in Figure 4.3.

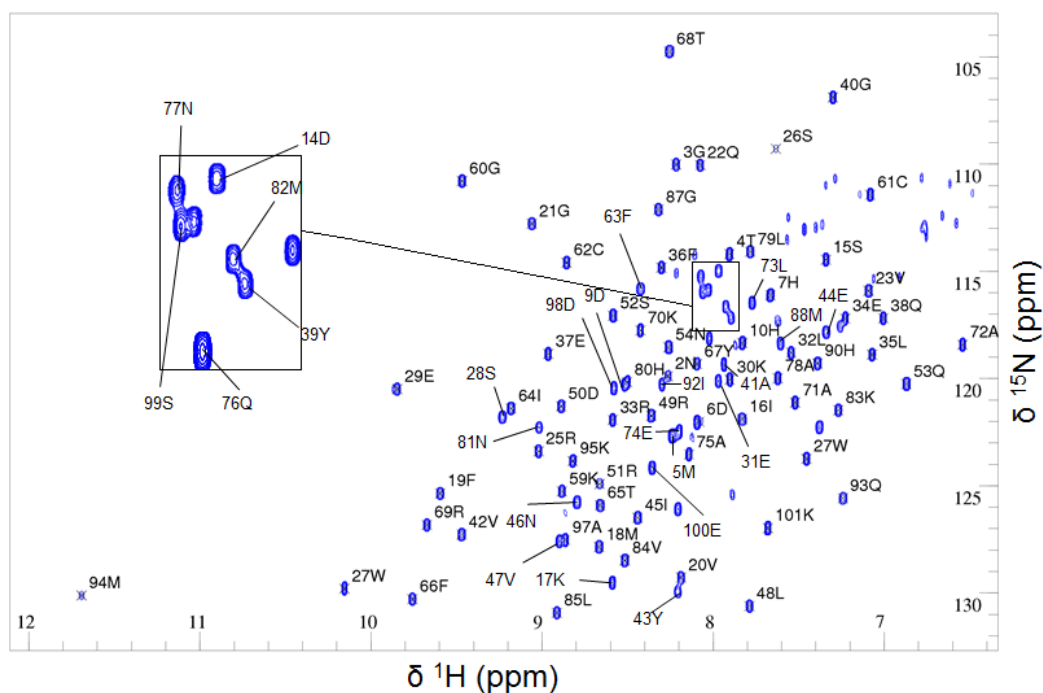


Figure 4.3: Assignment of the ^1H - ^{15}N HSQC of RRM1 (residues 1 - 101). There are some additional peaks from side chain NH_2 groups visible in the upper right region of the spectrum, which have not been assigned. Chemical shifts for all assigned residues are tabulated in the appendix.

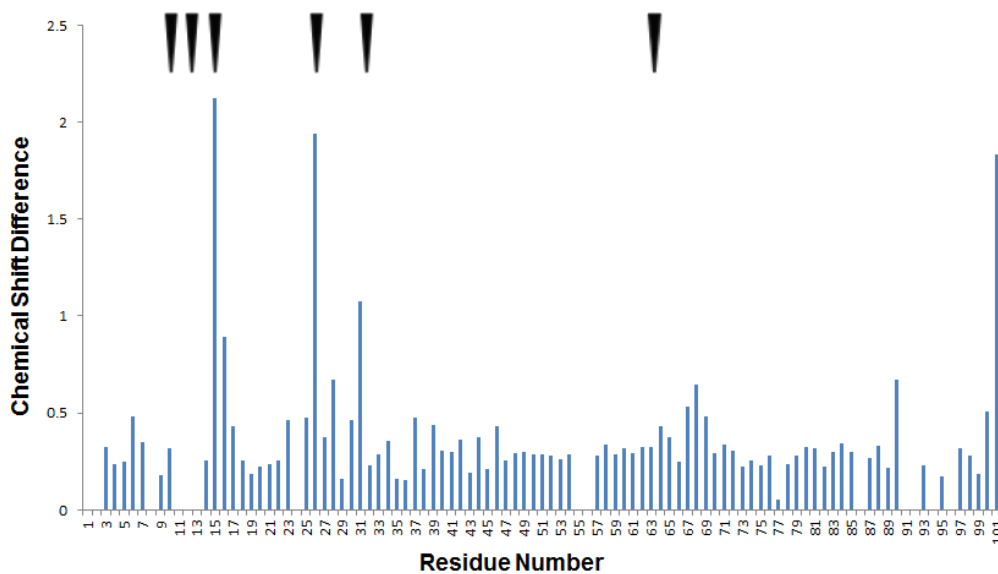


Figure 4: Histogram comparing the chemical shifts in Jun *et al.*'s available assignments with our assignments. Difference is calculated using the same method as for chemical shift perturbations, as outlined in section 2.2. Our data is for *Xenopus* CELF1, while Jun *et al.*'s data is for human CELF1. Residues which are not conserved between these homologs are highlighted with black arrows. Gaps indicate residues for which assignments are not available in one or both of the datasets.

There is generally good agreement between our assignments and those of Jun *et al.* The largest discrepancies are for residues 15, 16, 26 and 31 which are all either not conserved between these constructs, or directly adjacent to a non-conserved residue. Lys101 also shows a large difference, but this is to be expected as it is the C-terminal residue in this construct, as opposed to being in the middle of Jun *et al.*'s construct.

4.1.3 Purification of RRM2

The RRM2 construct was produced by PCR amplification of the DNA for residues 108 - 187 of *Xenopus* CELF1 using the primers specified in section 11.1. This insert was then cloned into the Xho I/Hind III sites of the multiple cloning site of the pET28b(+) vector (Novagen) and transformed into *E. Coli* XL1 Blue cells. As with RRM1 the construct is expressed with an N-terminal 6-His-tag, cleavable with thrombin, to allow purification using IMAC. After sequencing had confirmed the sequence of the RRM2 construct was correct, the plasmid DNA was transformed into *E. Coli* BL21 (DE3) cells for expression of the protein. Test growths and inductions confirmed RRM2 was successfully overexpressed, and remained in the soluble fraction after a 16 hour induction at 30°C.

Large scale expression and purification of RRM2 was carried out using the same protocols as for RRM1. Since the RRM2 construct contains no tryptophan or tyrosine residues it has almost no absorbance at 280 nm. Protein containing fractions at the gel filtration and desalting steps therefore had to be identified by SDS-PAGE. ¹⁵N and ¹³C/¹⁵N isotopically labelled protein was produced for NMR assignment and characterisation.



Figure 4.5: SDS-PAGE of washes and elution fractions from the IMAC column stage of the RRM2 purification. Significant quantities of protein were eluted by the 10 mM imidazole wash, which was reduced to 1 mM for the later purifications. The expected mass of the protein, allowing for the 6-His tag, was 9.6 kDa. The presence of multiple faint bands above the main RRM2 band suggests impurities bound to the protein.

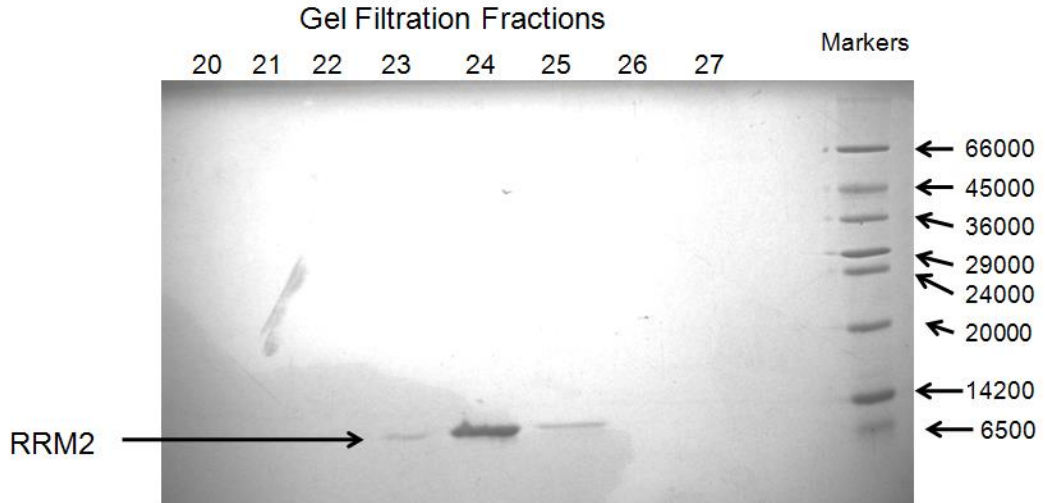


Figure 4.6: SDS-PAGE of elution fractions from the gel filtration stage of the purification, using a Superdex GF75 column. A single clean band is now visible, confirming the impurities from the IMAC column stage were removed.

The overall yields for this protein were lower than for RRM1 at approximately 12 mg/l from LB growths, and 8 mg/l from M9 minimal media. Due to the lack of absorbance at 280 nm protein concentrations when preparing samples were based on the mass of the lyophilised protein, as measured on a balance accurate to 0.1 mg.

4.1.4 NMR Assignment of RRM2

The TROSY technique was not used for NMR data collection on RRM2 since its small size (9.6 kDa) results in minimal loss of signal intensity from relaxation, and a conventional HSQC has twice the inherent sensitivity. Doubly labelled RRM2 was prepared, and 3D NMR data collected for assignment purposes. HN(CA)CO, HNCO, CBCANH and CBCA(CO)NH spectra were acquired on a 1 mM sample of ^{13}C and ^{15}N labelled RRM2. HCCH TOCSY data was also acquired for the purpose of side chain assignment.

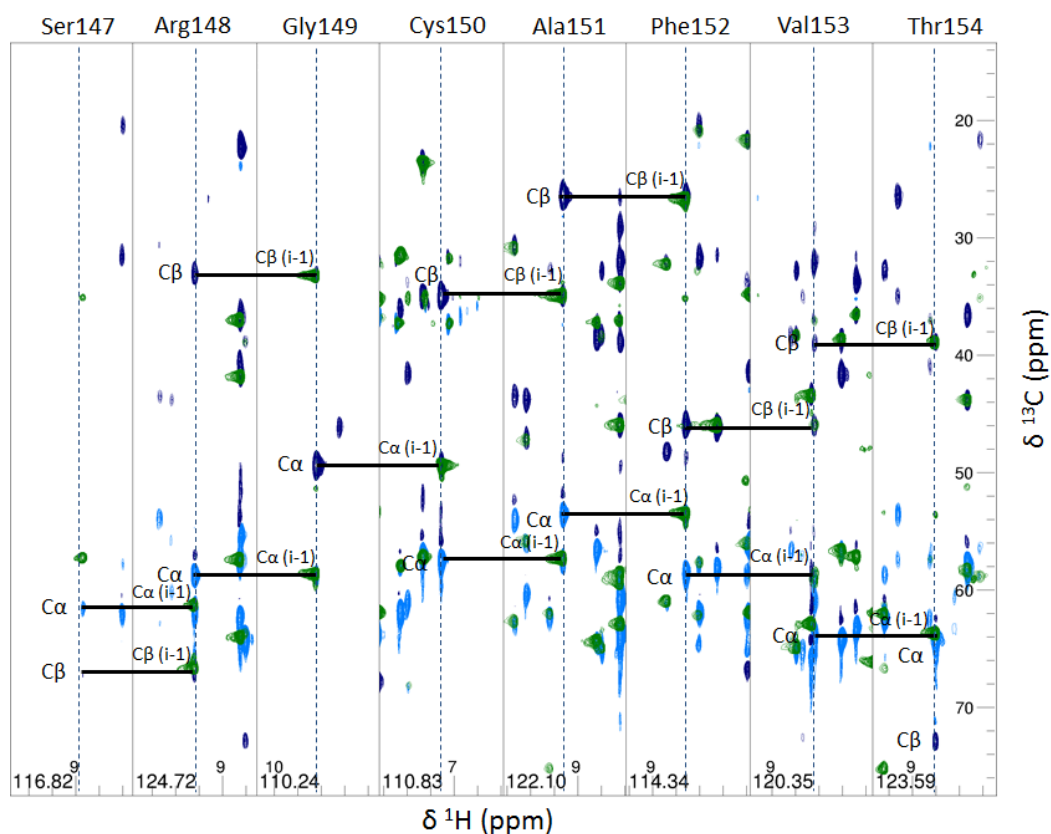


Figure 4.7: This figure shows strips through the three dimensional HNCACB and HNCOCACB data for residues 147 – 154 of the RRM2 construct. Peaks in the HN(CO)CACB spectra are shown in green. Peaks from the HNCACB spectra are shown in light and dark blue. Negative phase peaks, corresponding to Cβs (and Cas of glycines) are in dark blue. Positive phase peaks, corresponding to the Cas of all residues except glycines are shown in light blue. In each strip the peaks are labelled, showing the matching chemical shifts between residue *i* and residue *i-1*. The black lines show the “backbone walk” through this section of the protein.

Based on the 3D heteronuclear data 98% percent of the backbone amide signals were assigned. Assignments were determined for all non-proline residues except Ser178. As with RRM1 there are additional signals from the remainder of the 6-His tag left after the thrombin cleave, which were not assigned. The assignment of RRM2 is shown in Figure 4.8.

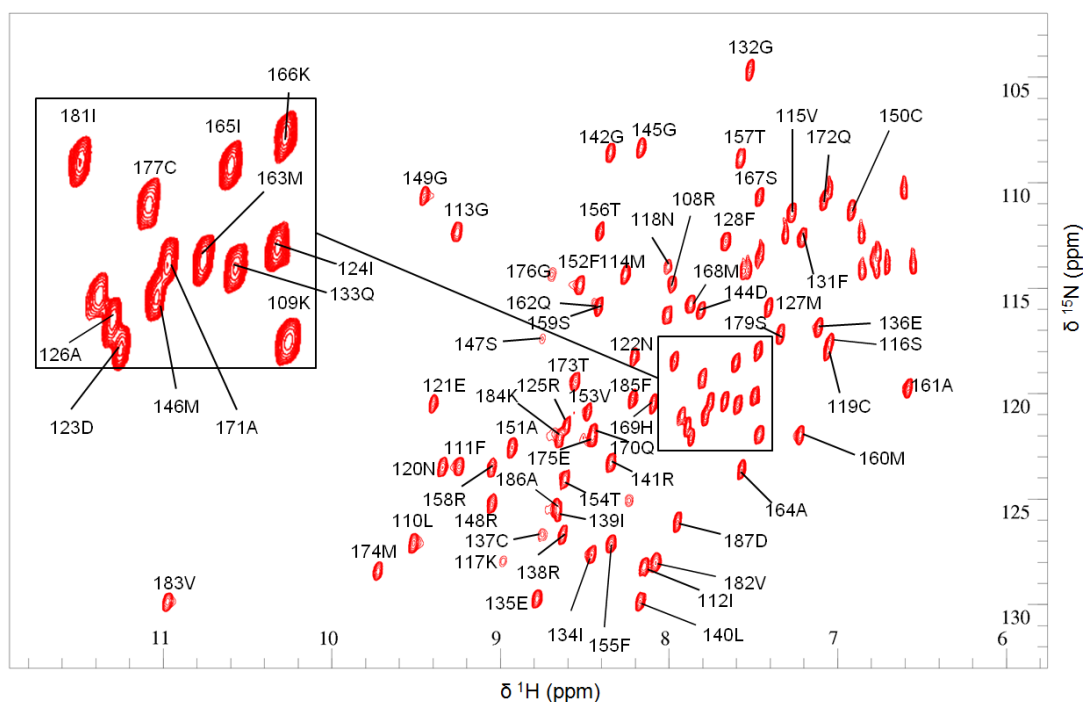


Figure 4.8: Assignment of the ^{15}N TROSY spectrum of RRM2 (residues 108 – 187 of CELF1). No assignment is available for Ser178. Additional peaks from side chain NH_2 groups are visible in the upper right region of the spectrum, which have not been assigned.

The assignments for most residues in RRM2 of human CELF1 were deposited in the BMRB by Jun *et al.* (Entry 6121)⁴⁸. A comparison of this data with our assignments is shown in Figure 4.9.

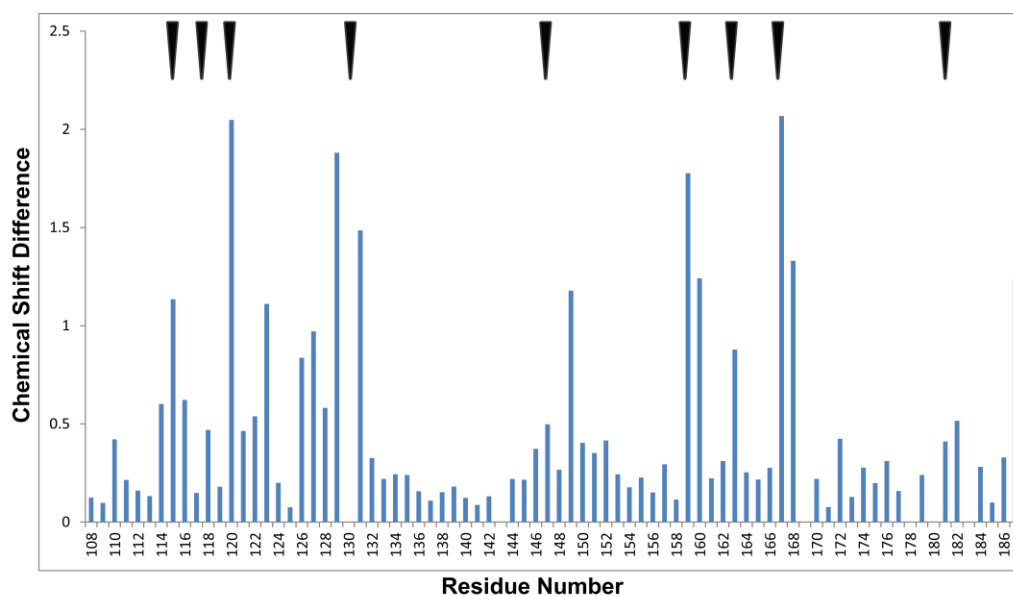


Figure 4.9: Histogram comparing the chemical shifts in Jun *et al.*'s available assignments with our assignments. Difference is calculated using the same method as for chemical shift perturbations, as outlined in section 2.2. Our data is for *Xenopus* CELF1, while Jun *et al.*'s data is for human CELF1. Residues which are not conserved between these homologs are highlighted with black arrows. Gaps indicate residues for which assignments are not available in one or both of the datasets (e.g. Val183, which is missing from Jun *et al.*'s assignments).

While some significant differences are seen, they correspond to residues which differ between the two constructs, and those in close proximity to them. In those sections of the protein which are well conserved there is good agreement our assignments and those of Jun *et al.*

4.1.5 Purification of RRM3

The RRM3 construct was produced from the wild type CELF1 plasmid DNA using a single step PCR method which deleted the DNA codons for residues 1 - 384, as outlined in section 3.15.6. This left an N-terminal 6-His tag attached to RRM3. A sufficiently long N-terminal extension was present in the construct that its involvement in RNA binding subsequently discovered by Tsuda *et al.* should still be possible. Protein expression and purification was carried out using the same methods as for RRM1 and RRM2. The RRM3 construct does not contain a tryptophan residue, so the 280 nm absorbance is relatively low, but there are

tyrosines present in this RRM. Protein containing fractions from the gel filtration stage could therefore still be identified by 280 nm absorbance, unlike RRM2.

The expression and purification used the same protocols as for the RRM1 construct. Analysis by SDS-PAGE, which is shown in Figure 4.10, confirmed that RRM3 was expressed intact.

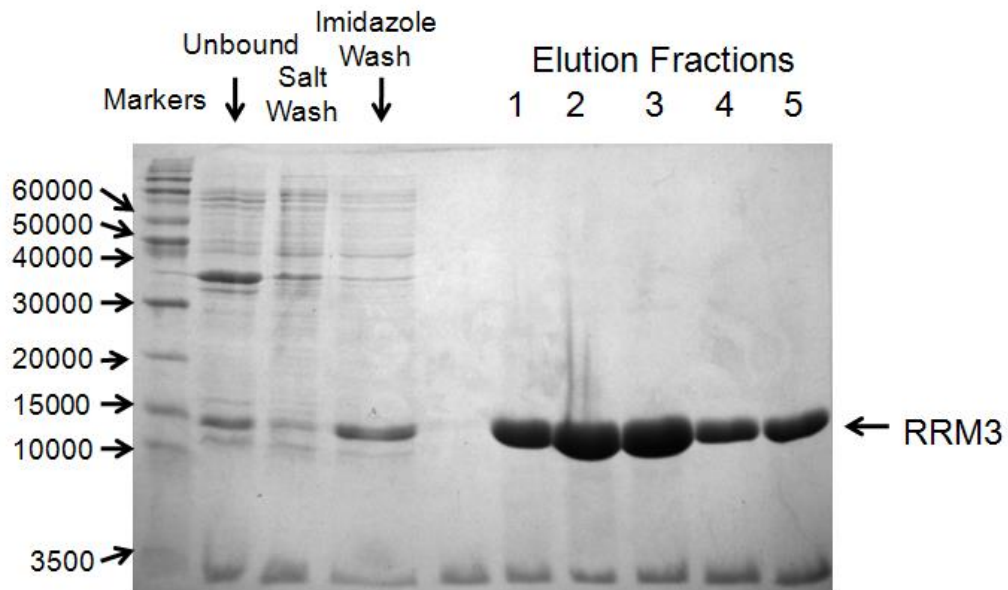


Figure 4.10: SDS-PAGE of samples from the IMAC column stage of the RRM3 purification. In lane 1 are reference markers (Novagen). Lane 2 is a diluted sample of the runoff from the IMAC column. Lanes 3 and 4 show proteins eluted in the two wash steps. Lanes 6 – 10 show the first five of the 0.75 M imidazole elution fractions. RRM3 was found to be relatively pure even at this stage, but was gel filtered through a Superdex 75 column to remove any trace impurities.

4.1.6 NMR Assignment of RRM3

A ^{15}N TROSY spectrum was collected, as well as HNCACB, HN(CO)CACB, HNCO and HN(CA)CO 3D heteronuclear experiments in order to assign the protein backbone. The assignment for this domain is shown in Figure 4.12. The flexible residues at the N-terminus resulted in very weak signals in the NMR spectra, hindering assignment of this region. 90% assignment of the backbone of the structured domain was achieved.

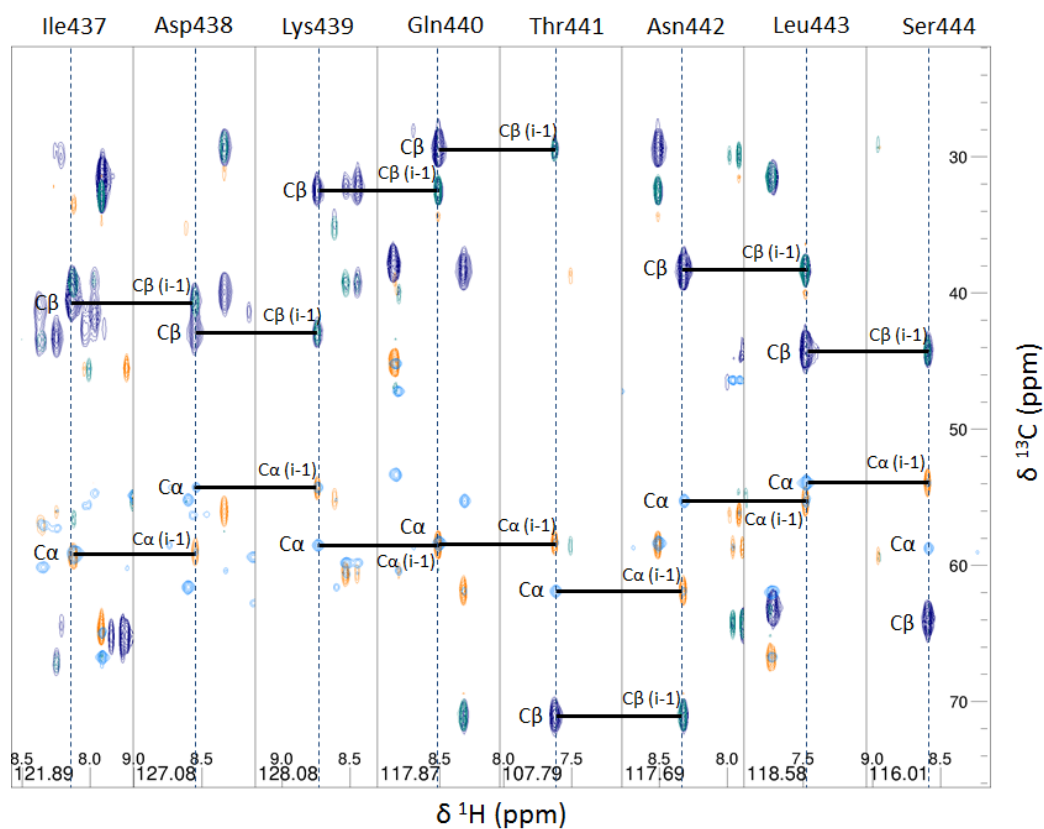


Figure 4.11: This figure shows strips through the three dimensional HNCACB and HNCOCACB data for residues 437 – 444 of the RRM1 construct. Peaks in the HN(CO)CACB spectra are shown in orange and green. Orange peaks correspond to $\text{C}\alpha$ s in the preceding residue, while green peaks correspond to $\text{C}\beta$ s. Peaks from the HNCACB spectra are shown in light and dark blue. Negative phase peaks, corresponding to $\text{C}\beta$ s are in dark blue. Positive phase peaks, corresponding to the $\text{C}\alpha$ s are shown in light blue. In each strip the peaks are labelled, showing the matching chemical shifts between residue i and residue $i-1$. The black lines show the “backbone walk” through this section of the protein.

Assignments are missing for five residues in the flexible N-terminal extension, Gly395 and for residues 481 - 484 at the C-terminus.

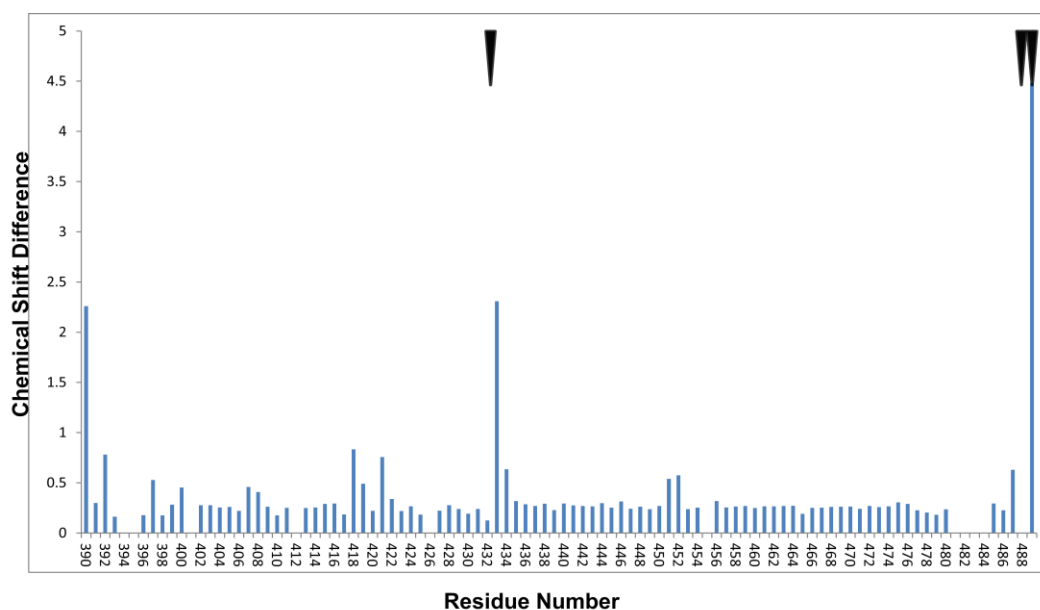


Figure 4.13: Histogram comparing the chemical shifts in Tsuda *et al.*'s available assignments with our assignments. Difference is calculated using the same method as for chemical shift perturbations, as outlined in section 2.2. The constructs used were not identical, and residues which differ between them have been highlighted with black arrows.

A good agreement is seen between our assignments and those of Tsuda *et al.* with the exception of residue 433, which is not conserved, and the terminal residues (due to the constructs being of different lengths, and the incorporation of non wild type residues at the C-terminus of Tsuda *et al.*'s construct).

4.2 Interaction of CELF1 RRMs with Guanine-Rich Elements

With the vast majority of the residues in each RRM assigned it was possible to determine by NMR whether any given RNA sequence was binding to an RRM, and the areas of the protein involved in the binding interaction. The highest affinity RNA substrates reported in the literature were the Guanine Rich Elements (GREs), consisting of a repeating UGUU pattern of nucleotides. Three or possibly four repeats of this pattern were suggested to be sufficient to bind all three RRMs of CELF1 (the EDEN11 and EDEN15 GREs). This seemed to imply each RRM could be recognising a UGUU site. The RRM fold has however been known to recognise anywhere from 2 – 8 nucleotides, so potentially a single

RRM could be recognising additional nucleotides on either side of the UGUU repeat. One of the RRMs recognising more than one UGUU repeat would also be a possible explanation for the fourth conserved UGU site in the EDEN15 consensus sequence reported by Graindorge *et al.* (2008). High affinity interactions have also been reported between CELF1 and UGUG repeats. This could imply that the fourth nucleotide is not involved in binding, and the RRMs are recognising UGU sites rather than UGUU sites. Alternatively the fourth nucleotide could be involved in binding, but the protein is tolerant of either U or G at that position.

In order to distinguish between these possibilities the RNA sequences UGUUUGU (termed EDEN7) and UGU (EDEN3) were selected for investigation. If an RRM is recognising more than one UGUU repeat or a four nucleotide UGU(U/G) site it would be expected either to not bind to the short UGU substrate, or to show a much smaller binding patch on the surface of the protein compared to the EDEN7 substrate. If however an RRM was recognising just a three nucleotide UGU site, it should show the same binding patch on the protein for both of these RNA substrates.

4.2.1 Interactions of RRM1 with Guanine-Rich Elements

¹⁵N labelled RRM1 was titrated with the RNA substrate EDEN7 (UGUUUGU). Significant chemical shift perturbations (CSPs) were seen for several residues, confirming that RRM1 does bind to the EDEN7 sequence. Most residues were in fast exchange, and so their assignments could simply be tracked from point to point throughout the titration. In Figure 4.14 are shown overlaid spectra of the unbound protein and the protein bound to RNA. Highlighted are the peaks for some of the residues which show the greatest perturbation throughout the titration.

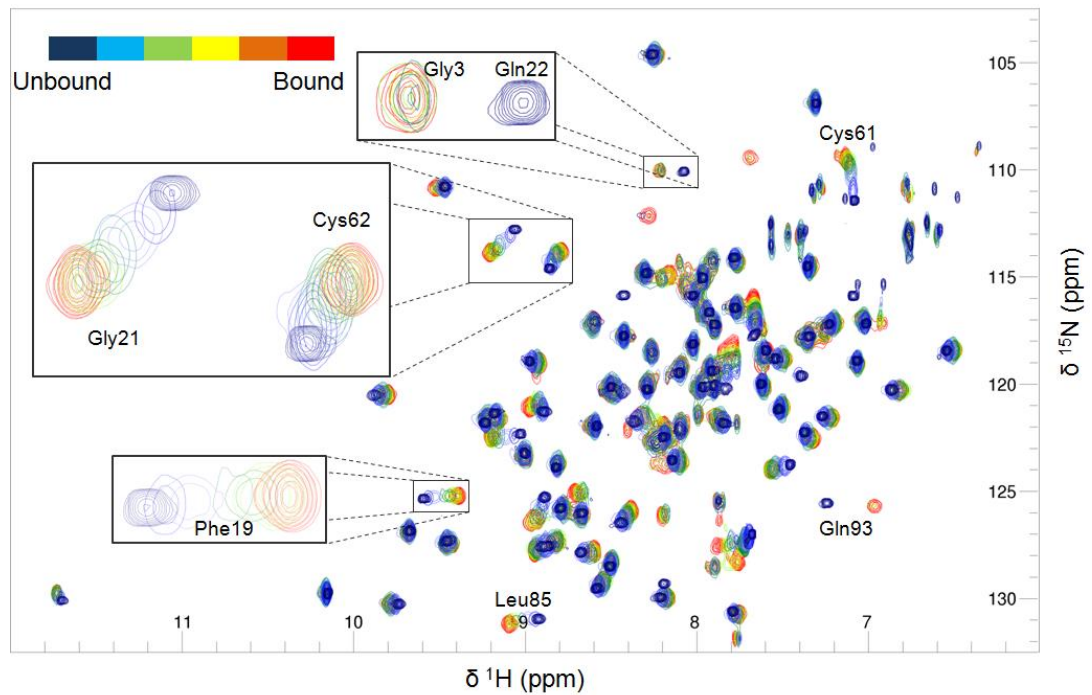


Figure 4.14: Overlaid ^{15}N TROSY spectra for the titration of RRM1 with the RNA substrate EDEN7 (UGUUUGU). The spectrum of the unbound protein is shown in blue, and the fully bound protein in red. Intermediate titration points are shown as a spectrum. Insets are expanded views of some of the most affected peaks. Most of the affected residues are in fast exchange, such as Phe19, Gly21, Cys61, Cys62 and Leu85. There are some residues that are in intermediate exchange such as Gln22, for which the peak from the free form is highlighted, but the bound peak is lost due to broadening. There are also residues in slow exchange such as Gln93, where both the peak is visible in both the free and fully bound forms, but not the intervening titration points. This prevents the peak being tracked through the titration, which can present problems in determining the assignment of the bound form.

While most residues are in fast exchange there are a few, such as Gln22 which are in intermediate exchange, and so broaden out and are lost in the early stages of the titration. Additional peaks also grow in during the later stages of the titration from the bound forms of residues in slow exchange, but the assignment of these new peaks is in some cases ambiguous due to overlap. It can be stated these residues are definitely involved in binding the RNA, but the chemical shift perturbation cannot be quantified unless the corresponding peak from the bound form can be located. In cases of slow exchange where bound assignments are unclear a minimum CSP can be stated based on the closest unassigned peak in the bound spectrum. This is not possible in some intermediate exchange situations as

the peak from the bound form may be too broad to observe. Residues in more dynamic regions of the protein are more likely to fall into this category as they tended to give weak, broad peaks even in the spectrum of the unbound protein.

The nitrogen chemical shift has a greater dispersion than the proton chemical shift. When combining the changes in the proton and nitrogen chemical shifts into a single chemical shift perturbation value (CSP), they must therefore be weighted so that changes in the proton dimension are not obscured. CSP values were calculated throughout using the formula below.

$$\text{CSP} = \left(\left(\frac{\Delta\delta\text{N}^2}{10} \right) + \Delta\delta\text{H}^2 \right)^{0.5}$$

Where $\Delta\delta\text{N}$ is the difference in chemical shift in the nitrogen dimension between the saturation point and the zero point of the titration and $\Delta\delta\text{H}$ is the corresponding difference in the proton dimension. The CSP values for each residue can then be plotted against residue number to show those regions of the protein that are involved in binding the RNA.

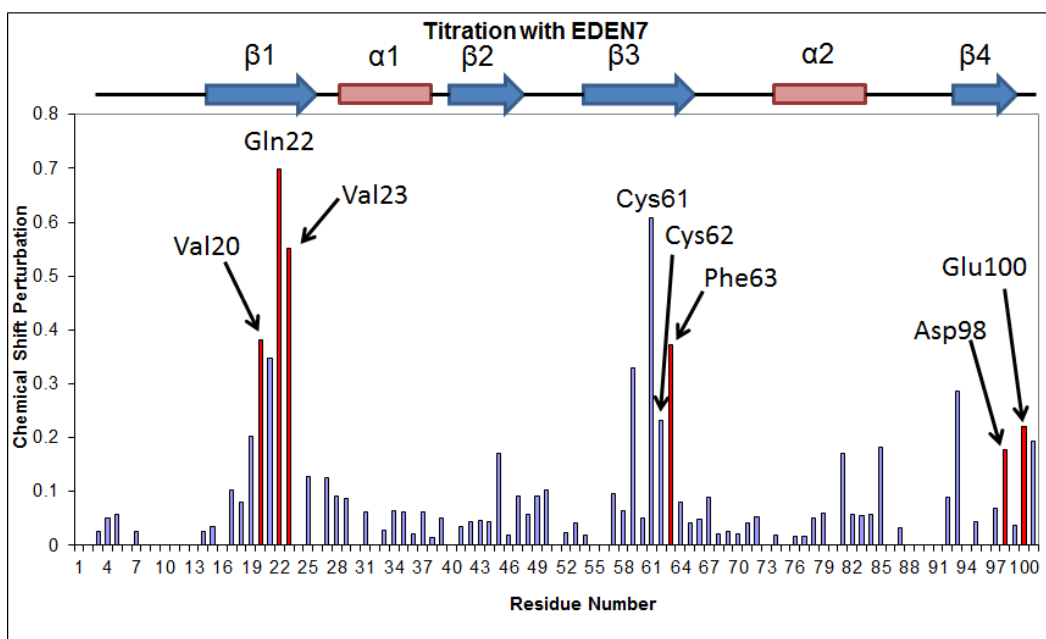


Figure 4.15: CSP values for each residue of RRM1 on titration with EDEN7. Residues which are in slow exchange, for which the values are therefore minimum CSPs rather than exact values, are highlighted in red. Gaps are due to prolines, unassigned residues and peaks for which CSPs could not be accurately calculated due to signal overlap.

When RRM1 binds to the EDEN7 RNA substrate, the most perturbed residues are concentrated in the 18 - 23, 59 - 63 and 93 - 101 regions. While these regions are far apart in the protein chain they actually form adjacent strands of the β -sheet in the folded protein, and so represent a single coherent RNA binding patch. This binding patch can be more easily visualised by mapping the CSP values for each residue onto the structure of the protein. In this case the CSPs were mapped onto the relevant part of the CELF1 RRM1 and RRM2 structure produced by Jun *et al*, which is available in the PDB (ID: 2DHS). This map of the binding surface is shown in Figure 4.16.

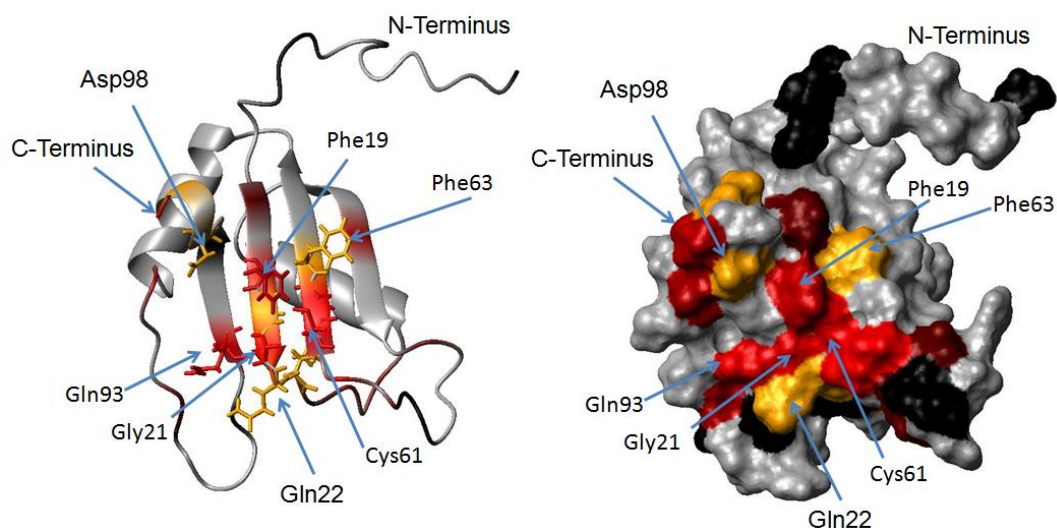


Figure 4.16: CSP maps on the structure of RRM1, produced by truncation of Jun *et al.*'s NMR solution structure of the first 187 residues of CELF1 from the PDB. RRM2 has been removed by deletion of residues 102 – 187. The CSP values have been mapped onto the structure in red: the brighter the red colour, the greater the magnitude of the CSP. Residues which are definitely affected but do not have quantified CSP values due to intermediate or slow exchange preventing the peaks from the bound form being located are shown in yellow. Residues for which no data can be obtained (i.e. prolines and unassigned residues) are shown in black. This image was produced using the molecular graphics package Molmol, as were all subsequent CSP maps.

In producing this map, residues with CSP values of less than 0.1 are considered to undergo no significant change on binding, and are shown in grey. Residues for which no data is available, specifically the prolines and the unassigned residues are shown in black. CSP values are displayed as a colour gradient, with bright red indicating the most affected residues, and dark red indicating lower CSPs. Residues without quantifiable CSPs due to slow exchange preventing location of the peak for the bound form are shown in yellow. As slow exchange is associated with a large difference in chemical shifts between the free and bound forms these residues are presumably the most disrupted on RNA binding, and would show the largest CSPs if exact values could be calculated.

From this CSP map, it can be seen that the RNA binding site is across the face of the β -sheet on the opposite side of the protein to the α -helices. There are also

some significantly perturbed residues in the loops at the lower edge of the β sheet as shown in Figure 4.16, such as Gln22. The most affected residues, such as Cys61 and Gly21 lie in the classic RNP regions in β -sheets 1 and 3. The conserved aromatic residues in the RNP regions (Phe19 and Phe63) are also affected. This is consistent with them forming stacking interactions with the RNA bases, as is commonly seen for RRMs. Some residues near the C-terminus (e.g. Asp98) appear to be involved in RNA binding despite being beyond the folded region of RRM1. It was not clear whether this was an artefact caused by the position at which the protein was truncated, or if some residues beyond the C-terminus of the structured domain are in fact involved in binding.

It was noted that this titration seemed to reach saturation rather earlier than would be expected for simple 1:1 binding, based on the point at which the ^{15}N TROSY spectrum ceased to vary significantly between titration points. Very few changes in chemical shift were seen after a 0.6: 1 ratio of RNA to protein was reached. Examples of the titration curves for some of the most affected residues, such as Gly21 and Cys61 are shown in Figure 4.17.

Titration Curves for RRM1/UGUUUGU

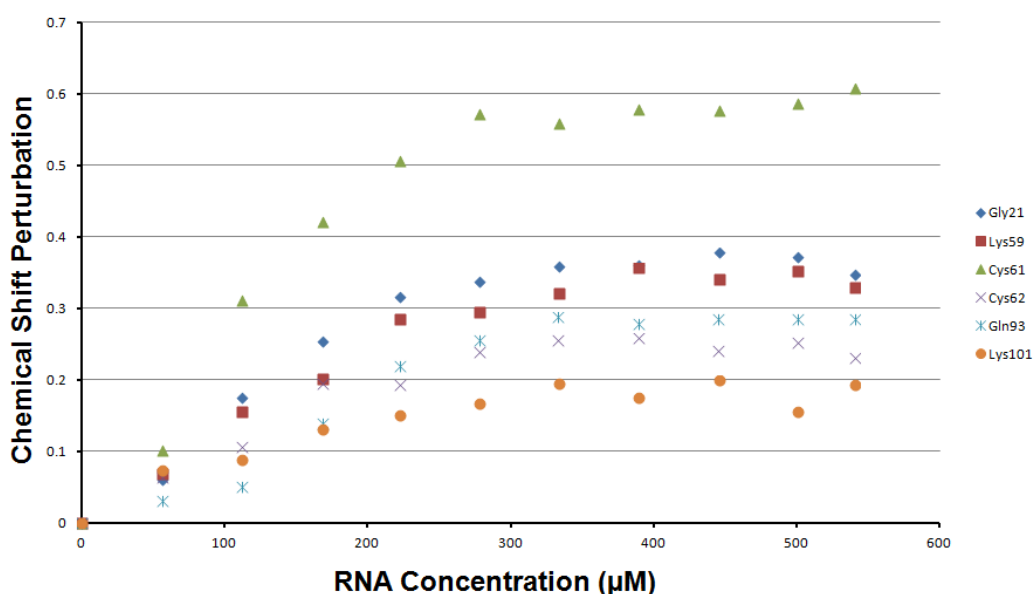


Figure 4.17: Chemical shift perturbations at each titration point for a selection of the most affected residues for which CSPs can be calculated throughout the titration. The protein concentration was 500 μM . All reach an apparent plateau before an RNA concentration of 500 μM is reached.

Since the protein concentration in this experiment was 500 μM , in a 1:1 model the titration would not be expected to reach saturation before this concentration of RNA was reached. A possible explanation for this was that the complex being formed did not have a simple 1:1 stoichiometry. If RRM1 is recognising a UGU site then the EDEN7 RNA used (UGUUUGU) potentially had two identical binding sites. This would permit a 2:1 protein to RNA complex to form, resulting in all of the protein being in the bound form after a 0.5:1 ratio of RNA to protein was reached.

The titration was repeated with the EDEN3 (UGU) RNA substrate. The protein concentration for this titration, and all further titrations with RRM1, was reduced to 400 μM .

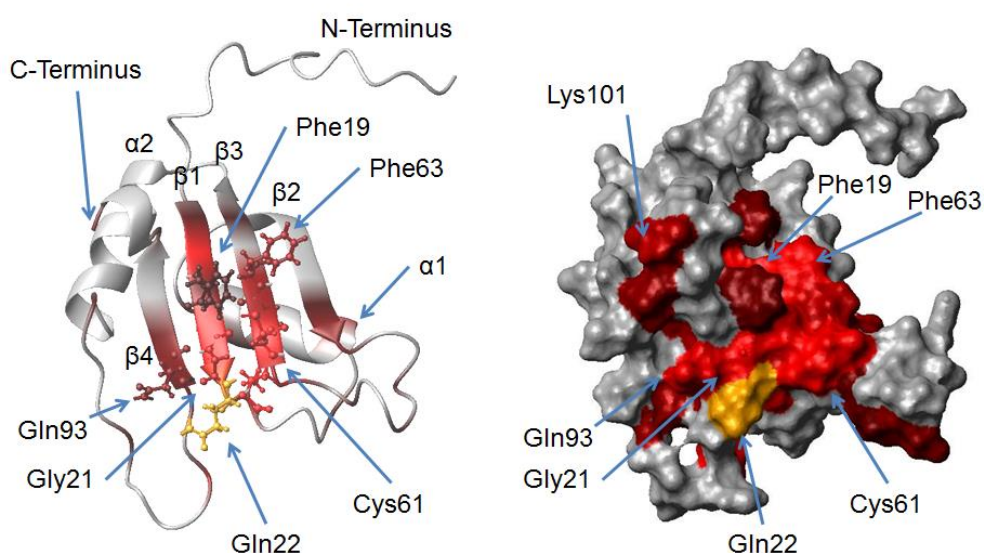
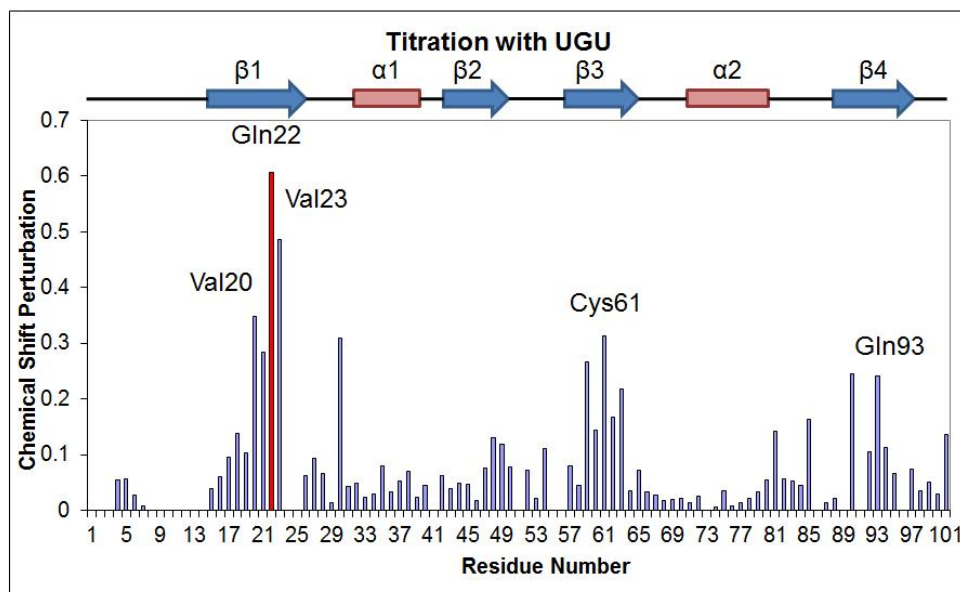


Figure 4.18: Above is a histogram of chemical shift perturbations for the titration of RRM1 with UGU. The assignment for the bound peak of Gln22 was unclear, so a minimum CSP estimate to the closest unassigned peak has been included for this residue. Below is the CSP map for the titration of RRM1 with EDEN3 (the trinucleotide UGU). The protein concentration was 400 μM , and the titration was conducted at 298 K.

The UGU RNA substrate was still bound by RRM1, with almost all residues in fast exchange in the NMR titration. Only Gln22 still appeared to be in slow exchange, and so only has a minimum CSP value. The same residues in the RNP regions are disrupted, including the aromatic residues Phe19 and Phe63, which can therefore be assumed to be still stacking with two of the three RNA bases. The only residues which appeared unaffected in the UGU titration, but showed

significant CSPs in the EDEN7 case are Asp98, Glu100 and some of the weakly affected residues such as Ile45 in β 2.

Significant CSPs show that RRM1 is still binding to this shorter RNA substrate, and the set of affected residues appears to be very similar. The UGU substrate was therefore not only binding to RRM1, but occupying the whole of the binding site across the β -sheet as effectively as the longer EDEN7 substrate. From this it was concluded that UGU sites are the key component of the EDEN motif, and are sufficient for binding of RRM1. It also supported the possibility of two RRM1 protein molecules binding to EDEN7 (UGUUUGU) with one protein at each UGU site.

The titration curves for some of the most affected residues suggest titration had not quite reached saturation point at a 1:1 ratio of RNA to protein (see Figure 4.19). Again this is consistent with the UGU substrate forming a 1:1 complex while EDEN7 forms a 2:1 complex with RRM1.

Titration Curves for RRM1/UGU

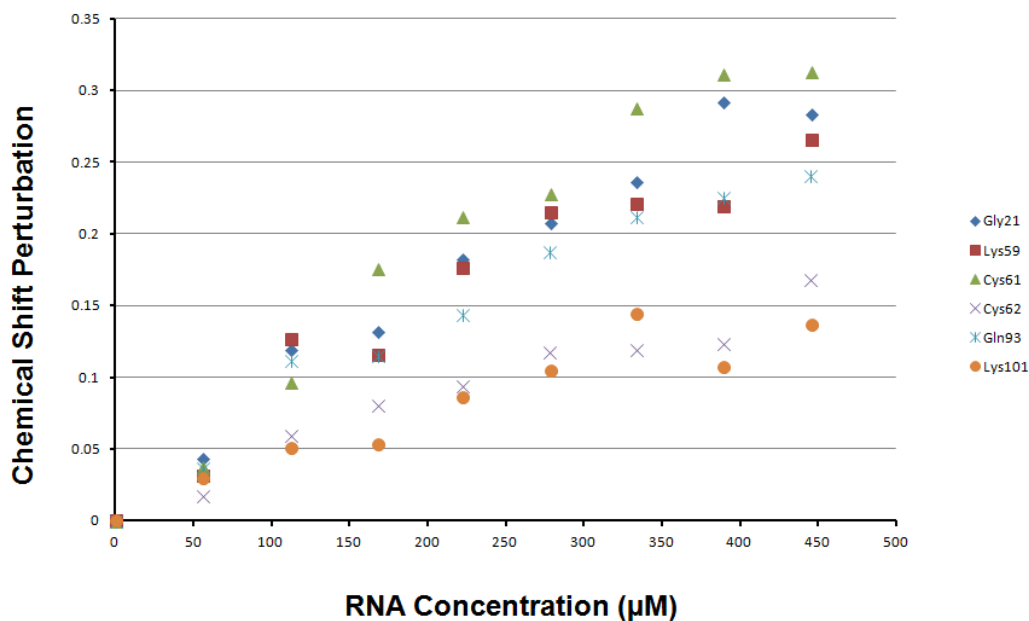


Figure 4.19: Titration curves for a selection of residues in the titration of the RNA sequence UGU into 400 μM RRM1. The curves for Gly21 and Cys61 definitely do not reach a maximum until an RNA concentration of 400 μM . This is less clear for the other residues shown.

4.2.2 Removal of one UGU site from the EDEN7 RNA Substrate

To confirm the 2:1 complex hypothesis, and hence that RRM1 was recognising just a UGU site, a version of the EDEN7 substrate with one of the two UGU sites removed was designed (UGUUUUAU). UAUU repeats had been previously reported in the literature to show at most a low affinity interaction with CELF1, so a switch from a UGU to a UAU site would be expected to eliminate, or at least greatly reduce binding to the second site.

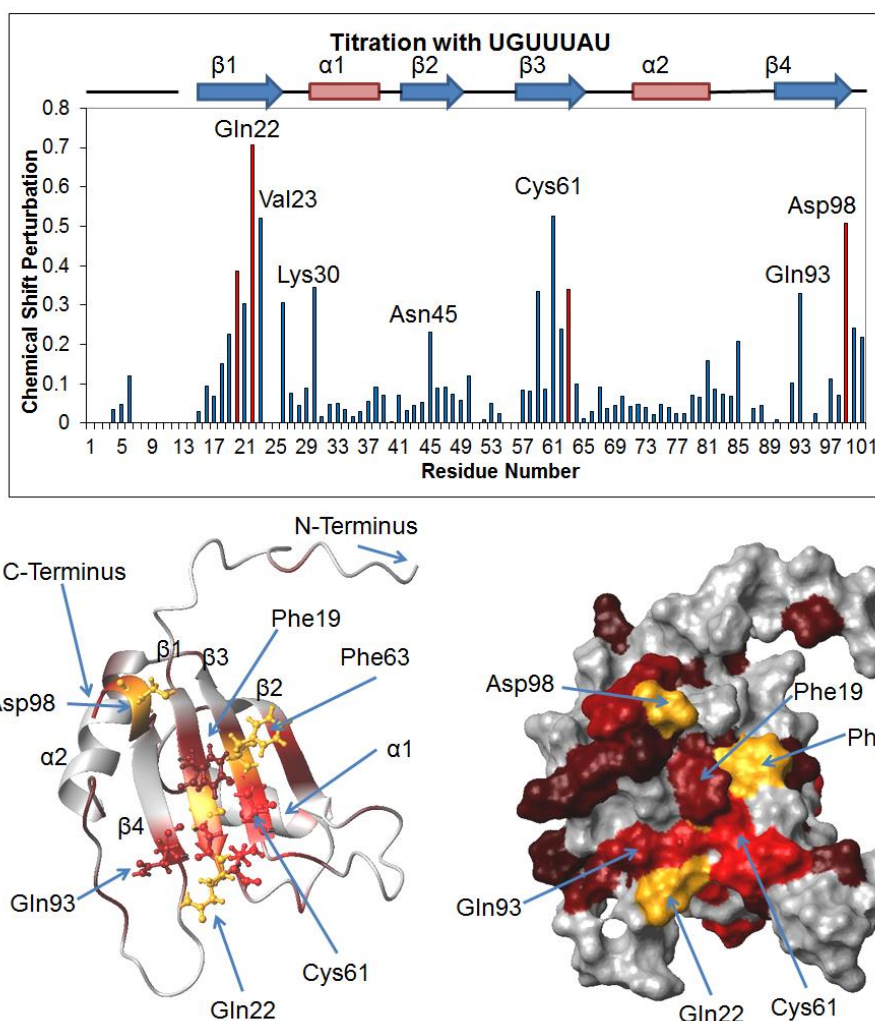


Figure 4.20: At the top is shown a plot of the CSP for each residue on binding to UGUUUUAU. Residues in slow exchange with minimum CSP estimates are highlighted in red. Below is a CSP map of RRM1 on titration with UGUUUUAU. Exact CSP values are shown in red, with brightness of colour indicating the magnitude. Affected residues with only minimum CSP estimates are shown in yellow. A similar binding patch is seen as in previous experiments. The protein concentration throughout the titration was 400 μ M.

The same set of affected residues is seen as for the EDEN7 substrate, consistent with RRM1 recognising a simple UGU site in each titration. Gly21, Gln22, Val23, Cys61 and Gln93 are all highly affected. Moderate CSPs are seen for Asp98 and Ile45, again matching the EDEN7 titration. The titration curves, examples of which are shown in Figure 4.21, do seem to reach saturation point at a slightly higher RNA to protein ratio than in the EDEN7 case, but it was ambiguous whether the stoichiometry of the complex had changed. This RNA

substrate was later clarified by mass spectrometry to be primarily forming a 1:1 complex, for which the data is shown in section 4.5.1.

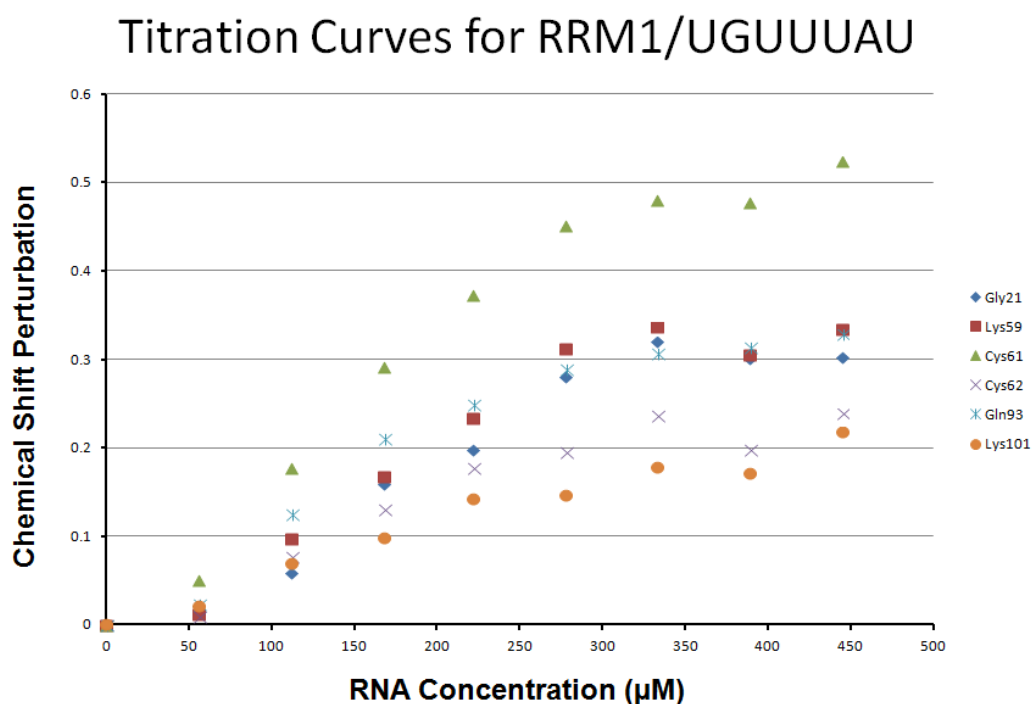


Figure 4.21: Binding curve for the titration of UGUUUUAU into 400 µM ¹⁵N-labelled RRM1. All curves show an increasing CSP up to an RNA: protein ratio of 0.85:1. The curves then appear to plateau, with the possible exception of Cys61.

4.2.3 Interactions of RRM2 with Guanine-Rich Elements

There are significant differences in the protein sequences of the three RRMs of CELF1, so it could not be assumed that they were all recognising the same site. Most of residues with large CSPs from the RRM1 titrations are conserved in RRM2, such as the two phenylalanine residues in the β-sheet, and one of the two cysteine residues in β3. There are some exceptions such as Gln22, which is replaced with methionine (Met114) in RRM2 and Gln93, which is replaced with valine (Val182). Our initial aim with RRM2 was to determine whether it was recognising a UGU site in the same manner as RRM1, or if it showed a

preference for a longer RNA sequence. The same titrations with the RNA substrates EDEN7 and UGU were carried out to determine this.

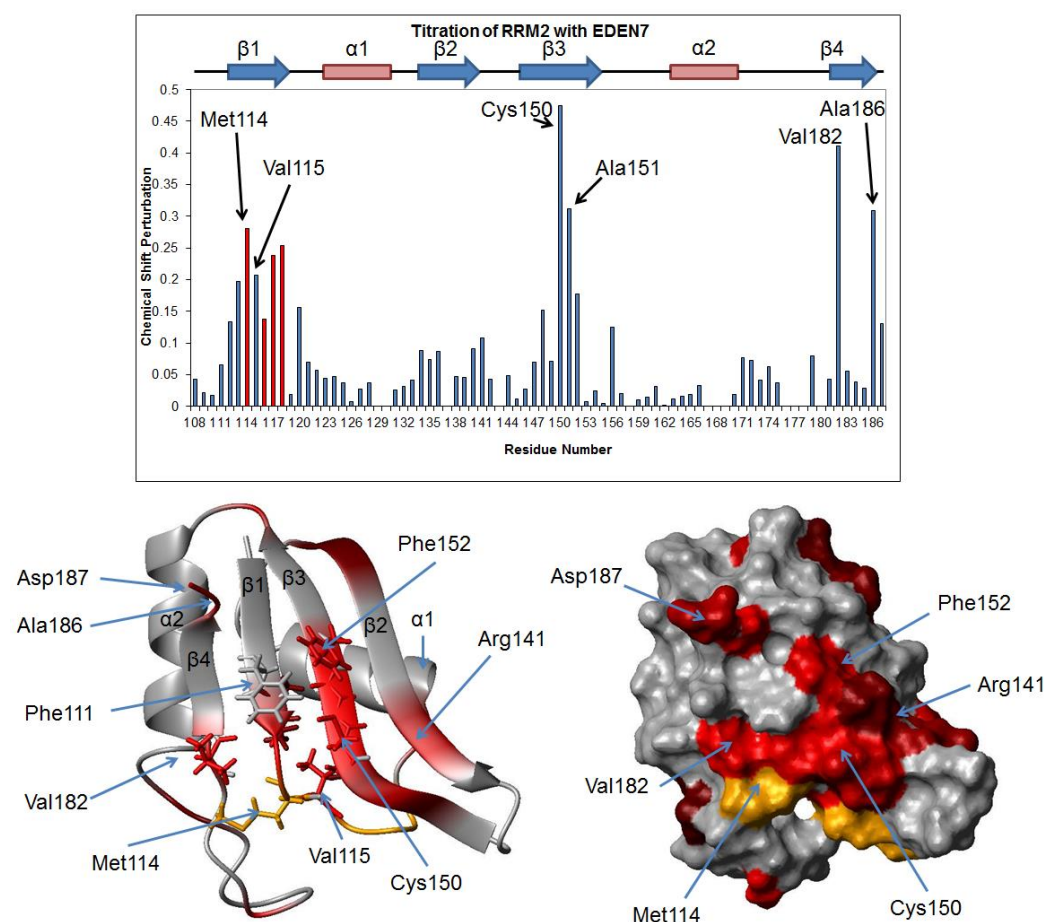


Figure 4.22: Above is shown a histogram of the CSPs for the titration of RRM2 with EDEN7. Values which are only minimum estimates, not exact values are highlighted in red. Also shown is the structure of RRM2, produced by truncation of Jun *et al.*'s solution structure of t187, with CSP values from the titration with EDEN7 mapped onto it. CSP values are shown in red with brightness of colour indicating magnitude of the effect. Residues with CSP values of <0.1 shown in grey. Residues for which only minimum CSPs are available due to loss of the peaks in slow exchange are shown in yellow. The overall protein concentration was 500 μ M.

As was the case for RRM1, the classic RNP regions of the RRM are the most affected, as well as some of the loops at the lower edge of the β sheet in Figure 4.22. The regions 112 - 120, 148 - 152 and 182 - 187 contain all those residues with CSPs of greater than 0.1. The most perturbed residue in RRM2 is Cys150, which is a conserved residue between RRM1 and 2 corresponding to Cys61 in RRM1. Cys61 was the most perturbed residue two of the three RRM1 titrations,

and the similar pattern of CSPs suggests the two RRMs are binding to the RNA in a similar manner. The non-conserved residues Met114 and Val182 are strongly affected, and so may be fulfilling the same role as Gln22 and Gln93 in RRM1. The C-terminal residue Asp187 (corresponding to Asp98 in RRM1) shows a moderate CSP, with a larger CSP seen for the preceding residue Ala186. The RRM2 construct was based on the existing t187 construct, resulting in a truncation point only two residues from the folded domain. Since this CSP map suggested some possible C-terminal involvement in RNA binding, the results were later checked with an extended construct (t242) to confirm no critical residues had been omitted at the C-terminus (see section 5.6.2).

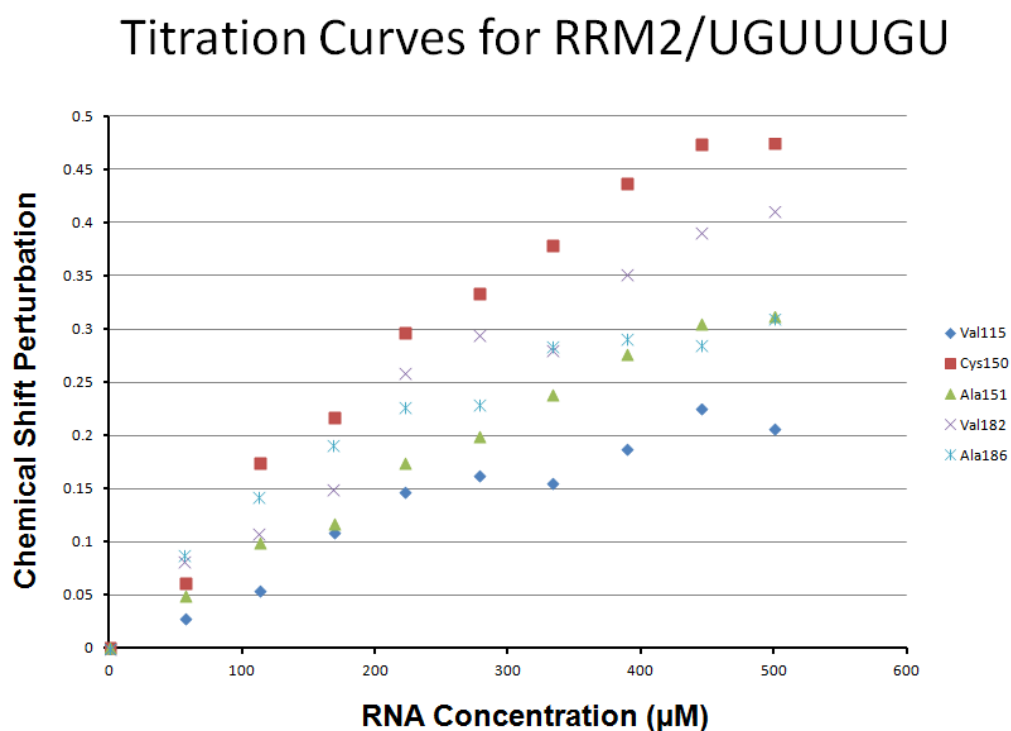


Figure 4.23: Binding curves for the RRM2/EDEN7 titration. Unlike the RRM1/EDEN7 titration this curve has clearly not reached a plateau by a 0.6:1 ratio of RNA to protein. The protein concentration was 500 μM .

There is one clear difference between the titration of RRM2 with the substrate UGUUUGU and the equivalent RRM1 titration. This titration had definitely not reached saturation point significantly before a 1:1 ratio of RNA to protein was

reached, as can be seen from the binding curves in Figure 4.23. This suggests that it is not possible to bind two RRM2 proteins simultaneously onto a single EDEN7 RNA molecule. The binding patch seen on the surface of the protein is not sufficiently large for RRM2 to be binding across both UGU sites in the EDEN7 substrate. Recognition of a fourth nucleotide could however be enough to prevent a second protein molecule from binding to the unoccupied UGU site. The implication of this was that RRM2 required a UGU(U/G) site rather than being able to tolerate a UGU site like RRM1.

This also has implications for the overall EDEN motif recognised by CELF1. In sequences such as the EDEN11 GRE there is only a single U between each of the UGU sites, just as in EDEN7. If RRM2 is obstructing binding to the adjacent UGU site to the one it is bound to, then it seemed unlikely it would be possible to bind both RRM1 and RRM2 onto the adjacent UGU(U/G) sites of the EDEN11 GRE. Since RRM2 did not appear to be forming a 2:1 complex with the EDEN7 substrate anyway, the titration with the UGUUUUAU sequence was not carried out. The data for the titration of RRM2 with the shorter UGU substrate is shown in Figure 4.24.

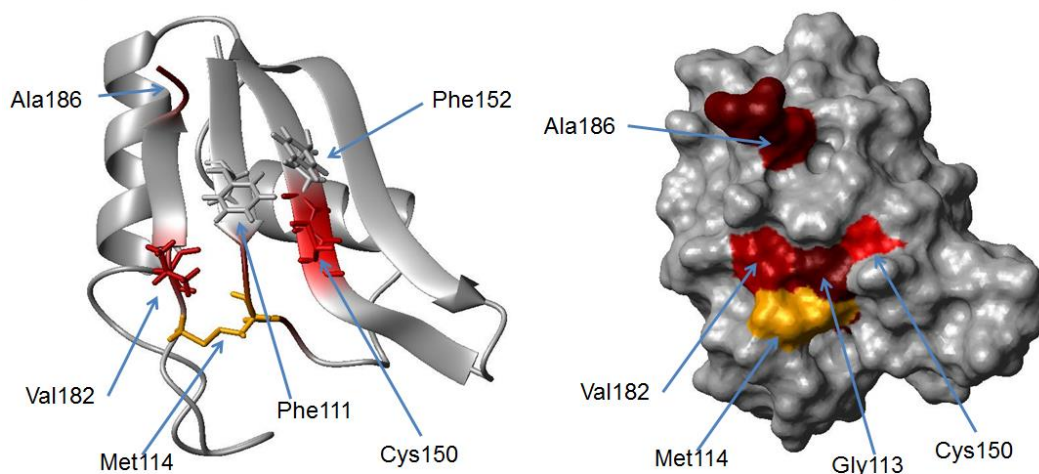
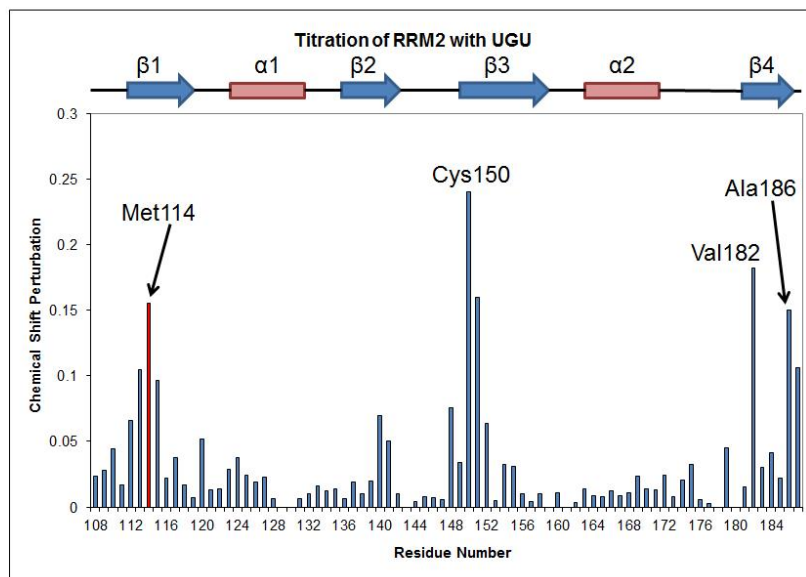


Figure 4.24: CSP data for the titration of 400 μM RRM2 with the RNA substrate UGU, acquired using a Bruker Avance III 600 MHz spectrometer. CSPs of greater than 0.1 ppm are regarded as significant and are shown in red, with brightness of colour indicating the magnitude. Residues which only have minimum CSP estimates are shown in yellow on the CSP map, and highlighted in red in the histogram.

Only a few residues in RRM2 show significant CSPs on titration with the shorter UGU substrate. Cys150 is the most affected residue again, with Gly113, Ala151, Val182, Ala186 and Asp187 also above the 0.1 ppm threshold. Met114 is again lost on titration, but the bound peak could not be located. Neither of the conserved aromatic residues Phe111 and Phe152 are significantly perturbed. Overall the binding patch is much smaller than that seen in the UGUUGU titration.

4.2.4 RRM3

The original intention was to carry out the EDEN7 and UGU RNA titrations on all three RRMs so they could be compared, and an isolated RRM3 construct was prepared for this purpose. However before the RNA titrations could be conducted Tsuda *et al.* (2009) published NMR and ITC studies on an isolated RRM3 construct both unbound and in complex with short UG rich RNA sequences. They determined that RRM3 was binding to the sequence UGUGUG with the highest affinity, with the core motif being UGU(U/G). The reported binding surface was somewhat larger than that seen for RRM1 and RRM2, and involved an N-terminal extension of the protein. These results implied RRM3 was recognising a longer sequence than the UGU site required for RRM1 binding, and possibly more than the UGU(U/G) site of RRM2. It would therefore not be expected to form a 2:1 complex with EDEN7. The binding affinity for these sites was significantly higher than seen for the isolated RRM1 and RRM2 constructs, with a reported K_d of 1.9 μM .

Tsuda *et al.*'s study of RRM3 also investigated binding other possible RNA substrates such as CUG repeat sequences, and adenosine rich elements (AREs) by NMR, which showed evidence of low affinity binding. ITC showed the K_d values for AREs to be around three orders of magnitude lower than the corresponding GREs. They were unable to detect any binding to the CUGCUG substrate by ITC.

4.2.5 Summary of NMR Titrations with GRE Sequences

It can be concluded that RRM1 is capable of binding to just the three nucleotides of a UGU site. Multiple copies of RRM1 can bind to UGU sites separated by only a single nucleotide, such as those in the UGUU repeating GRE RNA sequence.

RRM2 in contrast cannot bind to adjacent UGU sites separated by only a single nucleotide, consistent with it requiring a longer sequence such as a UGU(U/G) site. While some CSPs are seen on binding of RRM2 to the UGU substrate, their magnitude is greatly reduced compared to the corresponding EDEN7 titration, again suggesting a fourth nucleotide is required. Tsuda *et al*'s data on RRM3 indicates it is recognising at least four nucleotides in a UGU(U/G) site, and possibly as many as six (UGUGUG).

4.3 Interactions of CELF1 RRMs with CUG Repeat RNA Substrates

CELF1 was originally identified as an RNA binding protein by its ability to bind to a (CUG)₈ RNA probe. The higher affinity GRE sequences are more likely to be representative of the EDEN motif CELF1 recognises in its normal function, but the possibility of interactions with CUG repeat sequences is still of interest. In DM1 cells extended CUG repeat RNAs accumulate into foci, in which CELF1 is not found. It has however been proposed that a soluble fraction of these CUG repeat RNAs must also exist and may be interacting with CELF1, contributing to the DM1 phenotype. NMR titrations were therefore carried out to determine whether each RRM would bind to CUG repeat RNA. Also of interest was whether any binding patch found would overlap with that of the GRE substrates, resulting in competition between the two RNA substrates.

While these RNAs are usually described as CUG repeats, that does not necessarily mean that CELF1 is recognising a CUG site. The closest match to a UGU site in a CUG repeating RNA is the sequence UGC. When binding to a UGC site the first U and the G could then occupy exactly the same positions as when binding a UGU site. The second U would be exchanged for a C, which conceivably could occupy a similar part of the binding surface as they are both pyrimidines. If however CUG repeat sequences have a different binding patch on the protein, the number of nucleotides recognised might be completely different.

The RNA sequence CUGCUG was selected for these titrations as it contains a single UGC site.

4.3.1 RRM1

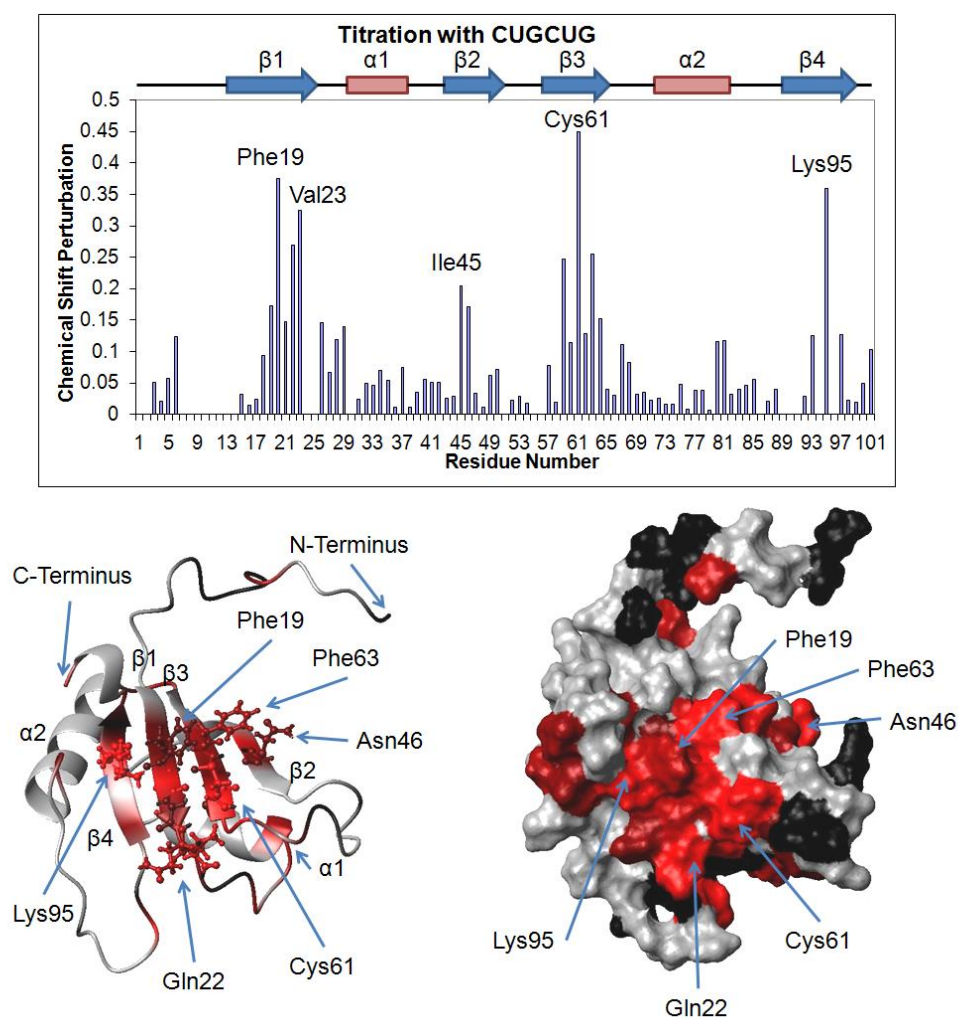


Figure 4.25: CSP map of RRM1 when titrated with CUGCUG. The protein concentration was 400 μM . Over the course of the titration the RNA concentration was raised to 450 μM in 50 μM increments.

RRM1 showed significant CSPs on titration with CUGCUG, confirming that it can bind to this type of RNA substrate. The titration reached an endpoint at around a 1:1 ratio of RNA to protein, as expected if a 1:1 complex is forming, and was entirely in fast exchange. It was immediately apparent that approximately the same regions of the protein were affected as in the titrations with EDEN7 and

UGU. Both of the aromatic residues Phe19 and Phe63 still show substantial CSPs, suggesting these stacking interactions are conserved between these RNA substrates. There are a few additional perturbed residues in the β 2 and β 4 strands, such as Lys95, Ile45 and Asn46 compared to the EDEN7 substrate, suggesting a slightly extended RNA binding surface.

Assuming RRM1 is recognising a UGC site, one potential explanation for this was that the RNA substrates selected were not the same length. In the EDEN7 RNA the UGU sites are at the ends of the sequence, while in CUGCUG the UGC site is in the centre, with additional nucleotides at both ends. The EDEN7 titration was repeated with an extended RNA substrate (EDEN9: UGUUUUGUU), which had an equivalent number of nucleotides on either side of the first binding site, but this did not show any similar increase in the CSPs for residues such as Lys95. A few additional residues from the bound form (in particular Val20 and Gln22) could however be located in the bound ^1H - ^{15}N HSQC.

4.3.2 Comparison of RRM1 Interaction with UGU and UGC Sites

In Figure 4.27 is shown a direct comparison between the CSPs for the CUGCUG and EDEN9 titrations. Residues with larger CSPs for CUGCUG are shown in red. Residues with larger CSPs for EDEN9 are shown in blue. Brightness of colour indicates the magnitude of the difference. Differences in the CSP values of less than 0.1 ppm are shown in grey, and treated as background noise.

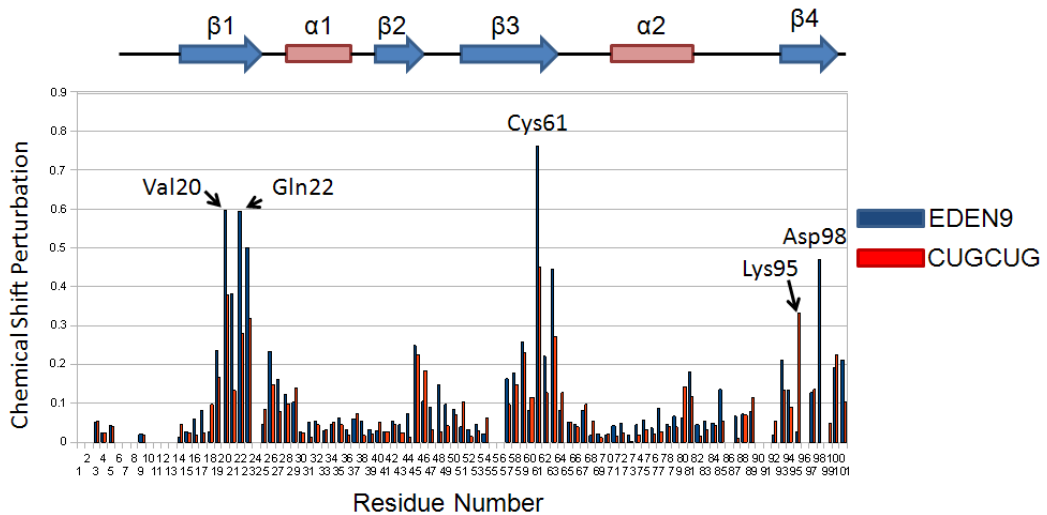


Figure 4.26: Direct comparison of chemical shift perturbations for titration of RRM1 with EDEN9 and with CUGCUG. For each residue the CSP for the EDEN9 titration is on the left in blue and the CSP for the CUGCUG titration is on the right in red. Some of the residues showing substantial differences between the two have been highlighted.

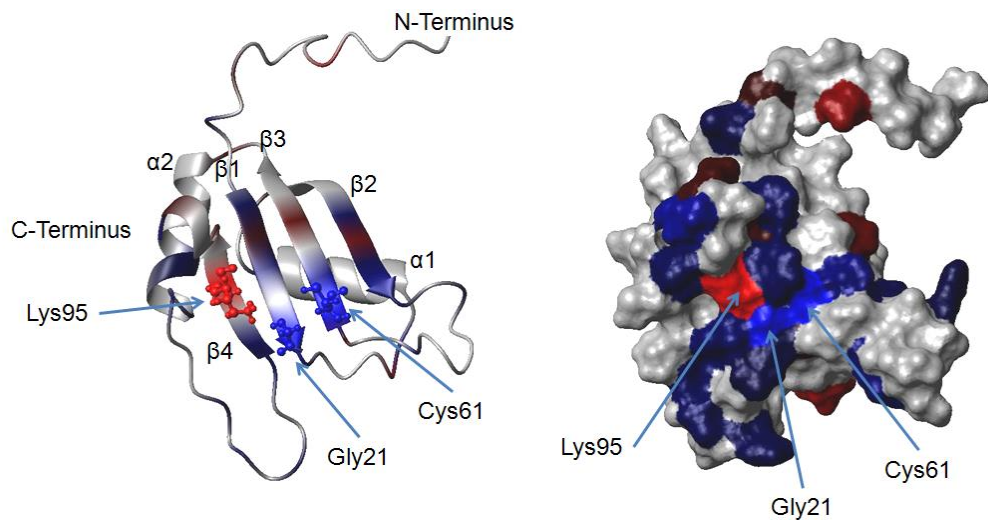


Figure 4.27: Map of the difference in CSPs in RRM1 between EDEN9 and CUGCUG substrates. Residues in red are more perturbed on addition of CUGCUG than EDEN9. Residues in blue are more perturbed by EDEN9 than CUGCUG. The brighter the colour, the greater the magnitude of the CSP difference. Residues in grey have less than a 0.1 difference in CSPs between the two cases.

The absolute magnitudes of the CSPs were in general somewhat larger for the EDEN9 substrate (with one clear exception for Lys95). A very similar pattern of affected residues is seen for the two RNAs, confirming they are occupying the same binding site on the protein, and so would be in competition. In both cases the most affected peaks are concentrated in the 19 - 23, 59 - 63 and 98 - 101 regions of the protein. The main RNP1 and RNP2 regions show significantly

larger CSPs when bound to the UGU site, as expected based on the overall preferences known for CELF1. The only residue with a dramatically larger CSP on binding to CUGCUG is Lys95 at the upper end of the $\beta 4$ strand.

Teplova *et al.* subsequently published a crystal structure of RRM1 in complex with a 13 nucleotide RNA substrate (UGUGUGUUGUGUG). Comparison of the bound conformation of this RNA with a repeating CUG sequence can help to rationalise some of the differences seen in the CSPs.

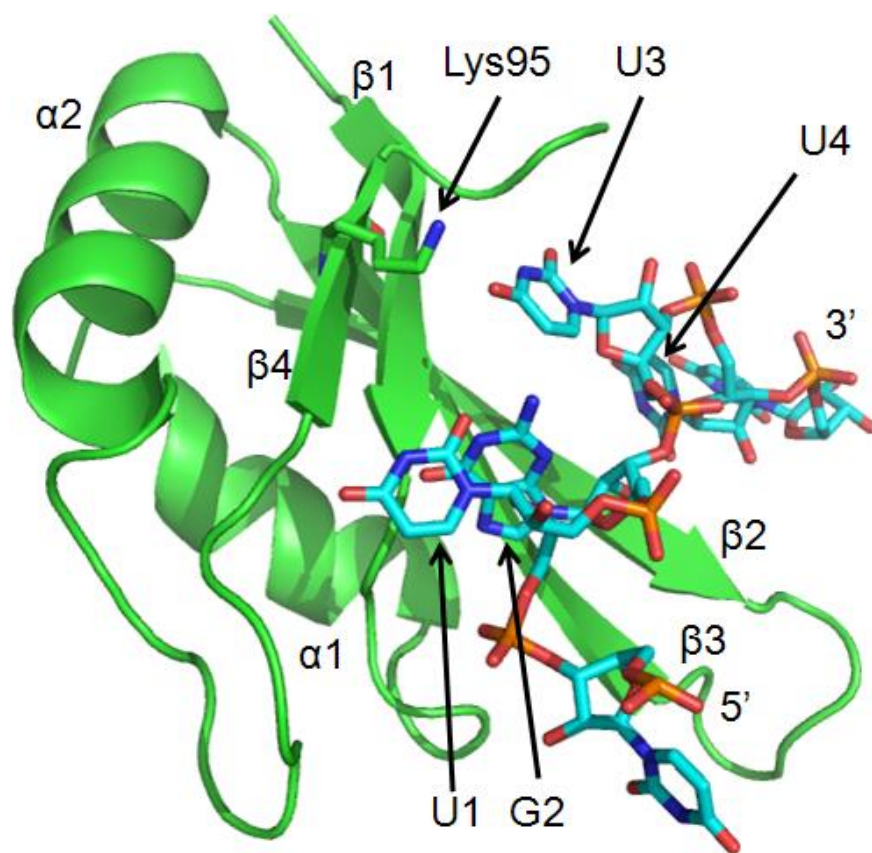


Figure 4.28: Structure of CELF1 RRM1 in complex with a UG rich RNA substrate, determined by Teplova *et al.* (2010) using x-ray crystallography. The position of Lys95 has been highlighted.

Based on this structure the increased disruption to Lys95 on binding to a UGC site can be rationalised, as this change would result in the carbonyl group on U3 closest to this residue being replaced with an NH_2 group.

4.3.3 Interactions of RRM2 with CUG Repeat RNAs

The comparison between the GRE and CUG repeat sequences was also conducted for RRM2. The protein concentration for these titrations was reduced to 400 μ M.

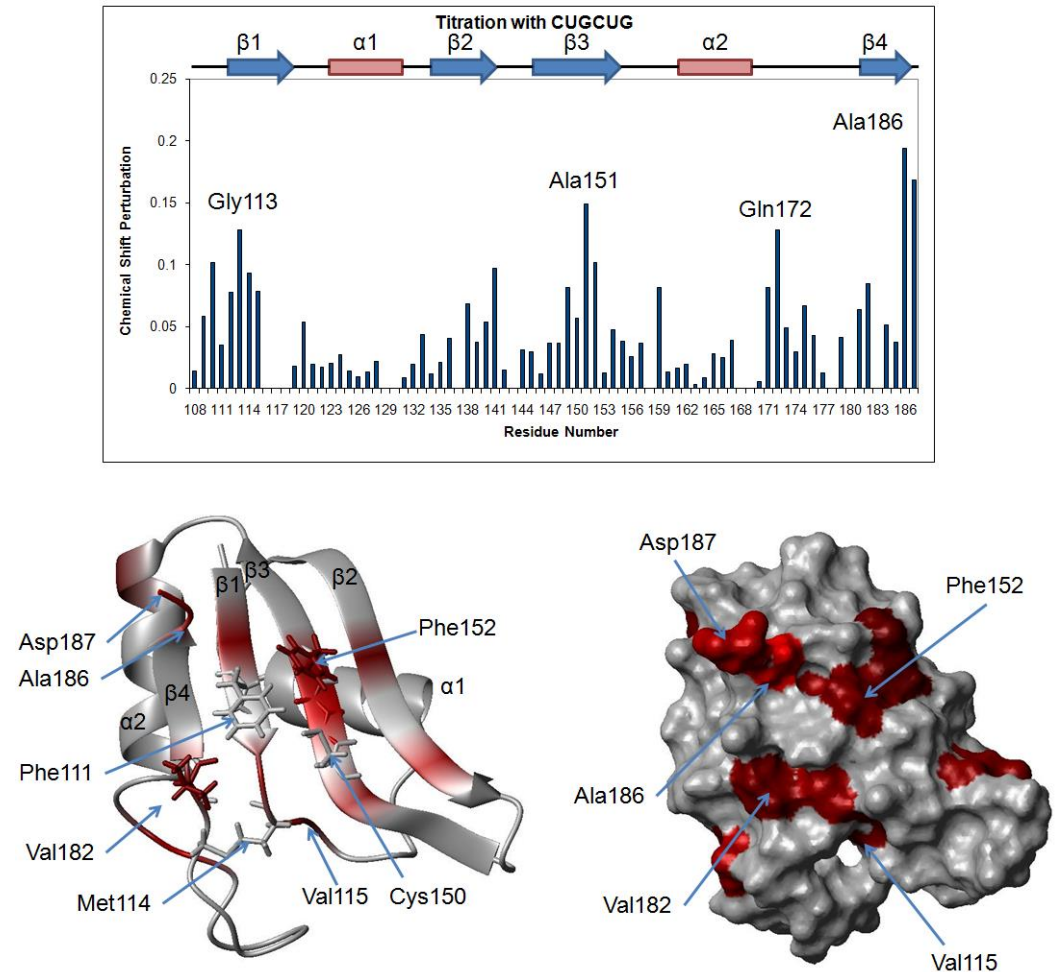


Figure 4.29: CSP data for the RRM2/CUGCUG titration. The CSP map shows all values greater than 0.05 in red as a colour gradient. The titration curve is consistent with a 1:1 complex.

While the usual RNP regions are still perturbed, the CSP values are in general reduced compared to those in the RRM2/EDEN7 titration. The RNP1 region of the protein in particular shows significantly reduced CSPs compared to the corresponding region in the RRM1/CUGCUG titration. Cys150 is no longer one of the most affected residues, which are now to be found at the C-terminus, specifically Ala186 and Asp187. Val182 also shows a limited perturbation of 0.1

ppm compared to 0.4 ppm in the titration with EDEN7. Met114 is not lost on titration as it was in the earlier titrations with substrates containing UGU sites.

While the CUGCUG substrate is still showing some limited interaction, RRM2 appeared to have more of a preference for UGU(U) sites over UGC(U) sites than was seen for RRM1. This difference cannot be accounted for by RRM2 recognising a fourth nucleotide, as in both titrations the base at position 4 would be U. RRM2 must therefore have a lower tolerance for the U to C substitution at position 3.

A side by side comparison for all residues is shown in Figure 4.30. Few residues in RRM2 show CSPs above the 0.1 ppm significance threshold when titrated with CUGCUG, and none are above 0.2 ppm, compared with Val115, Cys150, Ala151, Val182 and Ala186 in the titration with EDEN7. Unlike RRM1, there are no obvious examples of residues with much larger CSPs in the CUGCUG titration. Lys95 is a conserved residue between RRM1 and RRM2, but the corresponding Lys184 in RRM2 shows a CSP of less than 0.1 for both RNA substrates.

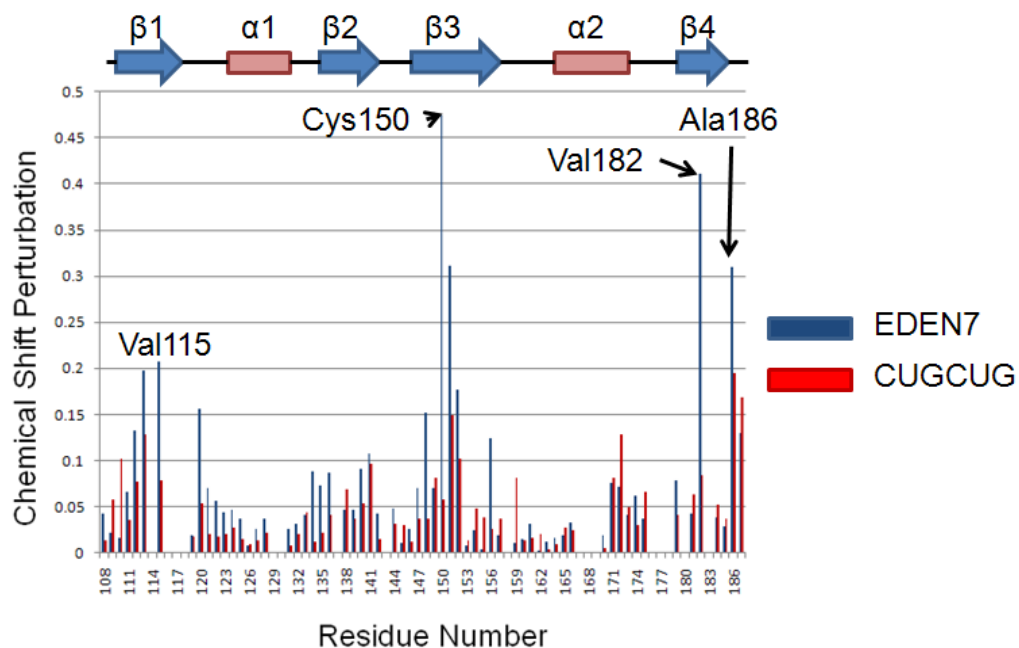


Figure 4.30: A comparison of the CSPs for each residue of RRM2 on titration with the RNA substrates EDEN7 (UGUUUGU) in blue and CUGCUG in red. Some of the residues showing significant differences have been highlighted.

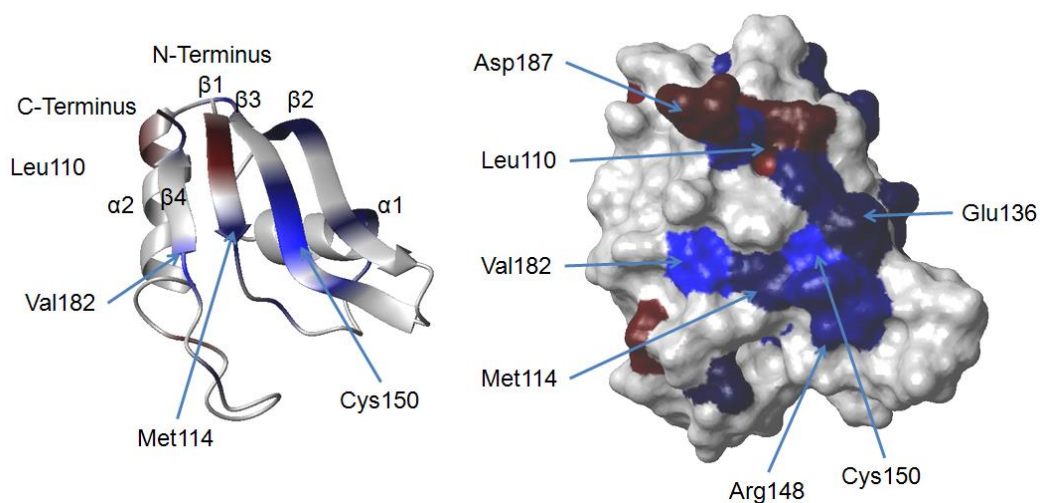


Figure 4.31: Map of the difference in CSPs between the EDEN7 and CUGCUG titrations onto the surface of RRM2. Residues in blue show a greater CSP on binding to EDEN7, residues in red show a greater CSP on binding to CUGCUG, with brightness of colour indicating the magnitude of the difference. Differences of less than 0.1 ppm are regarded as no significant, and the residues are shown in grey.

From this it can be concluded that UGC(U) sites are quite unfavourable for binding of RRM2. There is still some interaction, but the CSPs are greatly reduced overall.

4.3.4 Summary of Interactions between the CELF1 domains and CUG Repeat RNAs

For all three RRMs any interaction with CUG repeat RNA substrates appears to occur via the same RNA binding surface as the interaction with GRE sequences. These RNAs will therefore be in direct competition for binding, and if CELF1 does bind to the extended CUG repeat RNAs in DM1 cells it will interfere with the normal functions of the protein. It seems probable the RRMs are recognising a UGC(U) site in the sequence, as the closest match to the high affinity UGU(U) sites. There are noticeable differences between the three RRMs. RRM1 still shows quite large CSPs on binding to a UGC site, while RRM2 shows few residues above the 0.1 threshold. This suggests RRM1 is relatively tolerant of the U to C switch, while RRM2 is only interacting weakly with these sites. RRM3 was reported by Tsuda *et al* to have a much lower affinity for CUG repeats, suggesting most of the interaction with these substrates reported for CELF1 has been occurring via RRM1.

4.4 Interaction of CELF1 RRMs with Adenosine-Rich Elements

4.4.1 RRM1

The third category of RNA substrates reported to show at least some interaction with CELF1 was the AREs, particularly those containing UAU sites. The ARE equivalent of EDEN7 (UAUUUAU) was investigated.

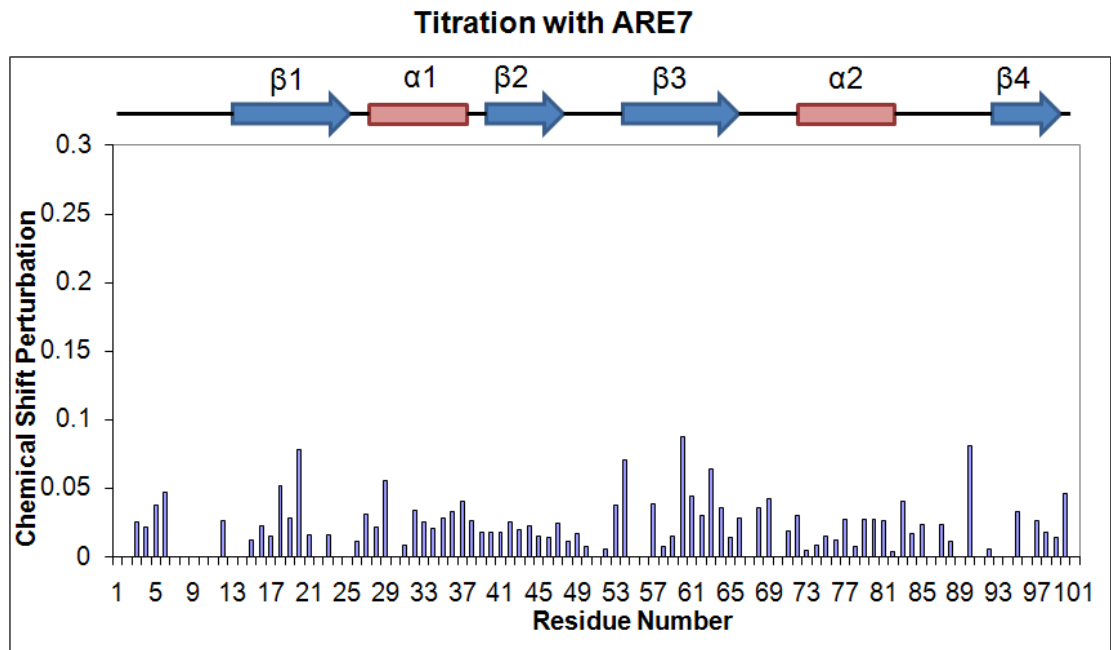


Figure 4.32: CSP values for a titration of ^{15}N RRM1 with ARE7. The protein concentration was 400 μM .

No residues showed CSP values above the 0.1 threshold. There is possibly some very slight disruption to residues such as Gly60 and Val20, but the low CSP values suggest this is a very weak non-specific interaction with the RNA. This experiment confirmed that this ARE7 sequence is not bound by RRM1. This also confirmed that ARE sequences are suitable for use as controls for this domain. The G to A substitution in UGUUUUAU should therefore have eliminated the second binding site in the earlier titration.

4.4.2 RRM2

Since RRM2 was suspected to be recognising a longer section of RNA from the GRE titrations, it was decided to use an extended ARE sequence; ARE15 (UAUUUAUUUAUUUAU) to ensure there were sufficient nucleotides on either side of at least one UAU site.

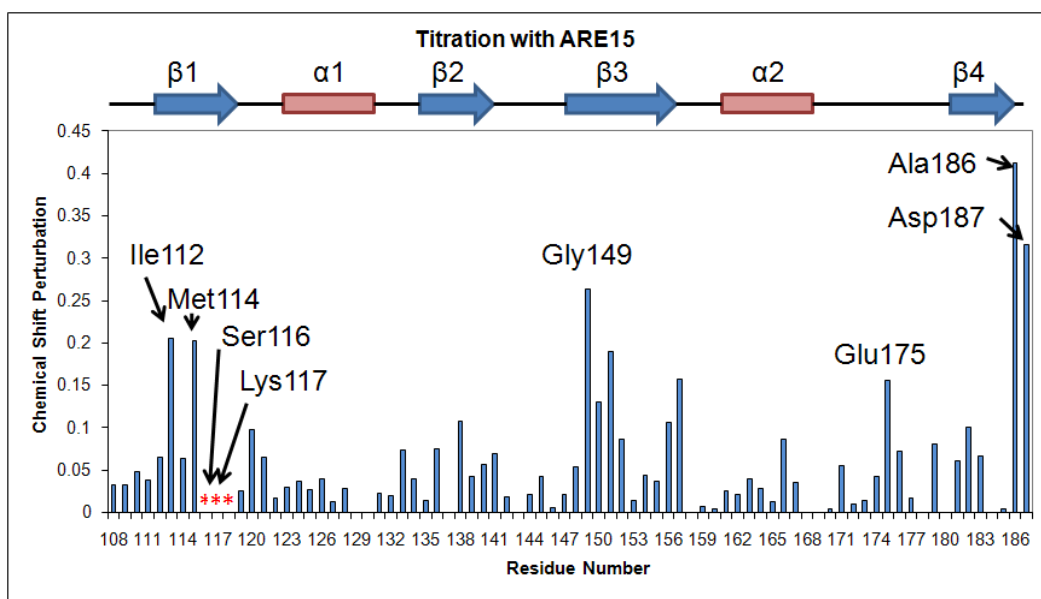


Figure 4.33: CSP values for a titration of ^{15}N RRM2 with ARE15. The protein concentration was $400 \mu\text{M}$. Red stars indicate peaks which disappear on titration, but no plausible peak corresponding to the bound form appears. These residues are therefore in intermediate exchange, and since none of the visible peaks correspond to the bound form it is not possible to calculate either an exact CSP, or estimate a minimum value for the CSP.

While the CSP values are substantially lower than for the titration with the EDEN7 sequence, in particular for residues such as Cys150 and Val182, there does still seem to be some weak/non-specific interaction between the RNA and the RNP1 and 2 regions of the protein. The overall intensities are significantly higher than those seen for the CUGCUG titration. Residues 186 and 187 are again the most affected, though these may have a tendency to be disproportionately perturbed as they form the flexible C-terminus. Substantially larger CSP values were seen in this titration than for the RRM1/ARE7 combination, where no residue showed a CSP of greater than 0.1. From this data it appears that RRM2 may have a greater tolerance for UAU(U) sites than RRM1.

4.5 Determination of Complex Stoichiometry by ESI Mass Spectrometry

The NMR data was supplemented using ESI mass spectrometry. This technique is useful for confirming the stoichiometry of complexes based on their overall mass. The NMR titration curves were ambiguous as to whether the EDEN7 and UGUUUUAU sequences could form 2:1 complexes with RRM1, so this point was clarified by ESI-MS.

4.5.1 RRM1

All mass spectrometry samples were produced from previously lyophilised and desalted protein by carrying out a second desalting step into 50 mM ammonium acetate. This was necessary to reduce the salt content to levels tolerated by ESI-MS. Without this second desalt step only very broad peaks could be observed due to a wide range of salt adducts of each species forming. All samples were run as native rather than denatured protein so the interactions with RNA could be investigated. Data was collected in both positive and negative ion mode since the negatively charged phosphate backbone of the RNA could potentially result in an overall negative charge on some complexes.

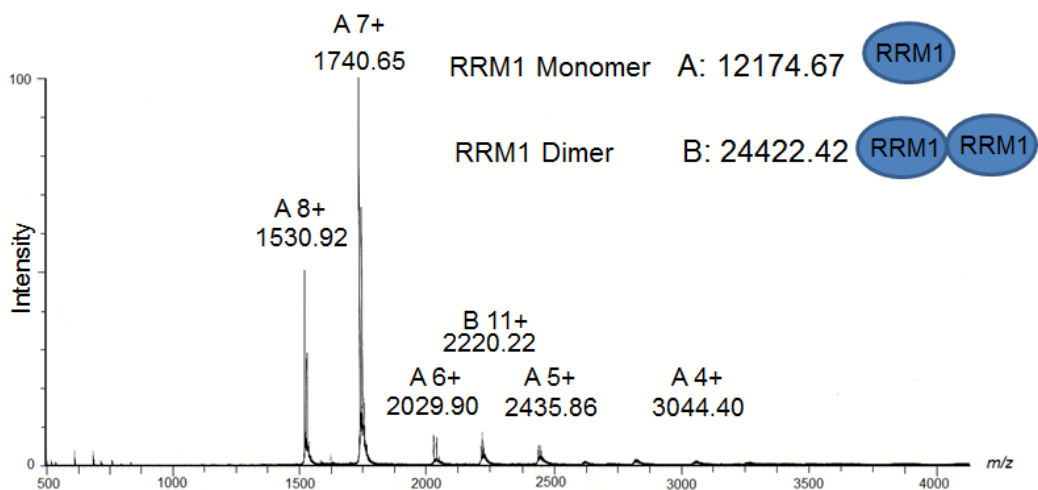


Figure 4.34: ESI mass spectrum of RRM1 only (sample concentration 10 μ M). One major species with a mass of 12174 Da seen. There are signs of a small population of a dimer, based on small peaks with apparent half-integer charge states at 5.5+ and 4.5+. While there is one report in the literature of *Xenopus* CELF1 forming a dimer, this was also stated only to occur in constructs containing RRM1, RRM2 and at least part of the RRM2 – RRM3 linker.

RRM1 has a theoretical mass of 12182 Da, allowing for the additional N-terminal residues left after thrombin cleavage of the histidine tag. Mass spectrometry showed one major species with a mass of 12174 Da. There were some intermediate peaks suggesting a small population of an RRM1 dimer may be present (theoretical mass 24364 Da). No evidence of dimerisation of RRM1 was observed by NMR or ITC, so this may be an artefact of the protein being in the gas phase.

To study the bound complexes RNA was added from a concentrated 5 mM stock dissolved in RNase free water to the sample of unbound RRM1 to a concentration of 2 μ M. On addition of the EDEN9 RNA substrate (UUGUUUGUU), the spectrum shown in Figure 4.35 was observed.

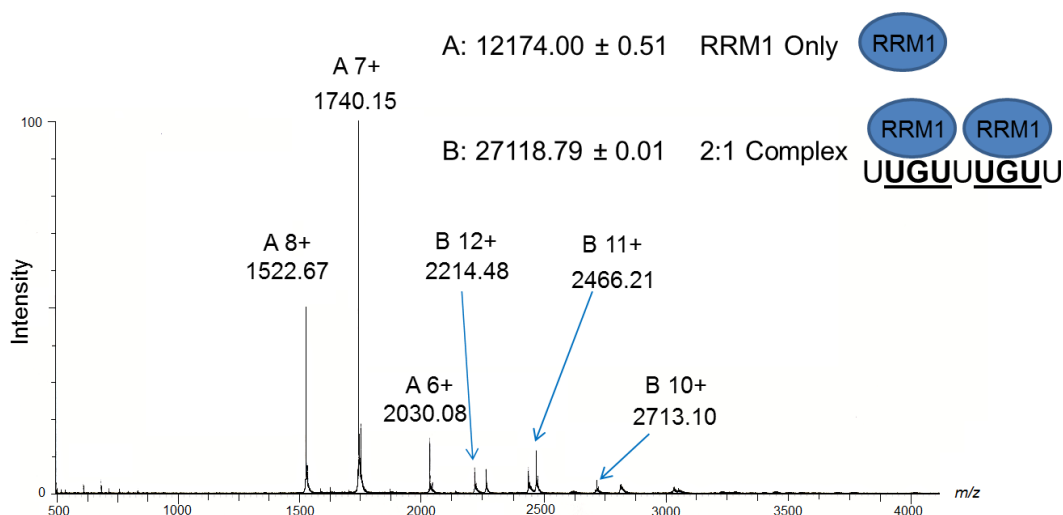


Figure 4.35: ESI mass spectrum of a mixture of RRM1 and EDEN9 (UUGUUUGUU), with RRM1 in excess. The protein concentration is 10 μ M, and the RNA concentration is 2 μ M. Two species seen, with masses of 12174 Da and 27118 Da. Species A is the unbound protein. Species B is a 2:1 complex of the protein and the RNA. No unbound RNA or 1:1 complex could be observed, but given the protein is in excess it would be expected that each RNA molecule would bind the largest number of proteins possible.

Two species were observed, one with a mass of 12174 Da and a second with a mass of 27118 Da. The first species is unbound protein (which is still in considerable excess in this experiment). The second species has a mass which is

consistent with a 2:1 protein - RNA complex (theoretical mass 27136 Da). No 1:1 complex is observed and also no unbound RNA. Since RRM1 is in excess, even allowing for the two possible binding sites, it is not surprising that the RNA would be saturated to form the 2:1 complex. ITC experiments with RRM1 binding to a UGU(U) site conducted by our group and Teplova et al. determined a K_d of 30 – 60 μM for this binding event. Under these conditions it would be expected that approximately 10% of the protein would be in the form of the complex, assuming that the binding of one RRM1 protein to EDEN9 does not interfere with the binding of the other. This experiment confirms that RRM1 can form a 2:1 complex with RNA substrates such as EDEN7. The experiment was then repeated with the EDEN7 knock out sequence UGUUUUAU. It was expected that this would have only one possible binding site for RRM1, and so no 2:1 complex would be observed. The results are shown in Figure 4.36.

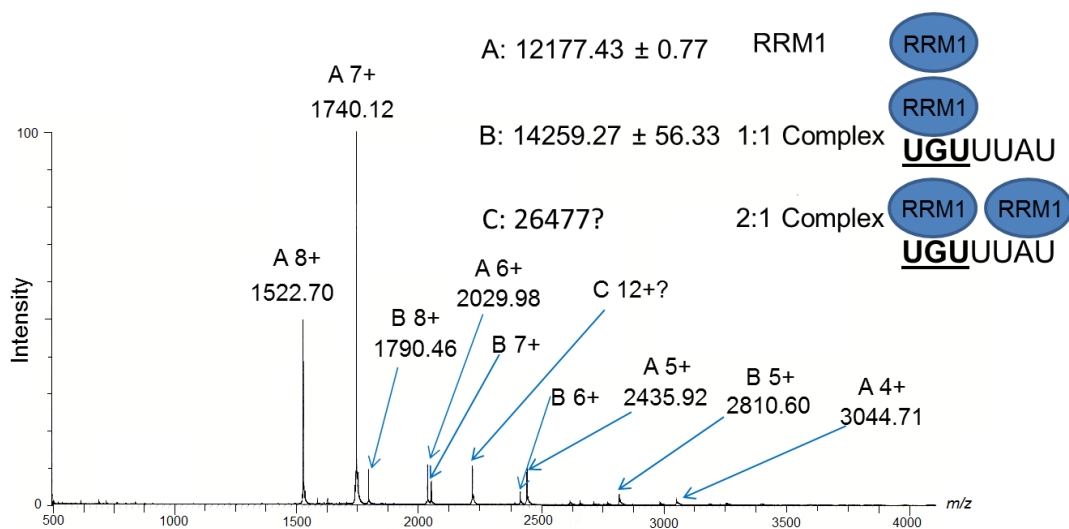


Figure 4.36: ESI mass spectrum of RRM1 + UGUUUUAU. The protein concentration is 10 μM and the RNA concentration is 2 μM . Two species, with masses of 12177 Da and 14259 Da were seen. One significant additional peak with an m/z of 2206 is present, but other charge states from this species could not be located.

RRM1 was again in a twofold excess, and the remaining unbound protein is visible as a species with an apparent mass of 12177 Da. A 1:1 complex of mass 14259 Da (theoretical mass 14340 Da) is definitely present with peaks from

charge states +5 to +8. A 2:1 complex would have theoretical mass of 26507 Da. One peak with an m/z of 2206 was observed and could not be accounted for by the other species, which would be consistent with the +12 charge state of a 2:1 complex, but other charge states of this species could not be located. The relatively large error margins on the mass of the complexes are believed to be due to sodium adducts of the RNA. While there may be a small population of the 2:1 complex present, the majority of the RNA formed a 1:1 complex, which was completely absent for the EDEN9 substrate. This is despite the presence of excess protein, which should encourage binding multiple proteins to each RNA molecule if possible. The switch from a UGU to a UAU site may not have totally eliminated the 2:1 complex, but has definitely made it much less favourable than the 1:1 complex.

4.5.2 RRM2

Native ESI mass spectrometry of RRM2 was also carried out, the results of which are shown below.

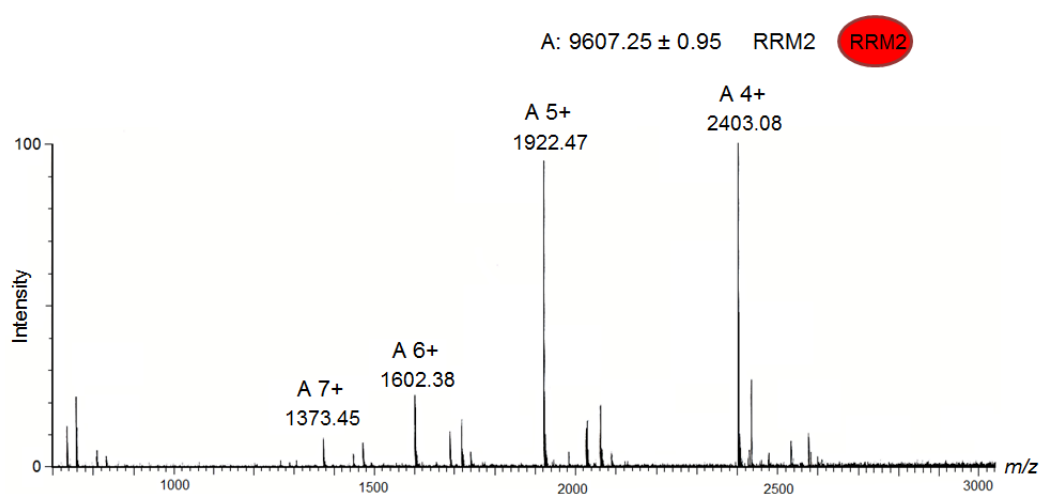


Figure 4.37: ESI mass spectrum of RRM2 only. Protein concentration estimated at 2 μ M based on mass of lyophilised protein used to produce a concentrated stock which was subsequently diluted. The lack of tryptophan and tyrosine residues in this construct results in a negligible absorbance at 280 nm preventing this from being confirmed by nanodrop, unlike the other constructs. One species was seen with a mass of 9607 Da.

RRM2 has a theoretical mass of 9613 Da (including the remaining N-terminal

residues GSHMASM after the removal of the 6-His-tag). A mass of 9607 Da was observed by ESI-MS, which is the unbound RRM2. Attempts were made to observe the complexes of RRM2 with EDEN9 and CUGCUG in order to confirm the stoichiometries, but these were not successful.

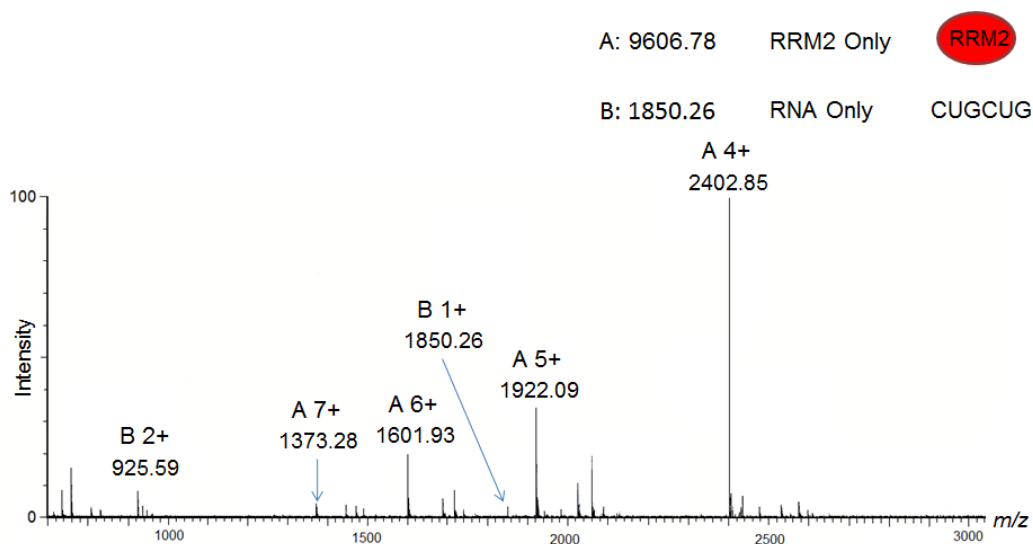


Figure 4.38: ESI mass spectrum of a mixture of 2 μM RRM2 and 1 μM CUGCUG. Two species were seen, of masses 1850 Da and 9607 Da.

Addition of the CUGCUG RNA to a concentration of 1 μM simply results in a new series of peaks from the unbound RNA appearing (theoretical mass 1851 Da). The same results were seen for addition of 1 μM EDEN9. We conducted ITC experiments on this system, and similar experiments were also published in 2010 by Teplova *et al.* Both sets of experiments showed the K_d for RRM2 binding to a UGU(U) site to be $\sim 60 \mu\text{M}$. Given this, only a small fraction of the protein ($\sim 1.5\%$) would be expected to be in the form of the complex, which may be insufficient to observe it. The exact K_d for binding of RRM2 to a CUGCUG sequence was not determined, but by NMR this interaction appeared to be of lower affinity than RRM2 with UGU(U). The K_d is therefore presumably larger than 60 μM , and the proportion of complex correspondingly even smaller, hence our inability to observe it in the mass spectrum.

4.6 Conclusions

RRM1 has been shown to be capable of binding to a three nucleotide site with the sequence UG(U/C). It can therefore bind to both UGU rich sequences such as the GRE and to single stranded CUG repeat RNA. Both RNA substrates have been confirmed by NMR CSP maps to bind to the same binding surface of the protein. The affinity for the UGU site appears to be higher than for UGC, but the difference is not as distinct as has been reported for RRM3 or for CELF1 constructs containing more than one RRM. This suggests RRM1 binds relatively promiscuously to RNA sequences, with the overall preference for U/G rich sequences being provided by at least one of the other RRMs of CELF1.

The EDEN7 sequence can accommodate two RRM1 proteins, but only one RRM2 protein, which suggests RRM2 requires a slightly longer RNA sequence for binding, such as UGU(U). The RRM2 titration with the shorter UGU substrate showed a greatly reduced binding patch compared to the UGUUUGU titration. The difference was not as pronounced in the RRM1 titration, again consistent with a fourth nucleotide being of greater importance for RRM2 binding than RRM1. Given the reported high affinity interactions with long UG repeat sequences RRM2 may tolerate some variation of the nucleotide at position 4 (i.e. a UGU(U/G) site). RRM2 appears to have a greater preference for UGU(U) sites over UGC(U) sites than was seen for RRM1. RRM2 did however show significant CSPs when titrated with UAU sequences (AREs) unlike RRM1. In combination the preferences of these two RRMs would account for the overall preference of the full length protein for U/G rich sequences which have high affinity sites for both RRMs rather than ARE or CUG repeat substrates which are unfavourable for at least one of the domains. Teplova *et al.* subsequently published crystal structures of RRM2 in complex with UGUU and UGUG sites and RRM1 in complex with a UGUU site⁵¹. Their reported structures of both domains show similar contacts to the base at position four when binding to the UGUU sequence, in the case of RRM1 to residues K17, N46 and F63, and in the case of RRM2 to K109, R138 and F152. When RRM2 was bound to a UGUG site

they report additional hydrogen bonds between the G4 base and E136. Superimposing these structures showed near identical conformations for the first three nucleotides, with greater variation seen for the fourth. The authors did observe a higher binding affinity by ITC for RRM1 than RRM2, consistent with our results, which they attribute to additional hydrogen bonds between the U1 and G2 nucleotides and residues Q22 and Q93 of RRM1, which do not have counterparts in RRM2 where neither of these residues is conserved. This could imply that in RRM1 contacts to the first three nucleotides (UGU) represent a greater contribution to the overall binding than in RRM2, diminishing the importance of the contacts to the fourth nucleotide for RRM1.

RRM3 has been reported to be capable of recognising up to six nucleotides, assisted by an interaction between the RNA and an N-terminal extension of the domain. Nothing similar was seen for these isolated RRM1 or RRM2 domains, but the possibility of this was investigated later on with longer protein constructs. Tsuda *et al.* identified a core motif of UGU(U/G) for RRM3, similar to our predictions for the preferred RRM2 target site.

As all three domains can recognise a variation on a UGU site, these results are consistent with the full length protein recognising a sequence of the GRE type. The fact that RRM2 cannot bind to adjacent UGU sites that are only separated by a single nucleotide does however suggest that UGUU repeating sequences such as the EDEN11 GRE may not be suitable for recognition of the full length CELF1 protein. The importance of the spacing between UGU sites when binding multiple CELF1 domains simultaneously was investigated, with the results shown in chapter 5.

5 Tandem RNA Binding of the two N-terminal Domains of CELF1

To be able to predict natural target sequences of CELF1, it was necessary to determine not only that each RRM was recognising a UGU or UGU(U/G) site, but also what separation was required between the sites to allow the domains to bind at the same time. This was investigated using a construct containing the two N-terminal domains of CELF1 (RRM1 and RRM2) and the UGU(U) site spacing in the proposed EDEN motifs EDEN11 and EDEN15 as a starting point. A series of RNA substrates containing two UGU sites with a variable number of nucleotides separating them (UGU(U)_xUGU) were then used to determine the exact range of spacer lengths tolerated for binding RRMs onto both sites simultaneously.

In order to trigger deadenylation and hence translational repression in cells, CELF1 must form a high affinity interaction with its target mRNA. The interaction of each RRM with its core binding site had been shown to be relatively low affinity, particularly for the two N-terminal RRMs. K_d values of 20 – 60 μM were later reported for each of RRM1 and 2 with a UUGUU substrate, significantly lower than the K_d of 1.9 μM reported for RRM3. An important question was therefore whether the binding affinity would be enhanced when multiple RRMs of CELF1 interact simultaneously with the same RNA molecule. If an enhancement of binding affinity was seen then there was also the question of whether the lower affinity RNA substrates (the CUG repeat sequences and the AREs) would show increased affinity when binding multiple RRMs in tandem, or would remain as unfavourable non-specific interactions.

Finally it was important to verify whether any regions of the protein other than the three structured RRMs were involved in RNA binding. RRM3 had been found by Tsuda *et al.* (2009) to have a flexible N-terminal extension which could fold

back to assist in binding to RNA. Similar N and C-terminal involvement in RNA recognition is seen in several structures of RRMs from other proteins^{42, 173, 174}. Flexible extensions of some RRMs have also been reported to be indirectly involved by the formation of additional structured regions in the presence of the RNA, which stabilize the overall structure^{175, 176, 177}. Since the isolated RRM1 and RRM2 constructs were truncated within a few residues of the structured regions, it was important to check that no similar flexible extensions of these domains had been removed. NMR studies to check for involvement of the N-terminus of RRM1, the C-terminus of RRM2, and the flexible linker between the two RRMs were therefore conducted.

5.1.1 Purification of a Construct of the N-terminal domains of CELF1

A construct consisting of the first 187 residues of CELF1 was used in this investigation, and has been termed the t187 construct. This consists of both the RRM1 and RRM2 domains connected as in the native protein by the short linker of residues 102 – 107, which was not present in either of the isolated RRM constructs. The t187 construct was originally produced by Dr Emilie Malaurie (University of Nottingham). The mass of this construct is 21.1 kDa, not including the N-terminal 6-His tag and the thrombin cleavage site. Test expressions were carried out at 30°C and 37°C, which showed the protein was overexpressed, and remained soluble at 30°C after a 16 hour induction. The protein was purified using the same methods as for the isolated RRM1 and RRM2 constructs, as detailed in section 3.7. SDS-PAGE showed the protein to be intact both in the cell, and at the IMAC column stage of the purification.

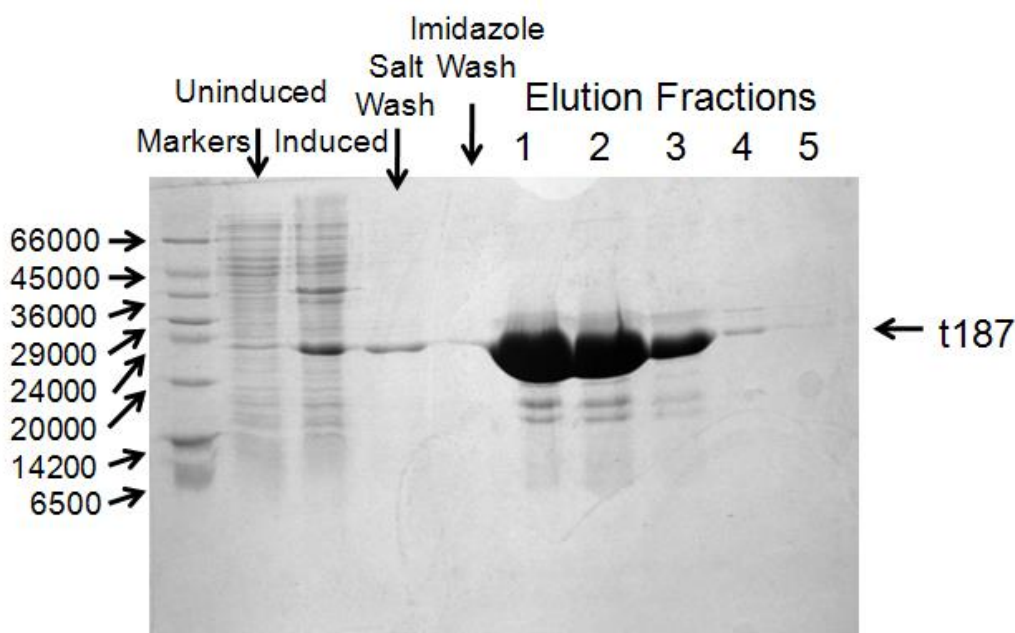


Figure 5.1: SDS-PAGE of the IMAC column washes and elution fractions from the first t187 purification. Low molecular weight markers (Sigma) are shown as a reference in lane 1, with the mass of each band shown in Daltons. Lanes 2 and 3 show diluted samples from the cell lysate of an uninduced growth, and a growth after a 16 hour induction. The t187 induction band is clearly visible. Lanes 4 and 5 show samples from the wash steps from the IMAC column stage. Lanes 6 – 10 show 2 ml elution fractions. The vast majority of the protein is eluted in the first 3 fractions.

The induction band can clearly be seen in lane 3, with a mass of approximately 24 kDa. A small amount of the protein was eluted by the high salt wash step (lane 4), and in later preparations the salt concentration used in this step was reduced from 2 M to 1 M in order to minimise this. The 1 mM imidazole wash (lane 5) did not cause any similar loss of protein. 0.75 M imidazole, 25 mM potassium phosphate, 50 mM NaCl, pH 7.0 buffer was used to elute the protein from the column. The bulk of the protein was eluted in fractions 1 - 3, though trace amounts are still visible in fractions 4 and 5. Significant quantities of impurities were still present, as can be seen by the additional bands in the SDS-PAGE for fractions 1 - 4, which were removed by the subsequent gel filtration step.

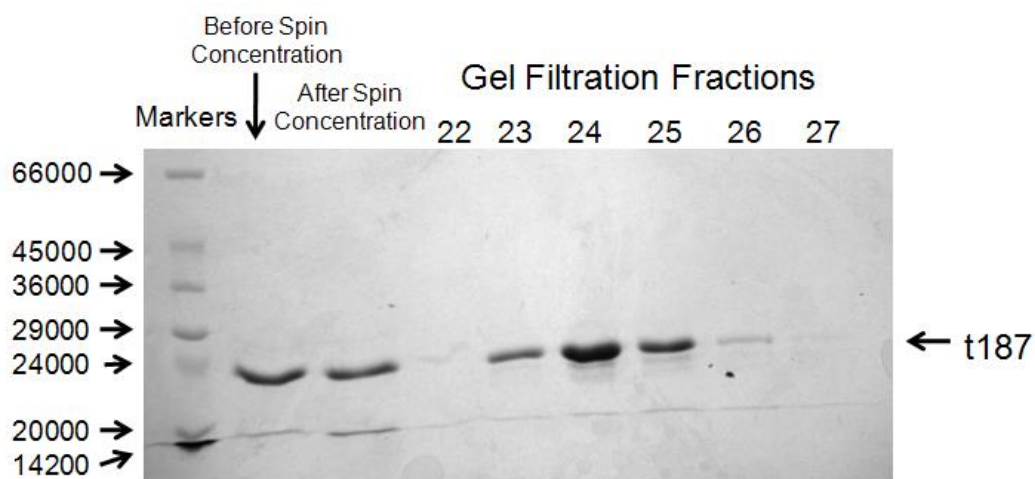


Figure 5.2: SDS-PAGE of gel filtration fractions from the t187 purification. T187 eluted from the Superdex 200 gel filtration column between 220 and 250 ml. There are still very faint bands from some impurities visible with a slightly lower mass than t187 that was not separated by the gel filtration.

Between the IMAC column stage shown in Figure 5.1 and the gel filtration stage shown above in Figure 5.2 the 6-His tag was removed with thrombin using the protocol in section 3.8. The tagged protein has a mass of 24911 Da, compared to 21719 Da after removal of the tag. The thrombin does not cleave immediately before the first residue of CELF1, but leaves the additional residues GSHMAS at the N-terminus, hence the slightly higher mass than for residues 1 – 187 alone. Comparison to the reference markers in the SDS-PAGE, and ESI mass spectrometry confirmed the tag had been successfully removed.

5.1.2 Comparison of the Isolated Domains and t187 Spectra

An initial 1D proton spectrum was collected on a Bruker Avance III 600 MHz spectrometer at 298K using unlabelled material. Lyophilised protein was dissolved in NMR buffer A. The dispersion of signals from the amide protons in this initial spectrum showed that the protein was correctly folded, with the downfield signals from Met94, Val183 and the Trp27 side chain clearly resolvable and matching their proton shifts from the isolated RRM. As the t187

construct has a mass of 21.7 kDa, the TROSY technique was used in all 2D and 3D NMR experiments to compensate for the faster relaxation rate compared to the isolated domains. High resolution ^{15}N TROSY spectra with well dispersed peaks could still be collected despite the larger size of the protein compared to the isolated RRM, and is shown in Figure 5.3.

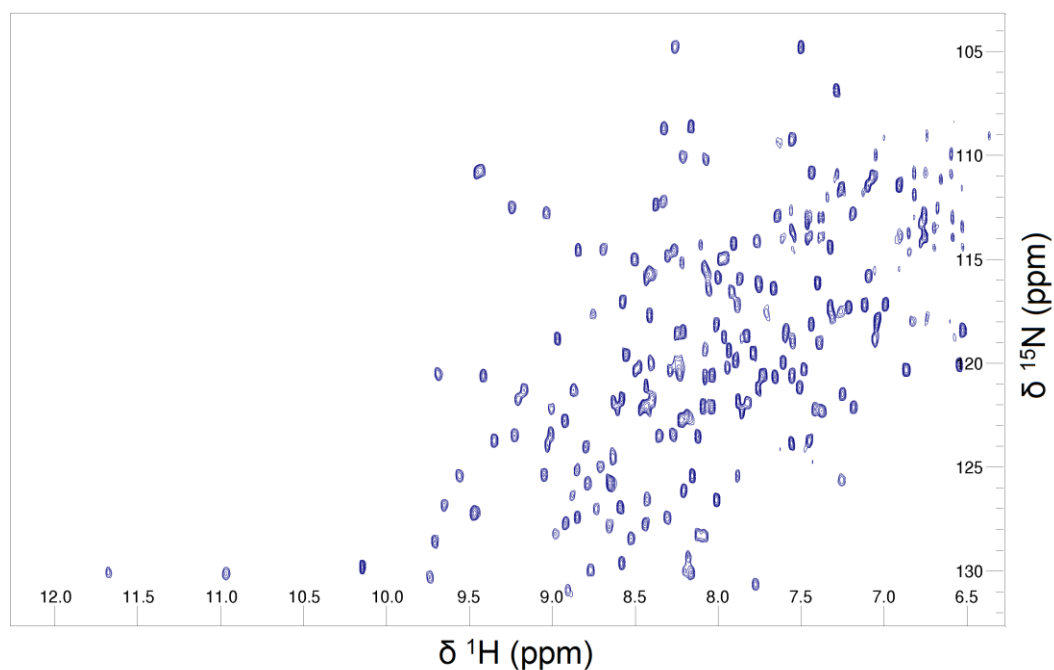


Figure 5.3: ^{15}N TROSY of t187, collected on a 500 μM sample using a Bruker Avance III 600 MHz spectrometer at 298 K. The sample was prepared by dissolving lyophilised protein in 25 mM potassium phosphate, 50 mM NaCl, 10% D_2O (v/v) pH 7.0 buffer.

In Figure 5.4 the ^{15}N TROSY spectrum of the t187 protein has been overlaid with those of RRM 1 in red and RRM2 in green.

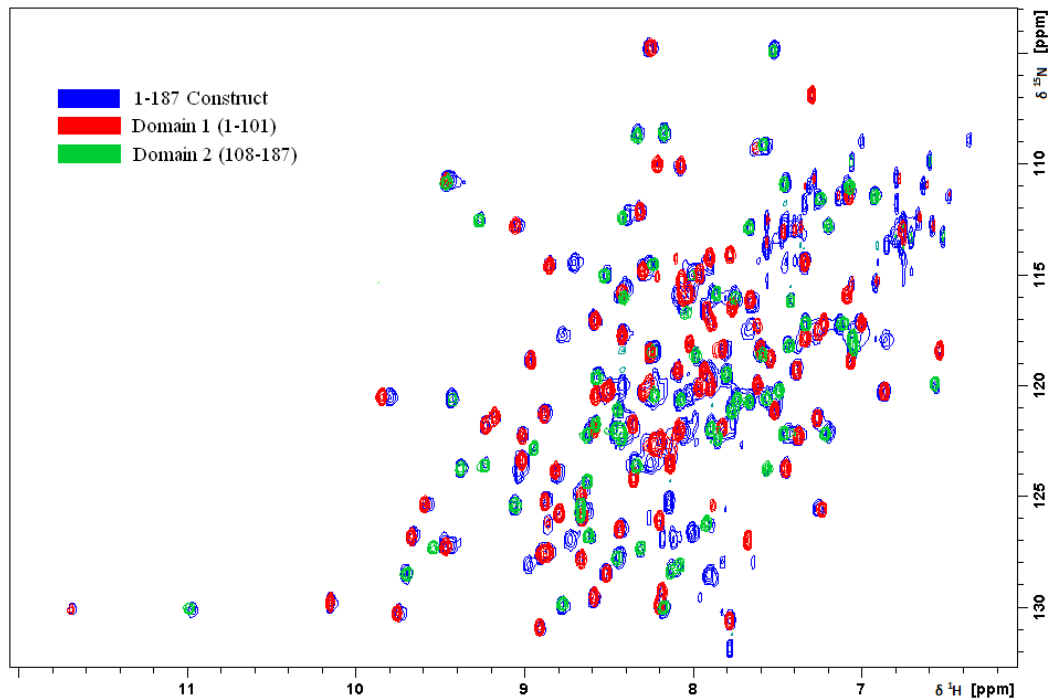


Figure 5.4: Overlaid ^{15}N TROSY spectra of t187 in blue, RRM1 in red and RRM2 in green. Virtually all the RRM1 and 2 peaks match to peaks in the t187 spectrum, confirming the chemical shifts of the residues have not been significantly perturbed by splitting the protein into two fragments. A small number of peaks are only seen in the t187 spectrum and are due to the linker region (102 - 107) which is not present in either of the smaller constructs.

The vast majority of peaks from the two isolated domain constructs overlay very closely with the corresponding peaks from the t187 construct. It can be concluded that the removal of RRM2 therefore has no effect on the environment and hence the chemical shifts of the residues in RRM1, and vice versa. This confirms that despite the short linker between them, the two domains of the protein are free to move fairly independently of each other, at least when not bound to RNA. This also aided assignment of the t187 spectrum, since in most cases assignments could be transferred directly from the spectra of the isolated RRMs.

A few residues do show very substantial changes in chemical shift, for example Lys101 (the RRM1 C-terminal residue), Arg108 and Lys109 (the RRM2 N-terminal residues), but since the environment of these residues changes from being in the middle of the protein sequence to being at the terminal regions this

was not surprising. In order to assign these residues, and those in the linker which were not present in either the RRM1 or RRM2 constructs, 3D heteronuclear NMR data was collected on the t187 construct.

5.1.3 Assignment of the ^{15}N TROSY Spectrum

NMR data on the first 187 residues of human CELF1 had previously been collected (Jun *et al.*, 2004), but there are still enough variations in chemical shifts compared to *Xenopus* CELF1 that assignments in the more crowded regions could not simply be transferred. There were also some missing assignments, such as the downfield peaks at >10 ppm which are not seen in Jun *et al.*'s human CELF1 NMR spectrum, possibly due to the collection of data over a spectral width range that was too narrow. For assignment purposes t187 was both ^{13}C and ^{15}N labelled by growing in M9 minimal media with appropriately labelled carbon and nitrogen sources. The purification yield was reduced to 13 mg/l, comparable to the yields of the isolated RRMs. HNCACB, HN(CO)CACB, HNCO, HN(CA)CO and HCCH TOCSY spectra were collected, allowing assignment of the linker region. Those assignments transferred from the spectra of the isolated RRMs were also verified using this 3D heteronuclear NMR data. All non-proline residues were assigned except for Met1, Asp12 and Ser178.

5.2 Interactions of the N-terminal Domains of CELF1 with Tandem UGU Sites in Guanine Rich Elements

By titrating an RNA substrate into ^{15}N labelled t187 protein, and collecting ^{15}N TROSY NMR spectra, it was possible to tell whether each of the domains was interacting with the RNA. If CSPs were seen in both RRMs, it would indicate they were both binding to the RNA, and so that the RNA substrate contained UGU sites with suitable spacing for CELF1 recognition. In contrast if CSPs were only seen in one, then the separation between the UGU sites was not suitable for tandem binding of the domains.

The EDEN11 GRE and EDEN15 consensus sequences reported by Vlasova *et al.* (2008) and Graindorge *et al.* (2008) respectively were proposed to be capable of forming a high affinity interaction with wild type CELF1, and so would be expected to be capable of binding both domains of the t187 construct in tandem. These sequences are shown in

Table 5-1, and contain up to four UGU sites in the case of EDEN15. By removing one UGU site at a time it was possible to deduce which of the possible UGU sites were involved in binding to these sequences, and so the spacing between them. With this as a starting point a series of RNAs with shorter and longer spacers between UGU sites were systematically investigated to find the exact range of spacer lengths that would permit both the N-terminal domains of CELF1 to bind in tandem. These RNAs were of the form UGU(U)_xUGU, where x is varied to alter the spacer length. The range of RNAs of this type used in this study is also listed in

Table 5-1.

RNA	Sequence
EDEN15 GRE	<u>UGUUUGUUUGUUUGU</u>
EDEN11 GRE	<u>UGUUUGUUUGU</u>
EDEN7	<u>UGUUUGU</u>
EDEN2U	<u>UGUUUUGU</u>
EDEN3U	<u>UGUUUUUGU</u>
EDEN4U	<u>UGUUUUUUGU</u>
EDEN5U	<u>UGUUUUUUUGU</u>
EDEN6U	<u>UGUUUUUUUUGU</u>
EDEN7U	<u>UGUUUUUUUUUGU</u>

Table 5-1: This lists the RNA substrates used in determining the UGU site spacing requirements for binding the N-terminal domains of CELF1 simultaneously. The positions of all UGU sites in the sequences have been underlined.

5.2.1 Interaction of the N-terminal Domains of CELF1 with the EDEN15 GRE.

In this titration, and all subsequent titrations with this protein construct, a 400 μM ^{15}N labelled t187 sample was prepared in 600 μl of NMR buffer A. The RNA concentration was raised in 50 μM increments by addition of 6 μl aliquots from a 5 mM stock dissolved in RNase free water. A ^{15}N TROSY spectrum was collected at each titration point on a 600 MHz Bruker Avance III spectrometer at 298K. Titrations were terminated once no variation could be seen between two successive spectra. In all cases this occurred shortly after a 1:1 ratio of RNA to protein was reached.

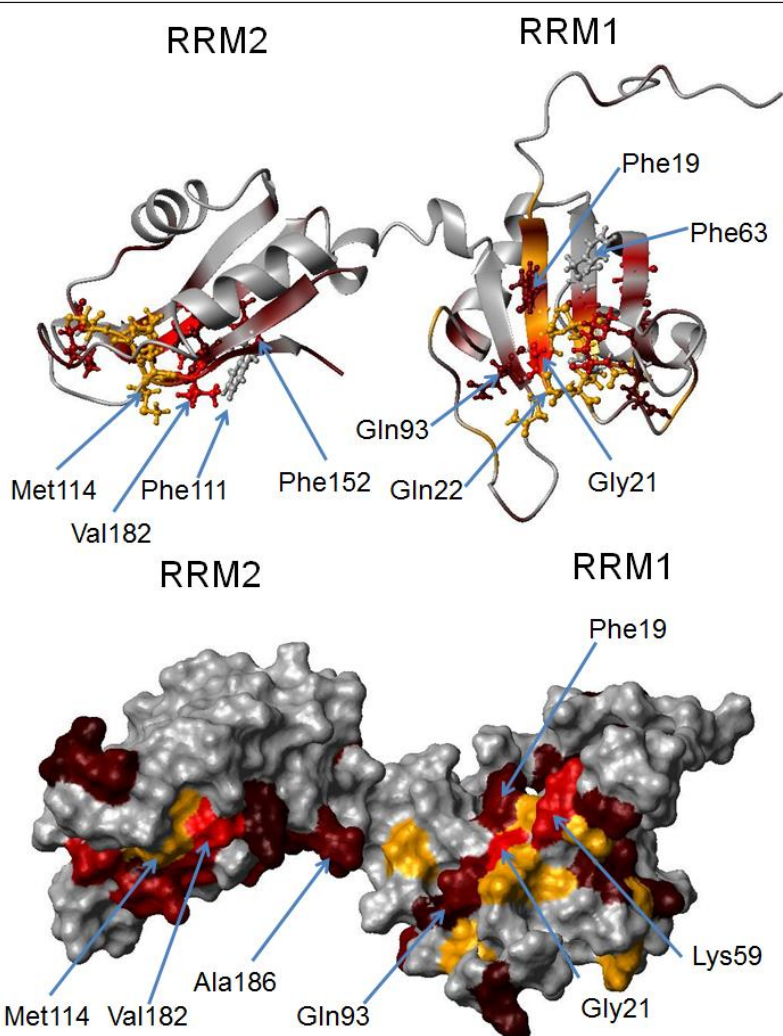
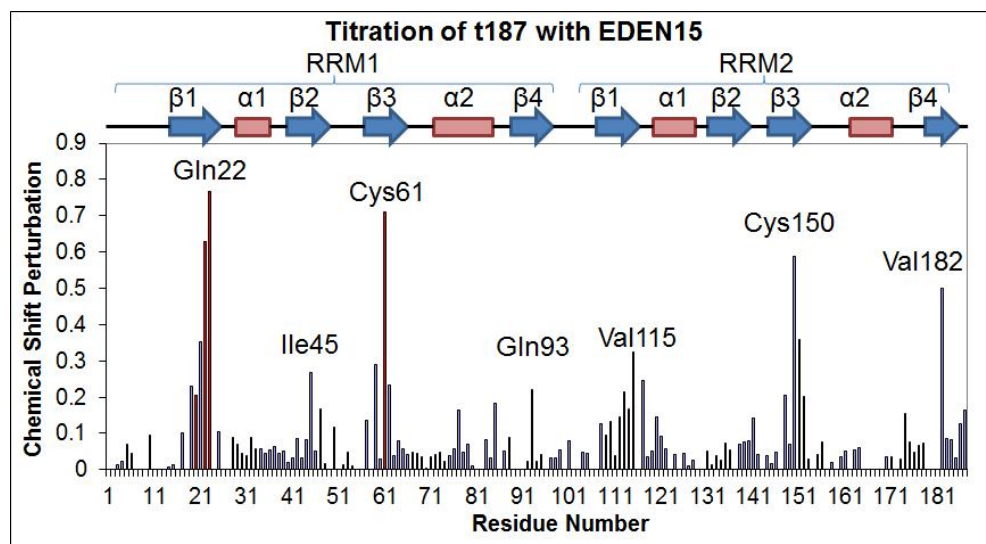


Figure 5.5: Graph of the CSP for each residue at the endpoint of the t187/EDEN15 titration. Also shown is a CSP map of the affected residues, with red indicating the most affected residues and yellow indicating residues with estimated minimum CSPs. The protein concentration was 400 μ M, and the titration was continued until no further variation in the spectrum was seen between titration points.

A mixture of residues in fast and slow exchange is seen. As was the case in the titrations with the isolated RRMs it was not always possible to locate the signals from the bound form for certain residues. This was due to a combination of signal overlap in crowded regions of the spectrum, and certain residues which did not appear to show a signal in the bound form (e.g. Met114).

Chemical shift perturbations are seen in both RRMs, confirming that the EDEN15 GRE is binding both the N-terminal domains of CELF1 in tandem. In RRM1 the affected residues are a similar set to those seen in the earlier RRM1/UGU titration. The β 1 and β 3 strands show several strongly affected residues, in particular Val20, Gly21, Gln22, Cys61 and Cys62. Of the two conserved aromatic residues on the β -sheet Phe19 shows a significant CSP of just over 0.2. However Phe63 has a negligible CSP of less than 0.05 contrasting with one of >0.1 in the RRM1/UGU titration. In β 2 there are significant CSPs for Ile45 and to a lesser extent Val47, suggesting an extended RNA binding surface across this part of the β -sheet. In β 4 only Gln93 shows a CSP above the 0.1 threshold. Asp98, which was an affected residue in slow exchange in the RRM1/EDEN7 titration, has a negligible CSP and does not appear to be involved in binding. Neither of the α -helices contain any affected residues.

In RRM2 CSPs are again concentrated in the β 1 and β 3 strands, in particular Gly113, Met114, Val115, Cys150 and Ala151. As with RRM1 only one of the two conserved aromatic residues on the β -sheet (Phe152) shows a significant CSP. Phe111 in contrast has a CSP of <0.05 . In β 4 Val182 is very strongly perturbed, as was the case in the isolated RRM2 construct. The α -helices do not have any affected residues, and there is also little disruption to the β 2 strand.

5.2.2 Interaction of the N-terminal Domains of CELF1 with the EDEN11 GRE.

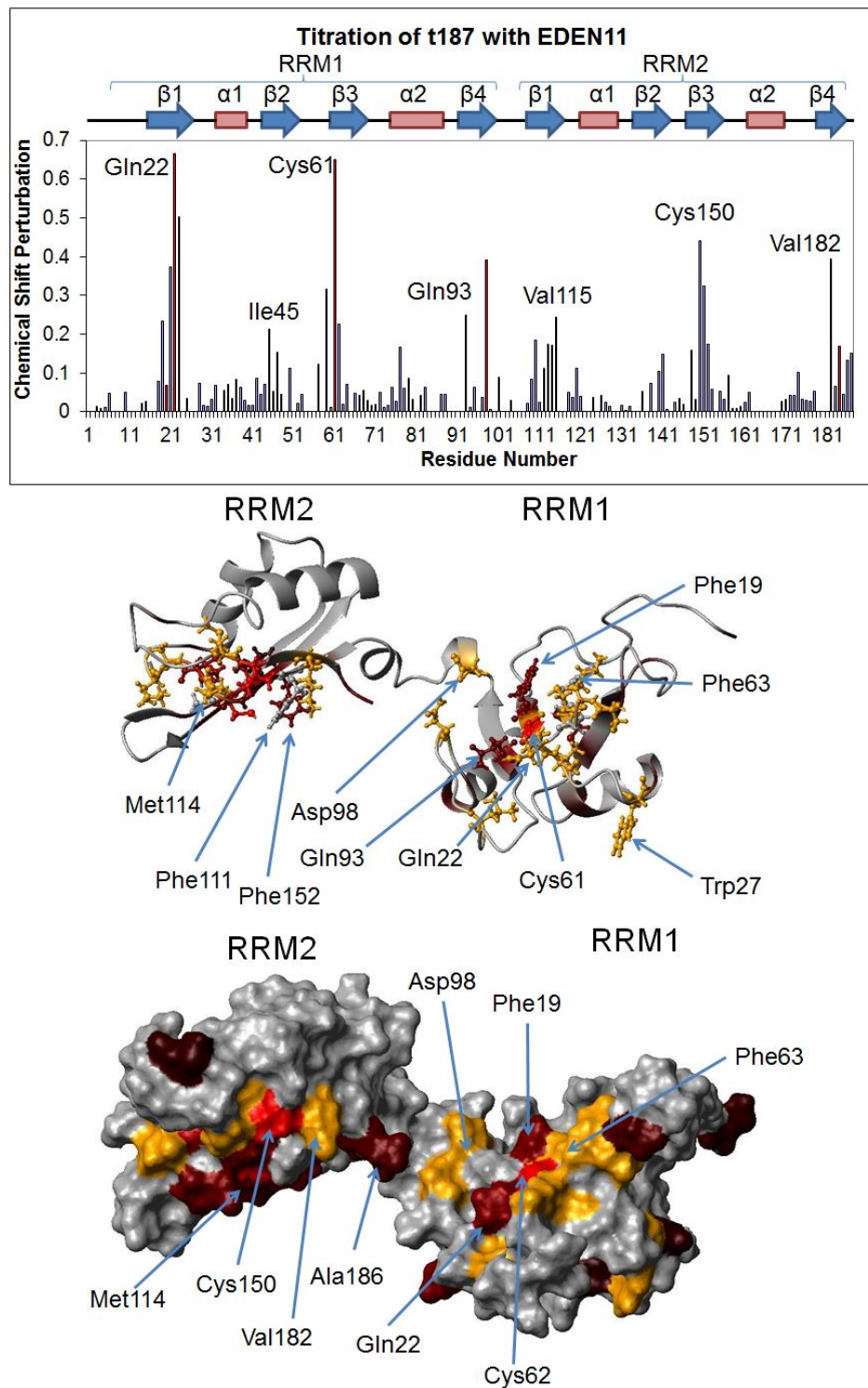


Figure 5.6: Graph of chemical shift perturbation for each residue at the endpoint of the t187/EDEN11 titration. A large number of residues in this titration appear to be in intermediate exchange, and so the peak from the bound form remains broadened out. This prevents minimum CSP estimation for many residues – estimates have been included for residues such as Gln22 where a plausible peak is present in the bound spectrum. These residues are shown in yellow in the CSP map.

The RNA sequence was shortened by one UGU(U) site to UGUUUGUUUGU, which corresponds to the EDEN11 GRE. The results of this titration are shown in Figure 5.6. Again there is a mixture of residues in fast and slow exchange. Significant CSPs are seen in both RRM, confirming this RNA substrate is binding both domains in tandem. The set of affected residues is generally the same as was seen for the EDEN15 GRE with few exceptions. The most noticeable difference is that Asp98 is now affected, though overlap of this peak in the bound form prevents accurate quantification of the CSP.

5.2.3 Interaction of the N-terminal Domains of CELF1 with the EDEN7 GRE.

The RNA was shortened by a further UGU(U) site to UGUUUGU (EDEN7). Unlike the previous titrations, where the affected signals were predominantly in fast exchange, this experiment appeared to show an intermediate exchange situation for most of the normally affected residues. In intermediate exchange the rate constant k is approximately equal to the difference in chemical shifts between the free and bound forms ($\delta\nu$)¹⁷⁸. This results in extremely broad signals at a population weighted average of the chemical shifts. In this case the signals for those residues with large $\delta\nu$ rapidly broaden out, but are not recovered, suggesting the intermediate exchange situation is broadening the peaks to an extent where they are not observable above the background noise. The lack of peaks specific to the bound form prevented direct CSP determination, or minimum CSP estimation based on the closest unknown peak.

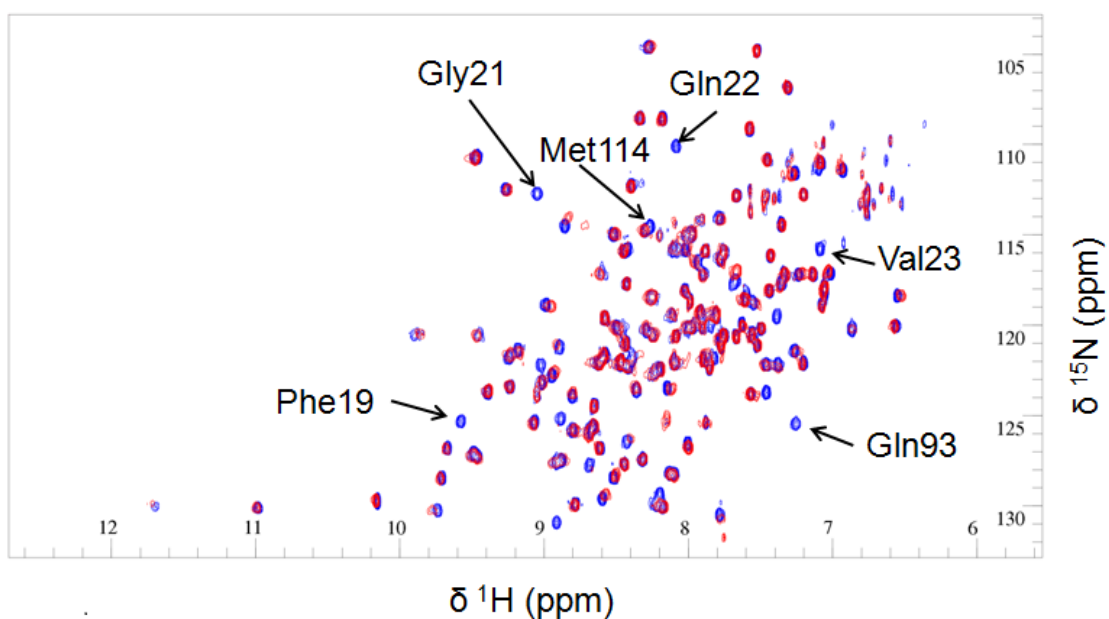


Figure 5.7: Overlaid ^{15}N TROSY spectra of t187 unbound (shown in blue) and after titration to a 1:1 ratio with EDEN7 (UGUUUGU – shown in red). Few peaks are seen to move in fast exchange over the course of the titration, and none of those in fast exchange show CSPs of >0.1 . A number of peaks are however lost, and therefore these residues must have a greater change in environment, resulting in an intermediate exchange situation. This permits the most affected region of the RNA binding surface to be identified, but without bound peaks no CSPs can be estimated.

The binding patch, and hence which domains were bound to the RNA could be identified based on which peaks from the free form were lost during the titration. This is shown in Figure 5.8.

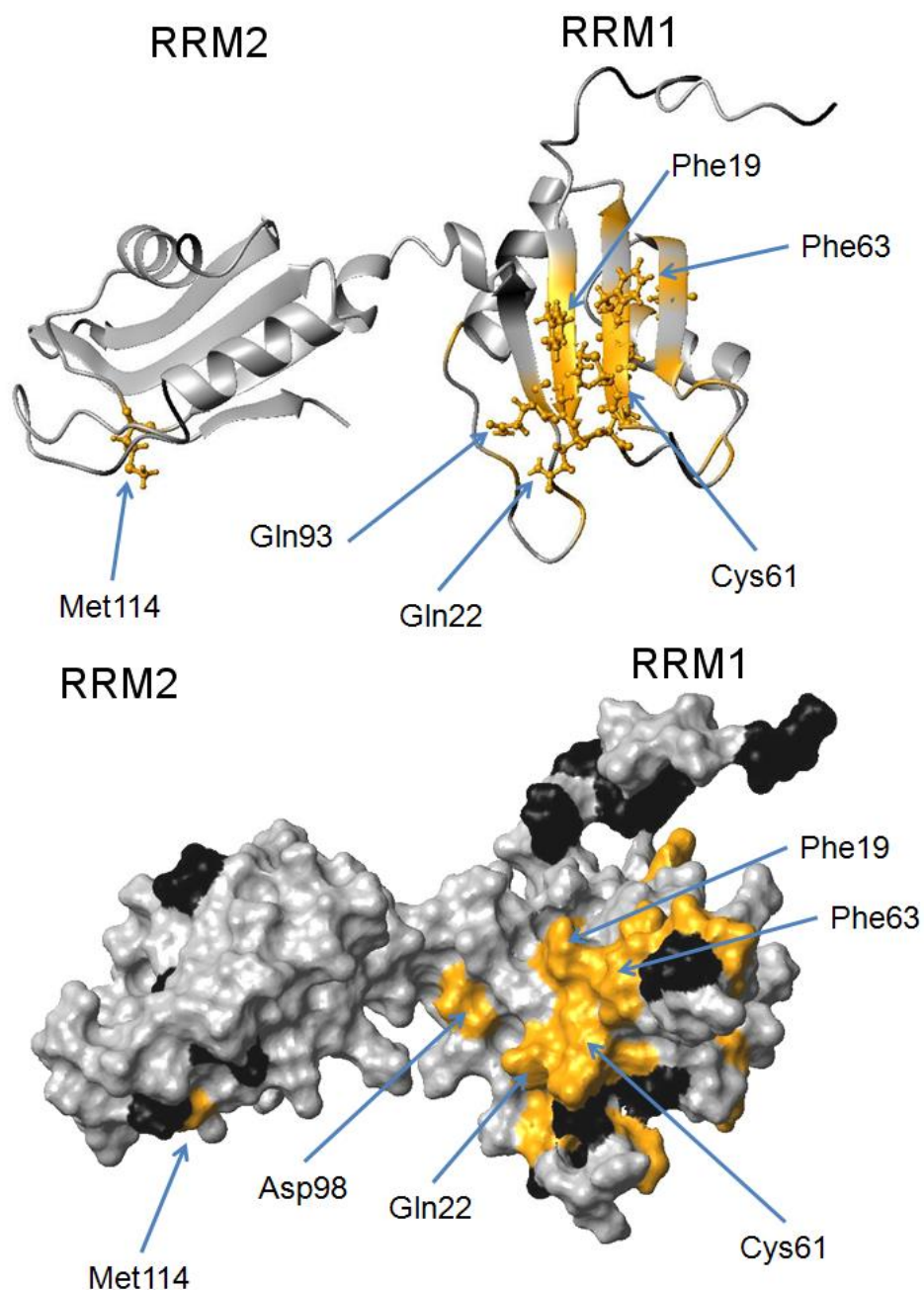


Figure 5.8: Map of the residues affected on titration with EDEN7 (UGUUUGU), plotted onto the NMR solution structure of RRM1 and 2 determined by Jun *et al.* Residues for which the peaks are lost on titration are shown in yellow. Residues with no data are shown in black. Since CSPs could not be quantified for the lost peaks there is no magnitude information in this figure, only an indication whether the peak for each residue is lost or not.

With a single exception (Met114) all of the affected residues are in RRM1. The RRM1 residues affected are generally the same as those in the earlier titrations. Val20, Gly21, Gln22, Cys61 and Cys62 are all lost over the course of the titration. Both of the conserved aromatic residues (Phe19 and Phe63) are also

affected. In β 4 Asp98 and Gln93 are lost. In β 2 Asn46 and Arg48 are lost, in contrast with Ile45 and Val47 in the earlier titrations. There is no effect on the α -helices.

5.2.4 Systematic Investigation of Spacing Requirements for Tandem Binding of the N-terminal domains of CELF1

The shortest GRE sequence to show tandem binding of the two N-terminal domains of CELF1 (the EDEN11 GRE) had a separation between the UGU sites of five nucleotides. RNAs with spacer lengths from 1 to 7 nucleotides were investigated by NMR in order to refine the exact spacing requirements between UGU sites for tandem binding. The NMR titrations were again carried out using a 400 μ M protein sample in NMR buffer A, and raising the RNA concentration in 50 μ M increments. All titrations were extended to a 1.5:1 ratio of RNA to protein to confirm that the sample was fully bound.

Virtually identical CSPs were observed for the residues in RRM1 for all spacer lengths from 2 - 7, while a greater range of effects were seen for residues in RRM2. In the RNA binding patch across the β -sheet Val20, Gly21, Gln22, Val23, Cys61, Cys62 and Gln93 show large CSPs for spacer lengths 2 - 7. A spacer length of 1 is equivalent to the earlier EDEN7 titration, where the signals for all of these residues are lost, but are not recovered. In RRM2 Ile112, Gly113, Met114, Val115, Cys150, Ala151 and Val182 show comparable CSPs to the titration with the EDEN11 GRE for spacer lengths of 2 – 5 inclusive. Cys150 and Val182 are consistently the most affected residues with CSPs of around 0.4 ppm in each titration. With a single nucleotide spacer only the Met114 signal is lost from RRM2. There are some slight perturbation of Cys150 and Val182, but in both cases it is only around 0.05 ppm, and is below the significance threshold. For spacers of length 6 and 7 significant CSPs were seen for all of the normally affected residues in RRM2, but were consistently reduced to around 50 – 60% of the magnitude of those seen for the 2 – 5 nucleotide spacers.

Figure 5.9 focuses on the peaks from the residues Cys61 and Cys150, which are in RRM1 and RRM2 respectively and show the greatest chemical shift perturbation in most of these titrations. Similar results are seen for the other affected residues, but the differences are most pronounced for these residues due to the larger absolute values of the CSPs.

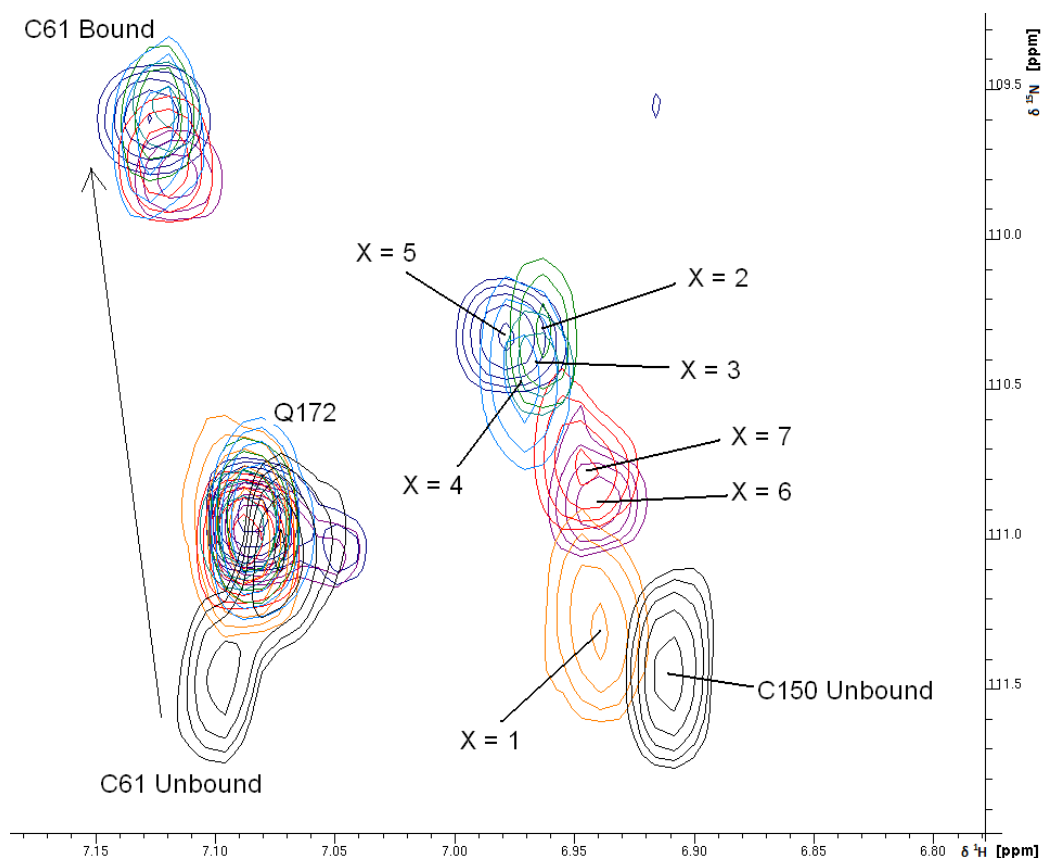


Figure 5.9: Overlaid ¹⁵N TROSY spectra for t187 unbound, and in the presence of a saturating amount of each of the seven RNA sequences EDEN1U – EDEN7U. The RNA sequences are of the form UGU(U)xUGU, with x = 1 – 7. This is a close up of a region of the spectra containing the signals from residue Cys61 in RRM1 and Cys62 in RRM2.

5.2.5 Interaction of the N-terminal Domains of CELF1 with GRE Sequences

Both the EDEN15 and EDEN11 GREs were found to be capable of binding the two N-terminal domains of CELF1 in tandem, consistent with these substrates

being targets for wild type CELF1. There are multiple possible UGU sites in these sequences (four in EDEN15 and three in EDEN11), some of which are expected to be redundant. The two domains could therefore be bound to sites with either one or five nucleotides separating them in the EDEN11 case. In the EDEN15 case one, five or nine nucleotide spacer lengths are possible depending which sites are being occupied by the two domains.

The EDEN7 (UGUUUGU) data clarifies how these two domains are recognising GRE sequences. In this titration all of the normally affected residues in RRM1, such as Gly21, Gln22, Cys61 and Gln93 are lost, showing that the RRM1 RNA binding surface is being fully occupied. In contrast Met114 is the only residue affected in RRM2, indicating that this domain is not binding to the RNA in the usual manner. This shows that this sequence, and hence a separation of one nucleotide between UGU sites, is not suitable for binding of the two N-terminal domains in tandem.

In the previous chapter this RNA sequence (UGUUUGU) was found to be capable of binding two copies of RRM1 simultaneously. It was not however capable of binding two copies of RRM2. It was speculated that RRM2 was recognising a slightly larger site of UGU(U/G) rather than the UGU site recognised by RRM1. If this is the case there would still be sites for both RRMs in this sequence, but with no separation between them, which could result in an unfavourable steric clash between the domains. Another possibility is that both domains might be able to fit onto the RNA when separated, but the short linker between them is not sufficiently flexible to allow the RRMs to adopt a suitable conformation relative to each other in order to bind simultaneously. The length of this linker may therefore play a role in regulating binding to CELF1's RNA targets by determining the separation between UGU sites that can permit tandem interaction with these domains. The EDEN7 RNA substrate is known to bind each of RRM1 and RRM2 in isolation. As they cannot bind at the same time when connected in the t187 construct, this titration behaves essentially as a

competition experiment. All but one of the affected residues are in RRM1, so it can also be concluded that RRM1 has a higher affinity for UGU(U) sites than RRM2.

The EDEN7 titration data shows unambiguously that the N-terminal domains cannot bind to sites with only a single nucleotide separating them. This eliminates one of the possible arrangements of the domains for binding to the EDEN11 GRE. The only remaining possible arrangement is for the two domains to bind to the outer two UGU sites, leaving the central site unoccupied. These sites are separated by five nucleotides. The longer EDEN15 GRE also has UGU sites with a five nucleotide separation, which the N-terminal domains of CELF1 could be recognising in the same manner. There was also still the possibility of binding to the outer two UGU sites in EDEN15, which would be a nine nucleotide separation.

The data from the GRE sequences had confirmed that a five nucleotide spacer between UGU sites was sufficient for tandem binding of RRM1 and RRM2, while a single nucleotide was insufficient. From this alone it was not possible to tell whether the separation had to be exactly five, or if a range of spacer lengths could be tolerated. The NMR data collected on the range of RNAs with spacer lengths from 2 – 7 nucleotides clarified this. For all spacer lengths the residues in RRM1 showed almost identical chemical shifts in the bound form. This is as expected, since the UGUUUGU titration showed that RRM1 is bound preferentially if the domains cannot bind in tandem. RRM2 however shows a larger range of effects.

With spacer lengths of 2 – 5 nucleotides the residues in RRM2 show very similar chemical shifts in the bound form to those in the EDEN11 GRE titration. This confirms that all of these spacer lengths (from UGUUUGU to UGUUUUUUUGU) can permit tandem binding of these two domains. The RNA

with the 5 nucleotide spacer also confirms that the central UGU site in the EDEN11 GRE is not playing any role in binding these two domains, since altering this G to a U has had no significant effect on the bound spectrum.

The longer 6 and 7 nucleotide spacers show a noticeable reduction in CSPs for the normally affected residues in RRM2. This was highlighted in Figure 5.9 for the highly perturbed residue Cys150, and a similar decline in CSP is seen for residues such as Ile112, Ala150 and Val182. In general they are reduced to 50 - 60% of the CSPs seen for the 2 – 5 nucleotide spacers. These CSPs are still above the 0.1 significance threshold for these residues, so tandem binding of RRM1 and RRM2 has not been completely eliminated as it appeared to be in the case of the single nucleotide spacer. The upper limit on the spacer length is therefore not as sharply defined as the lower limit. It does however appear that spacing of greater than 5 nucleotides between UGU sites is not optimal for tandem binding. It therefore seems likely that in the EDEN15 GRE the domains are binding to two of the UGU sites separated by five nucleotides, rather than the outer two sites which are separated by nine.

5.3 Enhanced Affinity when Binding Multiple Domains of CELF1 in Tandem

Our second aim was to determine whether tandem interaction of the two N-terminal domains results in enhanced binding affinity compared to their interactions in isolation. RRM1 had previously been determined by ITC to bind to substrates with UGU sites with a K_d of approximately 30 μM . RRM2 was found to have a slightly lower affinity for UGU sites of around 45 μM . ITC data was collected for titrations of the t187 construct with a UGU substrate, and with the series of RNA sequences with spacer lengths of 1 – 7 nucleotides between UGU sites. The UGU substrate would result in the domains binding separately, while spacer lengths of 2 – 5 nucleotides would permit tandem binding, based on the NMR data previously shown. Each titration was run with 25 μM RNA in the cell.

250 μM protein was injected from the syringe in thirty 10 μl aliquots, while stirring at a constant rate.

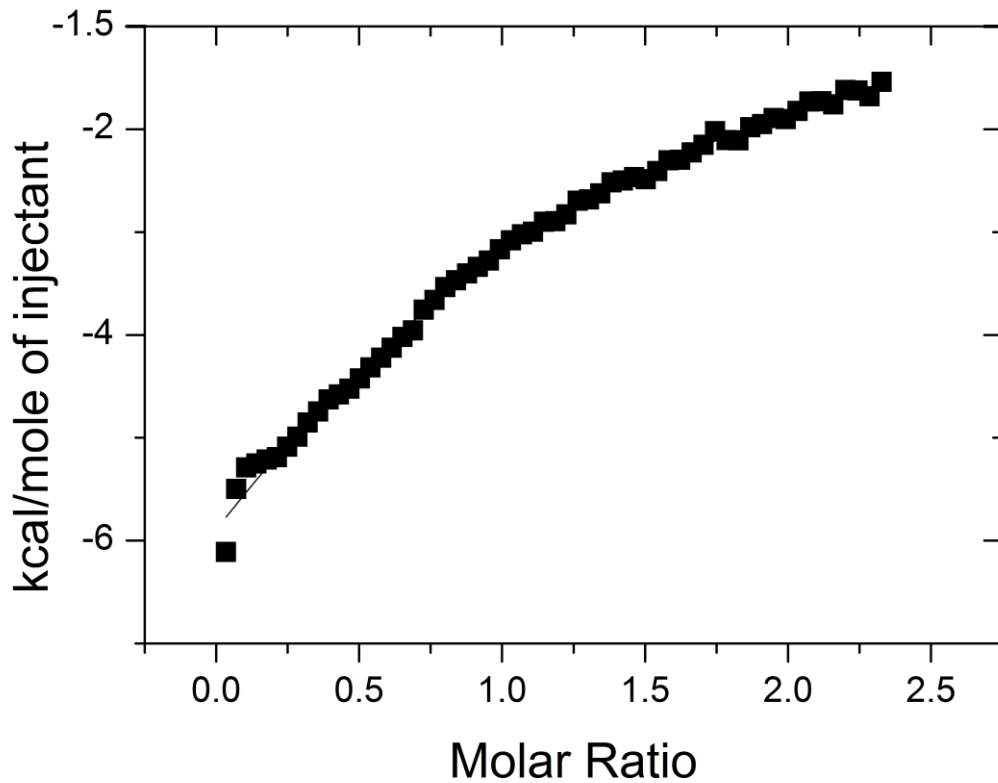
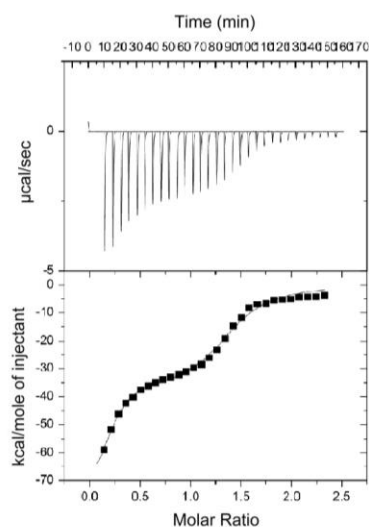


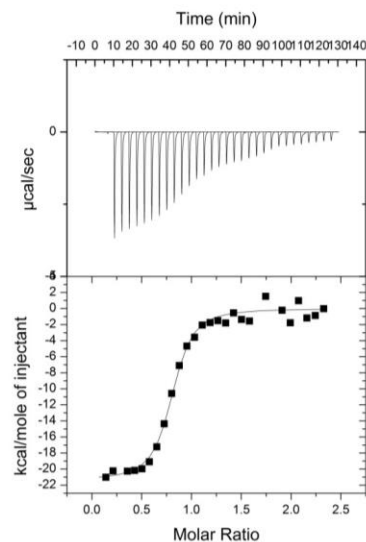
Figure 5.10: ITC trace for titration of 250 μM t187 protein into 25 μM RNA (UGU). The curve has been fitted using the MicroCal Origin 7.0 software package.

The K_d value for this interaction was calculated as $64.5 \pm 2 \mu\text{M}$, consistent with ITC data for the titration of UGU with the isolated domains. The stoichiometry is approximately 0.5 consistent with the two N-terminal domains of CELF1 binding separate UGU molecules.

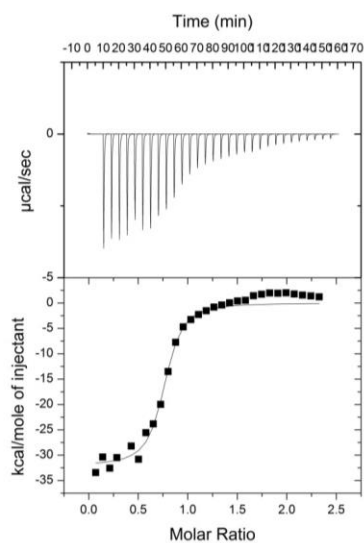
A) EDEN1U UGUUUUGU



B) EDEN2U UGUUUUGU



C) EDEN4U UGUUUUUUGU



D) EDEN6U UGUUUUUUUUGU

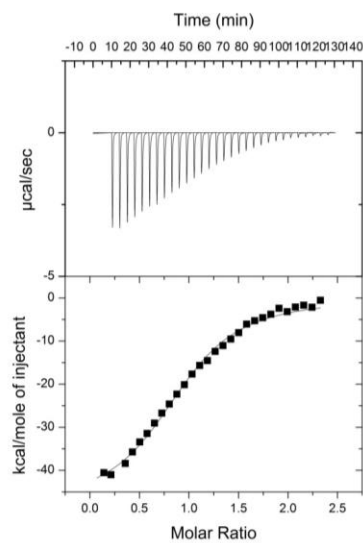


Figure 5.11: ITC binding curves for the X = 1, 2, 4 and 6 examples of the UGUUxUGU sequence. A) EDEN1U, previously called EDEN7, shows a biphasic titration curve distinct from all the others. No satisfactory fit to this curve could be obtained using the multiple site or sequential site binding models in the Origin 7.0 package. B) EDEN2U, showing a single phase curve, fitted to a one site model. C) EDEN4U, again showing only a single binding event, and fitted to a one site model. D) EDEN6U which, while it shows a single phase curve, the shallower gradient indicates a substantially lower binding affinity for the interaction. Data was also collected on the X = 3, 5 and 7 sequences.

In Figure 5.11 a) is shown the ITC trace for titration of the t187 construct into UGUUUGU (the substrate with the single nucleotide spacer). This shows a biphasic curve distinct from the single phase curves of the other RNAs investigated. Attempts were made to fit this to the multiple binding site and sequential binding site models in Origin 7.0, but no satisfactory fit could be obtained. In Figure 5.11 b) and c) are shown the ITC traces and fitted binding curves for the 2 and 4 nucleotide spacers. These fit to models with K_d values of $0.43 \pm 0.08 \mu\text{M}$ and $0.37 \pm 0.07 \mu\text{M}$ respectively. In contrast the trace for the 6 nucleotide spacer (Figure 5.11 d) shows a significantly lower affinity interaction, with a K_d around an order of magnitude larger at $3.4 \pm 0.3 \mu\text{M}$.

Binding affinities, stoichiometries and other calculated thermodynamic parameters for all RNA sequences investigated by ITC are shown below.

RNA	Sequence	K_d (μM)	N	ΔH (kcal/mol)	ΔS (cal/K/mol)
UGU	UGU	64.5 ± 2.0	0.94	-17.3	-41.0
EDEN2U	<u>UGUUUUGU</u>	0.47 ± 0.06	1.27	-17.0	-28.0
EDEN3U	<u>UGUUUUUGU</u>	1.60 ± 0.30	1.80	-20.1	-42.6
EDEN4U	<u>UGUUUUUUGU</u>	0.37 ± 0.06	1.35	-23.8	-50.5
EDEN5U	<u>UGUUUUUUUGU</u>	3.86 ± 0.79	0.99	-50.4	-144
EDEN6U	<u>UGUUUUUUUUGU</u>	3.38 ± 0.28	1.05	-45.5	-128
EDEN7U	<u>UGUUUUUUUUUGU</u>	3.50 ± 0.72	1.39	-39.4	-107

Table 5-2: ITC results for all spacer lengths, and also the titration of t187 into the UGU RNA substrate.

5.3.1 Dependence of Binding Affinity on the Separation between UGU Sites

The titration with the RNA substrate UGU showed a K_d of 64 μM , comparable to those seen for RRM1 and RRM2 binding in isolation. Since the RNA is only three nucleotides each domain must be binding to a separate RNA molecule, so there is no tandem binding to increase affinity. The RNA with the single nucleotide spacer (UGUUUGU) also does not permit tandem binding, as previously shown in the NMR data. Interpretation of these results was however complicated by the ITC trace showing two distinct binding events, with different affinities. This RNA substrate has previously been shown to be capable of binding two RRM1 proteins simultaneously, one to each UGU site. Two binding events are occurring and, since RRM2 is known not to be interacting from the NMR data, these must be two separate t187 proteins binding via their RRM1 domains. At low protein concentrations t187 binds to one UGU site of an RNA molecule via RRM1, but the spacer length does not permit RRM2 to bind in tandem, leaving the second UGU site vacant. When the protein concentration is increased until the protein is in excess this vacant UGU site can be occupied by the RRM1 domain of a second t187 protein, hence the second binding event seen in the ITC trace. A diagram of this complex is shown in Figure 5.12. The difference in binding affinity indicates that the two events are not equivalent and suggests negative cooperativity, possibly due to steric difficulties in binding the second protein onto the short RNA sequence. This may also imply that the bound conformation of the second RRM1 to bind may not be identical to that of the first RRM1. The presence of more than one bound conformation of RRM1 would result in broadening of the signals in the NMR, contributing to the lack of clear signals from the bound form.



Figure 5.12: This shows a possible 2:1 complex of t187 with the EDEN7 RNA substrate, which would account for the two binding events observed by ITC.

The RNAs with spacer lengths of 2 – 7 nucleotides all show simple sigmoidal curves, consistent with the two domains binding in tandem to form a 1:1 complex. The binding affinity is significantly enhanced for all of these compared to the RRMs binding in isolation. The lowest K_d values are seen for the 2 and 4 nucleotide spacers, both at around 0.4 μM . This is more than a 100-fold improvement in affinity compared to the protein binding two unconnected UGU sites. The 6 and 7 nucleotide spacers are, as seen in the NMR data, less favourable but with K_d values of around 3 μM they still show more than a 10 fold improvement in binding affinity. This is consistent with RRM2 still interacting to some extent, permitting some degree of tandem binding. The five nucleotide spacer showed a K_d value of 3.86 μM , indicating somewhat weaker binding than the 2 – 4 nucleotide spacers. This suggests that the five nucleotide spacing between occupied UGU sites in the EDEN11 and EDEN15 GREs may still be slightly larger than is optimal for tandem binding.

Based on these results, the optimal sequence for tandem binding of the N-terminal domains of CELF1 appears to be UGU(U) x UGU where X is 2 - 4 inclusive. X = 1 results in almost complete loss of binding to RRM2. X \geq 5 results in some loss of binding affinity, possibly due to binding becoming less entropically favourable as the spacer length increases. This upper limit is not as sharply defined as the lower limit, and it is possible that an RNA sequence with a longer spacer containing secondary structure to hold the UGU sites in close proximity might also show comparably favourable binding to the 2 - 4 spacers. This data clearly demonstrates that tandem interaction of the two domains leads to a significant enhancement in binding affinity. This is consistent with CELF1

forming a high affinity complex with its target mRNAs by recognition of an EDEN motif that extends across all three RRM s.

A model of the complex of the two N-terminal domains with the shortest of the optimal RNA substrates (UGUUUUGU) was constructed based on the available crystal structures of the isolated domains. Teplova *et al.* had published structures of RRM1 in complex with the UGU sites of a 12 nucleotide RNA (GUUGUUUUGUUU). The unit cell contains two RNA molecules each with two RRM1 proteins, one bound to each UGU site. They also published a structure of a construct of both RRM1 and RRM2 (residues 14 – 187) in complex with this sequence, but with only RRM2 in contact with the RNA. In order to construct this model the RNA in the RRM1 structure was truncated to the sequence UUGU, leaving a single RRM1 protein bound to the UGU site. The residues of this RRM1 were then superimposed onto the RRM1 region of the structure containing both domains, minimising RMSD for the protein. The RNA molecule bound to RRM2 in this structure was truncated to the core UGUU sequence in contact with the protein. This resulted in a structure of the two N-terminal domains, each bound to a four nucleotide section of RNA in the same manner as in the crystal structure.

The RNA fragments UGUU (bound to RRM2) and UUGU (bound to RRM1) were then connected to form the RNA UGUUUUGU, determined experimentally to be the shortest sequence capable of binding the domains in tandem. Due to the orientation of the two domains in Teplova *et al.*'s structure this required the introduction of an implausibly long bond connecting the two RNA fragments in this initial structure. The complex was placed in a truncated octahedron of TIP3PBOX water, with sodium ions to achieve an overall neutral charge. Energy minimisation was conducted in Amber with an initial restraint mask applied to the protein and RNA. The force constant of this restraint mask was reduced to zero over several stages (100, 50, 25, 10, 5, 2, 1), allowing the domains and RNA to shift until the bond where the two RNA fragments were connected had been

reduced to a normal length. Molecular dynamics simulations were then run in Amber, using the parameters in section 3.22, with a final step at 300 K with no restraint mask for 1 ns. The resulting model is shown in Figure 5.13.

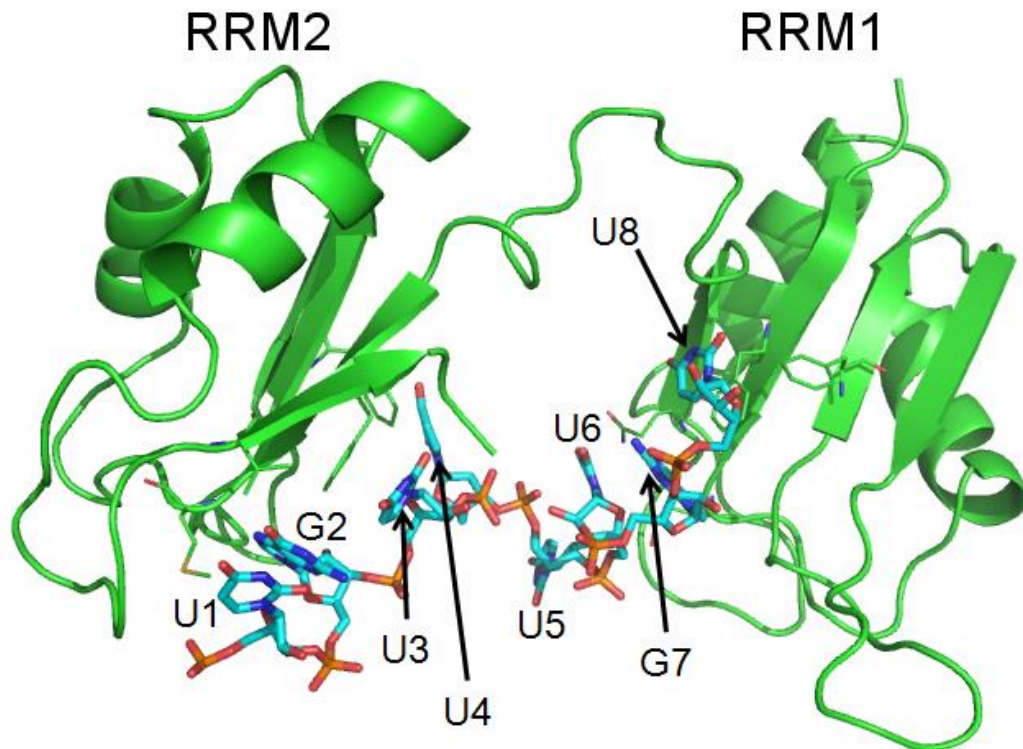


Figure 5.13: Model of the N-terminal domains of CELF1 in complex with the RNA substrate UGUUUUGU. The protein is shown in green as a ribbon diagram with the amino acid side chains of key residues in the binding surface shown as lines. The RNA is shown in light blue.

This is the shortest RNA sequence capable of binding both domains in tandem. Bases 1 – 4 of the RNA form contacts with the β -sheet and some of the loop regions of RRM2. U3 is forming a stacking interaction with Phe111, and U4 is forming a similar interaction with Phe152. U5 is relatively distant from the protein surface, with only the side chain of His90 in close proximity. U6, G7 and U8 interact with the β -sheet of RRM1. U8 forms a stacking interaction with Phe19. Phe63 does not stack with any of the RNA bases, though it is also quite close to the U8 base.

5.4 Determining the Stoichiometry of Complexes with GRE Substrates by Mass Spectrometry

The titration of t187 into UGUUUGU highlighted the potential for the formation of complexes with stoichiometries other than 1:1 when multiple UGU sites are present in an RNA substrate. The EDEN15 and EDEN11 GREs both have unoccupied UGU sites even after the N-terminal domains are bound in tandem. The masses of the complexes of t187 with these RNA substrates were therefore measured by ESI-MS to check for the presence of higher stoichiometries. As for the isolated domains, purified protein was put through a second desalting step into 25 mM ammonium acetate to further reduce the salt concentration, and hence the presence of salt adducts.

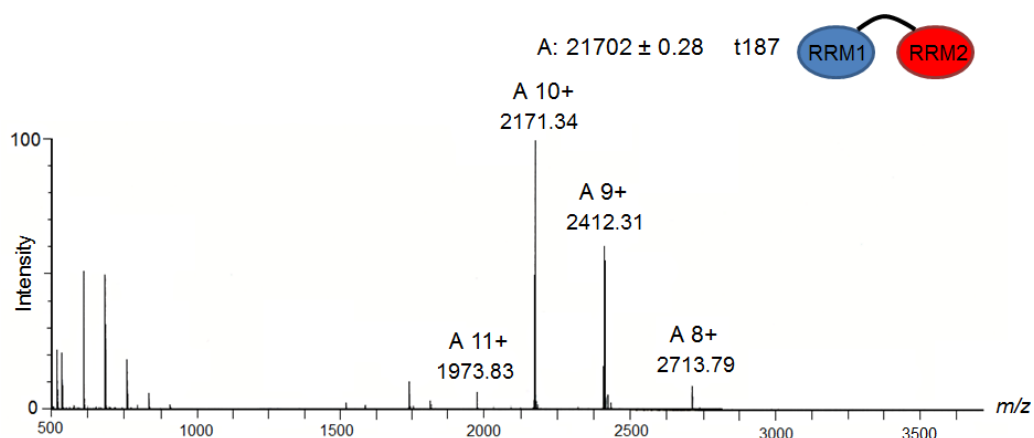


Figure 5.14: ESI mass spectrum of t187. The protein concentration is 5 μ M. One species is seen with a mass of 21702 Da.

The t187 construct, including the additional N-terminal residues left after removal of the 6-His-tag, has a theoretical mass of 21719 Da. The mass spectrum, shown in Figure 5.14, measures the protein's mass to be 21702 Da.

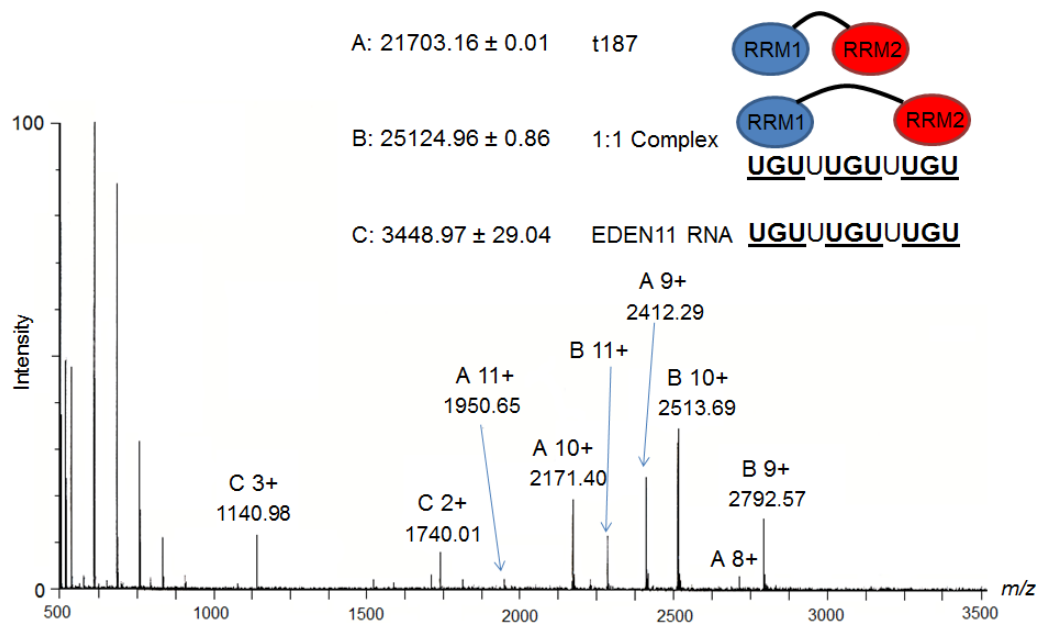


Figure 5.15: ESI mass spectrum of t187 + EDEN11. Both the protein and RNA concentrations are 5 μ M. Three species were seen, of masses 21702 Da, 25134 Da and 3449 Da, corresponding to unbound t187, 1:1 complex and unbound EDEN11 respectively.

RNA was added from a 5 mM stock in RNase free water until a 1:1 ratio of RNA to protein was reached. On addition of the EDEN11 GRE substrate a complex with a mass of 25134 Da was observed, which is a close match to the 25142 Da theoretical mass of a 1:1 complex. A small amount of unbound RNA is observable. Comparable amounts of unbound protein and 1:1 complex are present. ITC of this protein construct binding to the similar RNA sequence UGUUUUUUGU observed a K_d of 3.86 μ M. Under these conditions just over 40% of the protein would be expected to be in the form of the complex, which is consistent with mass spectrometry results.

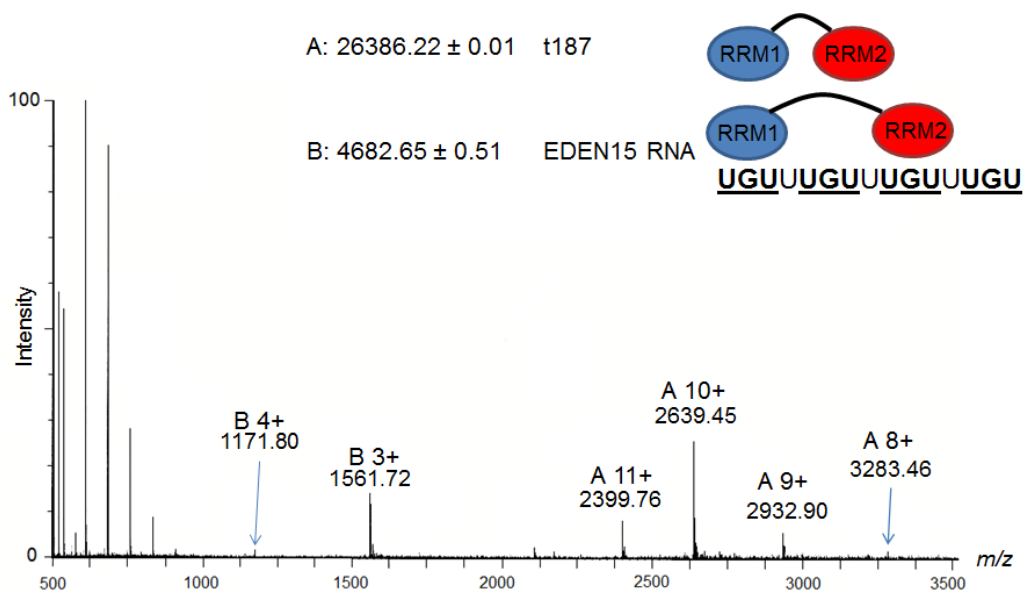


Figure 5.16: ESI mass spectrum of t187 + EDEN15. Both the protein and RNA concentrations were 5 μ M. Two species were seen, of masses 26386 Da and 4683 Da, corresponding to a 1:1 complex of t187 and EDEN15 and unbound RNA respectively.

Figure 5.16 shows the ESI mass spectrum after the addition of the EDEN15 GRE substrate. The 1:1 complex is visible. Its theoretical mass is 26405 Da, compared to an observed mass of 26389 Da. Unbound RNA is also visible, with a mass of 4683 Da. No free protein was observed at a 1:1 protein to RNA ratio. We were unable to fit a curve to the biphasic ITC trace for binding of this protein construct to EDEN15, preventing an accurate K_d for either of the binding events being determined. The fact the vast majority of the protein appears to be in the form of the 1:1 complex under these conditions does however suggest significantly tighter binding than in the EDEN11 case, where a mixture of unbound protein and complex was seen.

No 2:1 complex is observed. The biphasic ITC trace observed for this system does suggest it is possible for a second protein molecule to bind to this RNA. If however the second protein molecule can only bind via one of its two domains, the binding affinity will be far lower than for the first protein molecule binding. RRM1 binds to a UGU site in isolation with a K_d of ~ 30 μ M, and it is possible that negative cooperativity will further reduce the binding affinity. The proportion

of the protein in the 2:1 complex may simply be too small to be observed.

In conclusion both the EDEN11 and EDEN15 GREs were confirmed to form high affinity 1:1 complexes with t187, with the longer EDEN15 GRE appearing to be significantly more favourable than EDEN11. We were not able to observe any 2:1 complex but given the affinity for the second binding event would be expected to be much lower than for the first, and potentially even lower than for the isolated domains binding, this does not exclude the possibility 2:1 complex formation.

5.5 Investigation of Binding Affinity Enhancement in Tandem binding to UGC and UAU Sites

In the previous chapter UGC sites were found to be bound by the RRMs of CELF1, though with a somewhat reduced affinity in the case of RRM1, and only very weakly with RRM2. UAU sites conversely were found to show moderate CSPs for RRM2, but showed no significant interaction with RRM1. An important question was whether a longer RNA with multiple UGC or UAU sites could bind the domains in tandem, with an enhancement in binding affinity similar to that seen for UGU sites. This was particularly of interest for UGC sites, due to their presence in the extended CUG repeat RNAs in DM1 cells. NMR and ITC data was therefore collected on RNA sequences containing multiple UGC and UAU sites. The sequences CUG15 and ARE15, shown below in Table 5-3 were selected, as they were of comparable size to the EDEN15 GRE, and had at least two sites with spacing consistent with tandem binding.

RNA	Sequence
CUG15	<u>CUGC</u> CUGC <u>CUGC</u> CUGCUG
ARE15	<u>UAUU</u> UAUUUAUUUAU

Table 5-3: RNA sequences used to check for enhanced binding affinity when the N-terminal domains of CELF1 bind to tandem UGC and UAU sites.

5.5.1 Tandem Binding to UGC Sites

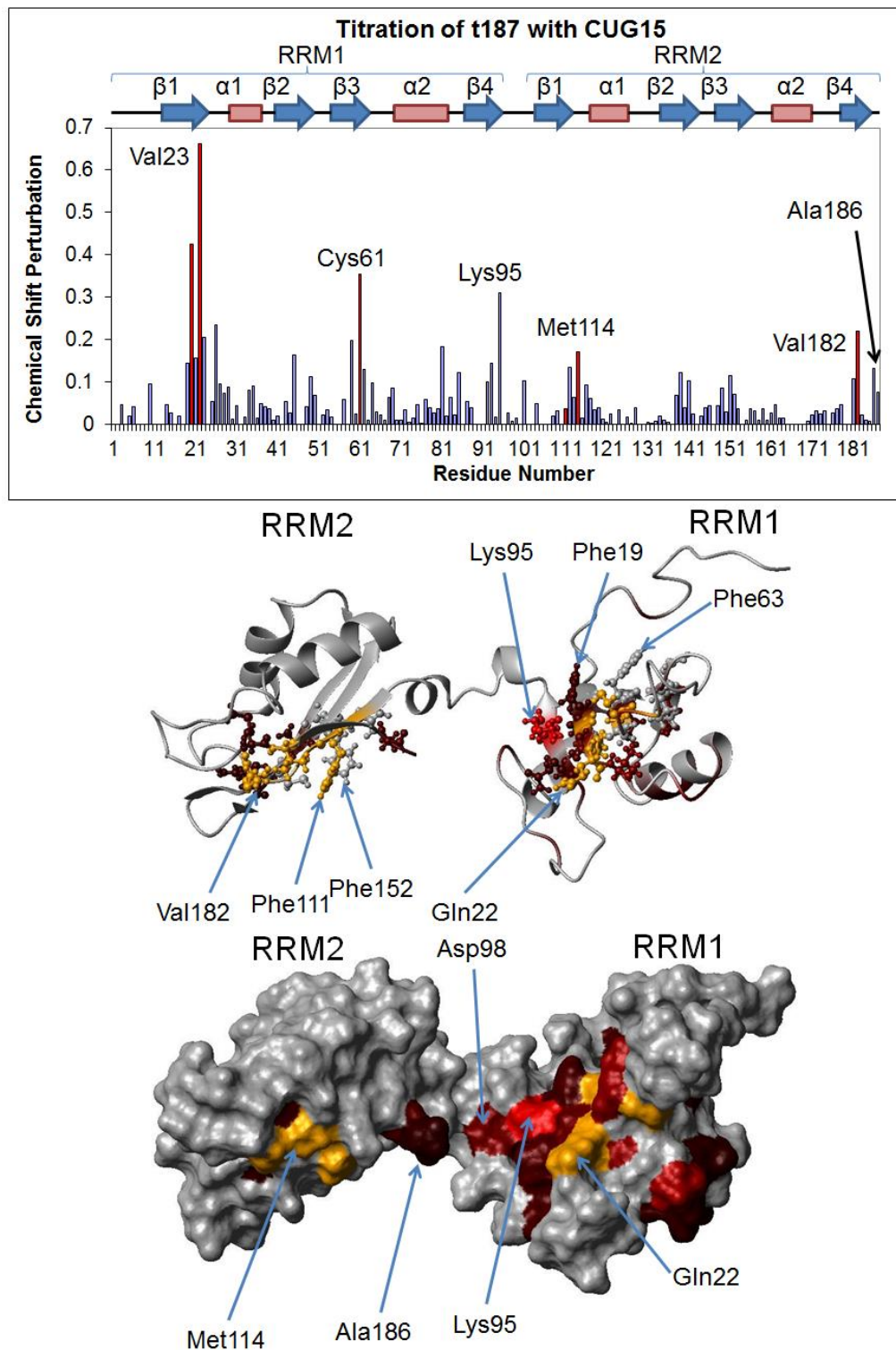


Figure 5.17: CSPs at the endpoint of the t187/CUG15 titration. The brightness of the red colour indicates the magnitude of the CSPs, with the bright red in the RNP regions of RRM1 indicating relatively large CSPs, while the darker red in RRM2 shows residues only just above the 0.1 significance threshold. Residues in yellow have only estimated CSPs, which are shown in red in the histogram. The protein concentration was 400 μ M throughout, and the RNA concentration was raised in 50 μ M increments up to a 1.5: 1 excess of RNA. The titration was run at 298 K, in NMR buffer A.

RRM1 shows CSPs across most of the β -sheet residues, with some of comparable magnitude to those in the EDEN15 titration. In β 1 Phe19, Gly21 and Val23 all show CSPs of greater than 0.15. In β 2 Ile45 and Asn46 show similar CSPs, as do Lys59 and Cys62 in β 3. In β 4 Lys95 shows a large CSP of >0.25 , contrasting with <0.05 in the EDEN15 titration. RRM2 however shows very limited CSPs. In particular the 110 - 115 and 149 - 155 regions, which showed the largest CSPs on binding to UGU sites, have no residues in fast exchange with CSPs of magnitudes above 0.1. The peaks for Phe111 and Met114 are still lost on titration. Val182 shows a CSP of just over 0.1, compared to 0.4 for binding to UGU sites. In this region Ala186 also has a CSP just over the significance threshold. As with the other t187 titrations, a mixture of residues in fast and slow exchange is seen. The ITC trace had an unusual shape, as shown in Figure 5.18, which was unlike any of those seen for the titrations with UGU substrates.

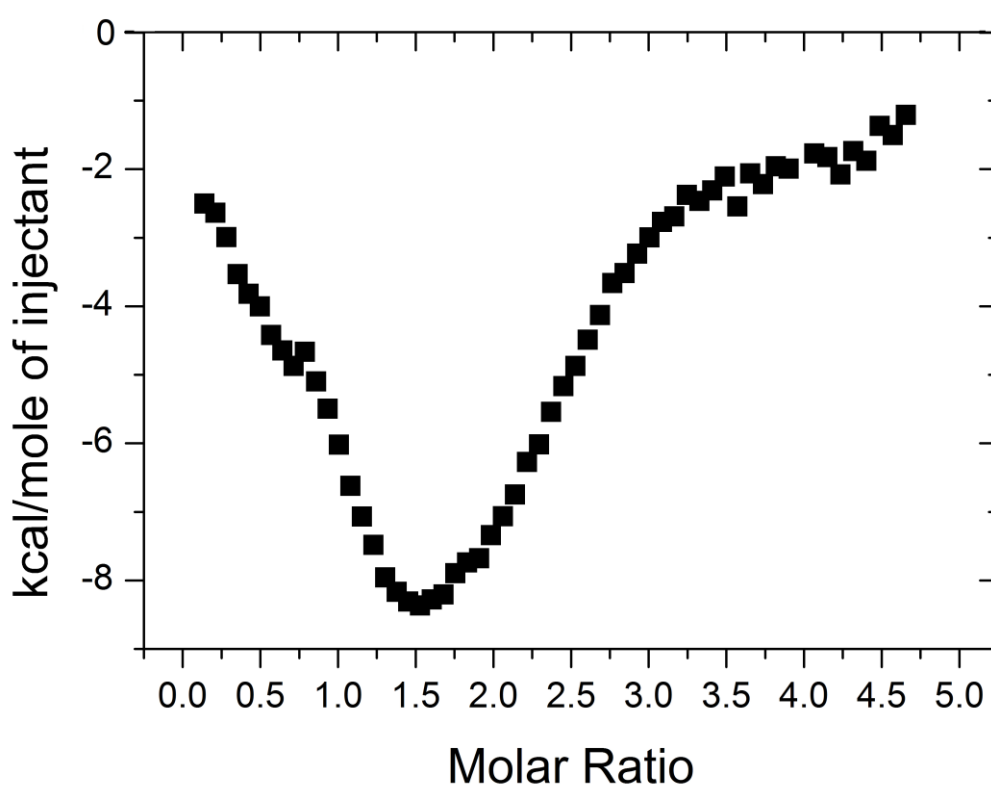


Figure 5.18: ITC curve for a titration of 500 μ M t187 protein into 25 μ M CUG15 at 298K. All samples were dissolved in RNase free water and degassed.

A plausible fit to the curve could not be produced using any of the available binding models in Origin 7.0, preventing any thermodynamic parameters from being calculated. From the NMR data it appears that RRM1 is binding to the UGC site with comparable affinity to the UGU site. However RRM2 still shows only very weak CSPs, suggesting that even when the domains bind in tandem the overall affinity for sequences with UGC sites is not significantly enhanced.

A complication in this titration is the issue of RNA secondary structure. Long CUG repeating sequences such as those found in DM1 cells have been shown to form hairpin structures. These consist of a stem of C – G Watson-Crick base pairs, separated by U – U mismatches. Atomic force microscopy by Michalowski *et al* (1999) showed that CELF1 could not bind to this double stranded stem. Binding could only occur to short single stranded sections of the RNA at the ends of the hairpin. The possibility of similar hairpin structures in the relatively short CUG repeat sequences used in these experiments had to be considered. The mFOLD RNA secondary structure prediction webservice¹⁷⁹ predicted no secondary structure for the short CUGCUG sequence, or any of the sequences with UGU or UAU sites. It did however predict that CUG15 would form a short hairpin structure with two C-G base pairs ($\Delta G = -1.0$ kcal/mol).

This could account for the unusual shape of the ITC trace. The endothermic section at the start of this titration, which was not seen for any other RNA substrate, could be caused by the breaking apart of the RNA hairpin. Since CELF1 has been confirmed to only bind to single stranded CUG repeat sequences by AFM, and the NMR shows that it is binding to CUG15, any secondary structure in the RNA must be breaking down. CUG15 is still a relatively short sequence compared to the extended CUG RNAs present in DM1 cells which can run to thousands of repeats. While this ITC experiment does suggest CELF1 is capable of breaking apart at least a short section of RNA hairpin in order to bind, it may not be able to do this except at the ends of the RNA hairpins in DM1 cells.

5.5.2 Tandem Binding to Adenosine Rich Elements

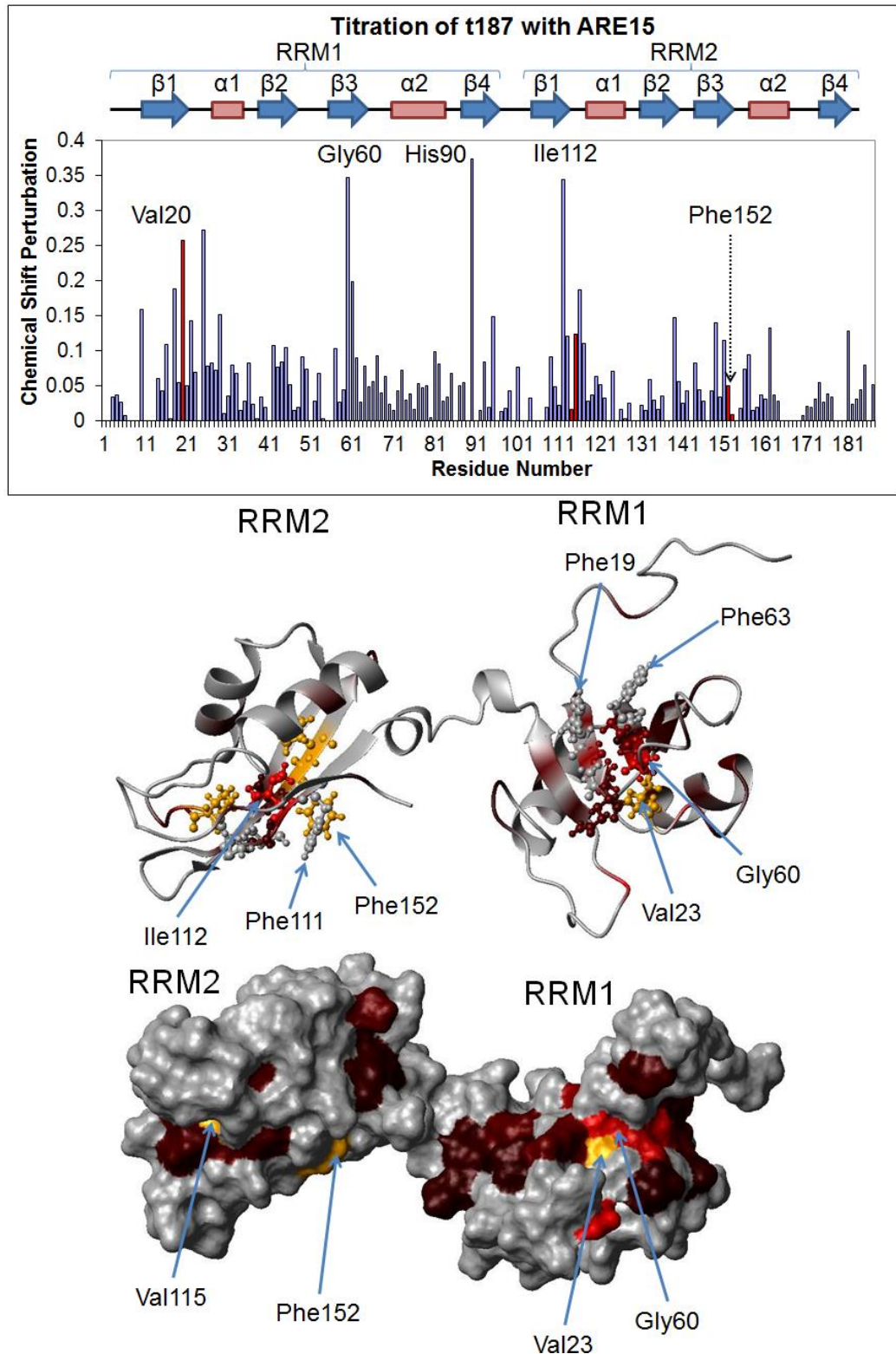


Figure 5.19: CSPs at the endpoint of the t187/ARE15 titration. This titration was largely in fast exchange, and shows residues in both RRMs above the 0.1 significance threshold. The titration was carried out on a 400 μM protein sample in NMR buffer A at 298 K. The RNA concentration was raised in 50 μM increments until no further variation in the spectrum was seen. Residues lost on titration are shown in yellow on the CSP map, and minimum CSP estimates are highlighted in red in the histogram.

Significant CSPs of up to 0.4 ppm were seen, comparable to those in the EDEN15 titration, were seen in both domains. In RRM1 β 1 and β 3 both show strongly affected residues, such as Gly21, Val23 and Gly60. The conserved aromatic residues Phe19 and Phe63 are not perturbed. B2 and β 4 show relatively low CSPs, though His90 in the loop connecting α 2 and β 4 has a high CSP of almost 0.3 ppm. In RRM2 most of the effects are in β 1, in particular Ile112. The other parts of the β -sheet are less affected, though Phe152 in β 3 is lost on titration.

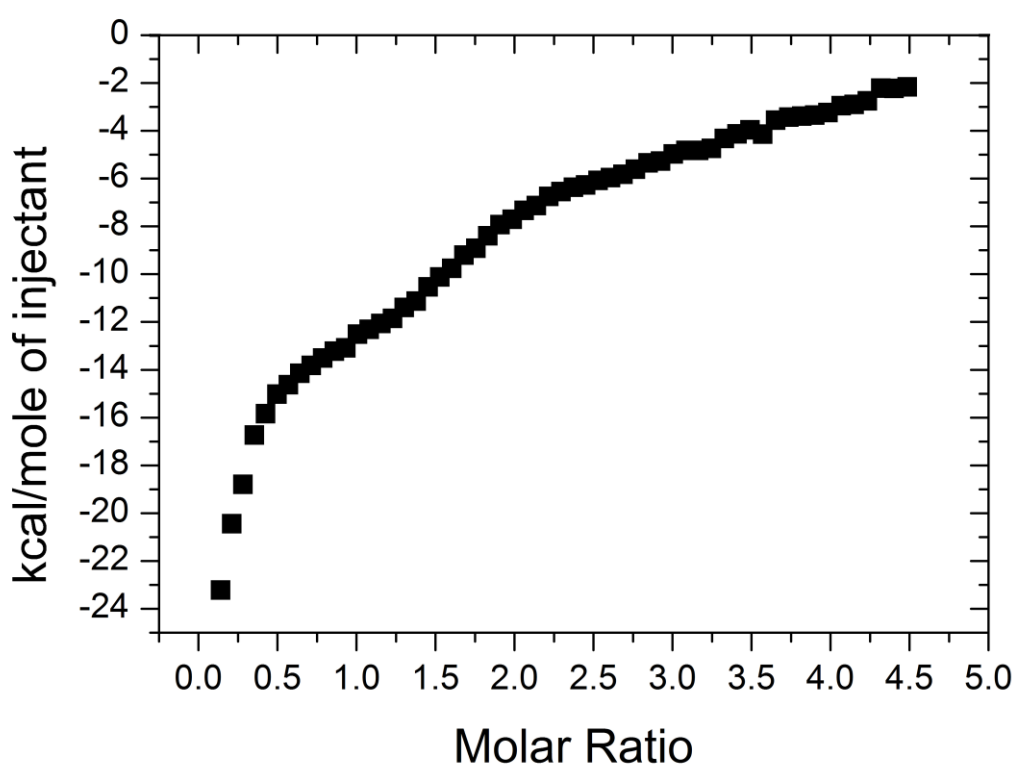


Figure 5.20: ITC curve for a titration of 500 μ M t187 into 25 μ M ARE15. Binding is occurring, with multiple events as can be seen from the shape of the curve. It was not possible to achieve a good fit to this data using any of the binding models in the Origin 7.0 software package.

A titration of t187 protein into the ARE15 RNA substrate showed a curve, indicating that binding was occurring. While not as pronounced as in the titration with EDEN7, there are clearly at least two phases to the binding curve, indicating

at least two binding events are occurring. The multi-site binding model did not produce a plausible fit.

From the NMR data it can be concluded that the N-terminal domains of CELF1 are binding in tandem to two sites in the ARE15 substrate, as there are substantial CSPs across both domains. This contrasts with the isolated domain results. RRM2 did show moderate CSPs with an ARE substrate, but RRM1 showed no significant CSPs at all when titrated with ARE7 (UAUUUAU). This suggests that binding the two domains in tandem has enhanced the affinity of the N-terminal domains of CELF1 for UAU sites. From the ITC it does not appear to be forming a simple 1:1 complex with ARE15. Possibly the two redundant UAU sites permit a second t187 protein to bind when in large excess.

Based on the ITC data the substrate ARE15 does not appear to form a high affinity 1:1 complex like EDEN15 does, so AREs can still be considered as relatively low affinity targets. There is enough of an interaction however that they may not be a good choice as control sequences, particularly when multiple domains of CELF1 can bind simultaneously to improve the binding affinity.

5.6 Investigating the Involvement of Unstructured Regions Flanking RRM1 and RRM2 in RNA Binding

In 2009 Tsuda *et al* published a structure of RRM3 in complex with the RNA substrate UGUGUG. One notable feature of this structure was that a flexible section at the N-terminus of the protein was folded back across the β -sheet, making additional contacts with the RNA and enhancing binding affinity. It was therefore important to investigate if any similar regions flanking the structured RRM1 and RRM2 domains were involved in RNA binding. This was particularly important to determine for the C-terminus of RRM2, since the t187 construct cut

the protein only one residue after the end of the structured domain. If any unstructured region was involved in the wild type, it would be truncated in the t187 construct, potentially altering the RNA target or binding affinity. Also the unstructured N-terminus of RRM1 and the linker between RRM1 and RRM2 were investigated. This was accomplished using a combination of ^{15}N heteronuclear NOE experiments, and an extended protein construct (t242).

5.6.1 Evidence for Conformational Flexibility from ^{15}N Heteronuclear NOEs

By measuring the $^1\text{H} - ^{15}\text{N}$ heteronuclear NOE it is possible to measure the flexibility of each residue in the protein¹⁸⁰. Heteronuclear NOEs are sensitive to motion on a timescale of $10^{-8} - 10^{-12}$ seconds, which is a typical range for internal protein dynamics¹⁸¹. Heteronuclear NOEs are generally highest in rigid areas of the protein, with a theoretical maximum value of 0.82.¹⁸² Some values higher than 0.82 are seen in practice due to the margin of error in measuring signal intensities. Values from 0 – 0.6 generally indicate relatively dynamic regions of the protein. Completely unstructured regions can produce negative values. ^{15}N heteronuclear NOE experiments have the disadvantage of low sensitivity compared to an ordinary $^1\text{H}-^{15}\text{N}$ HSQC experiment, and so require long acquisition times which can present a problem with unstable samples. They also require accurate measurement of the intensity of each peak in the spectrum. As a result heteronuclear NOEs cannot be accurately calculated for any overlapping peaks.

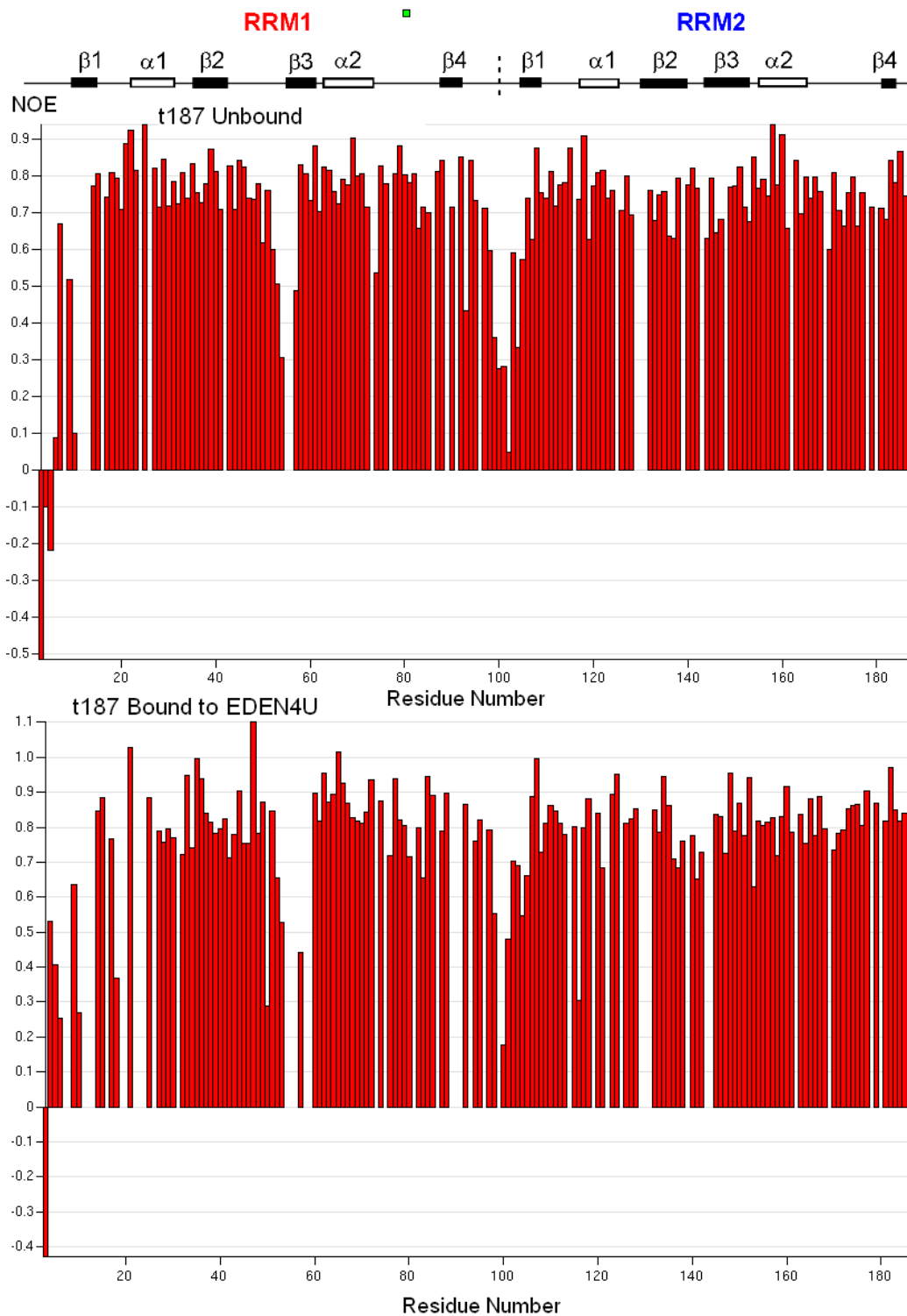


Figure 5.21: The upper graph shows the ^{15}N heteronuclear NOEs seen for each residue in the unbound t187 protein. The lower graph shows the same protein after the addition of an excess of the EDEN4U RNA substrate (known to be an optimal target to form a 1:1 complex with t187). Data was collected on an 800 MHz NMR spectrometer with cryoprobe, with 40 scans at a resolution of 2048 x 128 points for each of the two interleaved experiments comprising the ^{15}N heteronuclear NOE experiment.

In the folded domains of t187 NOEs are typically 0.7 or greater, indicating slow isotropic tumbling consistent with a compact, rigid structure. An exception is the loop connecting β -sheets 2 and 3 of RRM1 where the NOEs are significantly lower, indicating faster internal motion and suggesting this loop is somewhat more dynamic than the rest of the domain. This is consistent with the greater range of conformations seen for this loop compared to the rest of the domain in the available crystal structures of RRM1⁵¹, and the NMR structural ensemble of the N-terminal domains previously reported by Jun *et al*⁴⁸. The N-terminus of the construct also shows very low, and some negative NOEs, indicating unstructured protein. Residues 98 - 105 show relatively low heteronuclear NOEs, consistent with the linker between RRM1 and 2 being fairly dynamic.

The experiment for t187 in complex with the EDEN4U substrate showed a similar overall pattern of NOEs, showing that it is not becoming significantly more rigid on binding to RNA. The relatively flexible loop between the β 2 and β 3 strands of RRM1 is also remaining flexible when bound to the RNA, as is the N-terminus. The N-terminus possibly shows a slight increase in the NOE for residues 2 – 5, but still remains quite dynamic compared to the structured domains.

From this data it can be concluded from this that there is no involvement of the flexible N-terminus of RRM1 in binding the RNA, unlike that seen for RRM3. If it were, it would be expected to become significantly less dynamic when bound to RNA. Similarly the short linker between RRM1 and RRM2 appears to remain dynamic even when the domains bind in tandem, consistent with a lack of any N-terminal involvement in RRM2 binding.

5.6.2 Investigation of Involvement of the RRM2 C-Terminus Using an Extended CELF1 Construct

It had been suggested in the literature that not only the first two domains, but also

some additional residues from the unstructured region between RRM2 and 3 are required for high affinity binding of RNA^{103,54}. The t187 construct was however capable of binding RNA with affinities in the low μM to high nM range even without this region. We examined the effects of this proposed extension of RRM2 using a construct of the first 242 residues of CELF1 (t242). The t242 construct was originally produced by Dr. Emilie Malaurie (University of Nottingham), but due to lower yields from purifications and poor solubility, work was focused on the shorter t187 construct. It contains an additional 55 residues from the linker region between RRM2 and 3, which are believed to be completely unstructured. The purification was carried out using the same protocol as for t187 construct.

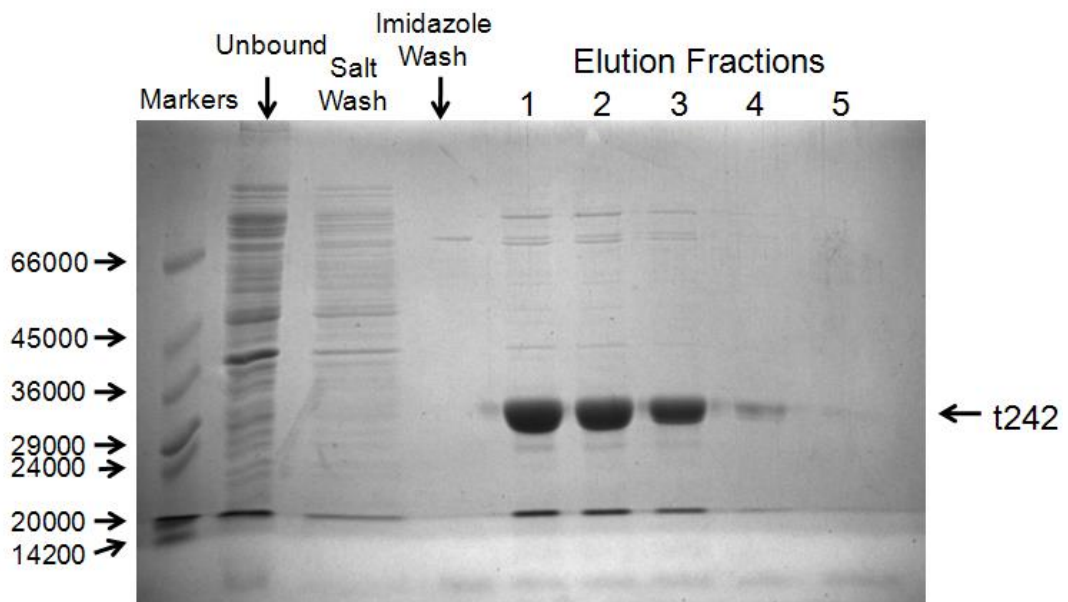


Figure 5.22: SDS PAGE of ¹⁵N labelled t242 purification. The protein mass is consistent with t242, and there is no sign of truncation of the flexible C-terminal tail. From left to right the lanes show: 1) Standard molecular weight markers (Sigma), 2) The supernatant after the protein has bound to the His-Pur column, containing the non-binding proteins. 3) Proteins eluted by the 2 M NaCl wash. 4) Proteins eluted by the 1 mM imidazole wash. 6) – 10). The first 5 fractions of elution buffer containing 0.75 M imidazole. The elution fraction volume was 2 ml.

From SDS-PAGE the increased size of the protein can be seen. It runs slightly above the 29 kDa marker, consistent with its theoretical mass of 30475 (including the 6-His-tag). The purification yield was severely reduced, to 2.5 mg/l when

grown in minimal media. The protein solubility was also reduced, to approximately 100 μM in the phosphate NMR buffer A. Increasing the salt concentration to 200 mM only marginally increased the protein solubility, and substantially reduced the quality of the resulting NMR spectrum, so buffer A was still used for collection of all NMR data on the t242 construct. The NMR data was collected using the TROSY technique on a Bruker Avance III 600 MHz spectrometer with a TXI probe at 298K.

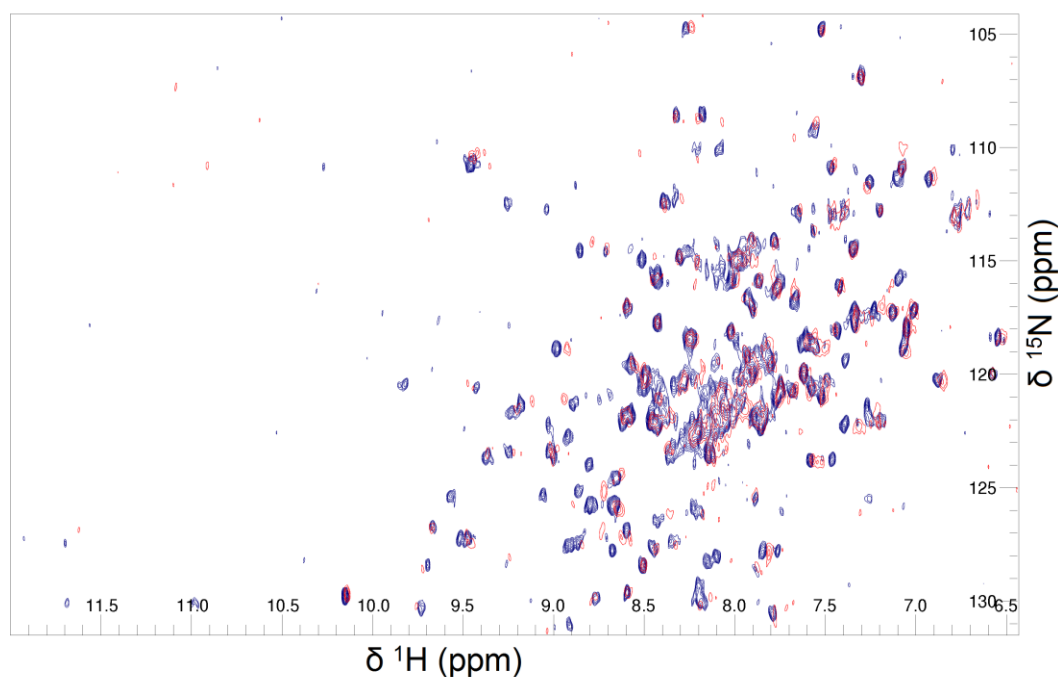


Figure 5.23: ^{15}N TROSY of t242, collected on a Bruker Avance III 600 MHz spectrometer, shown in blue. ^{15}N TROSY of t187 overlaid in red for comparison. 55 additional peaks would be expected in the t242 spectrum. Most of the additional peaks in the t242 spectrum are however tightly clustered in the 7.5 - 8.5ppm proton region and are difficult to resolve. This indicates they are in an unstructured region of the protein, which is consistent with the available information on the structure of CELF1.

Given the difficulty of resolving the heavily overlapped peaks from the unstructured 188 - 242 region and the poor signal/noise ratio, it was decided not to attempt assigning these, but instead to repeat the earlier titrations with a GRE sequence and the CUG15 sequence to check for any differences in the CSPs of the structured domains between the two constructs. The low protein concentration also prevented the acquisition of 3D heteronuclear NMR data, which would be necessary for assignment of a protein of this size.

Due to the limited solubility of t242, a very low sample concentration (~100 μM) had to be used for all NMR experiments. The number of scans taken at each titration point was increased to compensate. The RNA concentration was raised in 25 μM increments until an excess of RNA was present.

A larger than normal percentage of the peaks do not have quantifiable CSPs, since their low initial intensities results in them being more easily lost over the course of the titration. Also some peaks which are normally resolvable in the t187 are obscured by the cluster of peaks from the unstructured C-terminal extension of the protein. The binding patch can still be identified from those residues for which the signals from the free form disappear over the course of the titration.

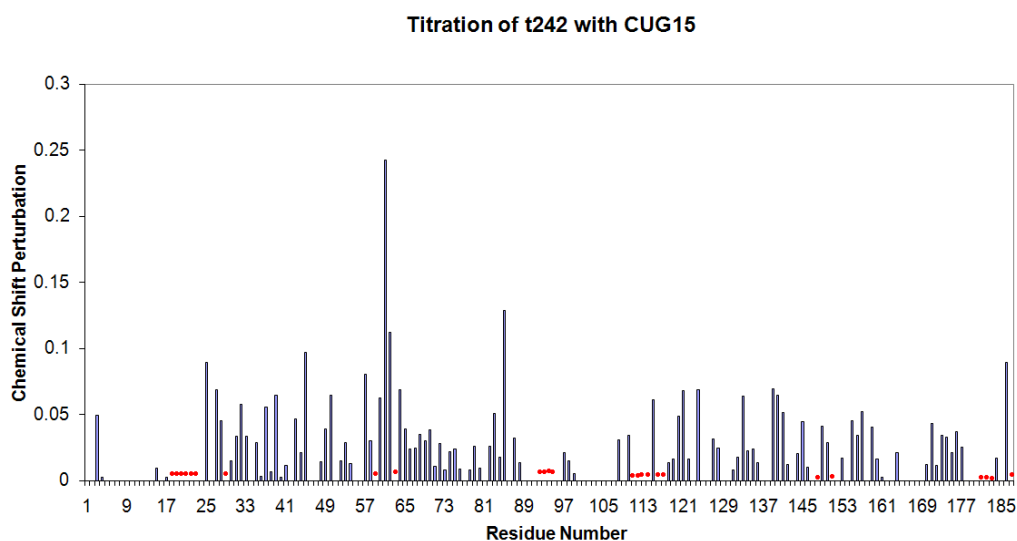


Figure 5.24: Graph of CSP values for titration of t242 with CUG15. Red asterisks indicate residues that are resolvable in the initial spectrum, but lost on titration. No values are shown for residues 187 – 242 as these were not assigned. Minimum values for the CSPs of residues lost on titration have not been estimated, since there are insufficient visible peaks in the bound form to account for all residues. If the bound peak is not visible, as opposed to merely unassigned, the distance to the nearest unassigned peak could still be a large overestimate of the CSP.

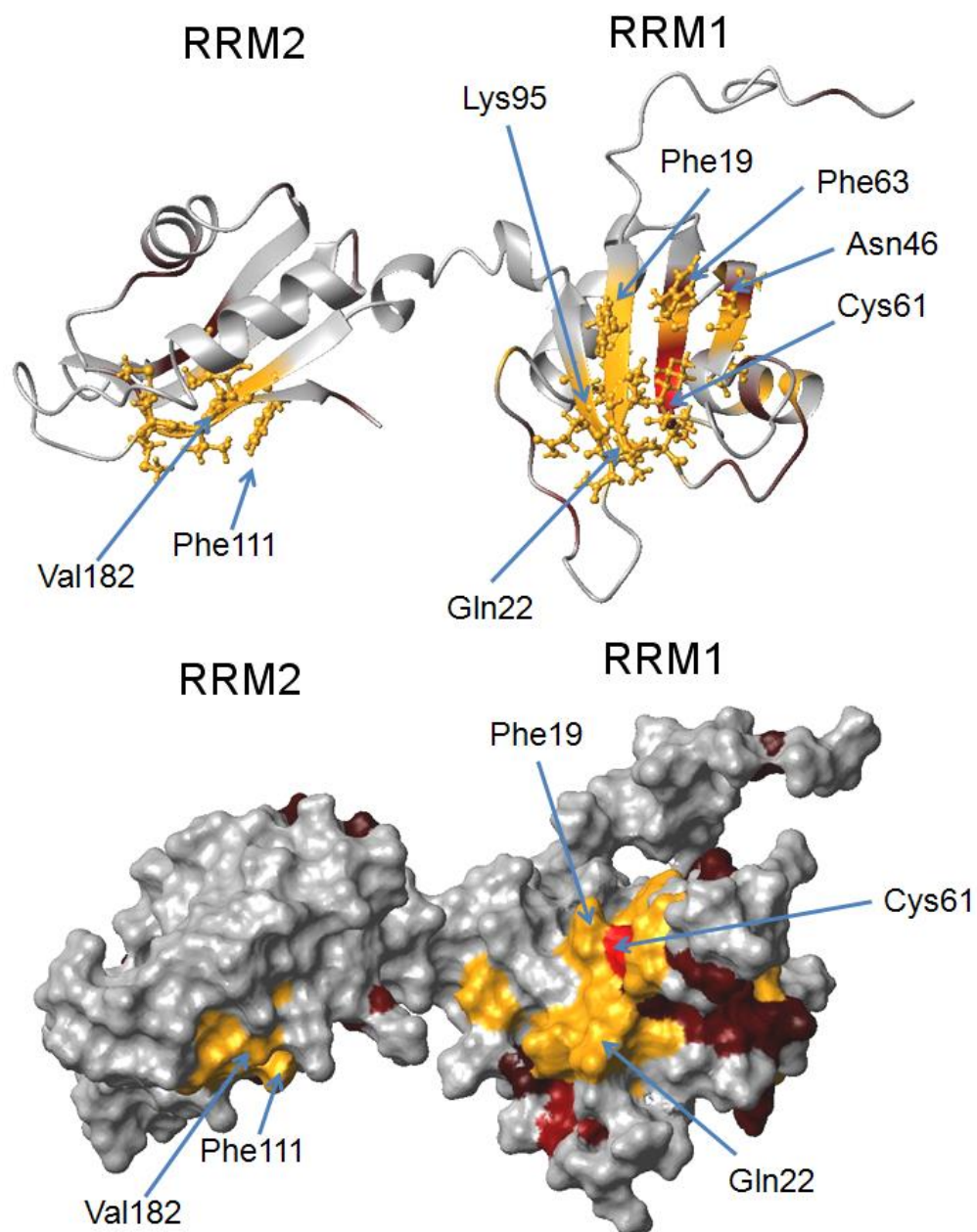


Figure 5.25: Map of CSP values onto the first 187 residues of t242. The additional 45 residues at the C-terminus are assumed to be unstructured, and there is no CSP data available for them. The affected residues are mostly in RRM1, as was expected based on the t187 data.

As with t187, most of the residues perturbed on titration with the CUG15 RNA are localized to RRM1, with only limited effects in RRM2. Cys61 is the most perturbed residue for which a CSP could be calculated. Both Phe19 and Phe63 are lost on titration, as are residues in all four strands of the β -sheet. The CSP for Lys95, could not be quantified as the peak from the bound form was obscured by

some of those from the unstructured region. Since the peak from the free form was lost Lys95 is definitely affected, consistent with the earlier titrations. In RRM2 the peaks from a few residues are lost, such as Phe111, Ala151 and Val182. Cys150 is not significantly affected, again consistent with the corresponding titration with the t187 construct. A repeat of the EDEN15 titration with t242 also matched the results for t187.

In conclusion, these experiments determined that there is no significant difference in the RNA binding properties of the t187 and t242 constructs, suggesting little involvement of the unstructured region immediately after RRM2. Since the spectrum of the unbound t242 matches very closely to that of the unbound t187 complex it can be concluded that there is no dimerisation occurring due to the additional residues from the RRM2 – RRM3 linker. If these residues did result in dimerisation, it would be expected that there would be significant changes in chemical shift for the residues in the dimerisation interface. While the protein concentration in these experiments was relatively low at 100 μM , if a physiologically relevant dimerisation event is occurring then at least some population of the dimer should be visible in these spectra. No variation in the t187 spectrum was seen for concentrations ranging from 10 μM to 1 mM.

These results confirmed that the C-terminus of RRM2 is not involved in binding to RNA. This in conjunction with the earlier ^{15}N heteronuclear NOE data shows that no critical regions for RNA binding have been omitted from the t187 and isolated domain constructs. The behaviour of these proteins is therefore representative of the behaviour of the domains of wild type CELF1.

5.7 Summary of Cooperative Binding by the N-terminal Domains of CELF1 to RNA targets

The data presented in this chapter shows that tandem binding of multiple CELF1 domains to RNAs with more than one UGU site greatly increases the overall affinity of the interaction. K_d values are reduced from tens of micromolar for the domains binding in isolation to less than one micromolar for optimal RNA targets. This increase in affinity is most pronounced for cooperative binding of UGU sites. There does appear to be some increase in affinity for UAU sites when the domains bind in tandem, but not to the same extent as was seen for UGU sites. UGC sites do not appear to show any significant increase in affinity. As for the isolated domains most of the interaction with CUG repeat RNA substrates is occurring via RRM1, with minimal perturbation of residues in RRM2.

We have shown that the separation between UGU sites is critical in determining whether a given RNA sequence can bind both domains in tandem. For optimal binding an absolute minimum of 2 nucleotides between UGU sites is required. The upper limit is not as well defined, with a gradual decline in binding affinity seen for spacers of 5 or more nucleotides. Even with a seven nucleotide spacer there was still a tenfold increase in binding affinity compared to the isolated domains. The optimal target sequence of the N-terminal domains of CELF1 was therefore concluded to be UGU(U) x UGU with x between 2 and 4, which were found to have a K_d of around 400 nM.

The ^{15}N heteronuclear NOE data shows that even when bound to an optimal RNA target, there remain some intrinsic dynamics in the linker region that facilitates binding to RNAs with a range of spacer lengths. This in combination with the data collected on the extended t242 construct showed no involvement of the N- or C-terminal unstructured regions in RNA binding, contrasting with the N-terminal extension involvement reported for RRM3.

Both the EDEN11 GRE and EDEN15 sequences have been demonstrated to form high affinity complexes with the two N-terminal domains of CELF1, consistent with them being “EDEN” motifs targeted by the full length CELF1 protein. Both sequences have unoccupied UGU sites, which could potentially be bound by the third RRM, increasing the affinity even further.

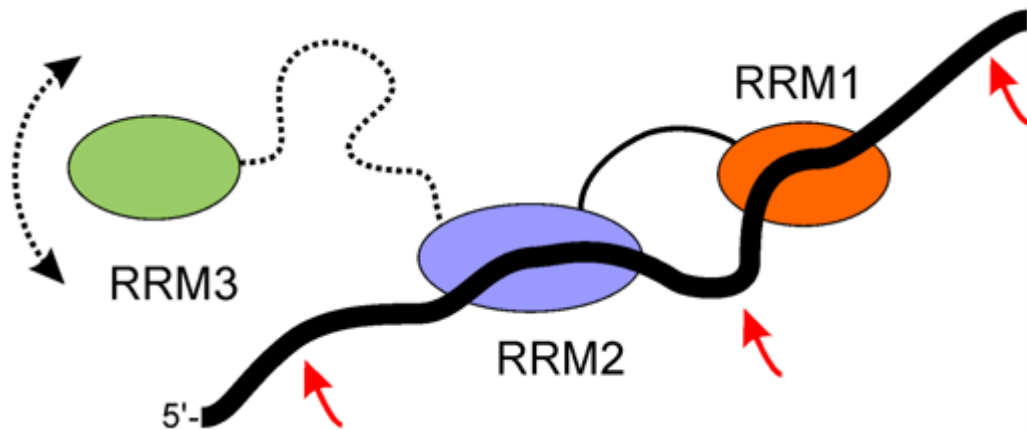


Figure 5.26: Possible arrangements of full length CELF1 on a repeating UGUU RNA substrate such as EDEN15 or EDEN11. Red arrows indicate possible locations of the binding site for RRM3 on the RNA strand. Since RRM1 and RRM2 have been shown to occupy the outer two UGU sites of EDEN11, there is potentially an unoccupied site between the domains. If this site cannot be bound by RRM3, then an additional UGU site must be added to the sequence towards either the 5' or 3' end of the RNA strand. The length and flexibility of the RRM2 – RRM3 linker meant that any of these positions initially appeared to be plausible. This was further investigated in chapter 6.

For the EDEN11 GRE to be binding all three RRM, RRM3 would have to occupy the central UGU site between RRM1 and RRM2, as shown by the central arrow in Figure 5.26. If this site is too hindered for RRM3 to bind then a longer RNA with an additional UGU site (such as the EDEN15 GRE) would be required. The length of the RRM2 – RRM3 linker is sufficient that it seems possible RRM3 could bind either towards the 5' end or to the 3' end of the other two domains.

6 Optimal RNA Targets of Full Length CELF1

6.1 Introduction

Wild type full length CELF1 is known to form a high affinity interaction with an RNA motif found in the 3' UTR of the mRNAs that the protein regulates. This had been termed the “EDEN motif”, but the sequence or range of sequences that could be recognised by CELF1 was not well defined. Some mRNAs, such as *c-mos*, *c-jun* and *TNF α* have been shown empirically to be bound by CELF1 triggering deadenylation, but it is not clear which regions of these sequences are being recognised. Without knowing the exact criteria for an EDEN motif, it is not possible to predict whether any given mRNA is regulated by CELF1.

Full length CELF1 consists of three RRM domains. The two N-terminal domains were investigated by NMR and ITC in the previous chapters. X-ray crystallography data on these domains was also collected by Teplova *et al.* (2010). The C-terminal RRM3 was investigated in isolation by Tsuda *et al.* (2009). However no data had been collected on the full length CELF1 protein containing all three domains, so it was not known how they worked together in order to bind a complete EDEN motif.

Some consensus sequences which constitute possible EDEN motifs have been discussed previously. Vlasova *et al.* suggested the EDEN11 GRE (UGUUUGUUUGU) and Graindorge *et al.* the longer EDEN15 (UGUUUGUUUGUUUGU) sequence. Rattenbacher *et al.* (2010) later suggested a long UG repeating sequence as a possible EDEN motif, while Masuda *et al.* (2012) suggested UGUUUGU (the EDEN7 sequence previously investigated). While all of these sequences were shown to be capable of binding to CELF1, it was not known if they were interacting with all three RRMs simultaneously, or sufficient to trigger deadenylation. These sequences could therefore be only

partial EDEN motifs, interacting with a subset of the CELF1 RRMs. The target identified by Masuda *et al.* (UGUUUGU) was already known to be incapable of interacting with both N-terminal RRMs simultaneously from work in the previous chapter. The question was therefore whether the longer EDEN11 GRE and EDEN15 sequences were complete, or merely partial targets for full length CELF1.

Previous *in vitro* studies of CELF1 had all used constructs of one or two RRMs rather than the full length protein. Our initial aim was therefore to devise a purification protocol for the complete CELF1 protein. Using this we would then determine by NMR and ITC whether the reported EDEN11 and/or EDEN15 GRE consensus sequences do in fact represent high affinity “EDEN motifs” targeted by CELF1. If these sequences were not complete EDEN motifs, we then aimed to design high affinity RNA sequences capable of binding all three RRMs based on our data on preferences of the smaller constructs. From this we would refine the overall criteria for an EDEN motif, and use these to explain how CELF1 is recognising known mRNA targets such as c-jun, c-mos and TNF α .

6.2 Purification of Wild Type CELF1

To study how all three RRMs of CELF1 interact, it was necessary to develop a purification protocol for the full length protein. This proved problematic due to the protein undergoing rapid proteolysis in the linker region between RRM2 and RRM3. The DNA for the full 489 residue CELF1 protein in a pET28b(+) vector (supplied by Dr. Emilie Malaurie, University of Nottingham) was transformed into XL1 Blue, and then BL21 (DE3) cells. Initial test growths showed some solubility issues. At 37°C the protein expressed, but rapidly became insoluble, as can be seen in the SDS-PAGE gel in Figure 6.1.

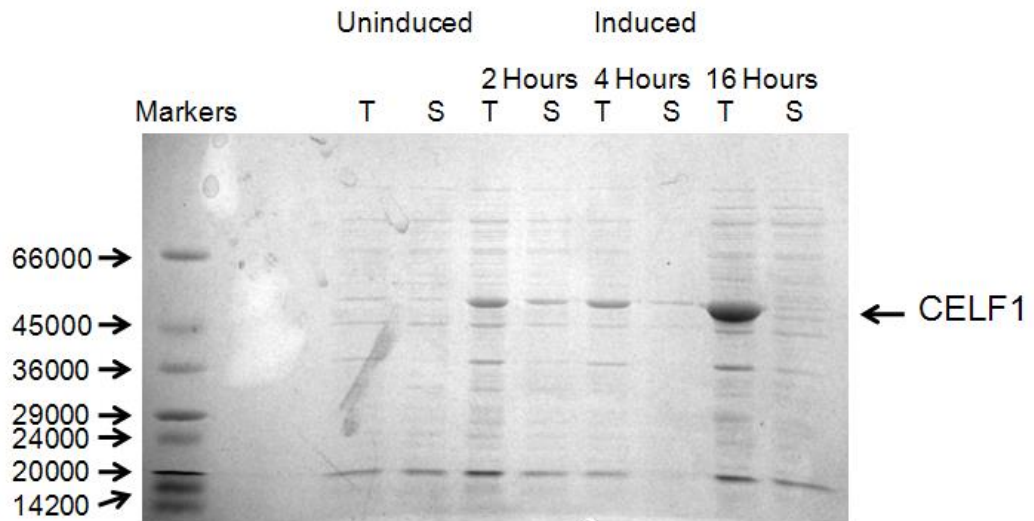


Figure 6.1: 20% SDS-PAGE of the test growth of full length wild type CELF1 at 37°C. At each time point the total fraction containing both soluble and insoluble proteins is shown in lane T, while the soluble fraction is shown in lane S. An expression band at the expected mass (~53kDa) is seen, but the percentage in the soluble fraction declines over time. No band is visible in the soluble fraction after 16 hours, and only a small fraction of the protein is in solution after 4 hours.

The decline in solubility over time indicates insoluble inclusion bodies are forming. The protein was mostly in the insoluble fraction 4 hours after induction, and completely in the insoluble fraction after this. The same problem was seen in test growths at 30°C and 25°C. To improve solubility it proved necessary to both reduce the induction temperature (to 20°C), and keep the induction period short at 4 hours. This resulted in soluble protein, as shown in Figure 6.2, but a very low overall yield of approximately 1 mg/l of growth.

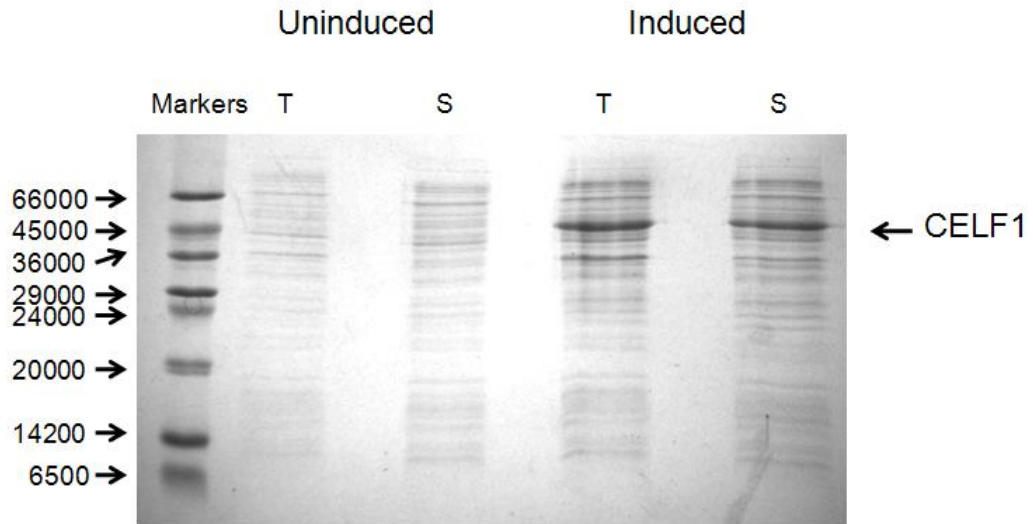


Figure 6.2: 20% SDS-PAGE from a short induction, low temperature test expression. The protein expression was induced with 1 ml of IPTG for 4 hours at 20°C to prevent formation of insoluble inclusion bodies. The CELF1 expression band is visible, and the majority of the protein seems to be in the soluble fraction. At this stage the protein is intact. Fragmentation of the RRM2 - RRM3 linker does not occur until after the cells are lysed.

While less protein was expressed in total, more of it is in the soluble fraction than after 4 hours at 30°C. These durations and temperatures were therefore used for large scale growths. Cell lysis and the IMAC column stage of the purification were initially carried out using the same basic protocol as for the t187 construct. A Roche EDTA free protease inhibitor cocktail was added to the resuspended cells prior to sonication. The time allowed for binding to the cobalt resin was restricted to one hour in order to minimise the time available for proteases to break down the protein. Samples from each stage of the purification were analysed by SDS-PAGE to check the condition of the eluted protein. The resulting gel is shown in Figure 6.3.



Figure 6.3: 20% SDS-PAGE of the IMAC column washes and elution fractions from a purification of unlabelled wild type CELF1. The wash step consisted of 25 ml of buffer A + 10 mM imidazole. The “unbound” lane is a diluted sample of the cell lysate drained from the IMAC column. The presence of multiple bands in the elution fractions indicate that the full length CELF1 has largely fragmented by this stage of the purification.

While a small amount of intact CELF1 was visible as the uppermost band on the gel (with a mass of approximately 53 kDa), the vast majority of the protein had been fragmented. The presence of multiple strong bands with masses of 24 - 36 kDa indicates that all these fragmentation sites are in the linker between RRM2 and RRM3. The protease inhibitor cocktail evidently was not effective in preventing proteolysis of the full length CELF1 protein. The elution fractions were combined and loaded onto a Superdex 200 gel filtration in an attempt to separate the remaining intact protein from the truncated forms. The thrombin cleave step was omitted. The trace of 280 nm absorbance showed multiple broad peaks. Analysis of the fractions by SDS-PAGE is shown in Figure 6.4.

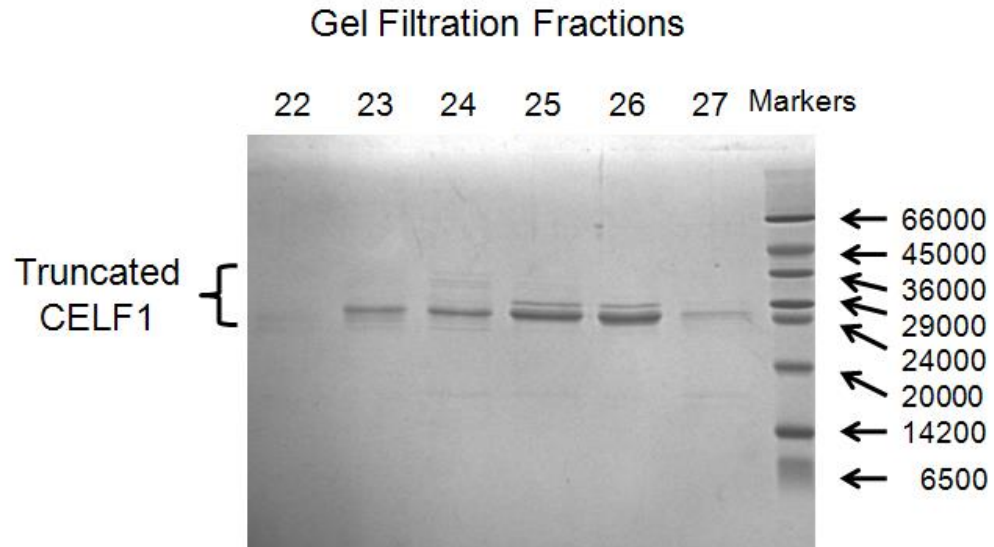


Figure 6.4: SDS-PAGE of the protein containing gel filtration fractions 22 – 30 from a purification of wild type CELF1 using a Superdex 200 column. Lanes are labelled with the elution fraction number (40 x 10 ml fractions were collected). The protein has continued to degrade since the drip column stage, and has now mostly been truncated to a stable fragment of between 24 and 29 kDa.

The void volume for this gel filtration column is 120 ml. No protein bands were observed in elution fractions from 130 – 210 ml. The vast majority of the material seen on this gel has a molecular mass of between 24 and 29 kDa, consistent with protein fragments slightly longer than the t242 construct. It appears the protein continued to break down during the gel filtration stage, until it reached the longest stable fragment. Analysis by ESI mass-spectrometry showed multiple species, even after an additional desalting step into ammonium acetate. Only a rough approximation of the exact mass of the longest stable fragment could be calculated.

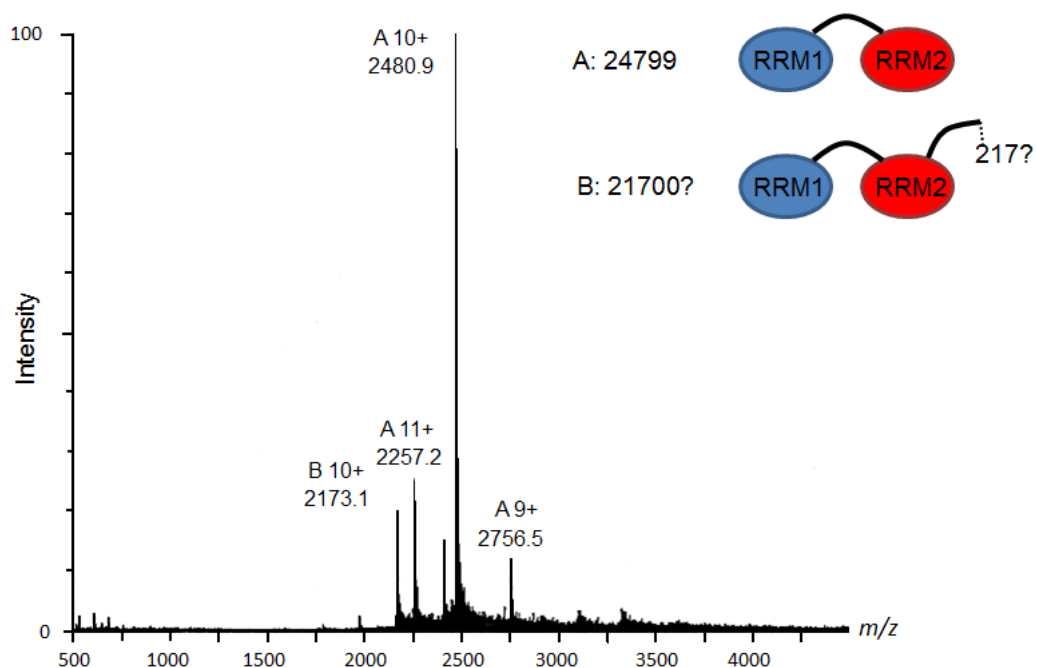


Figure 6.5: ESI mass spectrum of the degradation products of full length wild type CELF1. The total protein concentration was approximately 2 μ M. The major species has a mass of approximately 24799 Da. There is an additional minor species with a mass of approximately 21730 Da.

The major species appears to have a mass of approximately 24800, which does not match precisely to a fragmentation product of CELF1. The break site, assuming this is the N-terminal fragment, would be at around Leu217 or Thr218, though the observed mass does not match precisely to either. This is closer to the N-terminus than expected, given that the t242 construct appeared stable when analysed by SDS-PAGE. The C-terminal fragment could not be detected, but may have been removed at the gel filtration stage.

The earlier gels from the IMAC column stage of the purification also suggest that the fragmentation is occurring in several places in the linker region from the number of bands present. If only a small number of protease sites were present then they could have been removed by point mutation. However the number of protease sites required to give the range of species seen in the elution fractions and the difficulties of precisely locating them made this approach impractical. The main band of ~25 kDa after gel filtration is merely the longest stable

fragment, consisting of approximately the first 220 residues, and by this point in the purification the vast majority of the protein was fully degraded.

CELF1 is expressed intact, and remains so as long as it is in the cell, as can be seen by SDS-PAGE if all proteins are denatured immediately after cell lysis. Diluting the cell lysate immediately after sonication slowed the fragmentation process to some extent, but did not prevent it completely. It was found that lysing the cells under denaturing conditions (in the presence of 8 M urea) prevented fragmentation of CELF1, presumably due to denaturation of the proteases responsible as well. This also had the advantage of solubilising the insoluble fraction of the protein, allowing a longer induction time to be used resulting in an improved overall yield. A purification based on denaturing CELF1 at the cell lysis stage, and refolding it after the gel filtration step was attempted, but the peak dispersion in the 1D proton NMR spectra indicated that the protein was not correctly refolded. None of the normal dispersed peaks from the domains could be observed, and all signals were in a narrow band suggestive of random coil.

Reducing the concentration of urea in the lysis buffer to 4 M still prevented most of the fragmentation problems. Based on fluorescence experiments with varying concentrations of denaturant CELF1 should still be mostly folded under these conditions. Small amounts of intact material (1 - 2 mg per litre of M9 minimal media) were produced by this method, and confirmed to be folded based on the peak dispersion in the NMR spectra. The ^{15}N TROSY spectrum of this material is shown in Figure 6.6.

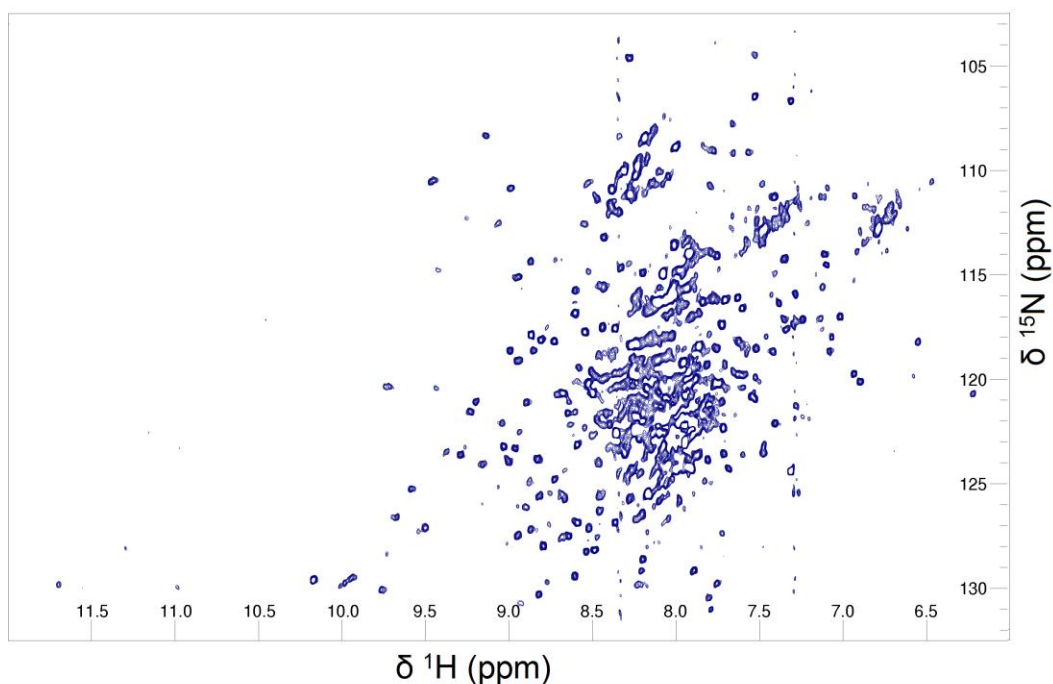


Figure 6.6: ^{15}N TROSY of full length wild type CELF1. This spectrum was collected on a 100 μM protein sample in 50 mM potassium phosphate, 200 mM NaCl, 10% (v/v) D_2O pH 7.0 NMR buffer, using an 800 MHz Bruker Avance III spectrometer with a QCI cryoprobe at 298 K. Due to the low signal to noise ratio 360 scans were required to obtain this quality of spectrum. The lengthy acquisition time and poor sample stability made it impractical to run titrations similar to those carried out on t187 and the isolated RRM3 using this sample.

Peaks with chemical shifts closely matching those of the residues of the isolated RRM1, RRM2 and RRM3 constructs can be seen. There are also a large number of peaks from the flexible RRM2 – RRM3 linker visible between 7.5 and 8.5 ppm in the proton dimension. Solubility remained a serious problem, as the protein could not be concentrated above $\sim 125 \mu\text{M}$ without a significant concentration of urea present. The protein was also insoluble in the 50 mM salt buffers used in previous experiments, requiring a 200 mM salt concentration in the NMR buffer resulting in a reduction in signal to noise ratio. The long acquisition times required made it difficult to carry out NMR titrations similar to those used to identify the preferred t187 RNA substrate.

6.2.1 Production of a Stable Construct Containing all three Domains

To bypass the solubility and stability issues encountered with wild type CELF1 it was decided to produce a construct in which a large section of the RRM2 - RRM3 linker was removed. This would remove the many fragmentation sites in this region, and was also expected to improve the solubility of the protein.

The first designed construct consisted of t242 fused to residues 385 - 489 based on Tsuda *et al*'s RRM3 construct which was reported to be stable, and the t242 construct which appeared to remain intact during the purification (see section 5.6.2). While fragmentation of the protein was greatly reduced, the solubility for this new construct remained low, with a maximum concentration of ~125 μ M in the 50 mM potassium phosphate, 200 mM NaCl buffer. The construct was therefore further shortened to residues 1 - 214 fused to 385 - 489 on the basis that t242 had been previously observed to have solubility issues, while RRM3 did not.

This shortened construct proved to be both stable and soluble to protein concentrations of at least 500 μ M in buffer A. Purification yields were improved to ~15 mg/l when grown in LB and 8 - 9 mg in M9 minimal media. The interaction of all three RRMs to bind long RNAs could be studied by NMR and ITC using this new construct, which was termed RRM123. With around 30 residues of flexible protein remaining between RRM2 and RRM3, the domains were still free to adopt any orientation relative to each other.

6.2.2 Production of Deletion Mutants Using a Single Step PCR

These constructs were produced using a one-step PCR deletion method as outlined by Qi *et al.* (2008), from the wild type CELF1 DNA, as specified in section 3.15.6. In this method the primers are designed so that the PCR amplifies the entire plasmid except for the section to be deleted. The primers consist of two sections; a short overlapping section with a low annealing temperature and a

longer non-overlapping section which will anneal to the template DNA at a temperature at least 5 K higher¹⁶⁶.

The PCR is run for 18 cycles at a temperature where the non-overlapping sections of the primer will anneal, but the overlapping sections will not. This amplifies the entire plasmid except the section to be deleted, and leaves complementary “sticky ends”. The temperature is then reduced so that these ends anneal to each other, reforming the plasmid into a circle, as shown below in Figure 6.7. This is followed by a final elongation step of 30 minutes.

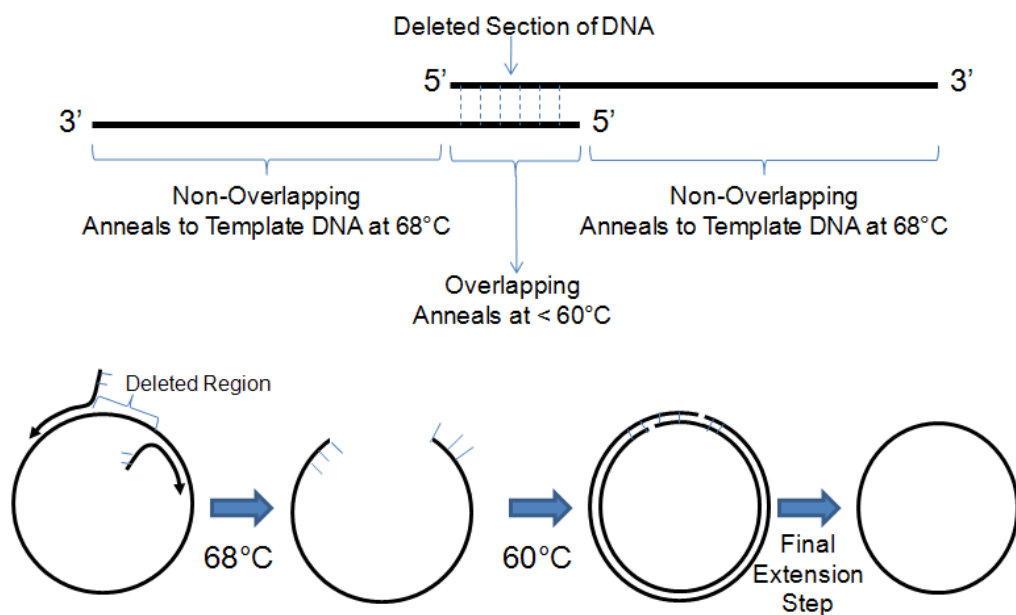


Figure 6.7: Above is shown the design of primers in this one step deletion method. In the initial higher temperature stage of the PCR the non-overlapping regions of the primers anneal, amplifying the entire plasmid except for the region to be deleted. The complementary sections of the primers anneal at the lower temperature.

As before the sequence of the resulting construct was verified by DNA sequencing. However the success of the deletion process could also be rapidly checked using an agarose gel. As the deleted section is relatively large, being in excess of 500 bases for each of these constructs, the difference in size between the template DNA and the PCR product is clearly visible after a successful reaction.

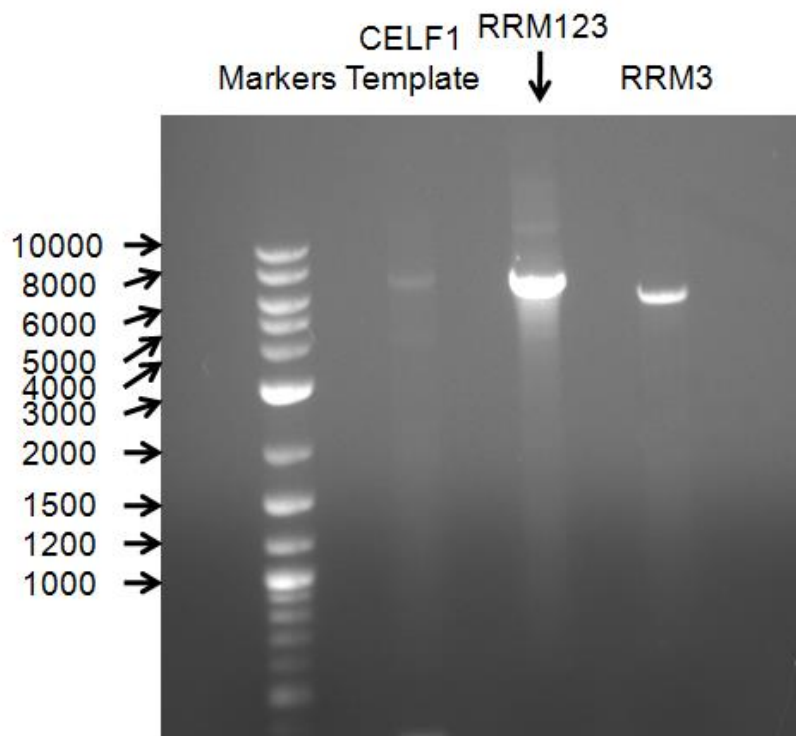


Figure 6.8: DNA gel showing the change in plasmid size in a successful deletion PCR. In the left hand lane is a 2-log DNA ladder (New England Biolabs) as a reference. In lane 2 is the template DNA, in this case the plasmid containing full length CELF1 in a pET28b vector with a total size of 6500 bp. In lane 3 is the PCR product from the reaction to produce the RRM123 construct. In lane 4 is the PCR product from a reaction to produce the RRM3 construct. The difference in size between these two PCR products and the template DNA is clear.

The plasmid DNA was transformed into XL1 Blue cells. The DNA was extracted from an overnight cell culture and sequenced to confirm the intended section had been deleted, after which it was transformed into BL21 (DE3) cells for expression.

6.3 Expression and Purification of RRM123

The expression and IMAC column stages of the purification used the same protocols as for the t187 construct. RRM123 was found to remain soluble in a 16 hour expression at 30°C, unlike the full length CELF1 protein.

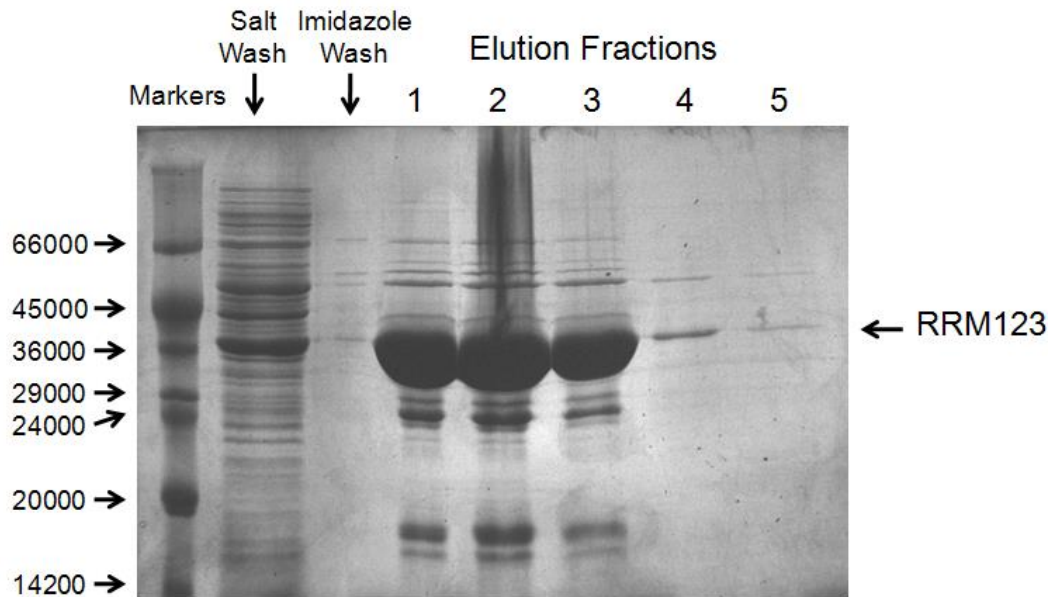


Figure 6.9: SDS-PAGE of the washes and elution fractions from the IMAC column stage of the RRM123 purification. The vast majority of the protein is now intact, and is of the expected molecular weight (38 kDa). The presence of low intensity bands at approximately 25 suggests a small amount of fragmentation is still occurring, but not to the same extent as seen in Figure 6.3 for the wild type CELF1.

The eluted protein was purified using a Superdex 200 gel filtration column, which separated out the lower molecular weight fragments of RRM123 as well as any other impurities. Those fractions containing protein were identified by their absorbance at 280 nm, and analysed by SDS-PAGE. The results of this are shown in Figure 6.10.

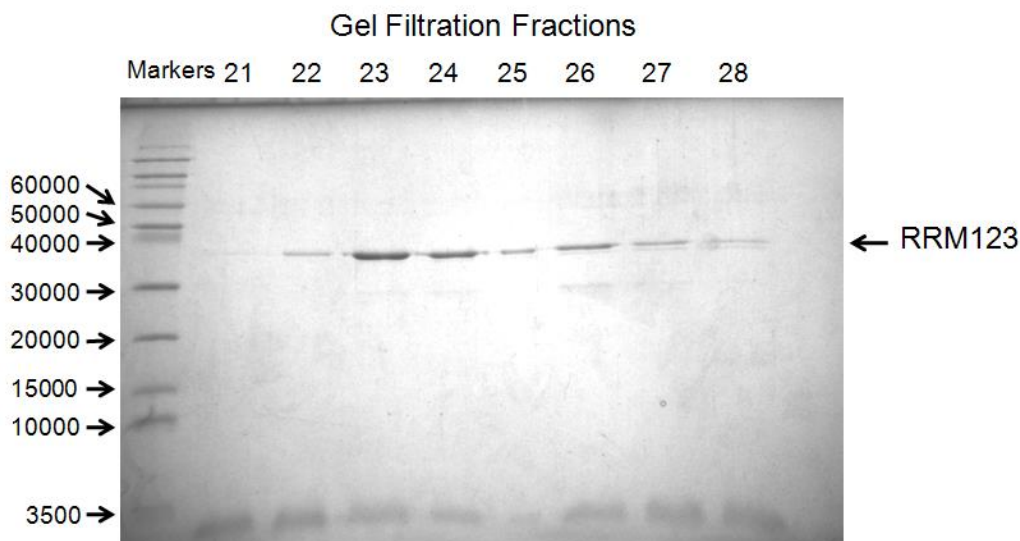


Figure 6.10: SDS-PAGE of gel filtration fractions. RRM123 is remaining intact and in solution throughout the gel filtration stage of the purification, although it does appear spread across an unusually large range of fractions.

The mass of the protein was determined by mass spectrometry to be 38348 ± 7 Da. RRM123 has a theoretical mass of 36026 Da, but this protein still has the N-terminal 6-His tag attached, giving a theoretical overall mass of 38348 Da. A much larger range of charge states is seen for this construct than for t187, as can be seen in Figure 6.11. This can be attributed to the unstructured linker region in RRM123, and the presence of the complete N-terminal His-tag. Denatured proteins tend to show a very large charge envelope due to the greater ability of the unstructured peptide chain to pick up additional charges, and this is presumably the case for the long unstructured regions in the larger CELF1 constructs.

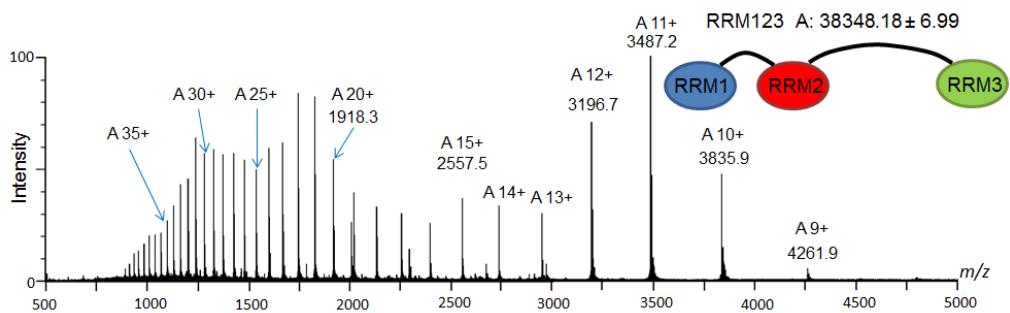


Figure 6.11: ESI mass spectrum of RRM123, under native conditions. The protein concentration was 5 μ M. A single species with a mass of 38348 Da is seen, consistent with the His-tagged RRM123 protein. Charge states ranging from +9 to +40 are seen. This large range compared to the other constructs is presumably due to both the remaining unstructured section of the RRM2 – RRM3 linker and the 6-His tag.

6.3.1 NMR Characterisation of RRM123

15 N labelled material was produced, and an initial 15 N TROSY spectrum was collected on a Bruker Avance III 600 MHz spectrometer. While it required higher scans and resolution than previous experiments with t187, a spectrum in which peaks from all three RRMs could be clearly resolved was acquired. A higher resolution spectrum was later collected at 800 MHz which is shown in Figure 6.12.

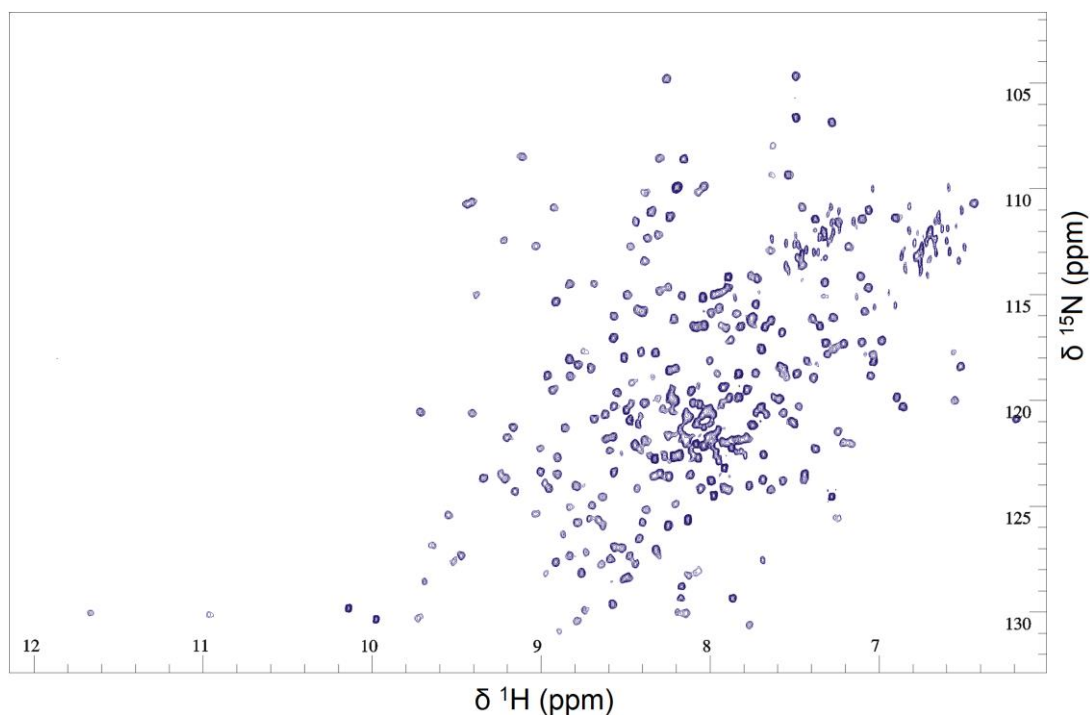


Figure 6.12: ^{15}N TROSY spectrum of the RRM123 construct. This was collected on a 250 μM sample in 25 mM potassium phosphate, 100 mM NaCl, 10% v/v D_2O pH 7.0 NMR buffer. Data was collected on a Bruker Avance III 800 MHz spectrometer with QCI cryoprobe at 298 K.

The quality of the spectrum is surprisingly good given this is a relatively large protein with a mass of 38 kDa. This is likely due to the favourable internal dynamics in the protein. Since the three structured RRMs are separated by flexible linkers and move fairly independently the relaxation rates are likely to be closer to those of a 12 kDa RRM than a 38 kDa globular protein. The linewidths of the peaks are therefore still quite narrow, allowing clear resolution of most peaks despite the spectrum being relatively crowded with signals from more than 300 residues.

Combining the spectra of the three separate RRMs gives a very good match to the RRM123 spectrum. There are still some additional peaks from the remaining section of the RRM2 - RRM3 linker, and these are clustered in a narrow band between 7.5 and 8.5 ppm, indicative of unstructured protein. RRM3 can therefore be concluded not to interact with the other RRMs or the flexible linker since the chemical shifts of its residues in the RRM123 spectrum are not significantly

different from those in the spectrum of the isolated domain. The RRM1 and RRM2 chemical shifts as expected match those in the t187 construct, with the exception of Ala186 and Asp187.

The increased sample solubility and improved signal to noise ratio from the lower salt concentration meant that adequate resolution of the peaks of all three RRMs required only 32 scans at a resolution of 2048 x 128 points. This meant that acquisition times were short enough that RNA titrations could be conducted easily using this construct.

Assignment of the peaks from all three RRMs was carried out by analogy to the smaller constructs. No assignment of the peaks from the RRM2 – RRM3 linker was attempted. This protein does give surprisingly high quality NMR spectra, and so it should be possible to collect 3D heteronuclear data. The unstructured nature of this linker would make the assignment strategy used so far problematic, but alternative assignment strategies for intrinsically disordered regions of proteins could be used. While the peaks from the side chain C α and C β shifts show very limited dispersion in intrinsically disordered regions, greater dispersion is seen for the ^{15}N and $^{13}\text{C}'$ shifts. Alternative HA-detect 3D experiments such as H(CA)NCO and H(CA)CON can be used to establish backbone connectivities from these nuclei¹⁸³. Further dispersion of peaks could be achieved by the use of 4D or 5D NMR experiments, with non-uniform sampling methods to reduce the acquisition time required^{184, 185, 186}.

6.3.2 ^{15}N Heteronuclear NOE

To characterise the relative flexibility of different sections of the protein ^{15}N heteronuclear NOE data was collected on an 800 MHz spectrometer with cryoprobe. 168 scans were accumulated at a resolution of 2048 x 256 points. Experiments with and without the NOE were interleaved to minimise artefacts from any changes in the spectrum over time.

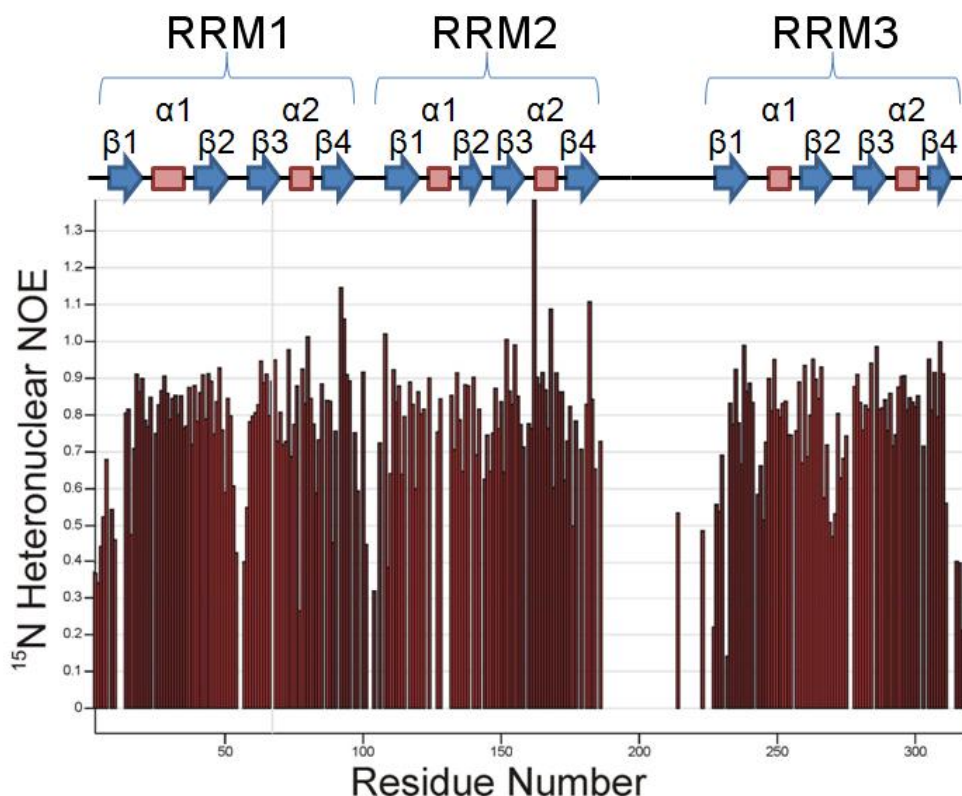


Figure 6.13: ^{15}N Heteronuclear NOE plotted against residue number. It can be seen that the three RRMs are highly structured, with the exception of some loop regions. Smaller NOEs are seen for the residues in the flexible regions between the domains, though assignments are not available for most of the RRM2 to RRM3 linker.

RRM1 and 2 show similar ^{15}N heteronuclear NOE values to the t187 construct. A few residues show NOE values of greater than 1, which is probably due to the relatively large margin of error in measuring the intensity of some of the weaker signals. Both domains are quite rigid, with the exception of the N-terminus, the linker around residues 100 - 107 and the loop from residues 52 - 57 which are moderately flexible. No assignments are available for most of the RRM2 to RRM3 linker. RRM3 is quite rigid, though there is a noticeable drop in the heteronuclear NOE for the N-terminal extension and the C-terminus of the protein. There is a slight decrease around residue 270, again due to a relatively flexible loop between two strands of the β -sheet. These loops do not appear to be involved in RNA recognition, based on NMR chemical shift perturbations and the available x-ray crystal structures.

These flexible linkers allow significant interdomain dynamics, which may contribute to the high quality NMR spectra that can be collected for this construct. The overall structure of the RRM123 construct (and presumably also the 53 kDa wild type CELF1) can be summarised as three “beads on a string”. The domains are free to move relatively independently with the result that their relaxation rates are closer to those of than isolated domains than for the average 38 kDa protein. This effect was observed for the RRM1 and RRM2 domains by Teplova *et al.* They reported rotational correlation times of 10.2 ns and 9.7 ns for RRM1 and RRM2 respectively, when connected as a construct of residues 14 – 187 of CELF1¹⁸⁷. These are both lower than the ~12 ns time which would be expected for a globular protein of the same mass^{188, 189}. Teplova *et al.* also noted a substantial increase in the rotational correlation times for both domains when bound in tandem to an RNA substrate, to 14.6 ns and 12.0 ns for RRM1 and RRM2 respectively. This was attributed to restriction of the relative motion of the domains by the RNA, though the significant difference seen for the two domains indicates the resulting structure is not completely rigid⁵¹.

6.4 Interactions of RRM123 with the EDEN11 GRE

With the aim of identifying RNA sequences which could bind all three RRMs simultaneously, NMR titrations were carried out on ¹⁵N-labelled RRM123, using an 800 MHz NMR spectrometer. The EDEN11 GRE (UGUUUGUUUGU) was considered as a possible candidate, containing three UGU sites. This RNA was titrated into a 250 μM sample of ¹⁵N-labelled RRM123.

Chemical shift perturbations were observed for residues on the binding surfaces of all three RRMs, with generally the same set of affected residues as were seen with the isolated domains. Gly21, Cys61 and Gln93 from RRM1 and Gly113, Cys150 and Val182 from RRM2 all show large CSPs. From RRM3 residues such as Cys446 and Gly448 are strongly perturbed, matching data reported by Tsuda *et*

al. for the binding of RRM3 to UGUGUG in isolation. This confirmed that all of the RRMs could recognise a UGU(U) site in the EDEN11 GRE. However the titration did not reach an endpoint until a 2:1 excess of RNA had been reached. At a 1:1 ratio the peaks were very broad, with far too few resolvable signals to account for all of the residues. This suggests the midpoint of a titration in intermediate exchange on the NMR timescale. The peaks from the perturbed residues are therefore extremely broad, and not observable in the spectra from the intermediate titration points. Since each of the smaller constructs generally reached saturation at about a 1:1 RNA to protein ratio this indicated that the EDEN11 GRE is not forming a tight 1:1 complex, but instead one with a higher stoichiometry, which would not be expected if the EDEN11 GRE represented a complete EDEN motif capable of binding all three domains of CELF1.

The fully bound spectrum at a 2:1 excess of RNA is a close match to a combination of the bound spectra of each of the three RRMs in isolation, and is shown in Figure 6.14.

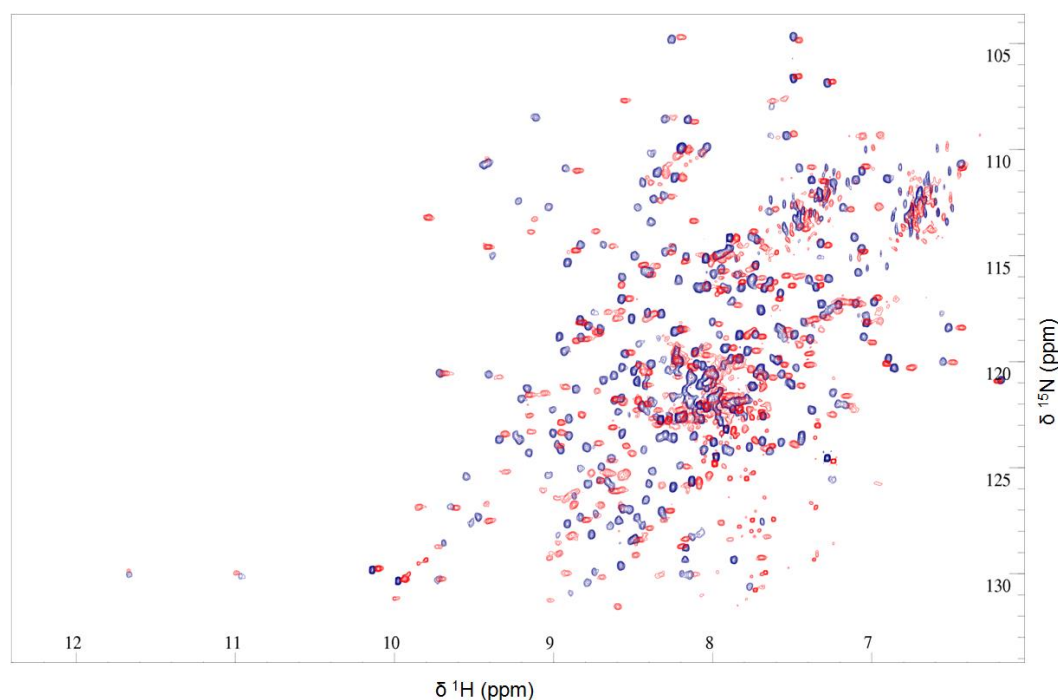


Figure 6.14: The ^{15}N TROSY of the unbound RRM123 is shown in blue. Overlaid in red is the spectrum of RRM123 after the addition of a 2:1 excess of the EDEN11 GRE RNA (UGUUUGUUUGU). Both spectra were collected on a Bruker Avance III 800 MHz spectrometer with a cryoprobe. The protein concentration was 250 μM . 32 scans were collected at a temperature of 298K.

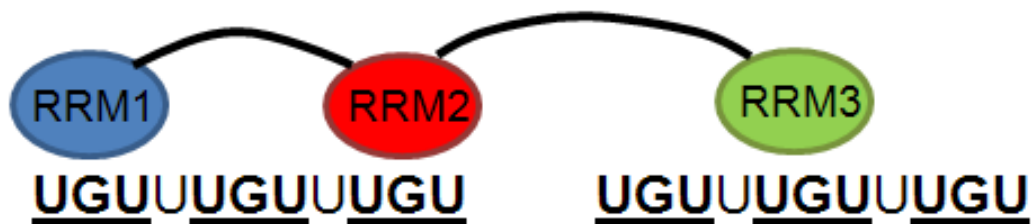


Figure 6.15: A possible 2:1 complex of RRM123 with the EDEN11 GRE, consistent with the NMR data.

The data suggest that the protein is binding two RNA molecules, one via RRM3, and the other by the tandem interaction of RRM1 and RRM2, as shown in Figure 6.15. If the binding affinity of RRM3 to the RNA is of comparable strength to the tandem binding of N-terminal domains to the RNA (as would be predicted based on the ITC results for t187, and the reported RRM3 ITC data from Tsuda *et al.* 2009) then at a 1:1 ratio a mixture of bound species would be present. Multiple species in intermediate exchange would account for the poor signal to noise seen across the residues in the binding interfaces of all three RRMs. Another possibility was that all three RRMs were binding onto a single RNA molecule, but with more than one conformation. For example, it might be possible to arrange the RRMs in a different order from the 5' to 3' end of the RNA substrate if the linkers between domains are sufficiently flexible. While this would account for a broadening of the line widths, it would not account for the apparent 2:1 stoichiometry observed for this titration.

As a control experiment a titration with the EDEN4U RNA substrate (UGUUUUUGU) was carried out under the same conditions. Since this sequence contains only two UGU sites, and was known to be an optimal target for the tandem binding of RRM1 and RRM2, it is definitely not capable of binding all three RRMs simultaneously. This control titration showed almost identical results to the EDEN11 GRE case, supporting the hypothesis of EDEN11 forming a 2:1 complex. Again, the signals were broad and poorly resolved at a 1:1 ratio, with a recovery of spectrum quality at around a 2:1 excess of RNA.

6.4.1 ITC of the EDEN11 GRE Binding to RRM123

The EDEN11 GRE was tested for formation of a 1:1 complex, again using EDEN4U as a control, with the results shown in Figure 6.16.

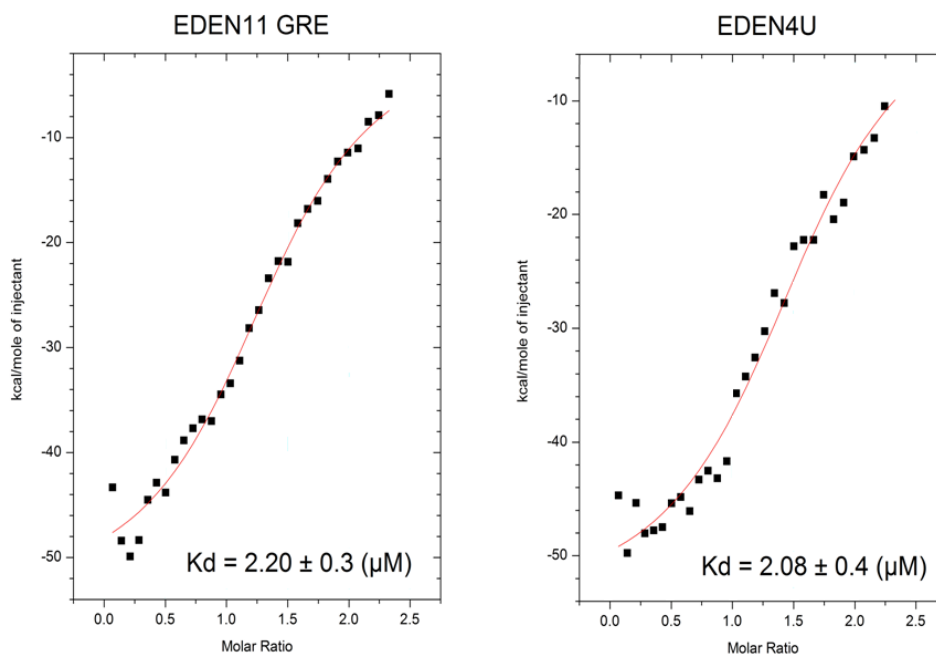


Figure 6.16: Binding curves for ITC of 125 μM EDEN11 GRE (UGUUUGUUUGU) and EDEN4U (UGUUUUUUGU) RNA substrates into 12.5 μM RRM123. Red lines show the best fitting match to a one-site binding model. Neither titration reaches full saturation at the endpoint (a 2.5:1 excess of RNA).

The EDEN11 GRE and EDEN4U RNA substrates give very similar binding curves on titration into RRM123. In both cases the titration fails to reach an endpoint until more than a 2:1 excess of RNA is present. K_d values of around 2 μM are seen for both sequences, which is comparable to that seen in the t187 ITC data. This is all consistent with the model of two EDEN11 molecules binding to each protein, with the two binding events having comparable K_d values. This confirms that RRM3 cannot occupy the central UGU site of an EDEN11 RNA molecule that has already bound to RRM1 and RRM2. This is consistent with the conclusion in the previous chapter that t187 is binding to the two terminal UGU sites of EDEN11, leaving the central UGU site sterically inaccessible.

From the K_d values of $\sim 3 \mu\text{M}$ determined in earlier experiments for t187 binding to EDEN5U, and $1.9 \mu\text{M}$ reported for RRM3 by Tsuda *et al.*, it seems likely that the two binding events in this titration do in fact have quite similar K_d values, making them competitive. This would account for unresolved binding events observed in the EDEN4U and EDEN11 ITC experiments, contrasting with the biphasic scheme seen for RRM1/EDEN7 where the K_d values for the two binding events are substantially different.

The NMR and ITC data enable us to conclude that the EDEN11 GRE is only a partial binding motif for CELF1. Its inability to bind all three RRMs simultaneously is likely to be due to steric effects between RRM3 and the other domains, as RRM3 would have to bind to the central UGU site. The crystal structure by Tsuda *et al.* suggests RRM3 is capable of forming contacts with up to six RNA bases, and so it was not surprising that it might require a greater spacing between binding sites than the other two RRMs.

6.5 CELF1 Recognition of the EDEN15 GRE

The ITC and NMR data collected on the shorter EDEN11 GRE showed unambiguously that it cannot bind all three RRMs simultaneously, and so does not represent a complete EDEN motif. Although the EDEN11 GRE has been presented as a consensus sequence in the recent literature, the analysis by Graindorge *et al.* in 2008 originally suggested a fourth UGU site might be conserved, giving the longer GRE sequence EDEN15 as a possible complete EDEN motif.

RNA	Sequence
EDEN11	<u>UGUUUGUUUGU</u>
EDEN15	<u>UGUUUGUUUGUUUGU</u>
(UGUC) ₄	<u>UGUCUGUCUGUCUGU</u>
GU15	<u>GUGUGUGUGUGUGUG</u>

The RNA substrate (UGUC)₄ was investigated by ITC. This has four potential UGUX sites, with the same spacing as the EDEN15 GRE. The binding curve showed both a higher affinity than the EDEN11 GRE ($K_d = 0.53 \mu\text{M}$), and stoichiometry consistent with a 1:1 complex ($n = 0.84$). A 15 nucleotide GU repeat RNA substrate, similar to that suggested by Rattenbacher *et al.* (2010) was also investigated and found to give similar results as shown in Figure 6.17.

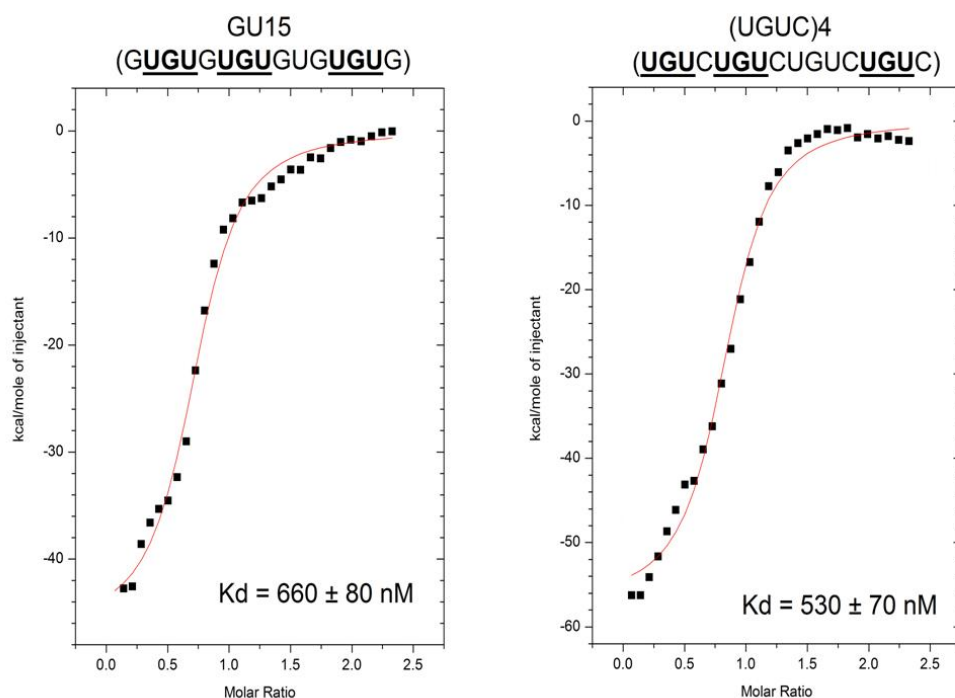


Figure 6.17: ITC Binding curves for the RNA substrates GU15 and (UGUC)₄. In red are shown the best fits to a 1: 1 binding model that could be obtained. Data processing carried out using MicroCal Origin 7.0.

From the ITC data it appears that both GU15 and (UGUC)₄ form a 1:1 complex with RRM123. Since EDEN15 has the same spacing between UGU sites as the (UGUC)₄ sequence, it could be concluded that the EDEN15 GRE will form a high affinity 1:1 complex with RRM123, and so appears to represent a complete EDEN motif. The binding affinities, while higher than for the EDEN11 GRE with RRM123 are still not much improved compared to those seen for tandem binding of the N-terminal domains. This suggests that while EDEN15 and similar sequences are capable of binding all three RRMs, the spacing between UGU sites may not be optimal.

In GU15 the separation between the UGU sites is 1 and 3 nucleotides, while in (UGUC)₄ it is 1 and 5 nucleotides. In both cases binding all three RRMs onto a single RNA molecule requires two of the RRMs to be occupying UGU sites with only a single nucleotide separating them, as illustrated in Figure 6.18. Since this was known not to be possible for the two N-terminal domains, it seemed to imply that RRM2 and RRM3 could tolerate this tight spacing between UGU sites. This was surprising, given that both of these domains were predicted to recognise UGUX sites and so would be expected to require more space than RRM1.

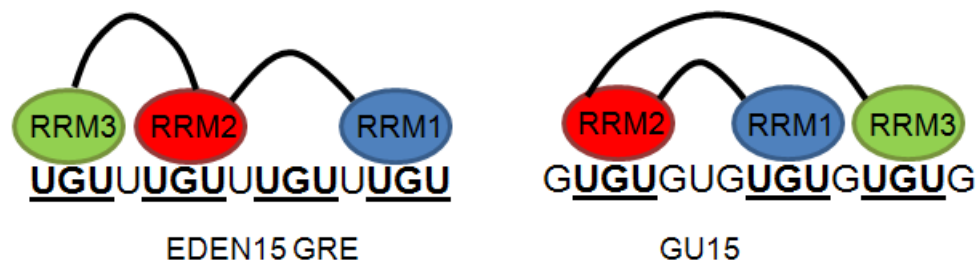


Figure 6.18: Possible arrangements of the three domains of CELF1 on the proposed EDEN motifs EDEN15 and GU15. In both cases two of the domains must occupy UGU sites separated by a single nucleotide, which is known not to be possible for the N-terminal domains RRM1 and 2.

6.6 Design of a High Affinity EDEN Motif

For optimal binding it was expected that RRM3 would need a greater spacing between the third UGU(U) site and the other two. Since the minimum spacing requirement for t187 had been determined it was possible to return to the known natural targets of CELF1, and examine the spacing between suitable sites for t187 and the next nearest UGU site. Based on these it was concluded that a spacing of 2 – 4 nucleotides between UGU sites was relatively common in the known natural targets.

c-fos: UGUUCAUUGUAAUGU

TNF α : UGUUCCCAUGU.....UGU

c-jun: UGUUUGGUAUCCUGCCAGUGUUGUUUGU...

c-mos: UAUAUGUAUGUGUUGUUUUAUGUGUGUGUGUGUGCU

This spacing was consistent with the *c-mos* and *c-fos* targets. It could also account for binding to *c-jun* if secondary structure in the spacing region could bring distant UGU sites together. This involvement of secondary structure appeared to be the only way to account for binding to TNF α , in which the third UGU site is separated by more than 30 nucleotides. Based on this observation the RNA substrate EDEN-2U/4U (UGUUUUGUUUUUUGU) was designed. RRM1 and 2 could potentially bind across either spacer with high affinity. RRM3 could be allowed up to four nucleotides between its site and the adjacent site, which was expected to improve the binding affinity compared to EDEN15 and similar RNA substrates. Also designed was a variant that used an RNA hairpin to bring two of the UGU sites into close proximity: EDEN-2U/HL (UGUUUUGUUCCCGAGGACGGGUUGU). These two RNAs were investigated by NMR and ITC to determine if they formed a 1:1 complex, and if the binding affinity was improved compared to the EDEN15 GRE.

6.6.1 NMR Studies of the EDEN-2U/4U Complex with RRM123

The initial titration of EDEN-2U/4U into ^{15}N -labelled RRM123 showed large CSPs for residues across the RNA binding surfaces of all three RRMs (see Figure 6.19).

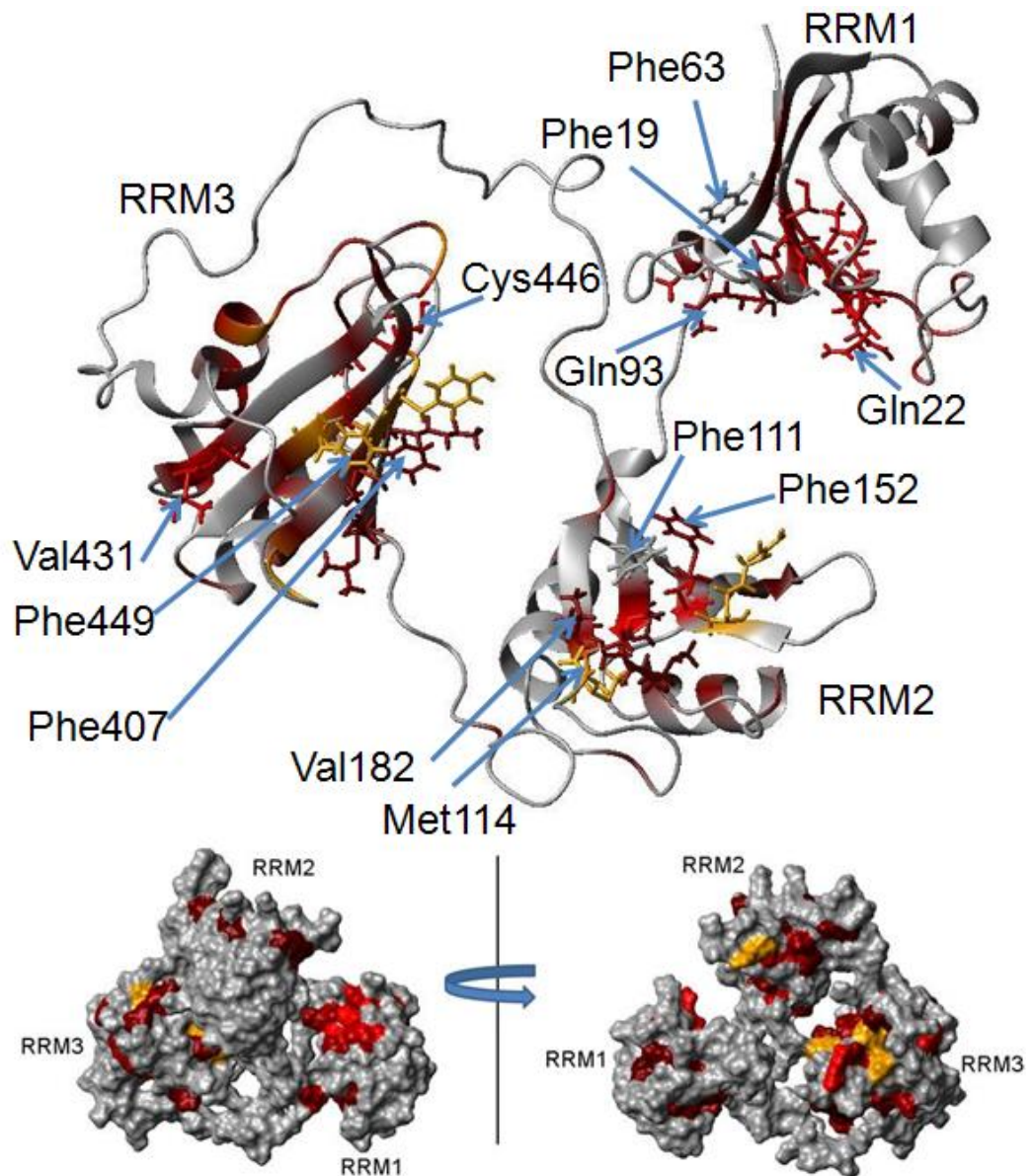


Figure 6.19: Chemical shift perturbations at a 1:1 ratio of EDEN2U/4U RNA to RRM123 protein. The brightness of the red colour indicates the magnitude of the perturbation. CSPs of less than 0.1 are assumed to be background noise, and are shown in grey. Effects are seen across the β -sheet surface of all three RRMs. Residues where the signal from the free form is rapidly lost, but no bound signal can be located are shown in yellow. Due to the presence of residues in intermediate exchange, where the peaks from the bound form are too broad to observe, minimum CSP estimates cannot be made in this situation.

With this RNA substrate there were some noticeable differences in the binding characteristics compared to earlier titrations. The signal to noise ratio remained poor throughout the titration, and was not recovered even at large excesses of RNA (3:1), unlike in the EDEN11 GRE and EDEN4U titrations. A ^{15}N TROSY spectrum with a greatly increased number of scans (720) was collected on a sample with a 1:1 ratio of RNA to protein, which showed only peaks corresponding to the bound spectrum for all three RRM s (shown in Figure 6.20). This can be seen most clearly for residues with large CSPs, such as Cys61, Cys150 and Gly478. The glycine and cysteine regions of the spectrum have been expanded and compared to the corresponding regions from the EDEN11 GRE titration in Figure 6.21.

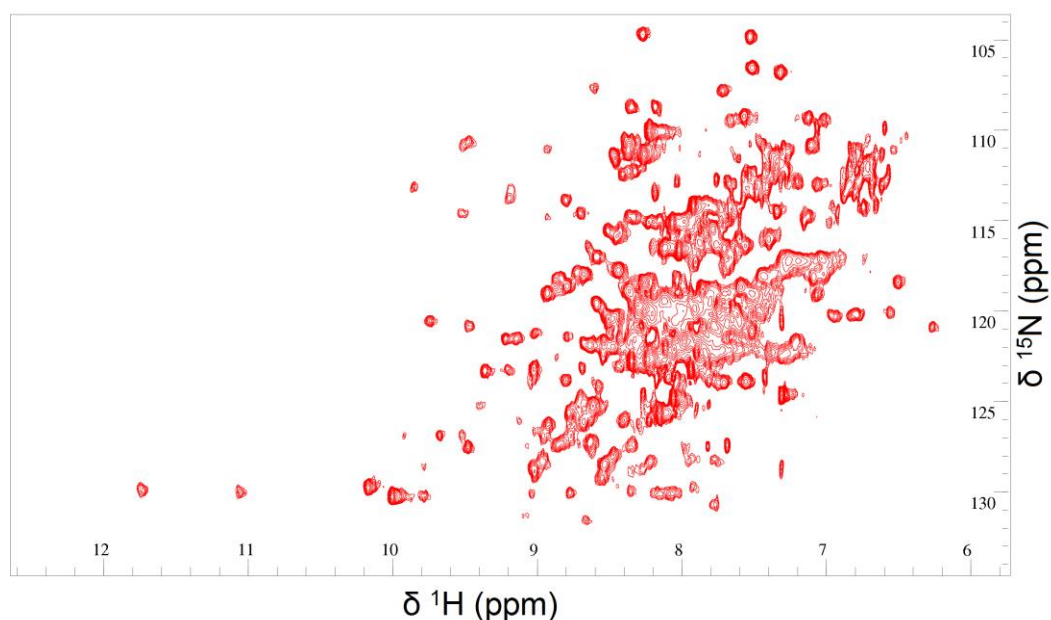


Figure 6.20: Complete ^{15}N TROSY at a 1:1 ratio of RRM123 and EDEN2U/4U, illustrating the decrease in spectrum quality compared to the free form, and the 2:1 complex with EDEN11 GRE. Peaks corresponding to the bound form of all three RRM s are visible. No peaks specific to the free form can be seen. This spectrum was acquired with 720 scans on a Bruker Avance III 800 MHz spectrometer with QCI cryoprobe at 298K.

Cys61 and Cys150 both show large CSPs, matching those seen for the titration of t187 with EDEN4U. In the glycine region of the spectrum from RRM1 Gly21, Gly60 and Cys62 also show significant CSPs. From RRM2 Gly113, Gly149 and

to a lesser extent Gln172 can be seen to move. RRM3 shows major CSPs for Gly416, Cys446 and Gly448, which match the observations reported for binding of RRM3 to a UGU site. The chemical shifts in the bound spectra for the 2:1 complex of EDEN11 with RRM123 and the 1:1 complex of EDEN-2U/4U with RRM123 are almost identical.

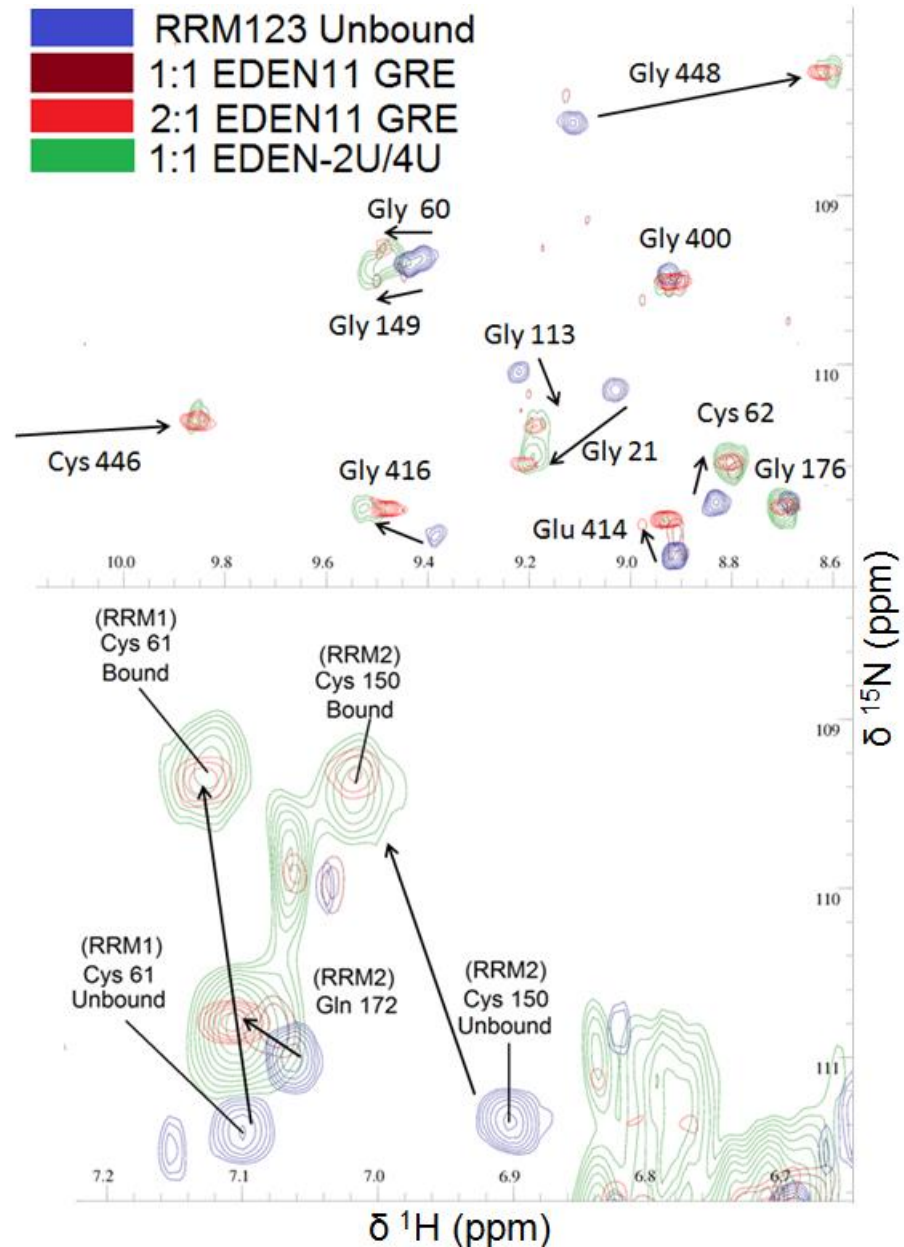


Figure 6.21: Expanded view of two regions of the ^{15}N TROSY spectrum, showing the residues most affected on binding to RNA. The spectrum of the unbound RRM123 is shown in blue. Overlaid in maroon is the spectrum at a 1:1 ratio with the EDEN11 RNA substrate, where very few peaks are visible. In green is the spectrum at a 1:1 ratio with the EDEN-2U/4U substrate, where peaks from the bound form are clearly visible. In red is the spectrum for a 2:1 ratio of EDEN11 to RRM123, where the peaks from the bound form have appeared.

No peaks specific to the free form could be observed in the EDEN-2U/4U case so it appears that the protein is fully bound at a ratio of 1:1. However the bound complex is showing a reduced signal to noise ratio and much broader linewidths compared to the end point of the EDEN11 titration. The poor signal to noise ratio cannot be attributed to intermediate exchange in this case. The peaks at a 1:1 ratio, while broad, match the bound chemical shifts of the isolated RRMs, and so are not at a population weighted average of the free and bound forms. The signal intensity is also not recovered for large excesses of RNA, which would be expected in the case of intermediate exchange.

The reduced spectrum quality could be due to the formation of a bound complex which is less dynamic and slower tumbling than the free protein. The high quality of the NMR spectra collected from unbound RRM123 samples has been attributed to the interdomain dynamics and resulting short rotational correlation times for the protein. If the dynamics of the protein change on binding, for example if it becomes more rigid and compact as all of the RRMs bind onto a single RNA molecule, this effect will be lost. The correlation times for RRM1 and RRM2 reported by Teplova *et al.* suggest this is occurring when the N-terminal domains bind in tandem⁵¹. It is therefore possible that a similar restriction is placed on the motion of RRM3 when all three domains are bound simultaneously to a single RNA molecule. Relaxation rates will become faster, resulting in more rapid loss of magnetisation and hence a poorer signal to noise ratio in the NMR spectrum. In contrast the signal to noise ratio was recovered in the EDEN11 GRE titration as RRM3 remained free to move relative to RRM1 and RRM2 due to binding a separate RNA molecule. Therefore the data for the complex of RRM123 with EDEN-2U/4U is consistent with a slow tumbling 1:1 complex with all three domains bound simultaneously.

6.6.2 Size Exclusion Chromatography

If the loss of signal is due to the protein becoming more compact on binding all three RRM s to a single RNA molecule, it would be expected that size exclusion chromatography (SEC) could confirm this. The rate at which the protein complex moves through the gel matrix is dependent not only on the mass, but also the shape of the protein. A more globular complex would be expected to elute significantly later than the unbound protein.

SEC however showed only a minimal difference between the free and bound RRM123. The bound complex eluted around 0.5 ml earlier than the unbound complex, as shown in Figure 6.22. It is possible this is due to the opposing influences of an increase in mass on binding to the RNA and the formation of a more compact protein complex. However the RRM123/EDEN11 complex was used as a control, and also showed little difference in the elution volume. This should have a higher mass than the RRM123/EDEN-2U/4U complex, and is not expected to be more compact than the free protein. From these results it was inconclusive whether the loss of signal in the NMR spectrum was due to a more compact bound form of the protein.

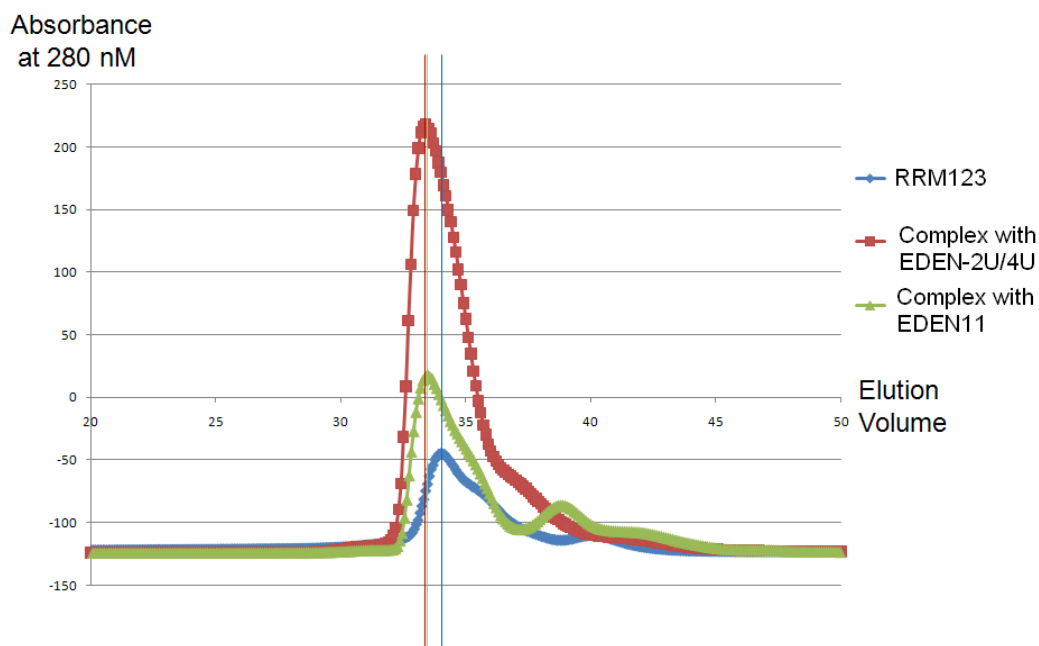


Figure 6.22: 280 nm absorption traces for size exclusion chromatography on an analytical Superdex GF200 column. The protein/RNA complexes are remaining intact when travelling through the column, as is clear from the increased 280 nm absorbance of the complexes compared to an equal concentration of the RRM123 protein. The maximum point of each peak has been marked with a vertical line in the same colour.

Ion mobility mass spectrometry to measure the cross-sectional area of the protein complex is another potential method to confirm this. In this technique the ions produced by ESI travel through a tube with an applied electric current. A carrier buffer gas flows in the opposite direction, impeding the motion of the ions. Depending on the size and shape of the ions, they have different collision cross sections for the buffer gas molecules to collide with. The ions therefore travel at different speeds to the detector depending on their collision cross sections. Unfortunately ESI-MS of the complex resulted in very broad signals and poor quality spectra, preventing a comparison to the unbound RRM123 being made. This is probably due to an increase in salt adducts due to the longer RNAs compared to those used in mass spectrometry of the isolated RRMs and the t187 construct.

6.6.3 RRM123 Binding to an RNA Substrate Containing a Hairpin Loop

The EDEN-2U/HL substrate (UGUUUUGUUCCCGAGGACGGGUUGU) was designed to test the hypothesis that secondary structure in the RNA could bring distant UGU sites together resulting in a higher overall binding affinity. This RNA contains a hairpin between the expected t187 and RRM3 sites with a predicted stability of -5.2 kcal/mol, as shown in Figure 6.23¹⁷⁹. The RNA was confirmed to form a hairpin in solution using 1D proton NMR, which identified imino peaks in the 12 - 14 ppm region of the spectrum.

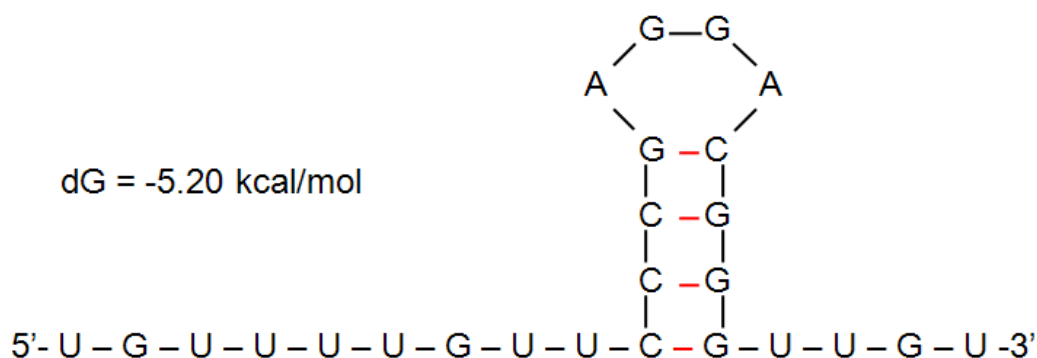


Figure 6.23: Secondary structure of the EDEN-2U/HL RNA substrate, as predicted by the RNA Institute mFOLD web service¹⁷⁹.

Hydrogen bonding between RNA bases results in distinctive chemical shifts downfield of the other RNA signals. With four C-G base pairs forming the “stem” of the hairpin, it would be expected to see four signals in this region if the hairpin is present. In the 1D proton NMR of the RNA three signals were observed, at shifts of 13.33, 12.65 and 12.18 ppm. The signal at 12.18 ppm is significantly more intense than the other two, and so may be caused by two protons with very similar shifts. This confirms that at least three of the C-G base pairs and hence the RNA hairpin is forming in solution.

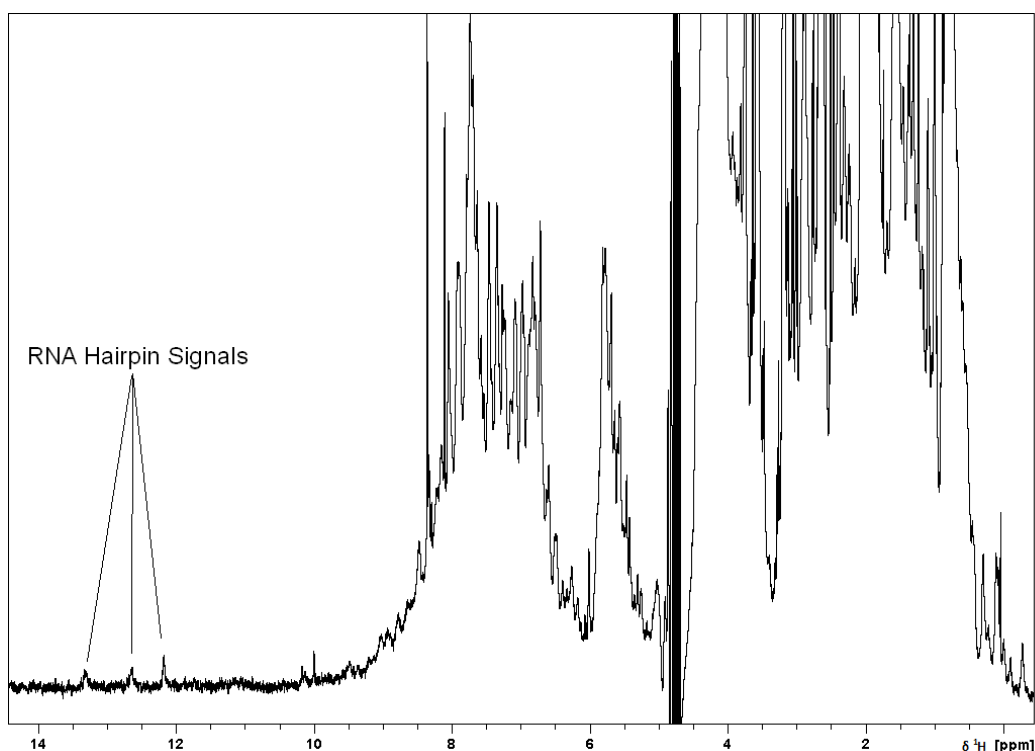


Figure 6.24: 1D proton NMR of the endpoint of the titration of ^{15}N labelled RRM123 with EDEN2U/HL. The imine peaks at the far left of the spectrum are clear indicators of the presence of RNA secondary structure. Theoretically there should be one peak for each of the four C – G base pairs in the hairpin. Only three clearly resolved peaks can be seen, but the more intense peak at 12.18 ppm may be due to two peaks with very similar proton chemical shifts.

As with the EDEN-2U/4U substrate, CSPs are seen across the RNA binding surfaces of all three RRMs. The same loss of spectrum quality is seen, and again is not recovered with a large excess of RNA. The 1:1 high affinity complex is therefore still forming, despite the insertion of the RNA hairpin between two of the UGU sites. The imino peaks from the RNA hairpin are present at the end of the titration, confirming that CELF1 is capable of binding across the base of the hairpin without breaking it apart. This is consistent with the AFM data reported by Michalowski *et al.* which showed CELF1 only binding to the single stranded ends of long CUG repeat hairpins and not to the stems.

6.6.4 ITC of RRM123 Binding to EDEN-2U/4U and EDEN-2U/HL

The EDEN-2U/4U and EDEN-2U/HL substrates which were identified as forming high affinity 1:1 complexes by NMR were also examined by ITC, with the results shown in Figure 6.25.

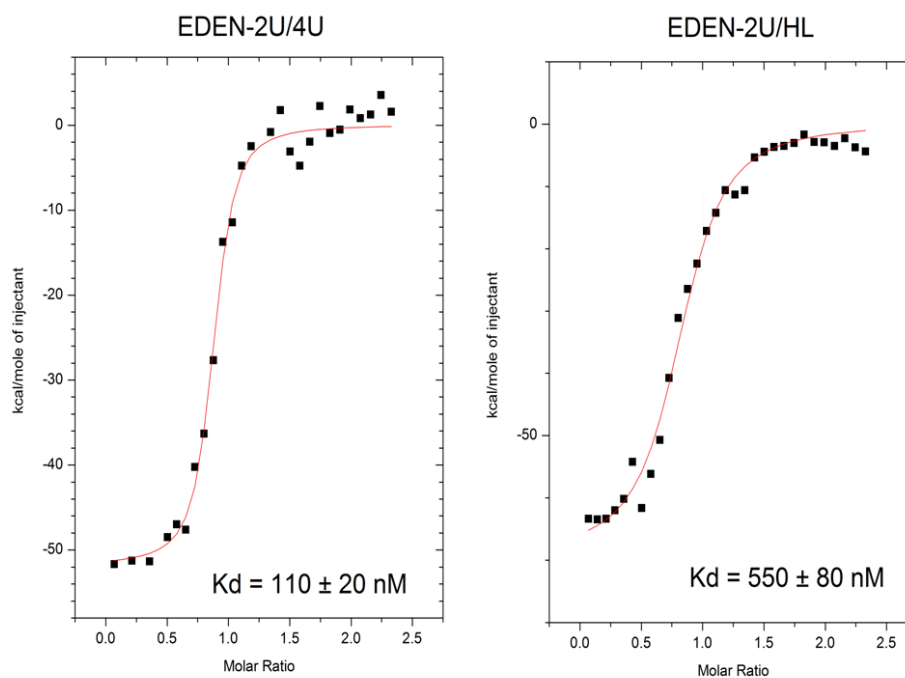


Figure 6.25: Binding curves from the titration of 125 μ M EDEN-2U/4U (UGUUUUUGUUUUUUUGU) and EDEN-2U/HL (UGUUUUUGUUCGGAGGACGGGUUGU) into 12.5 μ M RRM123. Red lines show the curves from the one site binding model the data is fitted to. The first data point has been removed from each data set because the volume of the first aliquot is generally inaccurate.

The EDEN-2U/4U substrate did produce a simple 1:1 curve when titrated into RRM123. Fitting to a one site binding model gave an n value of 0.85, showing a clear contrast with the n values of 1.45 and 1.64 observed for the EDEN11 and EDEN4U substrates. The K_d was calculated as 110 nM, which is the highest affinity so far observed by ITC for any combination of the CELF1 constructs and RNA substrates.

The EDEN-2U/HL RNA showed a similar binding curve, with a somewhat lower affinity ($K_d = 550$ nM). While the presence of a hairpin in the spacer may be

having a slight negative effect on the binding affinity, the stoichiometry appears to be the same as seen for EDEN-2U/4U ($n = 0.83$), which is consistent with the NMR data. Unlike the earlier ITC experiments with CUG repeat hairpins, there were no signs of the hairpin breaking apart on binding, which would have been expected to introduce a second endothermic event similar to that seen for the earlier t187/CUG15 titration, altering the overall shape of the ITC trace. This is consistent with the 1D proton NMR of the bound complex showing peaks in the 11 – 13 ppm region from Watson-Crick base pair hydrogen bonding in the stem of the hairpin.

ITC data was also collected for the EDEN-2U/4U and EDEN-2U/HL sequences as a reverse titration with the RNA in the cell and the RRM123 protein in the syringe. This was to examine how the protein behaved in the presence of large excesses of RNA, and to clarify whether the poor signal to noise in the NMR spectra at large excesses of RNA was due to multiple species forming.

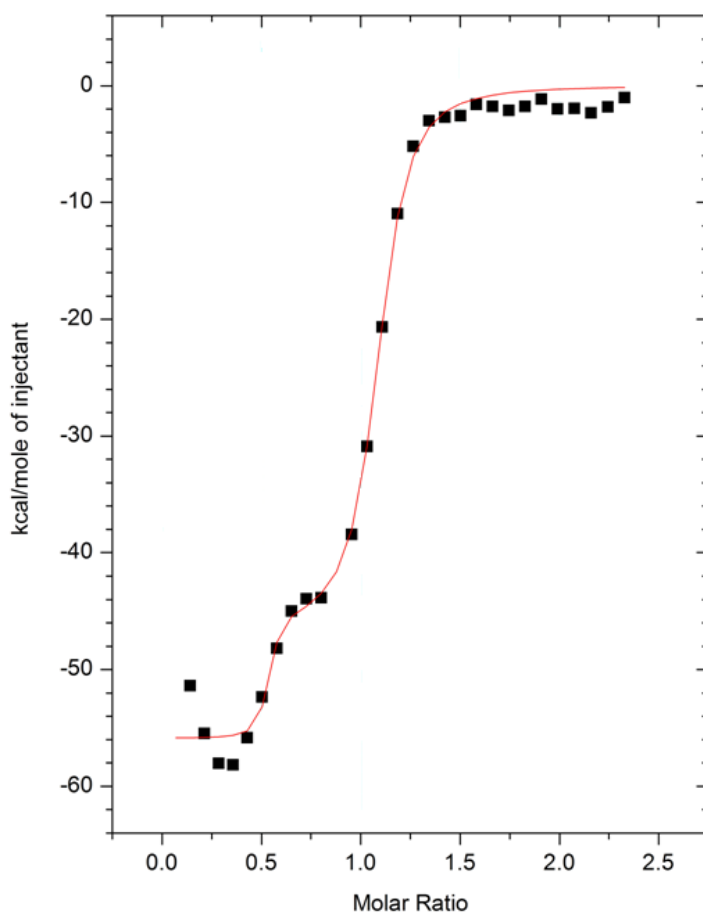


Figure 6.26: ITC curve for a titration of 250 μM RRM123 into 25 μM EDEN-2U/4U. 30 x 10 μl aliquots were injected at 5 minute intervals.

Both EDEN-2U/4U and EDEN-2U/HL showed an unusual shape to the start of the ITC curve, i.e. where there was a large excess of RNA present. The difference in the ITC traces for titrating protein into RNA compared to titrating RNA into protein can be rationalised. If this protein construct forms a high affinity complex with all three RRMs bound to this RNA sequence, then in a situation with a large excess of protein it would be expected that only simple 1:1 binding would be seen. Once a protein binds to the RNA substrate via one RRM, the chelate effect should strongly favour binding of the other two RRMs onto the same RNA molecule if there are suitable sites for them. This is the case for the RNA into protein titrations. In contrast if the RNA is in very large excess then the formation of complexes with two or possibly three RNA molecules per protein becomes more favourable. The formation and later dissociation of these complexes as the

protein to RNA ratio increases could account for the anomalous shape of the curve in the protein into RNA titrations for molar ratios of 0 to ~0.6 protein to RNA. Once the protein concentration increases, formation of the 1:1 complex becomes more favourable, resulting in the second part of the curve which shows similar K_d and enthalpy changes to those seen in the RNA into protein titration.

6.6.5 Comparison of ITC Data shows Two Distinct Binding Schemes

Since the titrations with the EDEN11, EDEN4U, EDEN-2U/4U and EDEN-2U/HL substrates were run under exactly the same conditions they could be compared directly by overlaying the ITC binding curves. This overlay is shown in Figure 6.27 and clearly shows that these four titrations can be divided into two distinct binding schemes, one indicative of 1:1 stoichiometry and one suggesting a higher stoichiometry.

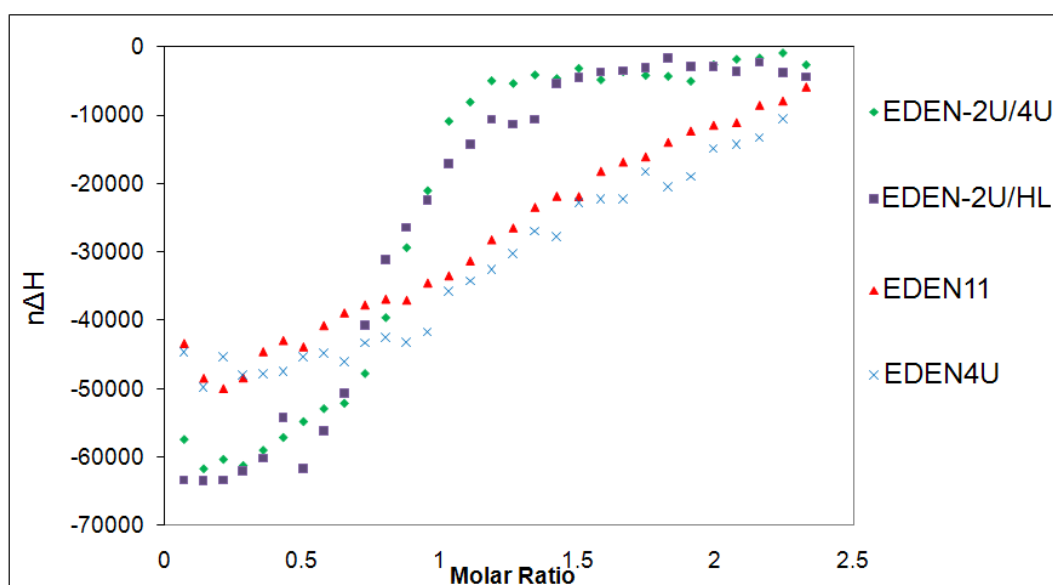


Figure 6.27: Comparison of the ITC traces for RRM123 on titration with EDEN4U, EDEN11, EDEN2U/4U and EDEN2U/HL. In all cases 125 μ M RNA was titrated into 12.5 μ M RRM123, in 30 x 10 μ l aliquots.

Where RRM123 can bind all three RRMs simultaneously to the RNA (in the EDEN-2U/4U and EDEN-2U/HL cases) the titration reaches saturation point

earlier, and there is a larger enthalpy change. When all the domains cannot bind simultaneously (in the EDEN11 and EDEN4U cases) the titration does not reach saturation until more than a 2:1 excess of RNA is present. This suggests that at a 1:1 ratio a mixture of species is present, with some proteins bound to the RNA via their N-terminal domains and some bound via the RRM3 domain, as shown in Figure 6.28. The binding affinities for these events are believed to be similar, accounting for the lack of resolvable binding events in the ITC trace. At a 2:1 excess all proteins can bind to two RNA molecules. In contrast in the scheme where all three RRMs can bind simultaneously the higher affinity 1:1 complex is not affected by addition of further RNA.

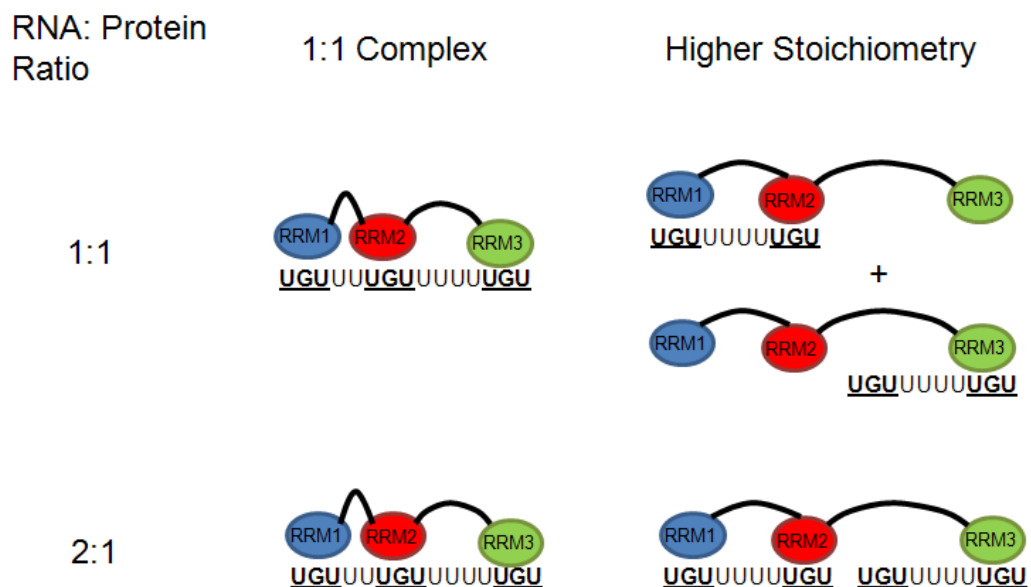


Figure 6.28: This diagram shows the species present in each of the two binding schemes at a 1:1 and 2:1 ratio of RNA to protein.

6.7 Refining the Criteria for an EDEN Motif

The spacer lengths of 2 and 4 nucleotides were originally selected based on a combination of known mRNA targets of CELF1, and the spacing requirements seen for the two N-terminal domains. Once these were known to permit the formation of a high affinity 1:1 complex it was necessary to investigate the

minimum and maximum spacer lengths tolerated as was done for the t187 construct, in order to determine the overall criteria for an EDEN motif. In addition, since the two spacers are not necessarily the same length, it was important to determine if CELF1 showed any preference in the 5' to 3' order of them.

6.7.1 EDEN4U/2U

The closest matching section to the EDEN-2U/4U RNA substrate from the naturally occurring mRNAs is a sequence from the c-fos ARE.

c-fos ARE 14-30: UGUUCAUUGUAAUGU

EDEN-2U/4U: UGUUUUGUUUUUUGU

There are differences, as some of the U spacers have been replaced with A and C bases, and the 2U/4U spacers have been reversed. However this still seemed a likely candidate to form a 1:1 complex with RRM123. Since it is possible that the RRMs have a preference for a specific 5' – 3' order on the RNA strand the arrangement of the spacer lengths may be relevant. The ITC experiment with the RNA EDEN-4U/2U (UGUUUUUUGUUUUGU) was used to check for any difference in binding affinity.

Reversing the spacers did result in some loss of binding affinity (the K_d was increased from 110 nM to 980 nM), but still permitted a 1:1 complex to form. It is not clear whether the change in binding from EDEN-2U/4U involves reversing the 5' to 3' arrangement of the RRMs on the RNA. It could simply be the case that RRM1 and RRM2 are still bound at the 5' end of the RNA, across the 4U spacer, while the 2U spacer is still sufficient for RRM3 to bind at the 3' end. The results of the EDEN15 titrations suggested that RRM3 can tolerate even a one nucleotide spacer. It therefore seems likely that RRM3 can bind across the 2U

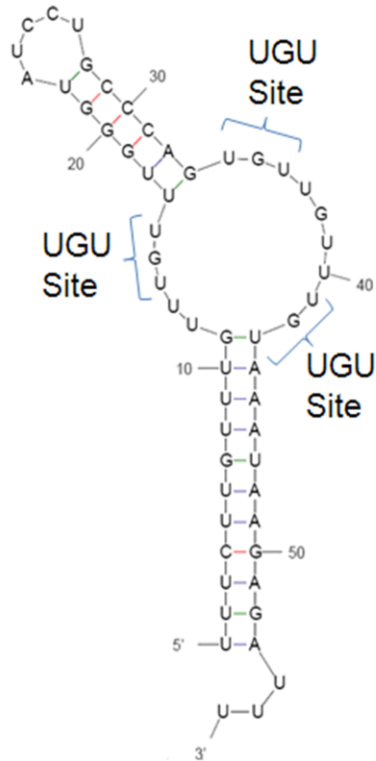
spacer as well as the 4U spacer. If RRM3 and the neighbouring RRM begin to clash when binding to UGU sites with only two uracils separating them, it could account for the reduction in binding affinity seen. Since this arrangement of spacers is tolerated it confirms that the section of the c-fos mRNA tentatively suggested by Moraes *et al.* in 2006 is a high affinity EDEN motif capable of fully binding CELF1.

6.7.2 Involvement of RNA Secondary Structure in CELF1 Binding

C-jun was reported by Paillard *et al.* (2002) to bind to both *Xenopus* and human CELF1, and trigger rapid deadenylation when present in the 3' UTR of an mRNA¹⁹⁰. Vlasova *et al.* reported a shorter version of the c-jun sequence which could also trigger deadenylation. Since the EDEN11 GRE has been shown to be insufficient this RNA does not contain a set of UGU sites with suitable spacing for CELF1 binding when considered only as a linear sequence. The TNF α sequence reported by Moraes *et al.* is another example, which has no instances of three UGU sites within 40 nucleotides of each other. The experiments with EDEN-2U/HL however showed that secondary structure could also create a high affinity CELF1 site by bringing distant UGU sites together. Similar secondary structure in the C-jun and TNF α sequences provide an explanation for their binding of CELF1. The secondary structures of the relevant regions of these two RNA, as predicted by the mFOLD web service, are shown in Figure 6.29.

C-jun

$\Delta G = -13.7$ kcal/mol



UGUU-GUGUUGUUUGU

TNF α

$\Delta G = -73.2$ kcal/mol

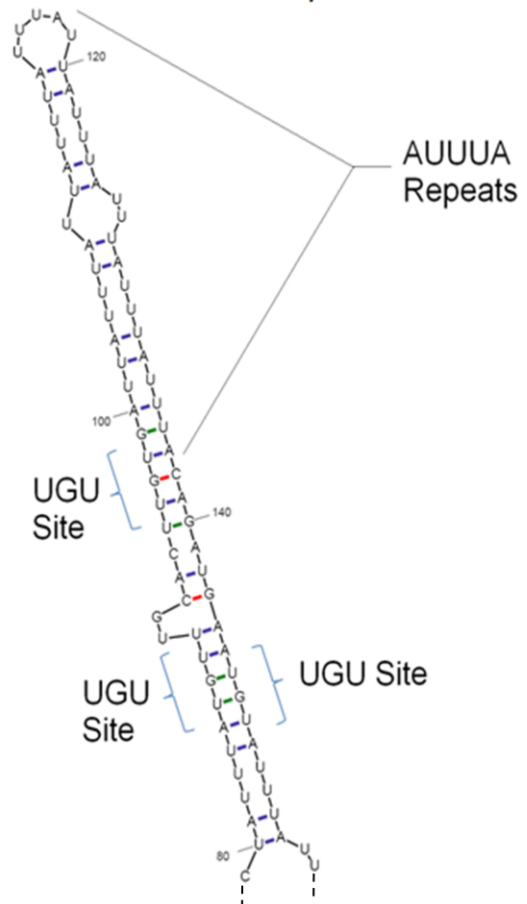


Figure 6.29: Left is shown the C-jun section shown by Vlasova *et al* to be capable of binding CELF1. Right is shown part of the TNF α substrate reported by Moraes *et al*. In each case the UGU sites which appear to be in the most favourable arrangement for binding CELF1 have been highlighted. RNA secondary structure predictions were made by the mFOLD web service¹⁷⁹.

The c-jun RNA shows two clear double stranded regions. One is from bases 17 – 31, which forms a hairpin held together primarily by three Watson-Crick C-G base pairs, similar to the hairpin in the EDEN-2U/HL sequence. The second double stranded region is between bases 1 – 11 and 44 – 53, mostly composed of U – A base pairs. This leaves a single stranded region between them, which contains five of the possible UGU sites in close proximity. The three highlighted UGU sites are essentially equivalent to the EDEN-2U/4U high affinity substrate, with a hairpin inserted into the 2U spacer. This seems the most probable site for

binding of all three RRM domains of CELF1.

TNF α is predicted to form an extended hairpin motif, formed largely by U – A base pairing in the AUUUA repeating region. As shown, this does bring three UGU sites into relatively close proximity. They are however predicted to be in double stranded regions of the RNA, which has been shown to prevent CELF1 binding in the long CUG repeat hairpins found in DM1 cells. The CELF1 interaction with UGU sites is of higher affinity, and there are more mismatched U-G and U-U bases in this hairpin than in the CUG repeat case. It is possible that some of this double stranded region can break apart in order to bind CELF1 (as was seen in the t187/CUG15 titration).

This also provides a possible explanation for the reported dependence of deadenylation efficiency on the presence of an AU rich element, in this case an AUUUA repeat. It can be hypothesised that deadenylation is more efficient when the AU rich elements are present because they form secondary structures that bring UGU sites into more favourable configurations for CELF1 binding, rather than any direct binding of CELF1 to the AU rich elements themselves.

6.7.3 Determination of the Minimal Binding Sequence for CELF1

If the earlier hypotheses about the spacing tolerances of each of the RRM domains are correct then the RNA substrate EDEN-2U/1U (UGUUUUGUUUGU) would be expected to be the minimum sequence capable of binding all three RRM domains. It would therefore represent the smallest possible EDEN motif, and confirm the minimum requirements for binding. ITC was carried out on this substrate, with the results shown in Figure 6.30.

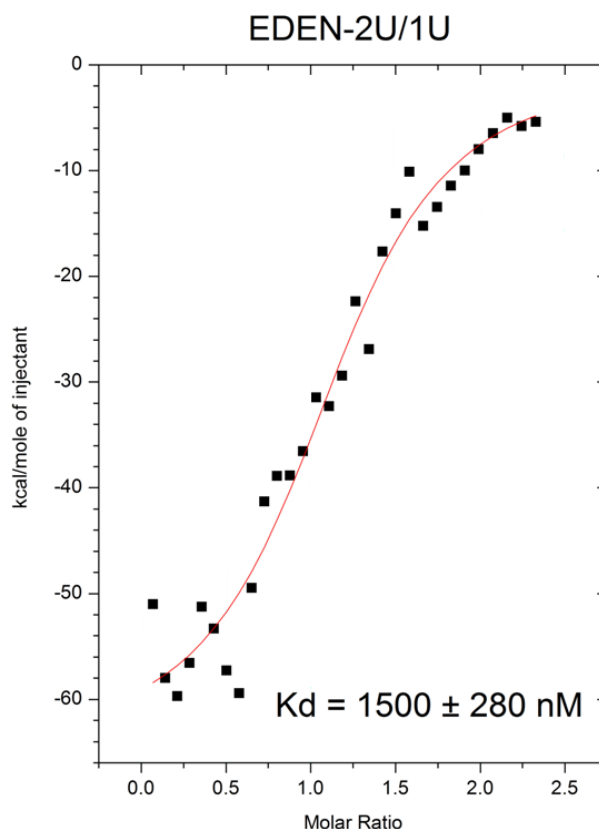


Figure 6.30: ITC binding curve for the titration of 125 μM EDEN-2U/1U into 12.5 μM RRM123.

The EDEN-2U/1U substrate seems to fall somewhere between the binding scenarios seen for the EDEN11 GRE and EDEN-2U/4U cases. The K_d indicates a higher affinity than the EDEN11 GRE, but more than a 10 fold reduction in affinity compared to the EDEN-2U/4U substrate. The n value is 1.19, roughly halfway between those of the EDEN11 GRE and EDEN-2U/4U RNAs. This RNA sequence was also investigated by NMR, which showed bound peaks for all three domains of CELF1 at a 1:1 ratio of protein to RNA, with the characteristic loss of signal to noise ratio, which suggests it probably is forming a 1:1 complex. As for EDEN-2U/4U, the spectrum quality was not recovered on addition of excess RNA. This RNA substrate therefore does represent a complete EDEN motif, but the short spacers between the UGU sites appear to be sufficiently unfavourable that there is only a marginal increase in affinity compared to binding of the N-terminal domains to the EDEN11 GRE.

6.7.4 Investigation of a Two Domain Construct of RRM2 and RRM3

As both the EDEN15 GRE and EDEN-2U/1U can bind all three RRMs, at least to some extent, then it was conceivable that RRM2 and RRM3 could bind simultaneously to the EDEN7 (UGUUUGU) sequence which previously failed to bind both RRMs of t187. To investigate this possibility a construct containing only the RRM2 and RRM3 domains was required. A construct retaining the wild type 200 residue linker between these two domains as expected had all of the same issues with solubility and stability as the full length wild type CELF1. For direct comparison with the RRM123 construct a version with the shortened RRM2 – RRM3 linker was needed.

Both the wild type and deletion mutant versions were produced using the same method of single step PCR deletion to remove the codons for residues 1 - 107 of CELF1 from the construct. The only difference in the PCR protocol was whether full length CELF1 or the RRM123 construct DNA was used as the template. The growth, expression and purification protocols were the same as for the RRM123 complex. The solubility and stability of the protein were found to be similar to RRM123, allowing NMR and ITC data to be collected.

The ¹⁵N TROSY spectrum of this construct was well resolved, and is shown in Figure 6.31. As expected the spectrum essentially a composite of the RRM2 and RRM3 spectra, with some additional peaks from the unstructured linker.

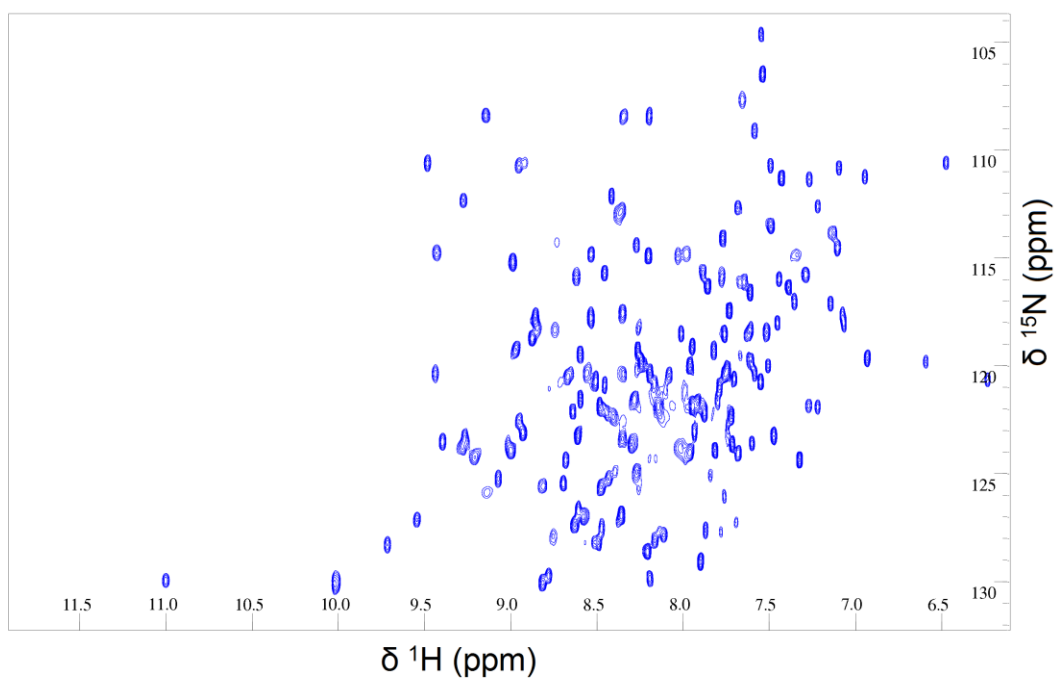


Figure 6.31: ^{15}N TROSY spectrum of a 250 μM sample of the RRM23 construct, collected on an 800 MHz spectrometer with cryoprobe at 298K.

This new construct was used to determine whether RRM2 and RRM3 could bind to UGU sites separated by only a single nucleotide, using a similar approach to that described for the t187 construct. The EDEN7 RNA substrate was titrated into ^{15}N -labelled RRM23.

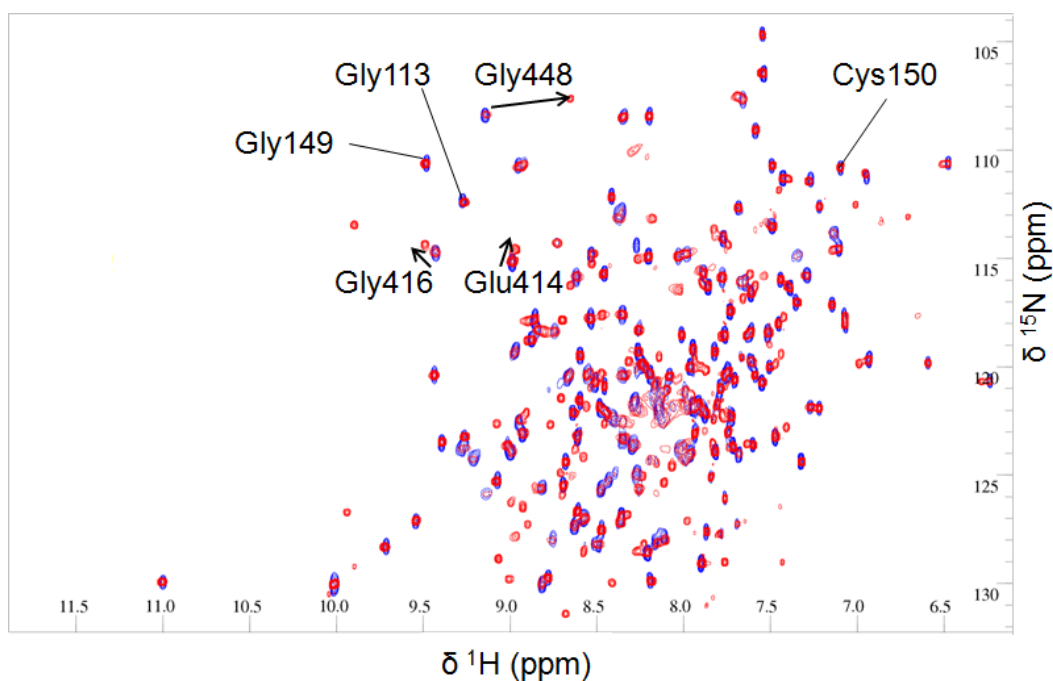


Figure 6.32: The ^{15}N TROSY spectrum of unbound RRM23 is shown in blue. Overlaid in red is the ^{15}N TROSY at the midpoint of the titration with EDEN7. As the titration is in slow exchange sharp peaks from both the free and bound form are clearly visible. CSPs are only seen for residues in RRM3. No effects are seen for any residues in RRM2. Some significantly perturbed residues in RRM3, and some residues that are normally perturbed on binding in RRM2 have been highlighted.

As shown in Figure 6.32, CSPs were only seen in RRM3, indicating that only this domain was binding to the EDEN7 substrate. The titration was entirely in slow exchange and peaks from both the free and bound forms of RRM3 can be clearly seen at the midpoint of the titration. No significant CSPs were seen for any residues in RRM2. When RRM2 and RRM3 are in competition RRM3 is bound preferentially. This is as expected since the ITC data showed that RRM3 had a significantly stronger binding affinity for UGU sites than RRM2, with a K_d that was at least an order of magnitude lower.

This was corroborated by ITC of RRM23 into EDEN7, which showed only a single binding event with a K_d of $0.52 \pm 0.12 \mu\text{M}$, consistent with only RRM3 binding (Figure 6.33). Due to the large difference in the affinities of the two domains, there would be expected to be a strong preference for binding of RRM3. No effects were seen for residues in RRM2 until after a 1:1 ratio of RNA to

protein was reached. It is unclear if this is due to an inability to bind the domains in tandem to the UGUUGU substrate, or simply the 100 fold difference in binding affinities between the domains.

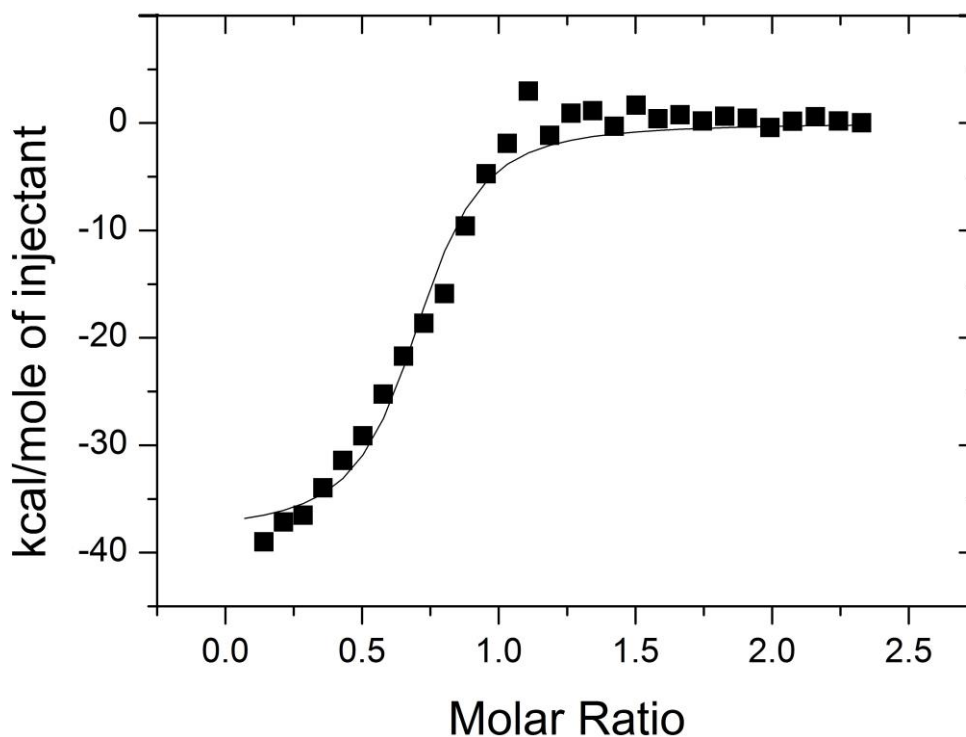


Figure 6.33: ITC curve for a titration of 125 μM RRM3 into 12.5 μM EDEN7. A single binding event is seen, indicating formation of a 1:1 complex.

These observations had failed to produce any evidence of tandem binding of RRM2 and RRM3 to UGU sites separated by only a single nucleotide. A remaining possibility in sequences such as EDEN-2U/1U was that RRM1 and RRM3 were occupying the UGU sites on either side of the single nucleotide spacer, leaving the RRMs arranged in the order RRM2 – RRM1 – RRM3 from the 5' to 3' end of the RNA substrate. Whether this was a viable arrangement of the domains was initially investigated by molecular modelling, and then investigated in solution by NMR using a paramagnetic relaxation enhancement technique as detailed in the next chapter.

6.8 Conclusions

Wild type CELF1 was found to be a difficult protein to investigate by most biophysical techniques due to its poor solubility and the low yield of the purification method. We did however succeed in producing the much more soluble and stable RRM123 construct allowing the behaviour of all three domains of CELF1 together to be investigated by NMR and ITC.

Using RRM123 we have shown that the EDEN11 GRE is not capable of forming a high affinity 1:1 complex with CELF1, and so only represents a partial EDEN motif. While it does contain three UGU sites the spacing between them is unsuitable for simultaneous binding of all three domains. The longer EDEN15 RNA substrate does however appear to be capable of binding all three RRMs and so is a complete EDEN motif. However the ITC results suggest the spacing is not optimal, as little enhancement of affinity was seen compared to binding of the N-terminal domains only. Based on the spacing requirements of the N-terminal domains deduced in the previous chapter, and the known natural mRNA targets of CELF1 we have designed the RNA substrate EDEN-2U/4U, which was found to be a complete EDEN motif with the highest binding affinity so far observed ($K_d = 110$ nM).

We have refined the criteria for the EDEN motif to UGU(x)UGU(y)UGU where $x = 2 - 4$ and $y = 1 - 5$ result in a 1:1 complex. There is a 5-fold difference in K_d for $y = 5$ vs. $y = 4$, and a 10-fold difference for $y = 1$ vs. $y = 4$. The combination $x = 2, y = 4$ results in the highest affinity interaction measured so far. However we have also shown using the RNA EDEN-2U/HL that much longer spacers can bind with comparable affinity if RNA secondary structure can bring distant UGU sites into close proximity. We have identified both c-jun and TNF α as possible natural examples of this. All other mRNAs previously demonstrated to trigger deadenylation by binding CELF1 contain sequences consistent with our EDEN motif criteria without the need for secondary structure involvement.

7 Characterisation of a Complex of CELF1 with a High Affinity EDEN Motif

We originally aimed to characterise the structure of the complex of CELF1 with a high affinity EDEN motif using either NMR or x-ray crystallography. Unfortunately the decrease in signal to noise ratio seen in the NMR spectra when the complex formed prevented the collection of sufficiently high quality NOE and RDC data to gather restraints for an NMR solution structure. Attempts were also made to co-crystallise RRM123 with high affinity RNA substrates in order to obtain a structure by x-ray crystallography, but no diffraction quality crystals were produced.

A different approach of modelling the structure of the complex, starting from the available structures of the isolated domains was therefore chosen. In constructing this model the main uncertainty to be resolved was the arrangement of the three structured domains on the three UGU(U) sites of a high affinity RNA substrate. There was also the question of whether there was a single preferred bound conformation, or if the inherent flexibility of the linkers between the domains would permit a range of conformations in solution. The range of possible RNA binding modes in multi-RRM systems has been previously found to present problems, particularly for x-ray crystallography. For example when the tandem interaction of RRM1 and RRM2 of U2AF65 with an RNA substrate was investigated by both NMR and x-ray crystallography, the resulting structures differed significantly^{191, 192, 193}. The potential for multi-RRM systems to have several possible binding modes, depending on the exact target RNA and the presence of any secondary structure therefore had to be considered.

7.1 Arrangement of the Domains on the RNA Substrate

A key question in constructing the model was the relative arrangement of the three domains when bound onto a single RNA molecule. The data in the previous chapter showed that substrates such as EDEN-2U/4U could bind all three domains, one to each of its three UGU sites, but did not indicate which domain was occupying which site. There are several possible ways of arranging the domains on the three UGU sites, but steric considerations allowed some possibilities to be eliminated. In the available crystal structures the RNA substrate is consistently positioned with the 5' end towards the β 4 side of the β -sheet and the 3' end on the β 2 side for all three RRMs of CELF1. This alignment of the RNA across the β -sheet is common for RRMs in general⁴³. The short linker between the N-terminal domains RRM1 and RRM2 of CELF1 imposes significant steric constraints on binding, and in order for each domain to bind in the same way as they do in isolation they must be arranged in the order RRM2 – RRM1 from 5' to 3' along the RNA. This arrangement is shown in Figure 7.1.

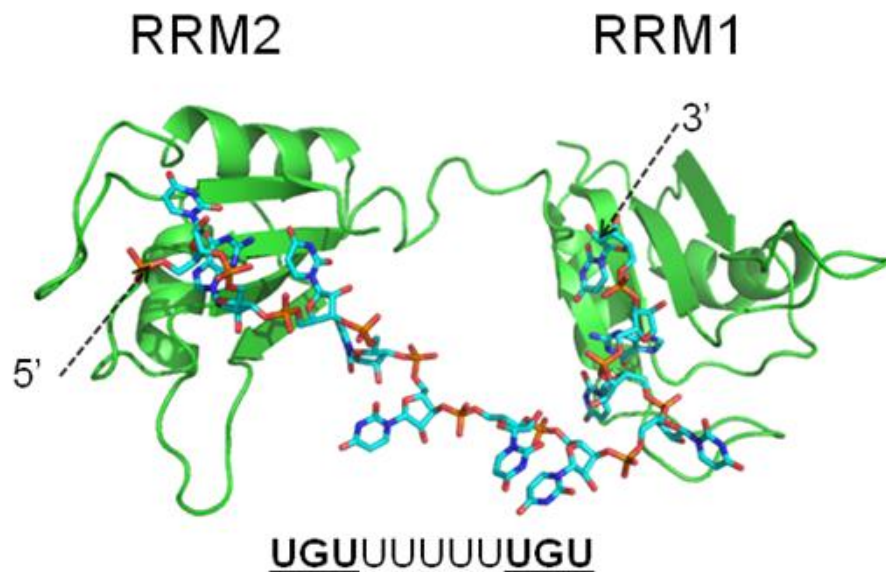


Figure 7.1: Model of the N-terminal domains RRM1 and RRM2 in complex with the RNA substrate UGUUUUUUUUGU. This was produced by constructing the RNA sequence UUUUUU in XLEAP, and superimposing the two terminal nucleotides with U4 and U5 of the t187/EDEN2U model shown earlier. The model was then minimised, and underwent a molecular dynamics run according to the protocol in section 3.22. The domains are in the order RRM2 – RRM1 from the 5' to 3' end of the RNA. The linker between the domains is not sufficiently long to allow the domains to adopt the other arrangement. Energy minimization and molecular dynamics were carried out in Amber. This image was produced using Pymol.

While there are no available structures in the protein databank showing tandem binding of any combination of the CELF1 domains onto a single RNA molecule, there are some structures of other multi-RRM systems available in the literature. Structural data is available for some examples of proteins containing two RRM domains separated by a comparably short linker to CELF1, such as Sx1³⁸, PABP¹⁹⁴ and Hrp1⁴⁴. Each of these proteins is capable of binding in tandem to an RNA substrate of between 7 and 10 nucleotides. Restricted by an interdomain linker of less than 10 residues in each case, these proteins have consistently been found to bind with RRM2 at the 5' end of the RNA, and RRM1 towards the 3' end (numbering the RRM domains from the N-terminus of each protein). These proteins displayed considerable cooperativity between the RRM domains, with them acting in tandem to form an extended β -sheet surface to recognise longer RNA sequences. While the CELF1 RRM domains appear to be rather more independent, the short linker still forces RRM2 to be positioned to the 5' end of the RNA relative to RRM1.

The location of RRM3 remained uncertain. With the restriction that RRM2 must be towards the 5' end relative to RRM1 there were three possible arrangements of the domains on the EDEN-2U/4U substrate, as shown in Figure 7.2.

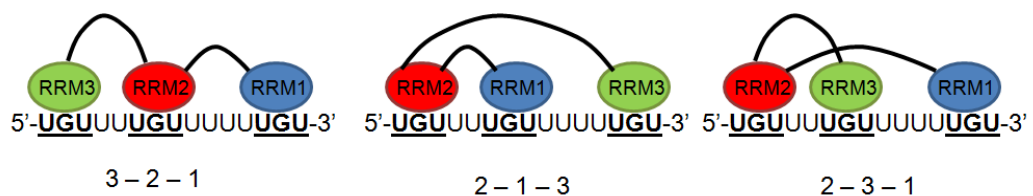


Figure 7.2: Possible arrangements of the three domains of CELF1 from 5' to 3' when bound to the RNA substrate EDEN-2U/4U.

The earlier investigation of the N-terminal domains in the t187 construct showed a significant decrease in binding affinity for UGU sites separated by more than 4 nucleotides. The 2 – 3 – 1 arrangement forces RRM1 and RRM2 to occupy sites

which are 9 nucleotides apart, which is therefore likely to be unfavourable. Based on this observation and the known inability of RRM3 to occupy to the central site of the EDEN11 GRE (UGUUUGUUUGU) it seemed unlikely that the 2 – 3 – 1 arrangement would be preferred.

This left the 3 – 2 – 1 and 2 – 1 – 3 arrangements as possibilities. In the RRM123 construct the linker between RRM2 and RRM3 consists of around 30 residues, which is sufficient to make either arrangement sterically plausible. In wild type CELF1 this linker is far longer at around 200 residues, allowing RRM3 even more freedom to move independently, again making either arrangement possible. In order to determine whether one of these arrangements is preferred, and if so which, a technique was required that could connect one of the domains to a specific UGU site. Paramagnetic relaxation enhancement was used for this purpose.

7.2 Modelling RRM123 in Complex with a High Affinity RNA Substrate

Models of the RRM123 construct bound to the EDEN-2U/4U and EDEN-2U/HL RNA sequences were constructed, as an initial check to ensure that no steric clashes or implausible strains on the interdomain linkers were present. These were constructed based on the available crystal and NMR structures in the Protein Data Bank produced by Teplova *et al.* and Tsuda *et al.* Since none of these structures had more than one of the RRMs bound to a single RNA substrate, it was necessary to splice the isolated structures together to produce the overall model of RRM123.

The model of RRM1 and RRM2 in complex with the RNA sequence UGUUUUGU (a two nucleotide spacer), shown earlier in Figure 5.13, was used as the N-terminal fragment of the protein. The structure of RRM3 in complex

with the RNA sequence UGUGUG produced by Tsuda *et al.* was used as the C-terminal fragment. Since no structural data existed for the RRM2 – RRM3 linker region a section of the RRM123 protein consisting of residues 186 - 216 was constructed in the program XLEAP, and then energy minimised in AMBER. This linker was then attached to the N-terminal fragment by superimposing residues 186 and 187 of the linker onto their counterparts in RRM2 of the N-terminal fragment (minimising RMSD). The C-terminal fragment was similarly attached by superimposing residues 215 and 216 of the RRM3 structure onto the corresponding residues in the RRM2 - RRM3 linker. This resulted in a complete RRM123 protein with two separate RNA fragments, one bound to the N-terminal domains and one to RRM3.

This model was energy minimised, and underwent molecular dynamics simulations in AMBER for 1 ns at 300 K. To produce the complete RNA the fragment bound to RRM3 was truncated to the UGU site. A section of RNA consisting of the sequence UUUUUU was constructed in XLEAP, energy minimised in AMBER, and attached to the RRM3 fragment by superposition of the 3' uracil with the 5' uracil of the UGU site. The 5' uracil of this RNA spacer was then superimposed onto the 3' U of the UGUUUUGU fragment, which necessitated the introduction of implausibly long bonds into the RNA backbone to make this connection. This structure, corresponding to RRM123 in complex with EDEN-2U/4U with the domains arranged in the order 2 – 1 – 3, was energy minimised with a restraint mask applied to the RNA, which was gradually reduced until all bonds had relaxed to normal lengths. The structure was then subjected to molecular dynamics simulations in AMBER for 2 ns.

A model of the same complex, but with the RRMs in the order 3 – 2 – 1 was also constructed by a similar method. The spacing in the RNA sequence UGUUUUGU, bound to the N-terminal fragment was expanded from 2U to 4U by superimposing the 5' and 3' nucleotides of a constructed UUUU sequence onto U4 and U5. This structure was then minimised and used as the starting point

for a molecular dynamics run as described in section 3.22. The RRM2 – RRM3 linker and the third domain were added by the same method as in the 2 – 1 – 3 model. Another constructed section of RNA, with the sequence UUUU was then used to connect the 3' end of the RRM3 bound UGU site to the 5' end of the UGUUUUUUGU sequence bound by the N-terminal domains. This starting structure then underwent energy minimisation and a molecular dynamics run, with a final 2 ns step at 300 K with no restraint applied to the protein or RNA. Both arrangements of the domains appeared sterically plausible, and the RNA remained bound throughout the molecular dynamics run. The model with the 2 – 1 – 3 arrangement is shown in Figure 7.3.

Models of RRM123 in complex with the EDEN-2U/HL RNA sequence were also constructed. The RNA hairpin (consisting of the sequence UCCCGAGGACGGGU folded to form hydrogen bonds between the bases in italics) was constructed in XLEAP, and energy minimised. The 5' and 3' uracils were then superimposed onto U9 and U12 respectively of EDEN-2U/4U in the complex of this RNA sequence with RRM123. U10 and U11 of the EDEN-2U/4U sequence were then deleting, leaving an overall RNA sequence matching EDEN-2U/HL. The model then underwent energy minimisation and a 2 ns molecular dynamics simulation. The structure appeared sterically plausible with either the 3 – 2 – 1 or 2 – 1 – 3 arrangement of the domains, and in both cases the RNA hairpin remained intact throughout the molecular dynamics run. The model with the 2 – 1 – 3 arrangement is shown in Figure 7.4.

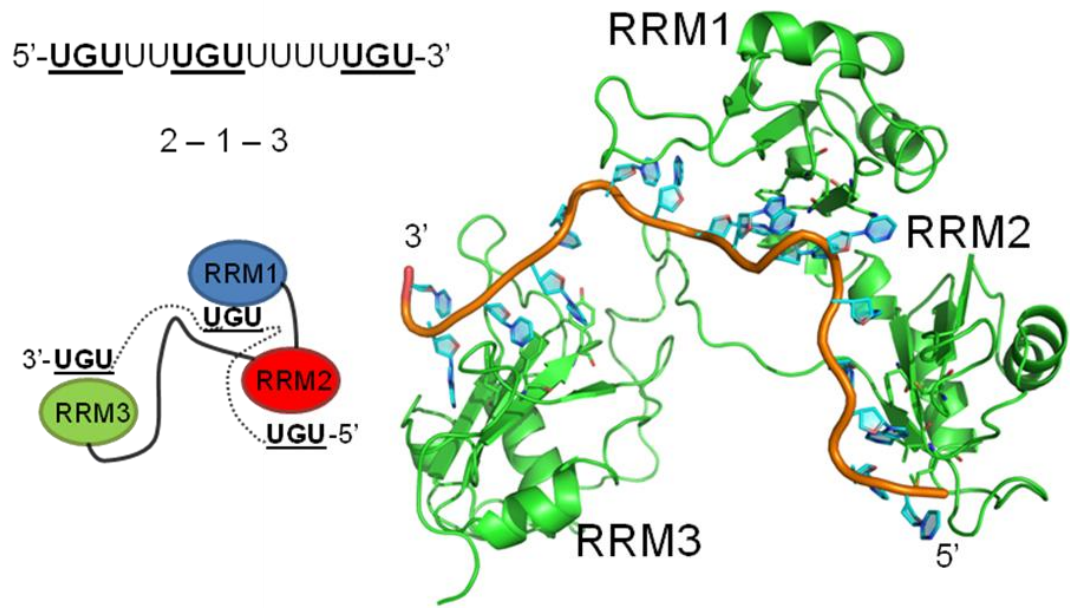


Figure 7.3: Model of RRM123 in complex with the EDEN-2U/4U substrate. The RRMs are in the 2 - 1 - 3 arrangement from the 5' to 3' end of the RNA strand.

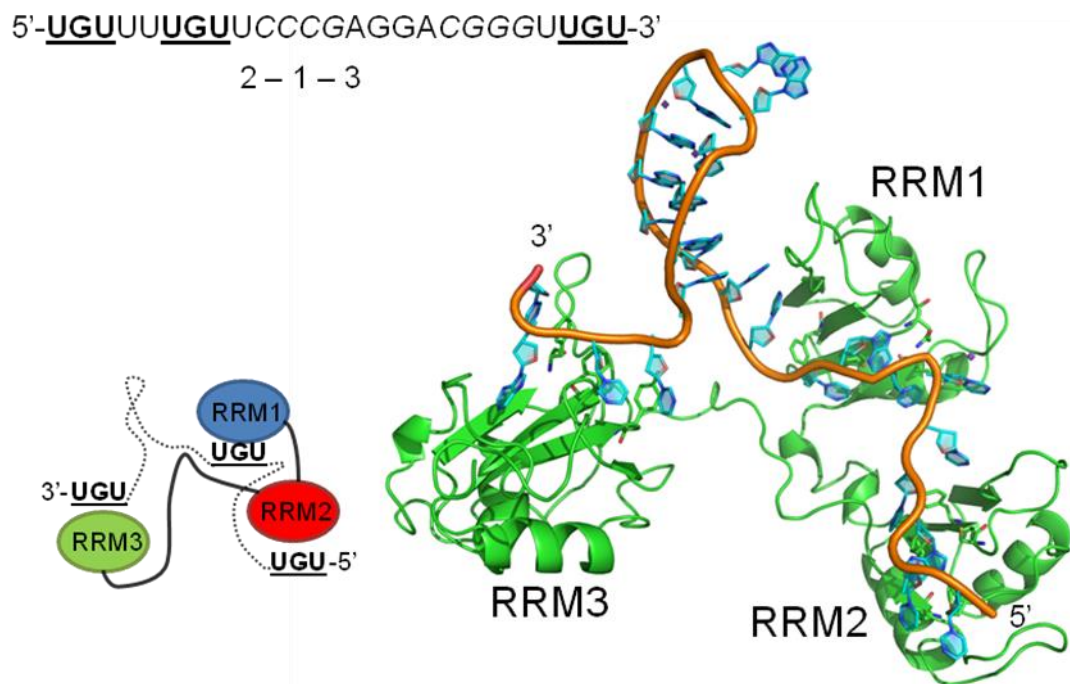


Figure 7.4: A model of the EDEN-2U/HL RNA substrate bound to the RRM123 protein. Modelling was carried out using Amber for energy minimization followed by molecular dynamics simulations as specified in section 3.22.

From the molecular modelling it was evident that there was still considerable flexibility in the structure from the RNA and interdomain linkers. This permits the domains to either form a compact structure, or a range of more extended structures.

7.3 Paramagnetic Relaxation Enhancement

When a paramagnetic centre is present in a protein the relaxation rates of surrounding nuclei are greatly increased, resulting in attenuation of their signals in NMR spectra. By observing which residues contain affected nuclei, the position of the paramagnetic centre within the structure can be determined¹⁹⁵. Some proteins contain endogenous paramagnetic centres such as Fe^{3+} , or metal ions which can be substituted for a paramagnetic lanthanide ion^{196, 197}. In addition to using existing metal ions in proteins it is also possible to add paramagnetic tags, containing either a lanthanide ion, or a stable radical such as a nitroxide group^{198, 199}. These are usually attached by a coupling reaction to a cysteine residue, either endogenous or introduced by point mutation. These tags can also be attached to ligands^{200, 201} and nucleic acids^{202, 203}.

The PRE effect has a much longer range than NOEs, of up to 25 Å. This is a sufficiently long distance that the effect could potentially extend between the domains of CELF1, allowing interdomain restraints to be generated. This technique would also distinguish between the 3 – 2 – 1 and 2 – 1 – 3 arrangements. If the tag were attached to one of the protein domains then measurement of the signal attenuation in the ¹⁵N TROSY spectrum for residues in each of the other two domains would show which domain was closest to the paramagnetic tag, and hence the overall arrangement. Alternatively the paramagnetic tag could be attached to the RNA, close to one of the UGU sites. The residues in the domain binding to that UGU site would then be expected show the greatest signal attenuation in the ¹⁵N TROSY spectrum.

The paramagnetic tag selected for these experiments was MTSL (*S*-(2,2,5,5-tetramethyl-2,5-dihydro-1H-pyrrol-3-yl)methyl methanesulfonylthioate) supplied by Toronto Research Chemicals Inc. MTSL consists of a stable nitroxide group attached to a sulfinic acid (CH_3SO_2) leaving group. This is normally reacted to form a disulphide link to a specific cysteine residue in the protein, but it can also be coupled to other sulphur containing groups. Since the RRM123 construct contains seven cysteine residues attaching the spin label to a specific cysteine would require a minimum of six point mutations. In addition some of these cysteines (specifically Cys61, Cys62 and Cys150) are located in the key RNP regions of the protein's binding surfaces, and form hydrogen bonds to the RNA in the reported crystal structures of the isolated domains. RNA binding would almost certainly be interfered with if the tag was attached to one of these residues. Altering these residues to, for example, serine or alanine would however potentially disrupt the normal RNA binding properties of the protein. Attaching the spin label to a specific site on the RNA was a more attractive option, as RNA sequences with modified bases at specific sites were commercially available from Dharmacon. MTSL can be coupled to a 4-thio-uridine base, as shown in Figure 7.5.

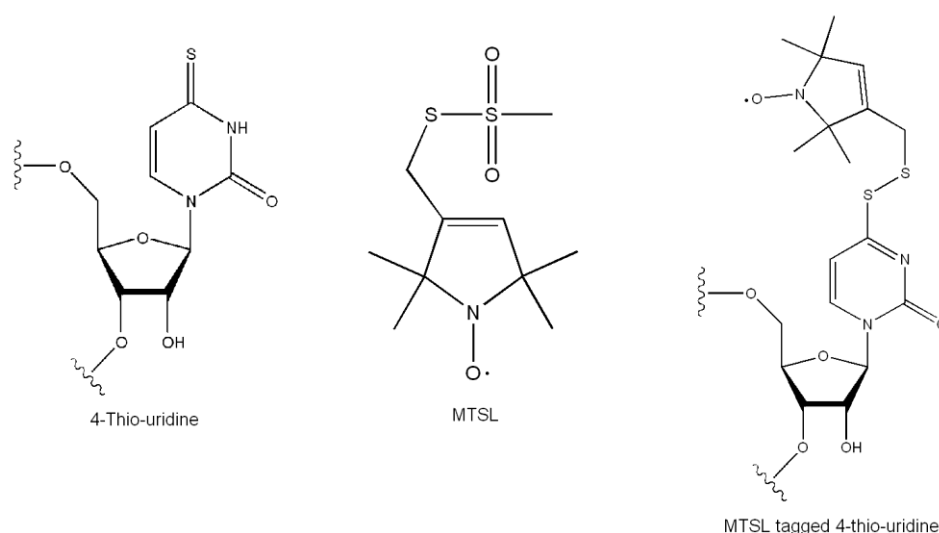


Figure 7.5: On the left is the structure of the 4-thio-uridine modified RNA base. In the centre is the structure of the MTSL, showing the unpaired electron of the nitroxide group which acts as the spin label. On the right is shown the structure of the modified RNA base after the coupling reaction with the MTSL.

With the tag attached to a modified base at one end of the RNA strand it would attenuate the signals of the nearby residues in the ^1H - ^{15}N HSQC spectrum, unambiguously showing which domain was binding closest to that end.

7.3.1 Paramagnetic Relaxation Enhancement in RRM1 on binding to MTSL Labelled UGUU

As an initial proof of concept the RNA tetramer U*GUU, where the 5' uridine had been replaced with 4-thiouridine was used. A 3x molar excess of MTSL was added to the RNA, and allowed to react in darkness at room temperature for two hours. This was then loaded onto a HiTrap desalting column and eluted into RNase free MilliQ H_2O to remove unreacted MTSL. The eluted RNA was then frozen using liquid nitrogen, and lyophilised, again in darkness.

Titration of this MTSL-tagged RNA into a ^{15}N labelled RRM1 sample resulted in attenuation of a large percentage of the amide signals in the spectrum. Those in β -strands 1 and 3 were most affected, with signals from residues such as 19 – 23 and 60 - 62 lost completely by the time a 1:1 ratio of RNA to protein was reached.

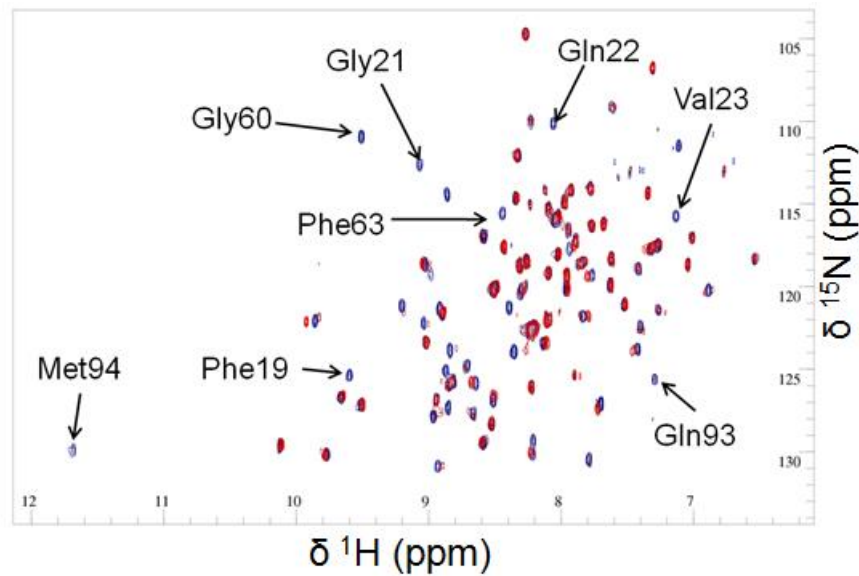


Figure 7.6: In blue is the ^1H - ^{15}N HSQC of the unbound RRM1 construct. Overlaid in maroon is the spectrum at a 1:1 ratio of MTSL coupled U*GUU to protein, and in red the spectrum at a 2:1 ratio. Very few peaks specific to the bound form can be seen.

Once the titration had reached saturation point 5 molar equivalents of a buffered sodium ascorbate solution was added to the NMR sample, and allowed to react for 15 hours. This was to reduce the sample, leaving no unpaired electrons and so removing all paramagnetic relaxation enhancement effects. The magnitude of the PRE could then be calculated as the ratio $I_{\text{para}}/I_{\text{dia}}$, where I_{para} is the signal intensity for a given residue in the presence of the spin label and I_{dia} is the signal intensity after reduction of the spin label.

Titration of RRM1 with U*GUU

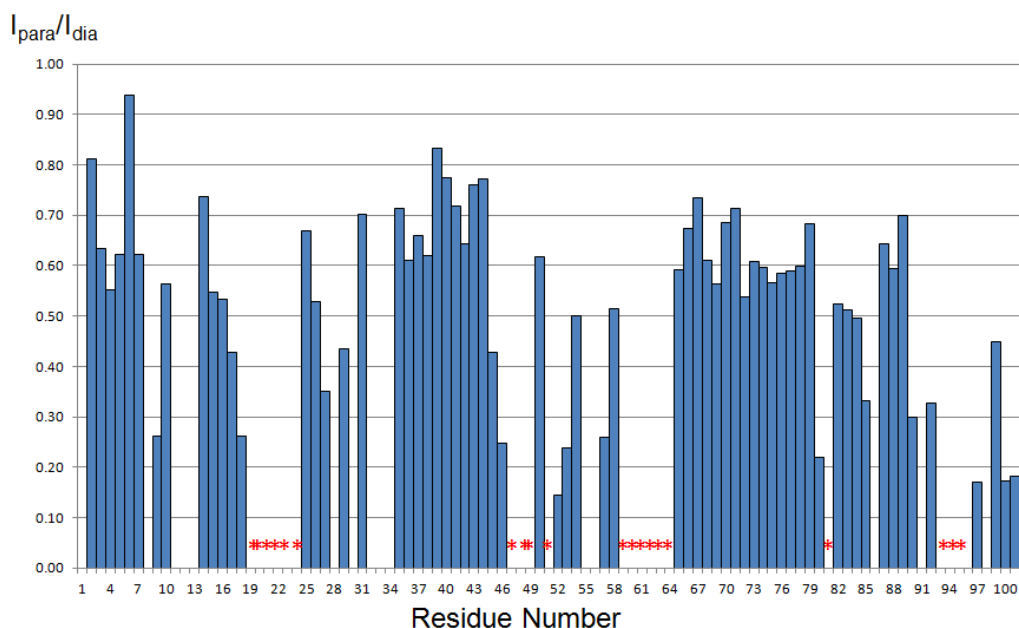


Figure 7.7: Graph of the ratio I_{para}/I_{dia} for the titration of RRM1 with U*GUU. Residues for which the signals are completely obliterated have been highlighted in red to distinguish them from the prolines and overlapped residues which have no data.

The most affected residues are 19 – 23, 47 – 51, 59 – 64, 81 and 93 – 95, the signals of which are all completely obliterated. These include most of the residues in the β -sheet, and almost all of those residues previously seen to be involved in RNA binding to this domain. Strong signal attenuation is also seen for the C-terminal residues, and for residues such as Ser52 and Gln53 in the loop connecting β 2 and β 3. Some attenuation of signal (around a 20 – 40% decrease in intensity) is seen even for the relatively unaffected regions of the protein. These are residues 2 – 7, 35 – 44 and 65 – 79, which make up the N-terminus and the α -helices of the protein. When the values for each residue are mapped onto the surface of the protein, a coherent patch of attenuated signals can be seen.

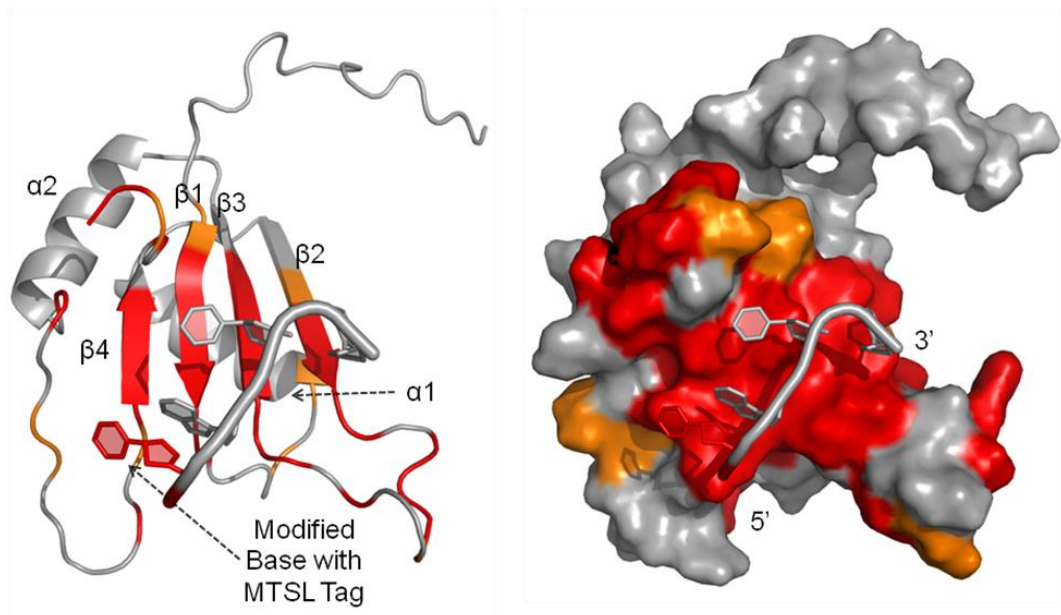


Figure 7.8: The largest paramagnetic enhancement effects are shown in red (residues where $I_{\text{para}}/I_{\text{dia}} < 0.3$). Moderate effects ($0.3 < I_{\text{para}}/I_{\text{dia}} < 0.5$) are shown in orange. Less affected residues are shown in grey ($I_{\text{para}}/I_{\text{dia}} > 0.5$). The RNA substrate is also shown, with the position of the modified base with the MTSL tag highlighted in red.

Figure 7.8 shows the most affected area of the protein in red, and the approximate position of the spin label based on the crystal structures. The most affected region covers a rather larger area of the protein surface than was generally seen in the CSP maps. The MTSL tag is attached to the 5' RNA base via a disulphide bond which allows it some range of movement relative to the RNA. This may allow the spin label some freedom of movement even when the RNA remains fixed in the binding site. There are additional affected residues above and to the left of the binding patch (visible in orange in Figure 7.8) which are greatly attenuated but not lost completely may be due to this. They are outside the normal RNA binding surface seen on CSP maps, but are plausibly within the range of motion of the MTSL tag.

There is a general loss of signal intensity of 20 - 40% over virtually all of the remaining surface area of the protein, including those residues in the α -helices on

the opposite face of the protein from the RNA. This can be attributed to the long range of the PRE effect (up to 25 Å) encompassing almost the entirety of RRM1.

7.3.2 PRE on labelling of the EDEN-2U/4U substrate with MTSL

The MTSL coupling method was used to attach a spin label to the EDEN-2U/4U sequence. As it is a rather bulky group, the MTSL tag was coupled to an additional 4-thio-uridine at the 5' end of the RNA rather than to one of the existing uridines in the EDEN-2U/4U substrate to ensure it did not interfere with binding of the protein to the UGU site at the 5' end of the RNA. The RNA sequence was therefore 5'-U*UGUUUUGUUUUUUGU-3'.

After completion of the titration the sample was treated with 5 molar equivalents of buffered sodium ascorbate for 16 hours. Comparison of the ¹⁵N TROSY spectrum after this with the bound spectrum from the RRM123 titration with unlabelled EDEN-2U/4U showed the spin label had been at best partially reduced. In particular the peaks for several residues in RRM2 were still of very low intensity compared to the conventional titration. 10 additional molar equivalents of buffered sodium ascorbate were therefore added and the sample was allowed to react at room temperature for an additional 24 hours. This achieved a greater recovery of signal intensity. It is unclear why the spin label was more difficult to reduce in this case compared to the RRM1/U*GUU titration. Possibly it had packed against the surface of the protein via some form of hydrophobic interaction with the MTSL group, making the nitroxide spin label harder to access.

The ratio of $I_{\text{para}}/I_{\text{dia}}$ was again calculated for each residue to quantify the PRE effect. The signal to noise ratio for the bound complex was poor even without the attenuation from the spin label, resulting in relatively large margins of error compared to the previous titration. There were also far more overlapping peaks in

this spectrum, for which it was not possible to accurately measure the signal intensity for each residue. The ratio is shown below in Figure 7.9 for all residues where it could be calculated.

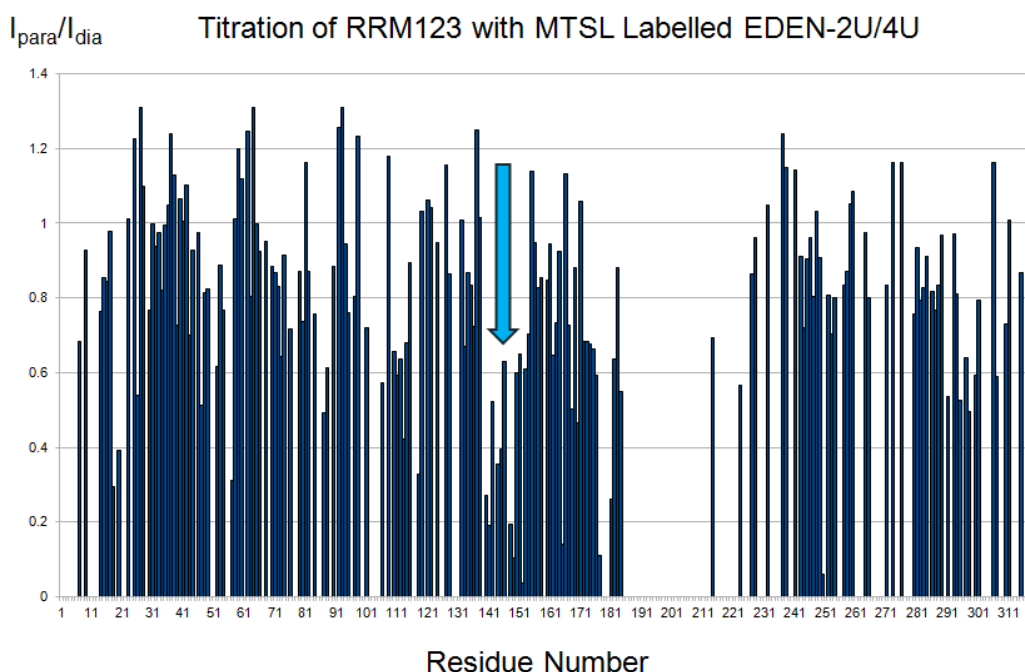


Figure 7.9: Graph of the PRE effects seen on the RRM123 construct on addition of MTSL labelled EDEN-2U/4U ($U^*-\underline{UGUUUUUGUUUUUUUGU}$). Values greater than 1 are seen for some residues due to the large margin of error. Moderate PRE effects (ratio = 0.4 – 0.8) are seen for some residues in all three domains. A noticeable cluster of strongly affected residues (ratio < 0.4) is seen in RRM2, and has been highlighted, though there are a few other strongly affected residues in the other domains.

The MTSL spin label is expected to have some freedom of movement due to both the disulphide link attaching it to the RNA base, and the fact the 4-thiouracil is an addition to the 5' end of the RNA and so does not interact directly with the protein. This accounts for the observation of PRE effects across a relatively large number of residues. While there is some attenuation of signals across all three domains, most of the strongly affected residues are concentrated in RRM2, as is shown in Figure 7.10. From this it can be concluded that CELF1 is preferentially binding with RRM2 at the 5' end of this RNA sequence. This indicates that the 2 – 1 – 3 arrangement of the domains from 5' to 3' is most favourable, not the 3 – 2 – 1 arrangement.

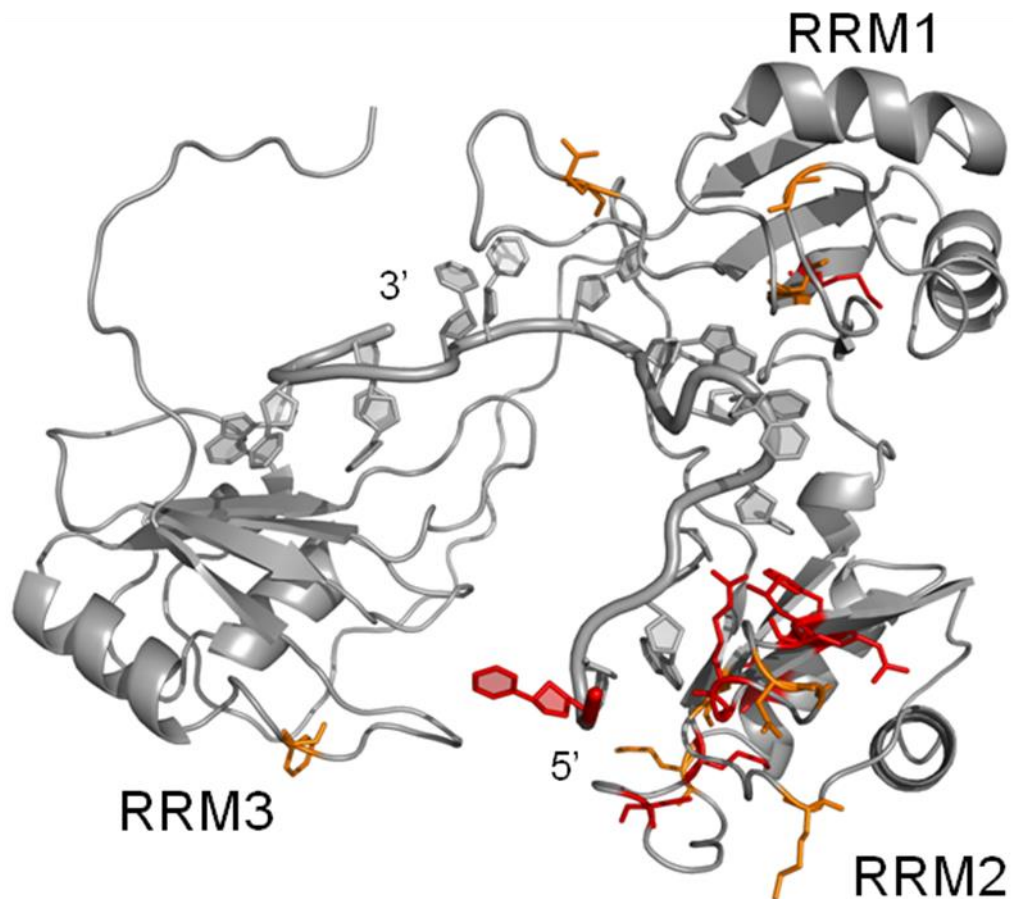


Figure 7.10: A model of RRM123 with PRE effects shown, in complex with the RNA substrate U*UGUUUUGUUUUUGU. Details of the model construction are explained in section 7.2. Large paramagnetic enhancement effects are shown in red (residues where $I_{para}/I_{dia} < 0.3$). Moderate effects ($0.3 < I_{para}/I_{dia} < 0.5$) are shown in orange. Less affected residues are shown in grey ($I_{para}/I_{dia} > 0.5$), as are any with no data such as the unassigned RRM2 – RRM3 linker. The RNA substrate is also shown, with the position of the modified base with the MTSL tag highlighted in red.

It seems likely that the signals in RRM2 that are almost completely obliterated are due to PRE from the directly bound RNA, while the much more widespread partial attenuation of signals may be due to non-specific intermolecular interactions, and represent the exposed surface of the protein. The most affected residues are shown in Figure 7.10 with those losing $>70\%$ of signal intensity shown in red, and those with 50 - 70% loss shown in orange.

With a single exception (Met18) the most affected residues are in RRM2, and generally are in the β -sheet and loop regions of the domain. There is also a concentration of moderately affected residues in this domain, with a few additional residues in RRM1 and RRM3 with 50 – 70% loss of signal intensity.

7.4 Small Angle X-ray Scattering

The loss of NMR spectrum quality on formation of a high affinity 1:1 complex was attributed to the protein becoming more globular and rigid on binding. Small angle X-ray scattering (SAXS) was used as a complementary technique to help investigate whether the complex was more rigid and compact than the unbound protein. SAXS data was collected for the RRM123 construct both unbound, and in complex with the high affinity EDEN-2U/4U substrate. Data for the protein/RNA complex was collected at two concentrations – 1 mg/ml and 5 mg/ml to check for any aggregation effects. Collection of the SAXS data was carried out by Dr. Chan Li (School of Pharmacy, University of Nottingham). We analysed the data to calculate Kratky and Guinier plots in the ATSAS software package. Advice during this analysis was provided by Dr. Katherine Carr (School of Pharmacy, University of Nottingham). Calculation of the 3D envelope was carried out by Dr. Jonas Emsley (School of Pharmacy, University of Nottingham).

7.4.1 Guinier Plots

The radius of gyration (R_g) of the protein and the complex can be calculated from a Guinier plot of the SAXS data. By comparing R_g values for the free RRM123 protein and the complex, it would be possible to tell if the overall protein geometry was changing. If a more compact complex was forming, it would be expected to have a lower radius of gyration. The Guinier plots for the unbound protein, the

complex at low concentration, and the complex at high concentration are shown in Figure 7.11.

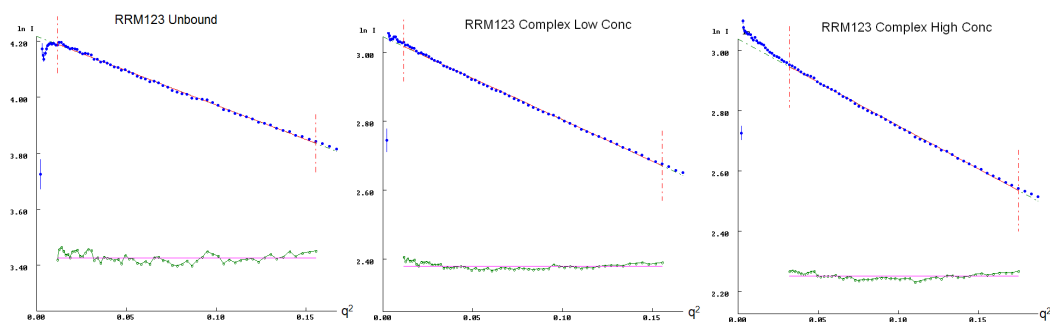


Figure 7.11: Left is the Guinier plot for the unbound CELF1. Centre is the plot for the RRM123/EDEN-2U/4U complex at low concentration (1 mg/ml) and right is the plot for the complex at higher concentration (5 mg/ml). Calculated R_g for the unbound protein was 2.72 nm, R_g for the complex was calculated as 2.69 nm from the low concentration plot and 2.94 nm at high concentration. Plots were produced using the ATSAS software package.

There is a slight deviation from linearity in the plot for the complex at high concentration, suggesting some aggregation is occurring in this sample. This is likely to be the reason for the slightly higher R_g seen for the complex at this concentration. At 1 mg/ml the Guinier plot is linear, and the calculated R_g should therefore be more accurate. R_g values of 27.2 Å for the unbound protein, and 26.9 Å for the complex were calculated. This difference in the radius of gyration for the free and bound RRM123 is negligible. This is somewhat surprising if the domains are forming into a more compact arrangement on binding, but is consistent with the earlier size exclusion chromatography data, which showed very little change for RRM123 on binding to the RNA.

7.4.2 Kratky Plots

Earlier in **Error! Reference source not found.** were shown examples of the Kratky plots for globular proteins, disordered proteins, and a protein with both structured

and disordered regions. If the complex of RRM123 with EDEN-2U/4U is more compact and rigid than the free RRM123 protein the Kratky plots, shown below in Figure 7.12, would be expected to show a significant difference.

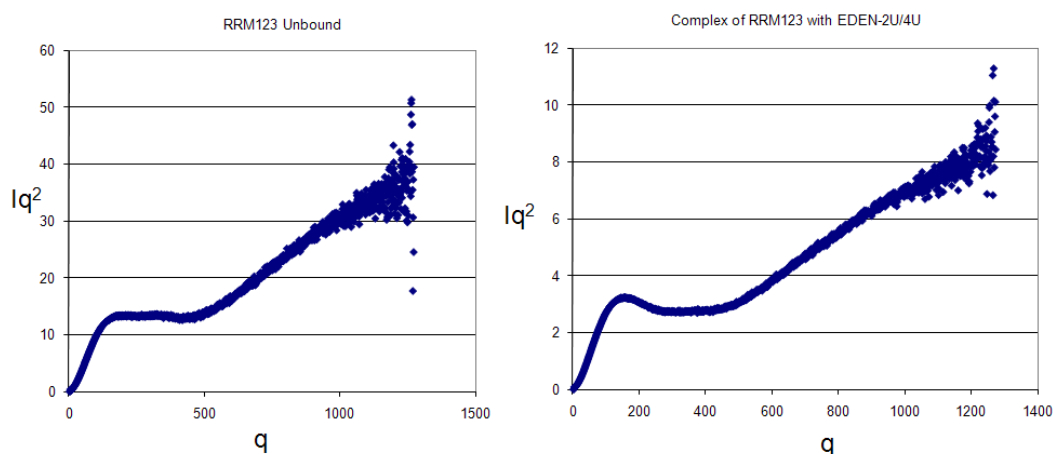


Figure 7.12: Kratky plots for unbound RRM123 (left) and the complex of RRM123 with EDEN-2U/4U (right).

Both the free protein and the complex show considerable flexibility, with a long increasing tail for high values of q . The complex shows a rather more clearly defined peak than the free protein, suggesting some population of a more compact form when bound to RNA. The Kratky plot does still show flexibility in the bound form though, so there may also be a range of more elongated conformations in solution.

7.4.3 Predicted Envelope

SAXS can be used to predict a low resolution 3D envelope of the particles in solution. Based on the data from the high concentration sample of the bound complex a 3D envelope was calculated by Dr. Jonas Emsley (School of Pharmacy, University of Nottingham), which is shown in Figure 7.13.

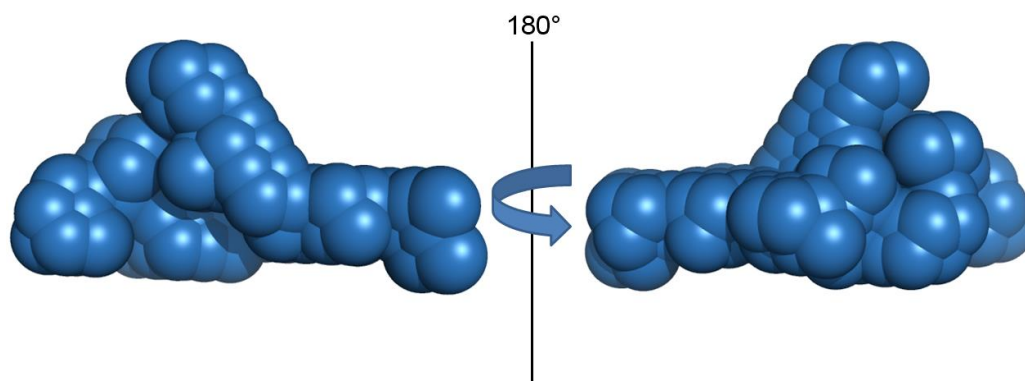


Figure 7.13: Autoenvelope calculated from the SAXS data for the RRM123/EDEN-2U/4U complex. Envelope calculated by Dr. Jonas Emsley (School of Pharmacy, University of Nottingham).

It is not immediately obvious how the three domains of CELF1 would occupy this volume. As shown in Figure 7.14 the envelope is large enough to accommodate a relatively linear arrangement of the domains, but this leaves a significant amount of unaccounted for volume in the envelope. Similarly a more compact form of CELF1 will fit reasonably well into the roughly triangular section to the left hand side in Figure 7.13, but again leaves a “tail” of unaccounted for volume to the right. It is possible that in solution there are a range of conformations between these two extremes, resulting in a calculated SAXS envelope which is not representative of any individual conformation.

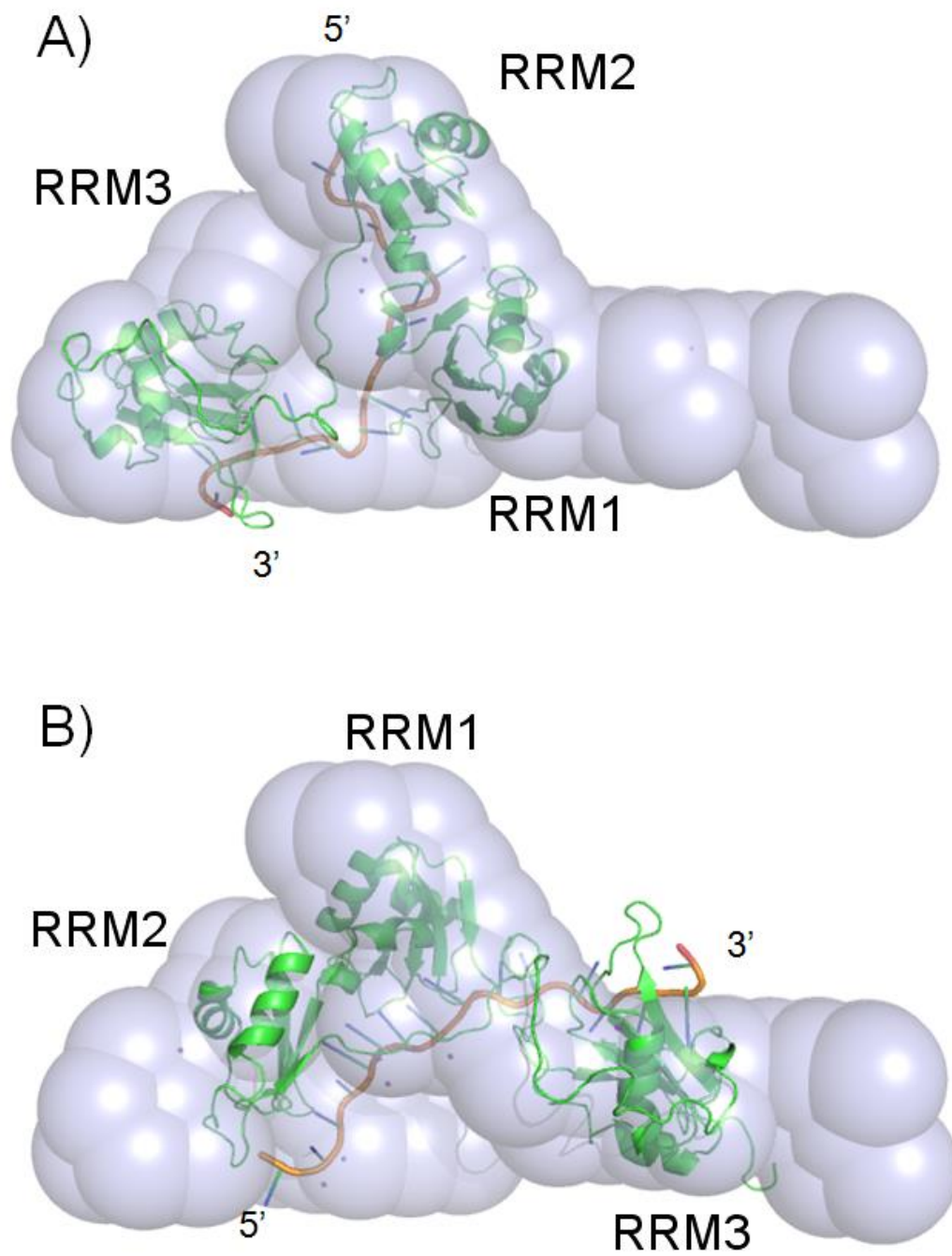


Figure 7.14: Possible arrangements of the domains within the SAXS envelope. A) shows a relatively compact arrangement of the three domains. B) shows a more extended model. In both cases the envelope is large enough to accommodate all three domains, but there are significant volumes unaccounted for.

7.5 Refining the Model

The initial model was refined using distance restraints based on the paramagnetic relaxation enhancement experiments. Due to the potential issues with intermolecular PRE effects, only those from the most affected residues ($I_{\text{para}}/I_{\text{dia}} < 0.5$) were used, though this left relatively few restraints between the tag and residues outside RRM2. Molecular dynamics simulations starting from either an “extended” or “compact” arrangement of the domains resulted in a very similar final model.

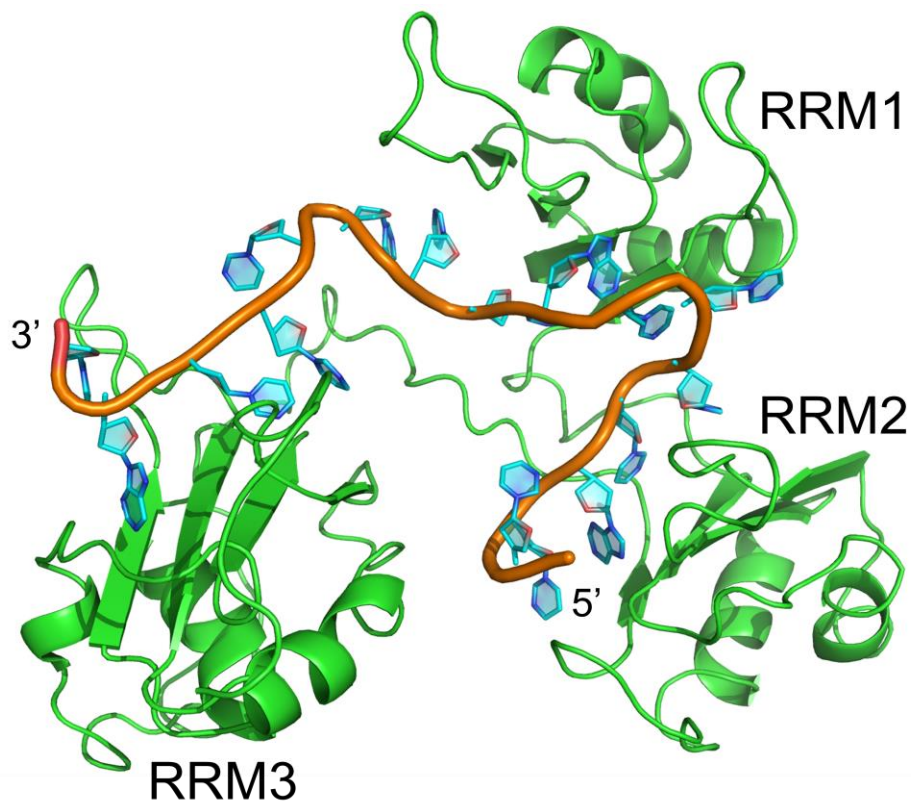


Figure 7.15: Refined model of RRM123 in complex with the EDEN-2U/4U RNA substrate, produced using restraints based on the most affected residues in the PRE experiment. Restraints were approximated as an upper limit of 24.5 Å between those residues where $I_{\text{para}}/I_{\text{dia}} < 0.3$ and the paramagnetic centre, and 29 Å for residues where $0.3 < I_{\text{para}}/I_{\text{dia}} < 0.5$.

The model could be refined further by repeating the experiment with the spin label at different positions in the RNA, for example at the 3' end and at a position

close to the middle UGU site. This would provide corroborating information on the 5' to 3' arrangement of the three RRM s and increase the number of long range distance restraints which could be used in molecular dynamics simulations.

7.6 Conclusions

We were not able to produce an NMR solution structure of the complex, but we were able to construct a model based on the structural data from the isolated domains supplemented by PRE and SAXS data. The intrinsic flexibility of the RRM2 – RRM3 linker sequence can be seen in the Kratky plots from the SAXS data, and is conserved in the bound state. This suggests that conformational flexibility, together with the long range distance dependence of the PRE effect may account for the attenuation of signals observed in all three domains. The largest effects appear to place the 5' MTSL label in close proximity to RRM2, which uniquely defines the alignment of all three domains on the RNA substrate. From this it appears that CELF1 forms a relatively compact complex with high affinity RNA substrates such as EDEN-2U/4U, with the RRM s preferentially arranged in the order 2 – 1 – 3 from the 5' to 3' end of the RNA. The possibility of a minor population in solution with a different domain arrangement, or a more extended conformation cannot be excluded.

8 CELF1 Phosphorylation and Interactions with Poly(A) Ribonuclease

8.1 Phosphorylation

CELF1 has been previously identified as a phosphoprotein, with multiple possible phosphorylation sites for different kinases¹¹. In DM1 cells it has been shown that CELF1 is hyperphosphorylated by protein kinase C, resulting in an extended protein half-life¹⁰⁵. So far the only phosphorylation sites to have been investigated and observed to have an effect on the properties of CELF1 are Ser28 in RRM1 and Ser302 in the RRM2 – RRM3 linker (cyclinD3/cdk4). Both of these have been reported to increase CELF1's affinity for RNA in general and possibly to influence the preferred RNA target sequence^{106, 109}. The Ser302 phosphorylation has also been reported to promote association with an initiation factor (eIF2), which would impact the translation of the target mRNAs²⁰⁴.

Other potential phosphorylation sites have been predicted for three other phosphatases. GSK3 at Thr277, Thr281, Ser285, Ser292 and Ser300. PKC delta at Thr163, Ser268 and Ser383. Finally Akt kinase has been predicted to also be capable of phosphorylation at Ser28. Most of these sites are in a serine and threonine rich region in the middle of the flexible linker between RRM2 and RRM3. The only sites in structured regions are Ser28 in RRM1 and Thr163 in RRM2. It is worth noting that Thr163 is not conserved between human and *Xenopus* CELF1, being replaced with methionine in *Xenopus*. Given human and *Xenopus* CELF1 have been shown to be functionally interchangeable it seems unlikely this residue plays any key role. Work by Salisbury *et al.* in 2008 was unable to confirm any activity by GSK3 or PKC delta on CELF1, but did show phosphorylation by Akt1 in vitro. Akt1 has also been noted to be upregulated in DM1 cells¹⁰⁹.

Salisbury *et al.* also reported increased affinity for the cyclin D1 mRNA sequence when CELF1 is phosphorylated. This sequence bears very little resemblance to any of the other sequences known to be targets of CELF1, with very few uracils, no UGU sites and only a single UGC site. It has been proposed that phosphorylation of CELF1 at Ser28 may serve as a “switch” capable of changing the RNA target of the protein from U/G rich sequences to C/G rich sequences, enabling the reported interaction with cyclin D1 RNA. Ser28 does not show a significant CSP when binding to any of the NMR substrates investigated earlier in this study, and did not show any contacts with the RNA substrate UUGUU in the crystal structure.

Cyclin D1: 5'-

CCCAGCCAGGACCCACAGCCCUCCCCAGCUGCCCAGGAAGAGCCCCA
GCC-3'

This sequence is clearly distinct from the U/G rich sequences capable of forming high affinity complexes with CELF1. To examine this potential range of additional RNA targets, a phosphomimetic mutant of CELF1: S28D was produced by site directed mutagenesis. This mutation was used in the original paper, and serine to aspartate mutations have been shown in many cases to mimic phosphorylation^{205, 206}. Mutants of the RRM1, t187 and RRM123 constructs were also produced. The purification methods used for the S28D mutants were identical to those for the wild type.

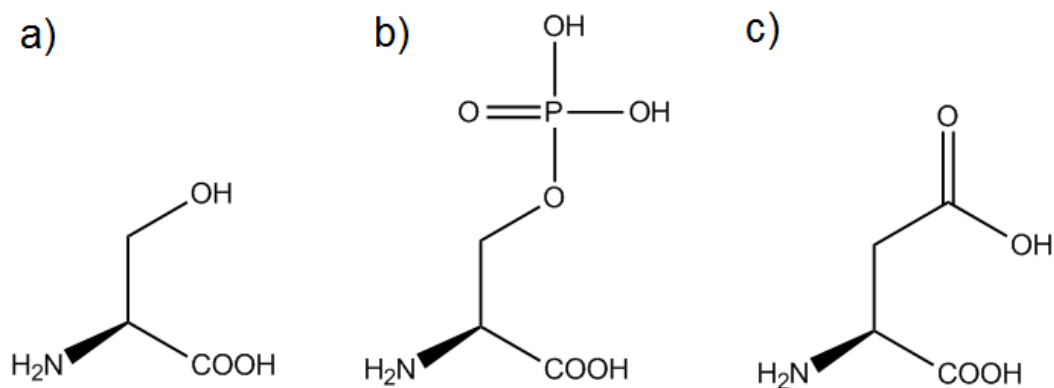


Figure 8.1: From left to right are shown structures of a) serine, b) phosphoserine from post translational modification, c) aspartic acid, used as a mimic for phosphoserine in the original study, and in this investigation. Glutamic acid can also be used as a phosphomimetic mutant.

¹⁵N labelling the protein and collecting a ¹⁵N TROSY showed moderate disruption to the spectrum, localised to those residues near the point mutation.

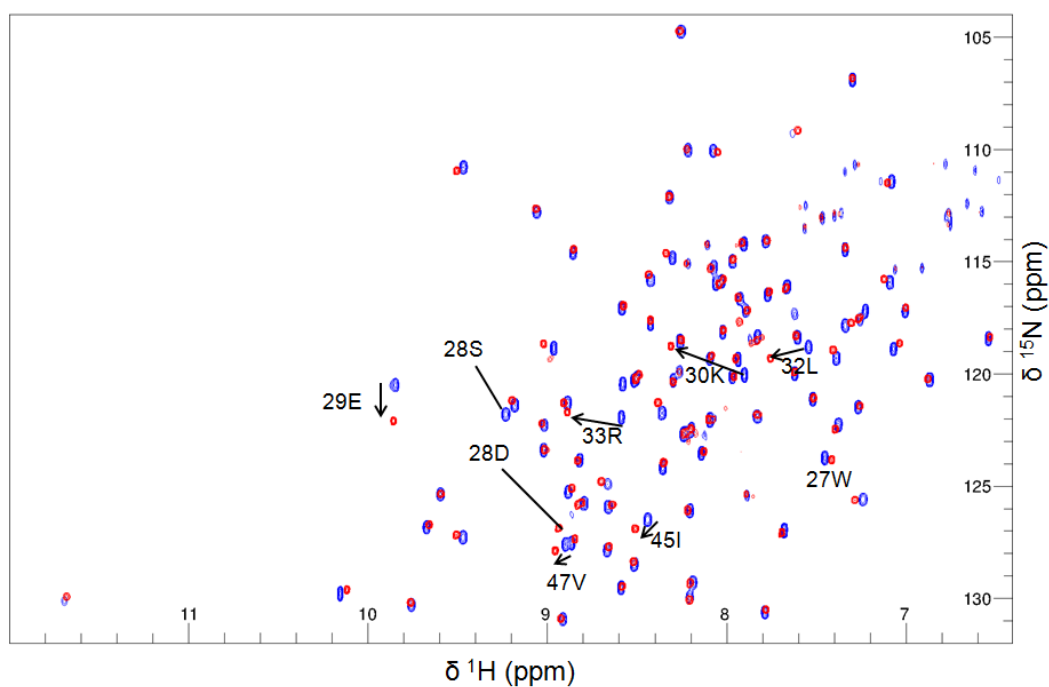


Figure 8.2: The ¹⁵N TROSY of the RRM1 S28D phosphomimetic mutant is shown in red, overlaid on the spectrum of wild type protein in blue. The signals for residue 28, and other strongly perturbed residues, are highlighted. The spectrum is generally very similar to that of the wild type RRM1, suggesting this phosphorylation is not drastically altering the fold of the protein. Data was collected on a Bruker Avance III 800 MHz spectrometer at 298 K.

Most residues could be assigned by analogy to the wild type protein. There were however several residues with large enough chemical shift changes between the wild type and S28D mutant to render assignments ambiguous (specifically for residues 30, 32, 33, and 34, in addition to residue 28 itself). Assignment of these residues was carried out using HNCACB and HN(CO)CACB spectra collected on a 250 μ M doubly labelled sample on an 800 MHz spectrometer with QCI cryoprobe.

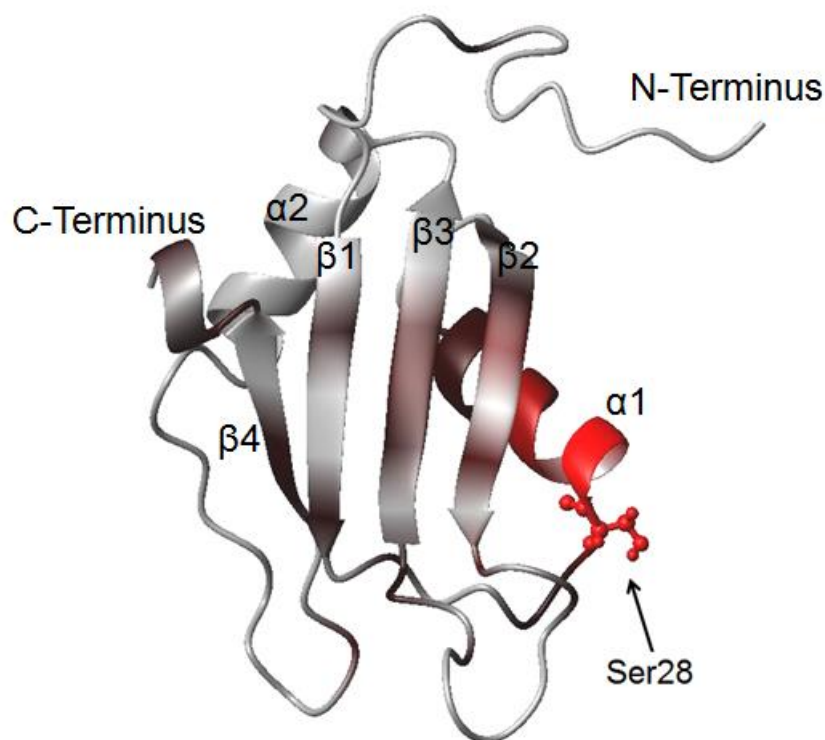


Figure 8.3: Structure of RRM1 with Ser28 shown using a ball and stick depiction. Those residues which show significant changes to their chemical shifts when Ser28 is mutated to aspartic acid are highlighted in red, with brightness of colour indicating the magnitude of the perturbation. The most affected residues consist of the first half of α -helix 1, and to a lesser extent a few residues in β -strand 2, which is packed against it.

In the wild type protein the side chain of Ser28 extends out into solution at the start of the first alpha helix. In the S28D mutant, there is disruption of the chemical shifts for all residues in the first two turns of this helix, with the exception of Glu31. There are minor shifts for Ile45, Val47 and Arg49 as well. The side chains of these residues extend from the underside of β 2, pointing

towards the disrupted residues in α -helix 1. There are negligible CSPs for Trp27 and Ser26, despite their close proximity to the mutation site.

From the changes in the NMR spectrum on mutation it appears that phosphorylation at this position does not greatly alter the overall fold of the protein. The effects are confined to the α -helix, which has not previously been seen to be involved in binding, and to a lesser extent the β 2 strand. This was consistently the least affected strand of the β -sheet in the titrations shown earlier, so again it would be surprising if this had a significant impact on the normal binding mode of the domain.

S28D mutants were also produced of the t187, RRM123 and full length CELF1 proteins with the assistance of Zoe Le Gray-Wise. The binding affinity of the S28D mutants relative to the wild type constructs was investigated by ITC, NMR and fluorescence methods. It was expected that the S28D mutant would show an increase in affinity for CUG repeating sequences, and/or a reduction in affinity for the sequences containing UGU sites. Comparison of the ITC data for wild type vs. S28D did not however show any significant difference on binding to the sequence UGUUUAU, as shown in Figure 8.4.

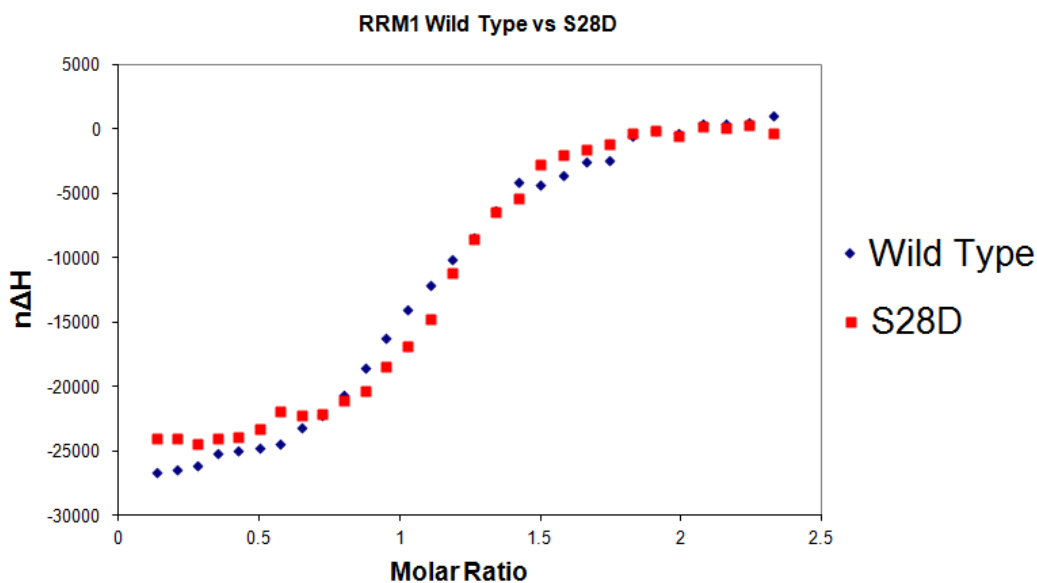


Figure 8.4: Comparison of ITC traces for the titration of RRM1 wild type and the S28D mutant with the RNA substrate UGUUUAU. This phosphomimetic mutation is not resulting in any loss of binding affinity to the normal UGU site.

In practice no significant differences in binding affinity (or stoichiometry) were seen for the S28D mutant binding to UGUGUG, EDEN11 or EDEN-2U/4U. To within the margin of error of these techniques the results were the same as for the wild type CELF1 constructs. The S28D mutant in fact showed a somewhat reduced affinity for CUG based sequences, with no detectable binding seen by ITC. NMR showed greatly reduced CSPs on binding to CUGCUG, and the titration required a much larger excess of RNA in order to reach an endpoint. Based on this it could be concluded that phosphorylation at Ser28 does not serve as any kind of regulatory switch between UGU and CUG targets of CELF1. The cyclin D1 mRNA from could perhaps be being recognised via some other motif, such as GCGC.

This leaves the possibility that phosphorylation may play a role in regulating the stability of CELF1, and its ability to interact with other proteins. The multiple sites in the serine rich region of the RRM2 to RRM3 linker are the most likely residues for this. The limited impact of Ser28 phosphorylation and the lack of

predicted phosphorylation sites in the other structured regions of the protein indicate that it does not regulate RNA recognition though.

8.2 Dimerisation of CELF1

Bonnet-Corven *et al.* (2002) reported dimerisation of *Xenopus* CELF1 using a yeast two hybrid assay⁵⁴. Biophysical techniques have not shown any sign of dimer formation except possibly in the ESI-MS of RRM1. No dimer population was seen for the t187 or RRM123 constructs, despite the fact the RRM123 construct still incorporates the section of the linker proposed to be involved in dimerisation¹⁰³. The elution point by gel filtration of all CELF1 constructs is consistent with a monomeric species. ITC of concentrated wild type CELF1 into buffer showed no significant enthalpy change. If a dimer was present then this dilution titration would be expected to show a dissociation curve.

There are signs of a small dimer population in some of the mass spectra, in particular the unbound RRM1 construct. This appears as a smaller set of peaks with m/z values that imply half-integer values of z . Since this is not possible, it indicates a second species consisting of a dimer. The NMR data shows no change in the spectrum of any of the CELF1 constructs on dilution from 400 μM to 20 μM . No change is seen on dilution for the high affinity RRM123/EDEN2U4U complex either. As the ITC and NMR do not show any evidence of dimerisation and the fraction of this species seen in the mass spectrum is very small it is possible this is an artefact of the experiment being in the gas phase. There were also no signs of dimerisation in the spectrum for the t187 or RRM123 constructs. Wild type CELF1 did not give clear enough mass spectrometry data for accurate determination of its mass, or to detect the presence of any low population species. The NMR spectrum of full length CELF1 was essentially the same as that of RRM123 for the structured region, so it seems unlikely that any dimerisation interface could exist in the RRMs. The spectrum did not show any changes on

dilution, so again there is no evidence of dimerisation of CELF1 by NMR.

8.3 Poly(A) Ribonuclease

In 2006 Moraes *et al.* reported a protein - protein interaction between CELF1 and poly(A) ribonuclease (PARN)⁵⁶. PARN is a 3'-exoribonuclease, which specifically degrades poly(A) tails^{207, 208, 209}. This presents a possible mechanism for CELF1 binding increasing deadenylation rates, as the protein could be directly recruiting PARN to the target mRNA substrate. This interaction was observed in the absence of RNA so it must occur between the proteins, and not simply be a case of the two proteins binding to the same RNA molecule. It was later shown that the presence of CELF1 affected patterns of mRNA deadenylation by PARN¹³. No structural information indicating which regions of these two proteins are involved in the interaction has been reported.

Poly(A) ribonuclease is a 72.8 kDa protein containing three structured domains; a 310 residue exoribonuclease domain, a 75 residue R3H domain, and an 80 residue RNA recognition motif²¹⁰. The R3H domain is inserted into a long flexible loop in the middle of the protein sequence of the nuclease domain. The RRM is separated from the other domains by an unstructured region, and there are an additional 120 residues of flexible protein forming the C-terminal end of the protein. A 54 kDa fragment of the protein has been found to be sufficient to specifically degrade poly(A) tails²¹¹.

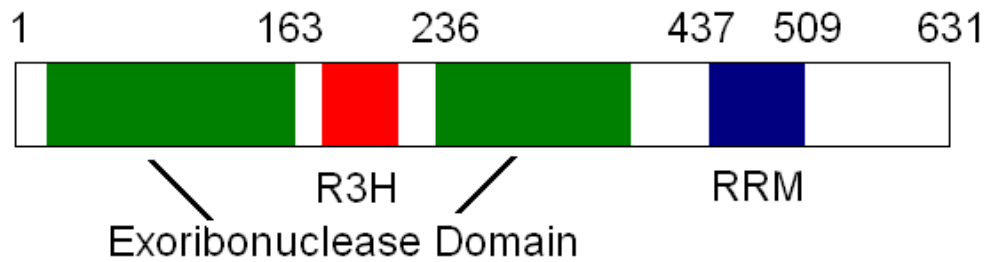


Figure 8.5: Domain layout of PARN. The R3H domain is inserted into an extended loop in the middle of the exoribonuclease domain.

PARN is believed to form a homodimer via the exoribonuclease domain²¹¹. Dimerisation of a construct of residues 443 - 560 has also been reported, and speculated to be mediated by a zipper motif in the C-terminal region²¹². Crystal structures of all three structured domains are available (PDB IDs: 1UG8, 1WHV and 2A1R), however no structure in which all three domains are visible simultaneously has yet been reported. Structural data is also available for the nuclease domain in complex with a poly(A) sequence²¹³ and for the RRM in complex with the 5' mRNA cap structure¹¹². The RRM has also been implicated in interactions with the poly(A) tail^{214, 215}. The largest complex which has been directly observed consisted of residues 1 - 510 of PARN in complex with RNA, but the R3H domain appeared unstructured in this crystal. In 2009 Wu *et al.* produced a possible model of the complete homodimeric protein in complex with both the 5' cap and the poly(A) tail of an mRNA based on a combination of the different crystal structures, which is shown in **Error! Reference source not found.**¹¹¹.

The reported dimerisation via the C-terminal zipper motif is however inconsistent with this model. While the C-terminus of the protein is not visible in the available crystal structures due to its flexibility, the model by Wu *et al.* would have these regions at opposite ends of the protein dimer. There is no indication of how CELF1 might interact with this complex

The R3H domain has been suggested to play a role in stabilizing the RRM, and hence the rest of the protein and the model does suggest a possible contact surface between these domains²¹⁶. In the model the R3H domain of each monomer is paired up with the RRM of the other monomer unit. PARN has been previously noted to truncate in the region of the RRM to give the p54 isoform, and removal of the R3H domain encourages this breakdown. PARN is also stabilised by the presence of Mg²⁺ ions, and requires them for catalytic activity²¹⁷.

8.4 Aims

Our initial aim was to express and purify poly (A) ribonuclease and determine whether it possible to acquire high resolution NMR data on this system. If NMR spectra of sufficient quality could be collected, we then aimed to observe the reported CELF1/PARN interaction using ¹⁵N TROSY spectra, and so determine which regions of the proteins were involved. This would enable us to determine if a ternary complex of CELF1, PARN and an EDEN motif could form, and so whether the proposed mechanism of PARN recruitment by CELF1 was plausible. As a complex of CELF1 with the PARN dimer would have a mass of around 200 kDa, this system is an ambitious target for NMR.

8.5 Expression and Purification of Poly(A) Ribonuclease

Expression plasmids of human and *Xenopus* PARN cloned into the pET33 vector were supplied by Dr. Cornelia de Moor (University of Nottingham). The expression and purification protocols were based on the methods reported by Nilsson *et al.* (2006), which had been shown to produce catalytically active PARN¹¹⁰ and so was expected to give intact and correctly folded protein.

Poly(A) ribonuclease was overexpressed successfully, though a significant fraction of the material was insoluble after a 16 hour induction at 30°C. Reducing

the induction temperature to 20°C resulted in almost all of the protein remaining in the soluble fraction. The intact protein was visible as a band just above the 66 kDa marker. There were also signs of truncation of the protein resulting in a significant band on the SDS-PAGE at approximately 55 kDa. Similar truncation products were seen in the purification by Nilsson *et al*, and were attributed to degradation of the unstructured C-terminus of PARN. Unlike CELF1, PARN did not appear to degrade further after the IMAC column stage, allowing the intact fraction of the protein to be separated from the truncation products.

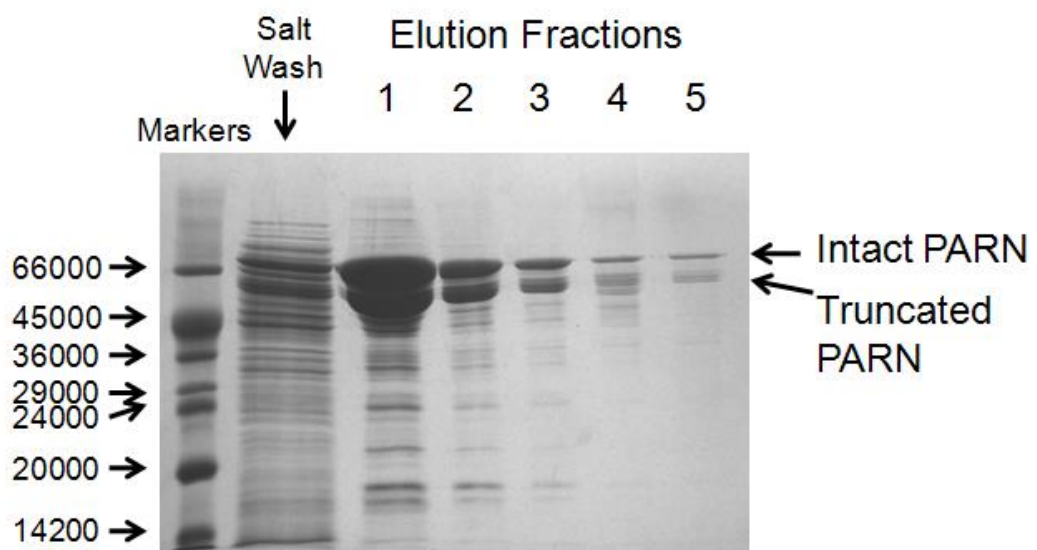


Figure 8.6: SDS-PAGE of the elution fractions from the IMAC column stage of the purification of poly(A) ribonuclease. Two strong bands are visible, one at more than 66 kDa, corresponding to the intact protein, and one just below, corresponding to a truncation product.

Gel filtration was found to be ineffective in separating the intact and truncated protein, as both eluted between 160 and 170 ml from a Superdex GF200 column. An ion exchange method similar to that used by Nilsson *et al*. was attempted, which succeeded in separating some of the truncation products.

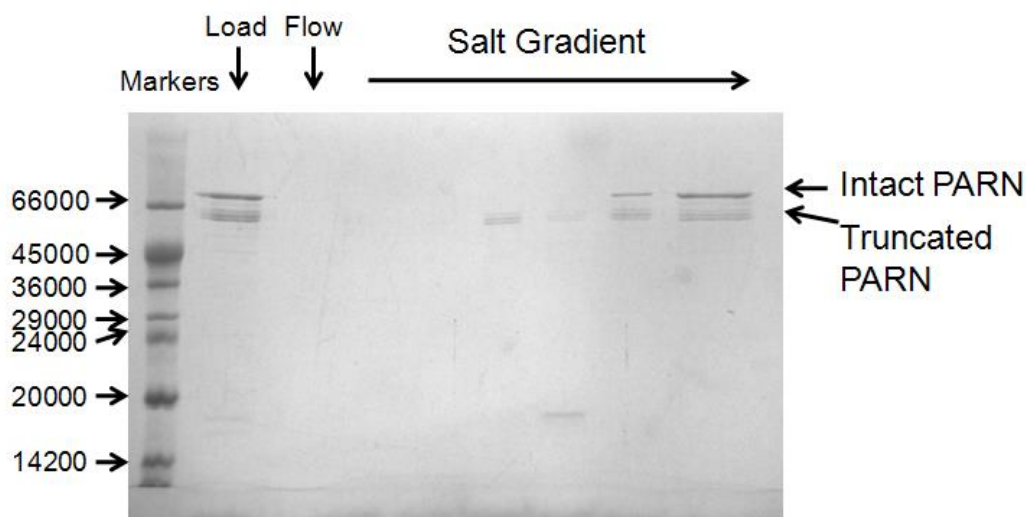


Figure 8.7: SDS-PAGE of samples from the ion exchange stage of the poly(A) ribonuclease purification. Lane 2 shows the proteins loaded onto the anion exchange column, lane 3 shows the proteins which were not bound. The remaining lanes show the proteins eluted by a 50 mM to 2 M NaCl gradient.

Some separation was achieved, though the truncation products were not completely removed. In the original purification by Nilsson *et al* these could not be completely eliminated either, though the resulting material was found to be catalytically active. The protein at this point was in a high salt buffer containing 10% (v/v) glycerol, which was not ideal for NMR, and prevented the protein from being lyophilised. The protein was therefore desalted into MilliQ water using a HiTrap desalting column.

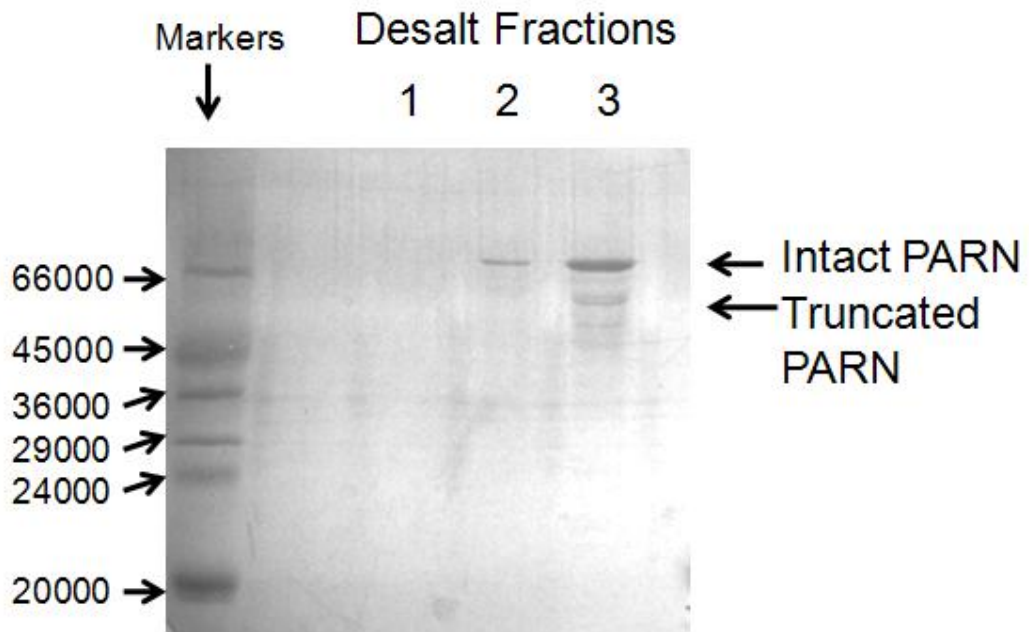


Figure 8.8: SDS-PAGE of the elution fractions from the desalt column. Fraction 2 contained intact protein only. Fraction 3 contained a greater quantity of intact protein, but also contained visible bands from the remaining truncation products.

Fraction 2 was lyophilised, and yielded 3 - 4 mg of pure protein per litre when grown in M9 minimal media. Fraction 3 was found to contain residual glycerol, and so could not be lyophilised, but additional material could be recovered by repetition of the desalting step.

8.6 NMR Studies of Poly(A) Ribonuclease

Since the protein has a mass of 72.8 kDa and was believed to form a homodimer, it seemed likely that rapid relaxation rates would result in a poor signal to noise ratio in the NMR spectrum, and that the protein would therefore be difficult to examine even using the TROSY method. ¹⁵N labelled material was purified and a TROSY spectrum was collected. With 720 scans acquired on a Bruker Avance III 800 MHz spectrometer some well dispersed peaks were resolvable, as shown in Figure 8.9.

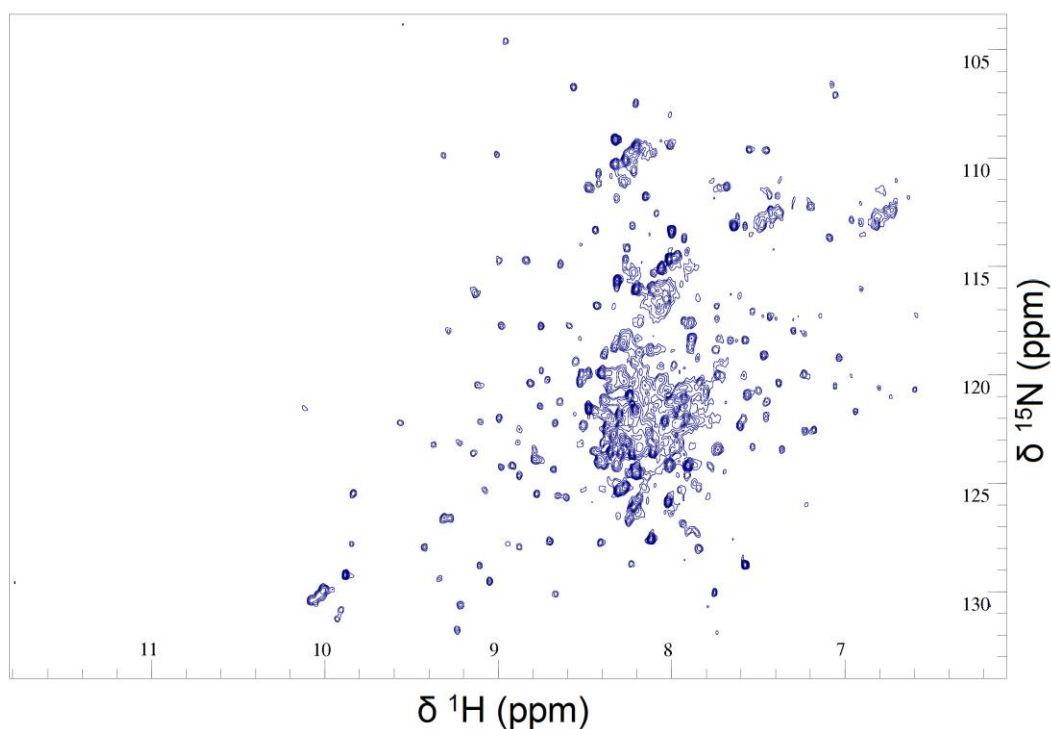


Figure 8.9: ^{15}N TROSY of full length PARN deadenylase. 720 scans were accumulated on an 800 MHz spectrometer with QCI cryoprobe. The protein was dissolved in 25 mM potassium phosphate, 200 mM NaCl, 10% (v/v) D_2O pH 7.0 buffer. The temperature was 298 K.

A large number of the peaks are heavily overlapped in a band with ^1H chemical shifts of between 7.5 and 8.5 ppm, consistent with unstructured protein. These presumably originate from the unstructured C-terminal region of the protein, and the long flexible sections flanking the R3H domain. There are around 120 well dispersed peaks, which are believed to be from structured regions of the protein. Based on the relative sizes of the domains in PARN it seems likely these are from the smaller RRM and R3H domains. The number of dispersed peaks is too large to be accounted for by just one of these domains, so it appears both the RRM and R3H domains are being observed. The larger exoribonuclease domain, while structured, should undergo much more rapid relaxation resulting in weaker signals in the NMR spectrum, accounting for the lack of signals seen for this domain.

NMR data for an isolated construct of the RRM (residues 430 - 516) was

published by Nagata *et al.* in 2008. The published ^1H - ^{15}N HSQC does not however match very closely to any subset of the well dispersed peaks in the spectrum of full length PARN. A possible explanation for this is that the RRM has been reported to be stabilized by interaction with the R3H domain. In the model by Wu *et al.* of the dimeric form the RRM domain of one protein subunit has contacts with the R3H domain of the other, consistent with this stabilisation. These contacts will not be present for the isolated RRM, which will exist as a simple monomeric protein accounting for the significant differences in the ^{15}N TROSY spectrum.

8.7 Interactions of CELF1 with Poly(A) Ribonuclease

An excess of unlabelled wild type CELF1 was added to a ^{15}N labelled PARN sample. The resulting ^{15}N TROSY spectrum is shown in Figure 8.10, overlaid on the spectrum of unbound PARN.

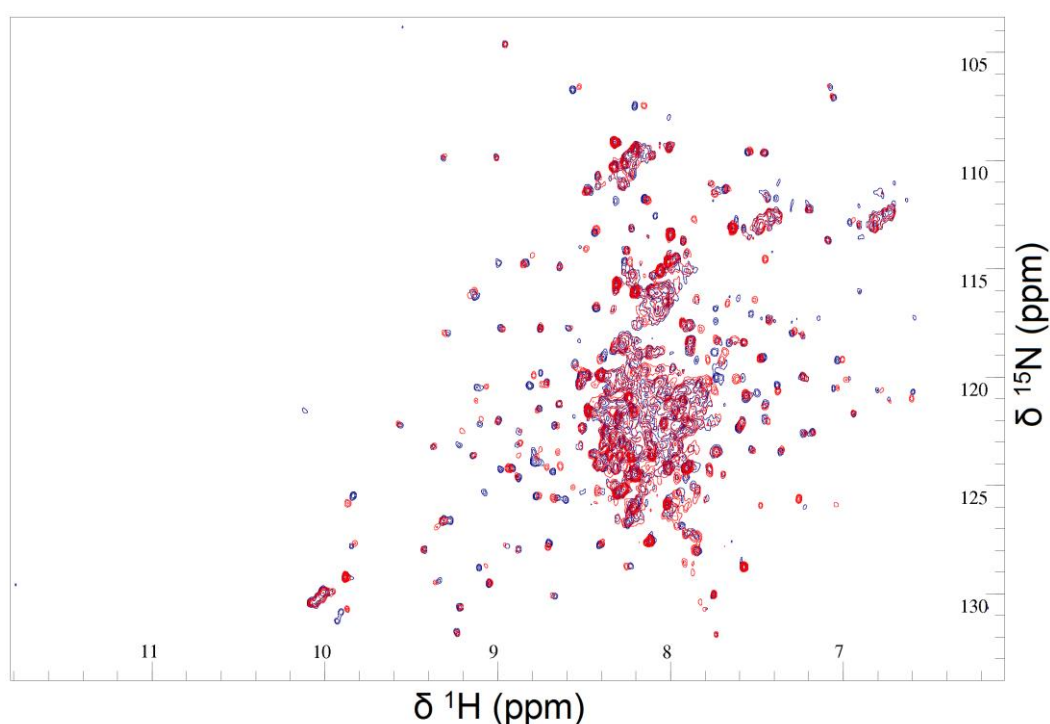


Figure 8.10: Spectrum of unbound ^{15}N labelled PARN shown in blue. Overlaid in red is ^{15}N PARN after the addition of an excess of unlabelled full length wild type CELF1. Acquisition was carried out on an 800 MHz spectrometer with QCI cryoprobe. Both spectra were collected with 720 scans at 298 K, with a resolution of 2048 x 128 points.

The poorly dispersed peaks from the unstructured region showed minimal perturbation on addition of CELF1. There were however some significant changes to the chemical shifts of some of the well dispersed peaks, presumed to be from the RRM and R3H domains. Without assignments it is not possible to unambiguously match up signals for the same residue bound and unbound and so calculate exact CSPs. However the distance between signals lost, and the closest signals that appear on addition of PARN allows a lower boundary for the CSPs to be set. It appears that several residues display CSPs of at least 0.4 ppm, indicating a significant change in environment. It can therefore be concluded that PARN and CELF1 do interact. As the most affected residues lie in the dispersed region of the spectrum it can be hypothesized that the interaction between these two proteins is mediated by the RRM or perhaps the R3H domain of PARN deadenylase.

The tryptophan side chains of PARN may provide some additional evidence as to which domain is interacting with CELF1. PARN contains six tryptophan residues, two of which are in the RRM. One tryptophan is located in the R3H domain, and the remaining three are in the unstructured C-terminal region. In the ^{15}N TROSY of PARN, a tight cluster of six peaks with chemical shifts characteristic of tryptophan side chains is visible.

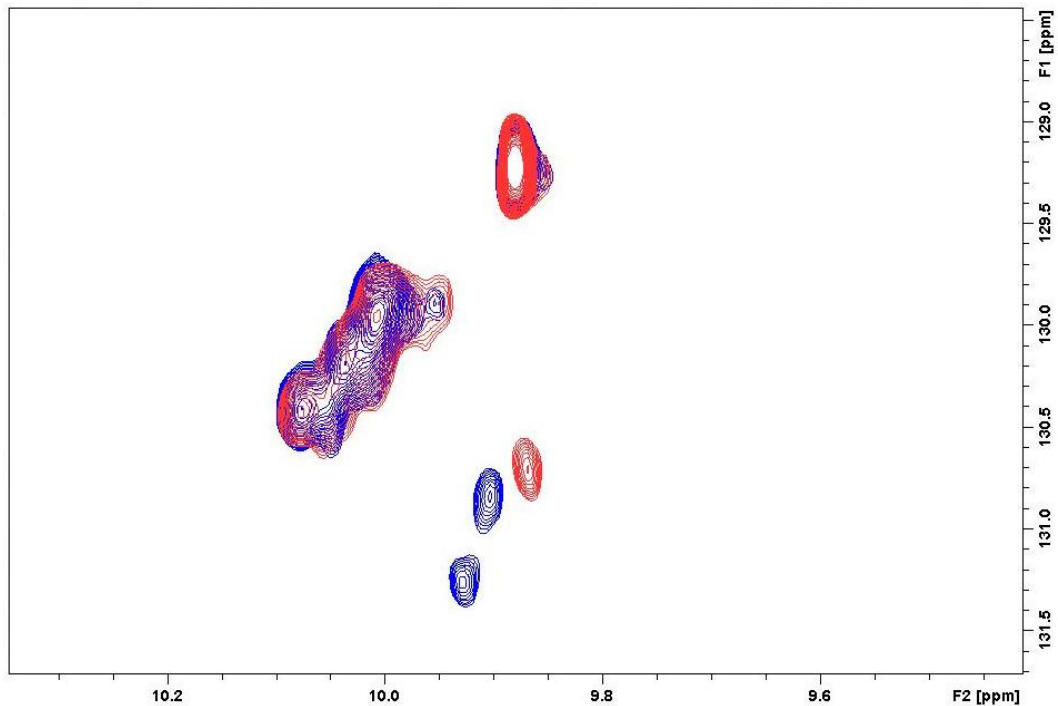


Figure 8.11: Tryptophan side chain region of the PARN ^{15}N TROSY spectrum. Unbound PARN is shown in blue. The spectrum after the addition of a saturating amount of unlabelled wild type CELF1 is overlaid in red. Six clear peaks can be seen in the unbound spectrum, of which two move significantly on binding. The remaining four, one of which is clearly the C-terminal tryptophan, are not affected.

Two of these peaks are perturbed by addition of unlabelled wild type CELF1, while the other four remain completely unaffected. As the only section of the protein with two tryptophan residues in close proximity is the RRM, this would seem to suggest this domain is mediating the PARN/CELF1 interaction.

There are some RRM domains which are known to mediate protein – protein interactions. One subgroup of RRM domains is known as U2AF homology motifs (UHM), and interact with other proteins via the α -helices on the opposite face from the normal RNA binding surface^{218, 219, 220}. In some cases RRM domains may bind both proteins and RNA simultaneously, as has been reported for PTB RRM2²²¹. Another subgroup of RRM domains is capable of forming protein – protein interactions via the β -sheet surface, though this generally prevents RNA binding^{222, 223, 224}. The PARN RRM has both a non-standard structure, with a third α -helix at the C-terminus, and a novel RNA binding site. The C-terminal α -helix blocks access to most of the β -sheet surface,

even in the presence of its target RNA (the m⁷GpppG cap structure). The RNA is instead bound by the loop regions, in particular a key tryptophan residue at the C-terminal end of $\beta 2$ ^{112, 33, 34}.

One possibility considered was that the interaction was between the PARN RRM and one of the three RRM of CELF1, perhaps via the opposite face to the RNA binding surface in the case of the CELF1 domain. To investigate this possibility the NMR experiment was run again with the labelling scheme reversed so the effects on the residues in CELF1 could be observed. An excess of unlabelled PARN deadenylase was added to ¹⁵N labelled wild type CELF1, resulting in the ¹⁵N TROSY spectra shown in Figure 8.12.

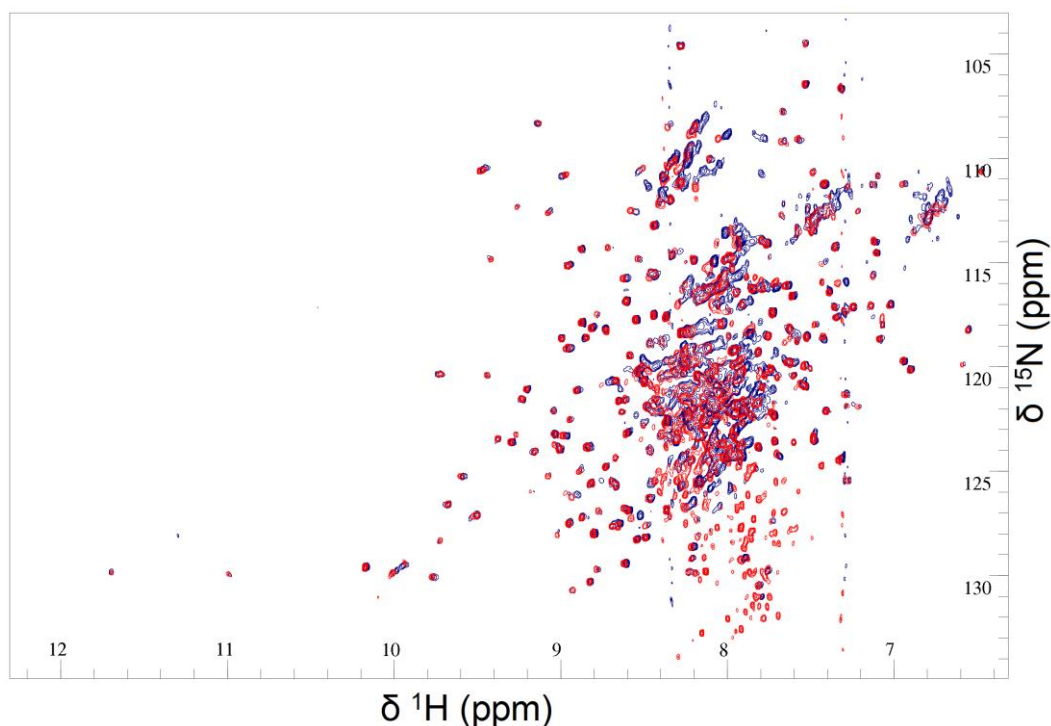


Figure 8.12: ¹⁵N TROSY of unbound wild type CELF1 shown in blue. Overlaid in red is the ¹⁵N TROSY after addition of unlabelled full length PARN. There are only very minor perturbations seen to the signals from the structured RRM3. A much greater disruption is seen for some signals from the unstructured RRM2-RRM3 linker, suggesting that PARN may be recognising some part of this sequence. Some degradation products of CELF1 are visible in the bound spectrum.

The addition of unlabelled PARN deadenylase had very little effect on the peaks

from any of the three RRMs of CELF1. There was some disruption to peaks in the unstructured region of CELF1, but without assignments the exact residues involved could not be determined. This indicates that the RRMs of CELF1 are not involved in any interaction with PARN. The remaining possibility is that the interaction is between the RRM and/or R3H domain of PARN and a peptide sequence in the long linker between RRM2 and RRM3. This is consistent with the disruption seen for the residues from the unstructured region of CELF1. It also implies that the interaction with PARN should not interfere with the normal RNA binding interactions of CELF1, and so a ternary complex could be formed.

If a section of the RRM2 - RRM3 linker is recognised by PARN it would be expected to be conserved across the different species where CELF1 and PARN homologs exist. Unfortunately this linker, while somewhat less conserved than the structured domains of CELF1, still has a high degree of sequence identity across species such as human, mouse, chicken, *Xenopus* and zebrafish. There are many conserved sections which could potentially be a binding motif for PARN. In Figure 8.13 is shown a sequence comparison of this region of the protein.

zebrafish.

If PARN is remaining as a dimer when it binds CELF1, the resulting complex would have a mass of around 200 kDa. It would be very surprising to see any clear peaks in the NMR for a system of this size. It is possible that the PARN dimer is disrupted by binding to CELF1, which would result in a monomer/CELF1 complex with a total mass of approximately 135 kDa. Given the NMR spectra of the complex are of at least the same quality as those of the free protein, it seems likely that the complex is not drastically larger than the PARN dimer.

8.7.1 Isolation of the PARN RRM

An initial attempt was made to confirm the regions of PARN involved in CELF1 binding by breaking the protein into isolated domains. The RRM was the simplest domain to isolate, using the one-step deletion PCR method to remove the codons for residues 1 – 430 from the full length protein plasmid. This construct retained the long unstructured C-terminus of the protein, which has been predicted to form a “zipper” motif dimer.

Expression and purification of this construct was carried out using the same protocols as for the full length protein. The solubility was considerably higher than for the full length protein, though SDS-PAGE did still show some C-terminal degradation of the protein after the IMAC column stage of the purification.

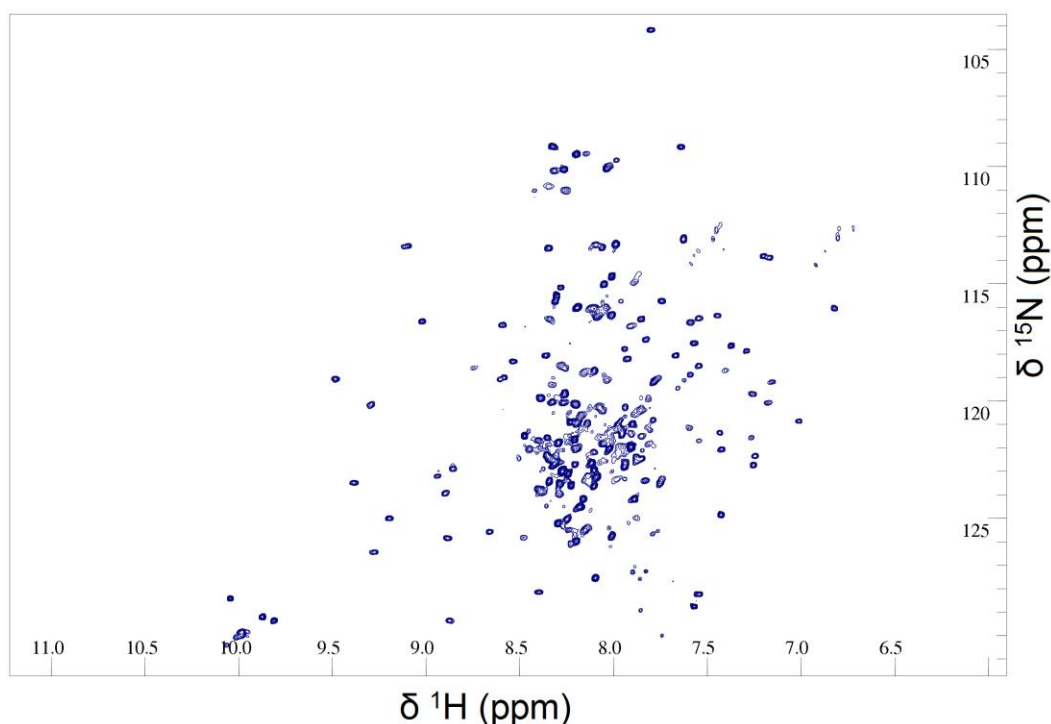


Figure 8.14: ^{15}N TROSY spectrum of the 431 – 631 construct of PARN deadenylase. Both well dispersed peaks from the structured RRM and heavily overlapped peaks from the unstructured C-terminus of the protein are visible. The unstructured peaks generally are a close match to a subset of those in the spectrum of the full length protein. The structured peaks do not match any of those in the full length protein, but do match the data in Nagata *et al.*'s 2008 paper.

The ^{15}N TROSY of this protein showed around 80 well dispersed peaks, consistent with the structured RRM domain. There are also clusters of intense peaks from the unstructured region. The signals from the unstructured region closely match a subset of the signals in the spectrum of the full length protein. The signals from the RRM however do not match the chemical shifts of any subset of the peaks in the spectrum of the full length protein. This can be attributed to a change from dimer to monomer in going from full length protein to the 431 – 631 construct. The well dispersed peaks are a reasonable match to the NMR data published by Nagata *et al.* in 2008, which was from a smaller monomeric construct, lacking the C-terminal region.

Addition of a saturating amount of wild type CELF1 had no apparent effect on the spectrum. From this it can be concluded that the RRM on its own is insufficient to bind to CELF1. Contacts with an R3H domain in the dimeric form of PARN may be required to form the binding site for CELF1, and/or stabilise the RRM. Since the domains are not functioning independently the approach of investigating each domain in isolation which was successful for CELF1, may not be suitable for locating the CELF1 binding site on PARN.

8.7.2 Supplementary Biophysical Techniques

Preliminary investigations of the CELF1/PARN interaction were also conducted using ITC and ESI-MS. Mass spectrometry of PARN was not successful. Some very broad signals were present, possibly indicating a range of species with different numbers of bound sodium ions. The SDS-PAGE analysis carried out during the purification suggested that the truncation products were not completely removed, which may also be contributing to the broad peaks seen in the mass spectrum

ITC experiments were conducted, titrating wild type CELF1 from the syringe into a dilute solution of PARN in the cell. The syringe and cell concentrations were reduced to 125 μM and 12.5 μM respectively due to the limited solubility of both wild type CELF1 and PARN. Titration of CELF1 into PARN showed a pronounced endothermic curve, shown in Figure 8.15, similar to that seen for dissociation of a dimer, though it could not be fitted to a simple dissociation model. Control experiments titrating CELF1 into buffer, and buffer into PARN showed no significant enthalpy change in either case, confirming that the curve seen was from direct interaction of the two proteins rather than simply the effect of diluting either protein.

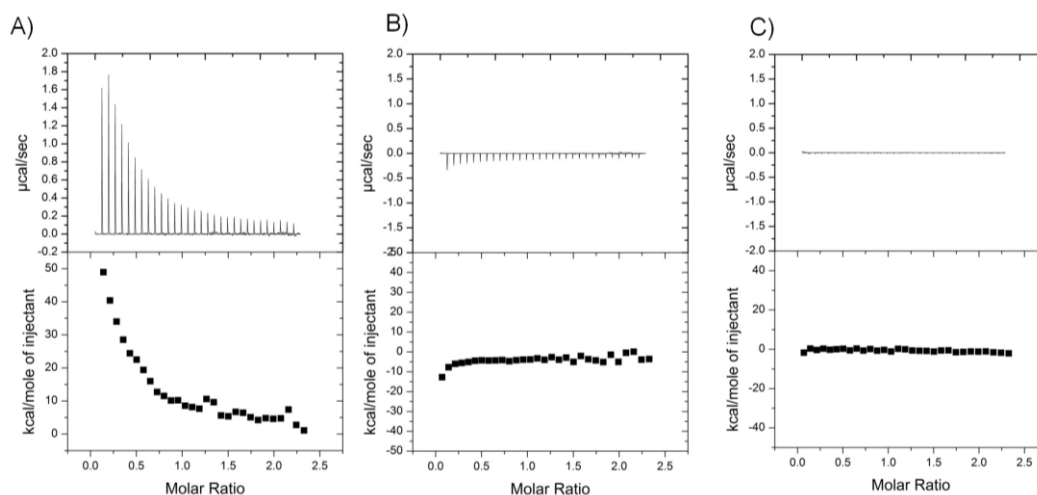


Figure 8.15: ITC traces collected for: A) Titration of 125 μM wild type CELF1 into 12.5 μM PARN. B) Control titration of 125 μM CELF1 into buffer. C) Control titration of buffer into 12.5 μM PARN. No satisfactory fit to the CELF1/PARN binding curve could be achieved using any of the binding models in Origin 7.0.

The curve suggests an entropically driven process, and could perhaps be due to the dissociation of the PARN dimer when binding to CELF1. Repeating the ITC experiment with the RRM123 construct showed no significant interaction, consistent with the requirement of some part of the linker between RRM2 and RRM3 of CELF1. It can also be concluded that the sequence recognised by PARN is not in the 188 – 214 or >385 regions which are retained in the RRM123 construct. A series of constructs incorporating different sections of the RRM2 – RRM3 linker could be used to narrow down the region involved in the interaction with PARN.

8.8 Conclusions

We have shown that despite its size at 72.8 kDa, and existence in solution as a 146 kDa homodimer, poly(A) ribonuclease can be investigated by NMR. Peaks from at least the RRM and R3H domains are clearly resolvable in the ^{15}N TROSY spectrum of the wild type protein. The interaction with CELF1 can therefore be investigated using this technique. The preliminary data collected on the isolated RRM does however show that the domains are not functioning independently.

The approach of studying each domain in isolation which proved effective for CELF1 may not be as successful for PARN.

The initial NMR and ITC data does support the hypothesis of a direct interaction between these two proteins. This interaction appears to be mediated by some part of the flexible section between RRM2 and 3 (the “divergent domain”) of CELF1. It is less clear which regions of PARN form the binding interface, though the NMR spectra do suggest that the RRM and/or the R3H domains are involved. The lack of interaction with the RRM123 construct seen by ITC shows that residues 188 – 214 of CELF1 do not include a binding site for PARN. The section of the CELF1 RRM2 – RRM3 linker recognised by PARN could be identified by producing a series of CELF1 constructs containing only a short section of this linker, and observing by ITC and NMR whether an interaction occurred with each one. Since the interaction with the EDEN motif and PARN appear to be mediated by completely separate regions of CELF1, this preliminary data is consistent with the formation of a ternary complex, and hence CELF1 triggering deadenylation by recruitment of PARN to the target mRNA.

9 Conclusions

Our first aim was to determine the minimum RNA sequence that would permit binding by each of the isolated domains. Using NMR and ITC we showed that RRM1 can bind to the three nucleotide RNA substrate UGU with a K_d of around 60 μM . This indicates only a slightly lower binding affinity than Teplova *et al.* later observed for a UUGUU substrate. The CSP map also showed little difference in the set of affected residues between the UGU and UGUUUGU substrates. From this it could be concluded that a UGU site is sufficient for RRM1 to bind, with the addition of a fourth nucleotide providing only a slight increase in binding affinity. This was corroborated by the observation that RRM1 will form a 2:1 complex with the UGUUUGU substrate, which was detected by ESI-MS. In contrast RRM2 showed a significantly smaller RNA binding patch in the CSP map when binding to a UGU substrate compared to UGUUUGU. It was also unable to form a 2:1 complex with the UGUUUGU substrate, unlike RRM1. We could therefore conclude that RRM2 requires a fourth nucleotide for high affinity binding, and hence needs a UGU(U/G) site.

For the lower affinity substrates RRM1 still showed significant CSPs on titration with a CUG repeat RNA, but not with an ARE. It was therefore concluded to be capable of recognising either a UGU or UGC site. RRM2 showed very limited interactions with a CUG substrate, but significant CSPs were seen on titration with an ARE. This suggests that the domain can tolerate a UAU(U/G) site as well as a UGU(U/G) site. Together these observations can account for the overall binding preferences seen for CELF1. Both can recognise sites in a UGU(U/G) repeating sequence, resulting in a high affinity complex. For CUG and ARE substrates only one of the two domains has a high affinity site, resulting in a low affinity interaction for the overall complex.

Our second aim was to determine the sequence requirements for tandem binding of the two N-terminal domains of CELF1. We demonstrated by NMR and ITC that for a sequence of the form UGU(U)_x(UGU) spacer lengths of $x = 2 - 4$ are optimal for tandem binding. ITC shows a substantial enhancement of the binding affinity from $\sim 60 \mu\text{M}$ to $\sim 0.4 \mu\text{M}$ when the domains can bind in tandem. $x = 1$ does not permit binding of both domains simultaneously, and in this situation RRM1 is bound preferentially. The upper limit was not as sharply defined, with spacer lengths of 5 nucleotides or more showing a reduction in binding affinity with K_d values of $\sim 3 \mu\text{M}$. This indicates the interaction is still of significantly higher affinity than for the domains binding in isolation, and the bound NMR spectrum for $x = 5$ matched that of the 2 – 4 nucleotide spacers. CSP maps did however show reduced perturbations in RRM2 for $x = 6$ and 7. We demonstrated that the EDEN11 GRE and EDEN15 consensus sequences will bind the N-terminal domains of CELF1 in tandem, to two of the UGU sites which are separated by 5 nucleotides.

An extended CUG repeat substrate still showed little interaction with RRM2 by NMR. An extended ARE however showed significant CSPs in both domains, unlike the isolated RRM1 construct, suggesting some enhancement of affinity when the domains bind in tandem to ARE substrates as well. RRM3 has been previously reported to have only very weak interactions with CUGCUG repeats. It can be concluded that any interaction of wild type CELF1 with single stranded CUG repeat RNA will be of very low affinity, and will be outcompeted by the preferred U/G rich sequences. We also confirmed that there is no RRM1 or RRM2 equivalent of the RRM3 N-terminal involvement in RNA binding. ¹⁵N heteronuclear NOE experiments showed that the RRM1 N-terminus and the interdomain linker between RRM1 and RRM2 remain dynamic even when both domains are bound to RNA. A construct with 50 additional residues at the C-terminus of RRM2 also showed no differences in RNA binding properties to the t187 construct. This confirms that the isolated domain and t187 constructs are not omitting any functional extensions of these domains, and so should behave in the same manner as in wild type CELF1.

Our third aim was to characterise the full EDEN motif capable of binding all three domains of CELF1 simultaneously. We were able to devise a purification to produce small amounts (~ 1-2 mg/l) of wild type CELF1, but the protein's poor solubility and vulnerability to proteolysis severely limited the data that could be collected using it. We therefore produced the RRM123 construct, in which residues 215 - 384 of CELF1 have been deleted, which was found to be stable, soluble, and allowed the acquisition of high quality NMR spectra. Using this construct we demonstrated that the EDEN11 GRE proposed as an EDEN motif by Vlasova *et al.* is not in fact capable of binding all three domains simultaneously. It can be concluded that neither the EDEN11 GRE, or the 11 nucleotide UG repeat proposed by Rattenbacher *et al.* represent complete EDEN motifs. The EDEN15 sequence proposed by Graindorge *et al.* did appear to permit the formation of a 1:1 complex with all three domains bound and so probably is a functional EDEN motif, but the affinity was not significantly enhanced compared to binding of just the N-terminal domains. It was therefore concluded that the while the spacing in this sequence can be tolerated by CELF1, it is not optimal.

We designed the sequence EDEN-2U/4U (UGUUUUGUUUUUGU) which formed the highest affinity 1:1 complex so far observed, with a K_d of 110 nM. We concluded that sequences of the form UGU(U) x UGU(U) y UGU, with $x = 2 - 5$ and $y = 1 - 4$ permitted a 1:1 complex with all three domains of CELF1 bound simultaneously, and therefore represented functional EDEN motifs. The shortest sequence for which formation of a 1:1 complex was observed was EDEN-2U/1U (UGUUUGUUUGU), though more than a 10-fold reduction in binding affinity was seen compared to EDEN-2U/4U. This is the minimum sequence capable of binding all three RRMs simultaneously. We also demonstrated that secondary structure in the RNA substrate can play an important role in forming a high affinity target for CELF1. The sequence EDEN-2U/HL still formed a 1:1 complex with comparable affinity to the EDEN15 sequence despite the 14 nucleotide spacer between two of the UGU sites. This was because the spacer was

capable of forming an RNA hairpin, which was confirmed to be present by NMR, bringing the UGU sites into close proximity and making the binding of CELF1 more favourable.

The fourth aim was to rationalise those RNA sequences which have been empirically demonstrated to be EDEN motifs by their ability to trigger deadenylation. All of the sequences shown to be EDEN motifs by Moraes *et al.*, Vlasova *et al.* and Rattenbacher *et al.* contain at least one set of UGU sites complying with our criteria for the formation of a 1:1 complex except TNF α and c-jun. Both of these sequences are however predicted to contain secondary structure which will bring distant UGU sites into close proximity, which can therefore account for CELF1 binding. Interestingly in the TNF α case this is due to the formation of a hairpin from the repeating AUUUA region of the RNA, which may account for the observation that this motif increases deadenylation efficiency when present.

The fifth aim was to characterise the structure of the high affinity 1:1 complex between CELF1 and an EDEN motif. We were however unable to produce an NMR or crystal structure of the complex. A substantial loss in NMR spectrum quality was seen when all three domains bound simultaneously to a single RNA molecule, which prevented acquisition of sufficient quality NOE restraints and RDC data to determine a structure. Attempts to co-crystallise the protein and RNA were unsuccessful preventing determination of the structure by x-ray crystallography. We were however able to produce a model of the complex based on the existing crystal structures of the isolated domains, supplemented by PRE and SAXS data. The PRE data showed a significant preference for arranging the domains in the order 2 – 1 – 3 from the 5' to 3' end of the RNA sequence. Kratky plots suggest the complex is slightly more globular than the unbound RRM123 protein. This may indicate a loss of internal dynamics in the protein, which could account for the reduction in the quality of the NMR spectra.

The sixth aim was to investigate whether phosphorylation at Ser28 could act as a “switch” changing CELF1’s preferred RNA target from U/G rich elements to C/G rich sequences. We produced and expressed phosphomimetic S28D mutants of all of our constructs of CELF1 which contained this residue. The disruption to the fold of the domain appeared very limited, with only six residues in α -helix 1 showing large CSPs when compared to the wild type. No significant difference in binding affinity was seen for U/G rich sequences between the wild type and the S28D mutant. No enhancement of binding affinity was seen for the S28D mutant when binding to a CUG repeat sequence. It is possible that recognition of some element other than the CG sites of the cyclin D1 RNA reported by Salisbury *et al.* is being enhanced, but we found no evidence to support this idea of a phosphorylation switch.

Our final aim was to determine whether it was possible to acquire high resolution NMR data on poly(A) ribonuclease, and its key regulatory complex with CELF1 reported by Moraes *et al.* We expressed and purified the full 631 residue poly (A) ribonuclease, though the protein was found to be prone to proteolysis of the unstructured C-terminal region. We were able to acquire the first ^{15}N TROSY spectrum of the complete protein (a 146 kDa dimer). Around 140 dispersed peaks could be clearly resolved which are believed to be from the smaller RRM and R3H domains, with the signals from the larger nuclease domain being lost due to rapid relaxation. This demonstrates that NMR can be used to study the behaviour of these domains even as part of the full length protein.

We observed significant CSPs for some of the well dispersed peaks in the PARN spectrum on addition of unlabelled wild type CELF1, confirming a direct interaction between these two proteins. This interaction is likely to involve the RRM and/or the R3H domains of PARN. Reversing the labels showed no CSPs in the three RRMs of wild type CELF1 on addition of unlabelled PARN, but did

appear to show some disruption to the poorly dispersed signals from the long linker between RRM2 and RRM3. If PARN is interacting with this region of CELF1 it is unlikely to interfere with the normal binding of CELF1's RRMs to the EDEN motif. This is consistent with CELF1 binding to both the EDEN motif and PARN simultaneously, and so the mechanism of CELF1 recruiting PARN to its mRNA targets in order to trigger deadenylation.

9.1 Future Work

The structure of the high affinity complex between CELF1 and an EDEN motif could be refined by additional paramagnetic relaxation enhancement experiments. If several titrations were conducted with the spin label placed at a different position in each one (such as at the 3' end of the RNA and either side of the central UGU site) a far greater number of distance restraints could be generated and a more accurate model could be produced.

Control experiments with the wild type CELF1 have shown no appreciable difference between its RNA binding preferences and those of the RRM123 construct. A further control experiment could be to replace the RRM2 to RRM3 linker with a more stable sequence of comparable length. This "dummy" linker would allow the same freedom of movement of the RRMs relative to each other, while bypassing the stability and solubility issues which have hindered the collection of data on the wild type protein. In particular it would allow SAXS data to be collected, which the low solubility of the wild type protein prevented. A longer linker between RRM2 and RRM3 would be expected to be more visible in the envelope, making the orientation of the protein domains much clearer.

While the S28D phosphomimetic mutant did not show any change in the binding preferences for U/G rich sequences and CUG repeats, there remains the possibility of increased affinity for some other motif present in the cyclin D1

mRNA. Systematic NMR titrations of CELF1 with short sections of the cyclin D1 RNA could locate any elements other than the single UGC site that are being recognised. Even if Ser28 proves not to have any important role in the function of CELF1, there are a number of other possible phosphorylation sites to be investigated. Most of these are within the unstructured RRM2 – RRM3 linker, and so could have a role in regulating the interaction with poly(A) ribonuclease. Phosphomimetic mutations could be produced at these sites, and any impact on the binding of PARN observed by ITC and NMR.

The exact region of CELF1 recognised by PARN could be determined by systematically testing short sections of the RRM2 – RRM3 linker for binding using NMR and ITC. These could either be isolated peptide sequences, or as deletion constructs of CELF1 produced by the same methods as RRM123. Locating the binding surface of PARN is more difficult due to the interaction between the domains. It might be possible to collect 3D heteronuclear NMR spectra of sufficient quality to assign the dispersed peaks in the ¹⁵N TROSY of the full length protein, and so determine the exact residues involved. An alternative approach would be to investigate whether in combination the PARN RRM and R3H domains can interact with CELF1. A construct with these domains, but not the large nuclease domain, would be expected to result in a substantial improvement in the NMR spectrum quality, and so the ease of assigning the spectrum.

The ability of CELF1 to bridge the end of an RNA hairpin, demonstrated using the RNA substrate EDEN-2U/HL presents a possible mechanism for its function as an alternative splicing regulator. By binding RRM1 and RRM2 in tandem to a partial EDEN motif on one side of an exon, and binding RRM3 to a UGU(U/G) site on the other side, it could encourage skipping of the exon. This is consistent with recently published results by Masuda *et al.* (2012), which reported that CELF1 binding sites are concentrated in intronic regions flanking alternative exons. In their study they were however treating the sequence UGUUUGU as a

CELF1 binding site, which we have shown in this thesis to be incapable of binding multiple CELF1 domains simultaneously. CELF1 would therefore need multiple copies of this RNA sequence for high affinity binding, which could be located on either side of the exon.

CELF1 presents a possible drug target, as if its “gain of function” in DM1 cells could be reversed then normal alternative splicing patterns should be restored and the DM1 phenotype mitigated. The recent publication by Masuda *et al.* (2012) also suggests that one of the mRNAs bound by CELF1, and hence translationally repressed, is the MBNL1 mRNA. Down-regulation of CELF1 should therefore result in upregulation of MBNL1, counterbalancing its sequestration by CUG repeat RNAs in DM1 cells. With the understanding of requirements for high affinity binding of CELF1 gained in this study it may be possible to design a ligand capable of binding with higher affinity than the natural substrates, and so sequestering CELF1. This would involve further studies to produce high affinity ligands, working from templates such as EDEN-2U/4U and possibly incorporating modified RNA bases.

10 References

1. Wu, J.; Li, C.; Zhao, S.; Mao, B., Differential expression of the Bruno/CELF family genes during *Xenopus laevis* early development. *International Journal of Developmental Biology* **2010**, *54* (1), 209-214.
2. Delaunay, J.; Mee, G.; Ezzeddine, N.; Labesse, G.; Terzian, C.; Capri, M.; Ait-Ahmed, O., The *Drosophila* Bruno paralogue Bru-3 specifically binds the EDEN translational repression element. *Nucleic Acids Research* **2004**, *32* (10), 3070-3082.
3. Chen, Q.; Herring, D.; Good, P., The role of the Bruno family of RNA-binding proteins in nervous system and muscle development. *Molecular Biology of the Cell* **1997**, *8*, 2064-2064.
4. Good, P.; Chen, Q.; Warner, S.; Herring, D., A family of human RNA-binding proteins related to the *Drosophila* Bruno translational regulator. *Journal of Biological Chemistry* **2000**, *275* (37), 28583-28592.
5. Barreau, C.; Paillard, L.; Méreau, A.; Osborne, H. B., Mammalian CELF/Bruno-like RNA-binding proteins: molecular characteristics and biological functions. *Biochimie* **2006**, *88* (5), 515-25.
6. Timchenko, L.; Timchenko, N.; Caskey, C.; Roberts, R., Novel proteins which bind CTG and CUG repeat sequences. *American Journal of Human Genetics* **1995**, *57* (4), 862-862.
7. Miller, J.; Swanson, M.; Timchenko, N.; Devore, D.; Lin, L.; Datar, K.; Roberts, R.; Caskey, C.; Timchenko, L., Identification of a CUG triplet repeat RNA-binding protein and its role in myotonic dystrophy. *Molecular Biology of the Cell* **1996**, *7*, 1755-1755.
8. Mankodi, A.; Takahashi, M.; Jiang, H.; Beck, C.; Bowers, W.; Moxley, R.; Cannon, S.; Thornton, C., Expanded CUG repeats trigger aberrant splicing of CIC-1 chloride channel pre-mRNA and hyperexcitability of skeletal muscle in myotonic dystrophy. *Molecular Cell* **2002**, *10* (1), 35-44.

9. Ho, T.; Bundman, D.; Armstrong, D.; Cooper, T., Transgenic mice expressing CUG-BP1 reproduce splicing mis-regulation observed in myotonic dystrophy. *Human Molecular Genetics* **2005**, *14* (11), 1539-1547.
10. Suzuki, H.; Jin, Y.; Otani, H.; Yasuda, K.; Inoue, K., Regulation of alternative splicing of alpha-actinin transcript by Bruno-like proteins. *Genes To Cells* **2002**, *7* (2), 133-141.
11. Roberts, R.; Timchenko, N.; Miller, J.; Reddy, S.; Caskey, C.; Swanson, M.; Timchenko, L., Altered phosphorylation and intracellular distribution of a (CUG)(n) triplet repeat RNA binding protein in patients with myotonic dystrophy and in myotonin protein kinase knockout mice. *Proceedings of the National Academy of Sciences of the United States of America* **1997**, *94* (24), 13221-13226.
12. Paillard, L.; Omilli, F.; Legagneux, V.; Bassez, T.; Maniey, D.; Osborne, H., EDEN and EDEN-BP, a cis element and an associated factor that mediate sequence-specific mRNA deadenylation in *Xenopus* embryos. *EMBO Journal* **1998**, *17* (1), 278-287.
13. Moraes, K.; Wilusz, C.; Wilusz, J., CUG-BP and 3'UTR sequences influence PARN-mediated deadenylation in mammalian cell extracts. *Genetics and Molecular Biology* **2007**, *30* (3), 646-655.
14. Goldstrohm, A.; Wickens, M., Multifunctional deadenylase complexes diversify mRNA control. *Nature Reviews Molecular Cell Biology* **2008**, *9* (4), 337-344.
15. Cooke, A.; Prigge, A.; Wickens, M., Translational Repression by Deadenylases. *Journal of Biological Chemistry* **2010**, *285* (37), 28506-28513.
16. Lu, P.; Vogel, C.; Wang, R.; Yao, X.; Marcotte, E., Absolute protein expression profiling estimates the relative contributions of transcriptional and translational regulation. *Nature Biotechnology* **2007**, *25* (1), 117-124.
17. Garneau, N.; Wilusz, J.; Wilusz, C., The highways and byways of mRNA decay. *Nature Reviews Molecular Cell Biology* **2007**, *8* (2), 113-126.
18. Cao, D.; Parker, R., Computational modeling of eukaryotic mRNA turnover. *Rna-a Publication of the RNA Society* **2001**, *7* (9), 1192-1212.

19. Parker, R.; Song, H., The enzymes and control of eukaryotic mRNA turnover. *Nature Structural & Molecular Biology* **2004**, *11* (2), 121-127.
20. Kapp, L.; Lorsch, J., The molecular mechanics of eukaryotic translation. *Annual Review of Biochemistry* **2004**, *73*, 657-704.
21. Ezzeddine, N.; Paillard, L.; Capri, M.; Maniey, D.; Bassez, T.; Ait-Ahmed, O.; Osborne, H., EDEN-dependent translational repression of maternal mRNAs is conserved between *Xenopus* and *Drosophila*. *Proceedings of the National Academy of Sciences of the United States of America* **2002**, *99* (1), 257-262.
22. Paillard, L.; Legagneux, V.; Maniey, D.; Osborne, H. B., c-Jun ARE targets mRNA deadenylation by an EDEN-BP (embryo deadenylation element-binding protein)-dependent pathway. *J Biol Chem* **2002**, *277* (5), 3232-5.
23. Paillard, L.; Legagneux, V.; Beverley Osborne, H., A functional deadenylation assay identifies human CUG-BP as a deadenylation factor. *Biol Cell* **2003**, *95* (2), 107-13.
24. Caskey, C.; Swanson, M.; Timchenko, L., Myotonic dystrophy: Discussion of molecular mechanism. *Cold Spring Harbor Symposia on Quantitative Biology* **1996**, *61*, 607-614.
25. Timchenko, L. T.; Miller, J. W.; Timchenko, N. A.; Devore, D. R.; Datar, K. V.; Lin, L.; Roberts, R.; Caskey, C. T.; Swanson, M. S., Identification of a (CUG)_n triplet repeat RNA-binding protein and its expression in myotonic dystrophy. *Nucleic Acids Res* **1996**, *24* (22), 4407-14.
26. Timchenko, L.; Timchenko, N.; Caskey, C.; Roberts, R., Novel proteins with binding specificity for DNA CTG repeats and RNA CUG repeats: Implications for myotonic dystrophy. *Human Molecular Genetics* **1996**, *5* (1), 115-121.
27. Philips, A. V.; Timchenko, L. T.; Cooper, T. A., Disruption of splicing regulated by a CUG-binding protein in myotonic dystrophy. *Science* **1998**, *280* (5364), 737-41.
28. Takahashi, N.; Sasagawa, N.; Suzuki, K.; Ishiura, S., The CUG-binding protein binds specifically to UG dinucleotide repeats in a yeast three-hybrid system. *Biochemical and Biophysical Research Communications* **2000**, *277* (2), 518-523.

29. Mori, D.; Sasagawa, N.; Kino, Y.; Ishiura, S., Quantitative analysis of CUG-BP1 binding to RNA repeats. *J Biochem* **2008**, *143* (3), 377-83.
30. Maruyama, K.; Sato, N.; Ohta, N., Conservation of structure and cold-regulation of RNA-binding proteins in cyanobacteria: probable convergent evolution with eukaryotic glycine-rich RNA-binding proteins. *Nucleic Acids Research* **1999**, *27* (9), 2029-2036.
31. Maris, C.; Dominguez, C.; Allain, F., The RNA recognition motif, a plastic RNA-binding platform to regulate post-transcriptional gene expression. *FEBS Journal* **2005**, *272* (9), 2118-2131.
32. Venter, J.; Adams, M.; Myers, E.; *et al.*, The sequence of the human genome. *Science* **2001**, *291* (5507), 1304-+.
33. Calero, G.; Wilson, K.; Ly, T.; Rios-Steiner, J.; Clardy, J.; Cerione, R., Structural basis of m(7)GpppG binding to the nuclear cap-binding protein complex. *Nature Structural Biology* **2002**, *9* (12), 912-917.
34. Mazza, C.; Segref, A.; Mattaj, I.; Cusack, S., Large-scale induced fit recognition of an m(7)GpppG cap analogue by the human nuclear cap-binding complex. *EMBO Journal* **2002**, *21* (20), 5548-5557.
35. Allain, F.; Bouvet, P.; Dieckmann, T.; Feigon, J., Molecular basis of sequence-specific recognition of pre-ribosomal RNA by nucleolin. *EMBO Journal* **2000**, *19* (24), 6870-6881.
36. Price, S.; Evens, P.; Nagai, K., Crystal structure of the spliceosomal U2B'-U2A' protein complex bound to a fragment of U2 small nuclear RNA. *Nature* **1998**, *394* (6694), 645-650.
37. Wang, X.; Hall, T., Structural basis for recognition of AU-rich element RNA by the HuD protein. *Nature Structural Biology* **2001**, *8* (2), 141-145.
38. Handa, N.; Nureki, O.; Kurimoto, K.; Kim, I.; Sakamoto, H.; Shimura, Y.; Muto, Y.; Yokoyama, S., Structural basis for recognition of the tra mRNA precursor by the sex-lethal protein. *Nature* **1999**, *398* (6728), 579-585.

39. Adam, S.; Nakagawa, T.; Swanson, M.; Woodruff, T.; Dreyfuss, G., Messenger-RNA polyadenylate-binding protein - gene isolation and sequencing and identification of a ribonucleoprotein consensus sequence. *Molecular and Cellular Biology* **1986**, *6* (8), 2932-2943.
40. Swanson, M.; Nakagawa, T.; Levan, K.; Dreyfuss, G., Primary structure of human nuclear ribonucleoprotein particle C-proteins - conservation of sequence and domain-structures in heterogeneous nuclear-RNA, messenger-RNA, and pre-ribosomal-RNA-binding proteins. *Molecular and Cellular Biology* **1987**, *7* (5), 1731-1739.
41. Allain, F.; Gubser, C.; Howe, P.; Nagai, K.; Neuhaus, D.; Varani, G., Specificity of ribonucleoprotein interaction determined by RNA folding during complex formation. *Nature* **1996**, *380* (6575), 646-650.
42. Oubridge, C.; Ito, N.; Evans, P.; Teo, C.; Nagai, K., Crystal-structure at 1.92 angstrom resolution of the RNA-binding domain of the U1A spliceosomal protein complexed with an RNA hairpin. *Nature* **1994**, *372* (6505), 432-438.
43. Clery, A.; Blatter, M.; Allain, F., RNA recognition motifs: boring? Not quite. *Current Opinion in Structural Biology* **2008**, *18* (3), 290-298.
44. Ding, J.; Hayashi, M.; Zhang, Y.; Manche, L.; Krainer, A.; Xu, R., Crystal structure of the two-RRM domain of hnRNP A1 (UP1) complexed with single-stranded telomeric DNA. *Genes & Development* **1999**, *13* (9), 1102-1115.
45. Crichlow, G.; Zhou, H.; Hsiao, H.; Frederick, K.; Debrosse, M.; Yang, Y.; Foltas-Stogniew, E.; Chung, H.; Fan, C.; De La Cruz, E.; Levens, D.; Lolis, E.; Braddock, D., Dimerization of FIR upon FUSE DNA binding suggests a mechanism of c-myc inhibition. *EMBO Journal* **2008**, *27* (1), 277-289.
46. Birney, E.; Kumar, S.; Krainer, A., Analysis of the RNA-recognition motif and RS and RGG domains - conservation in metazoan pre-messenger-RNA splicing factors. *Nucleic Acids Research* **1993**, *21* (25), 5803-5816.
47. Kenan, D.; Query, C.; Keene, J., RNA recognition - towards identifying determinants of specificity. *Trends in Biochemical Sciences* **1991**, *16* (6), 214-220.

48. Jun, K. Y.; Xia, Y.; Han, X.; Zhang, H.; Timchenko, L.; Swanson, M. S.; Gao, X., (1)H, (15)N and (13)C chemical shift assignments of RNA repeats binding protein -- CUGBP1ab. *J Biomol NMR* **2004**, *30* (3), 371-2.
49. Tsuda, K.; Kuwasako, K.; Takahashi, M.; Someya, T.; Inoue, M.; Terada, T.; Kobayashi, N.; Shirouzu, M.; Kigawa, T.; Tanaka, A.; Sugano, S.; Güntert, P.; Muto, Y.; Yokoyama, S., Structural basis for the sequence-specific RNA-recognition mechanism of human CUG-BP1 RRM3. *Nucleic Acids Res* **2009**, *37* (15), 5151-66.
50. Koradi, R.; Billeter, M.; Wuthrich, K., MOLMOL: A program for display and analysis of macromolecular structures. *Journal of Molecular Graphics* **1996**, *14* (1), 51-&.
51. Teplova, M.; Song, J.; Gaw, H.; Teplov, A.; Patel, D., Structural Insights into RNA Recognition by the Alternate-Splicing Regulator CUG-Binding Protein 1. *Structure* **2010**, *18* (10), 1364-1377.
52. Lu, X.; Timchenko, N.; Timchenko, L., Cardiac elav-type RNA-binding protein (ETR-3) binds to RNA CUG repeats expanded in myotonic dystrophy. *Human Molecular Genetics* **1999**, *8* (1), 53-60.
53. Audic, Y.; Omilli, F.; Osborne, H., Embryo deadenylation element-dependent deadenylation is enhanced by a cis element containing AUU repeats. *Molecular and Cellular Biology* **1998**, *18* (12), 6879-6884.
54. Bonnet-Corven, S.; Audic, Y.; Omilli, F.; Osborne, H., An analysis of the sequence requirements of EDEN-BP for specific RNA binding. *Nucleic Acids Research* **2002**, *30* (21), 4667-4674.
55. Marquis, J.; Paillard, L.; Audic, Y.; Cosson, B.; Danos, O.; Le Bec, C.; Osborne, H., CUG-BP1/CELF1 requires UGU-rich sequences for high-affinity binding. *Biochemical Journal* **2006**, *400*, 291-301.
56. Moraes, K. C.; Wilusz, C. J.; Wilusz, J., CUG-BP binds to RNA substrates and recruits PARN deadenylase. *RNA* **2006**, *12* (6), 1084-91.

57. Graindorge, A.; Le Tonqueze, O.; Thuret, R.; Pollet, N.; Osborne, H.; Audic, Y., Identification of CUG-BP1/EDEN-BP target mRNAs in *Xenopus tropicalis*. *Nucleic Acids Research* **2008**, *36* (6), 1861-1870.
58. Vlasova, I.; Tahoe, N.; Fan, D.; Larsson, O.; Rattenbacher, B.; John, J.; Vasdewani, J.; Karypis, G.; Reilly, C.; Bitterman, P.; Bohjanen, P., Conserved GU-rich elements mediate mRNA decay by binding to CUG-binding protein 1. *Molecular Cell* **2008**, *29* (2), 263-270.
59. Vlasova, I.; Bohjanen, P., Posttranscriptional regulation of gene networks by GU-rich elements and CELF proteins. *RNA Biology* **2008**, *5* (4), 201-207.
60. Rattenbacher, B.; Beisang, D.; Wiesner, D. L.; Jeschke, J. C.; Von Hohenberg, M.; St Louis-Vlasova, I. A.; Bohjanen, P. R., Analysis of CUGBP1 targets identifies GU-repeat sequences that mediate rapid mRNA decay. *Mol Cell Biol* **2010**, *30* (16), 3970-80.
61. Harper, P., Myotonic Dystrophy. Third ed.; 2001.
62. Mankodi, A.; Jiang, C.; Takahashi, M.; Beck, C.; Moxley, R.; Cannon, S.; Thornton, C., RNA splicing defect leads to chloride channelopathy and myotonia in myotonic dystrophy (DM). *Neurology* **2002**, *58* (7), A168-A169.
63. Charlet-B, N.; Savkur, R.; Singh, G.; Philips, A.; Grice, E.; Cooper, T., Loss of the muscle-specific chloride channel in type 1 myotonic dystrophy due to misregulated alternative splicing. *Molecular Cell* **2002**, *10* (1), 45-53.
64. Timchenko, N.; Patel, R.; Iakova, P.; Cai, Z.; Quan, L.; Timchenko, L., Overexpression of CUG triplet repeat-binding protein, CUGBP1, in mice inhibits myogenesis. *Journal of Biological Chemistry* **2004**, *279* (13), 13129-13139.
65. Ward, A. J.; Rimer, M.; Killian, J. M.; Dowling, J. J.; Cooper, T. A., CUGBP1 overexpression in mouse skeletal muscle reproduces features of myotonic dystrophy type 1. *Human Molecular Genetics* **2010**, *19* (18), 3614-22.
66. Koshelev, M.; Sarma, S.; Price, R.; Wehrens, X.; Cooper, T., Heart-specific overexpression of CUGBP1 reproduces functional and molecular abnormalities of myotonic dystrophy type 1. *Human Molecular Genetics* **2010**, *19* (6), 1066-1075.

67. Ho, T. H.; Bundman, D.; Armstrong, D. L.; Cooper, T. A., Transgenic mice expressing CUG-BP1 reproduce splicing mis-regulation observed in myotonic dystrophy. *Human Molecular Genetics* **2005**, *14* (11), 1539-47.
68. Aslanidis, C.; Jansen, G.; Amemiya, C.; Shutler, G.; Mahadevan, M.; Tsilfidis, C.; Chen, C.; Alleman, J.; Wormskamp, N.; Vooijs, M.; Buxton, J.; Johnson, K.; Smeets, H.; Lennon, G.; Carrano, A.; Korneluk, R.; Wieringa, B.; Dejong, P., cloning of the essential myotonic-dystrophy region and mapping of the putative defect. *Nature* **1992**, *355* (6360), 548-551.
69. Brook, J.; Mccurrach, M.; Harley, H.; Buckler, A.; Church, D.; Aburatani, H.; Hunter, K.; Stanton, V.; Thirion, J.; Hudson, T.; Sohn, R.; Zemelman, B.; Snell, R.; Rundle, S.; Crow, S.; Davies, J.; Shelbourne, P.; Buxton, J.; Jones, C.; Juvonen, V.; Johnson, K.; Harper, P.; Shaw, D.; Housman, D., molecular-basis of myotonic-dystrophy - expansion of a trinucleotide (CTG) repeat at the 3' end of a transcript encoding a protein-kinase family member. *Cell* **1992**, *68* (4), 799-808.
70. Buxton, J.; Shelbourne, P.; Davies, J.; Jones, C.; Vantongeren, T.; Aslanidis, C.; Dejong, P.; Jansen, G.; Anvret, M.; Riley, B.; Williamson, R.; Johnson, K., Detection of an unstable fragment of DNA specific to individuals with myotonic-dystrophy. *Nature* **1992**, *355* (6360), 547-548.
71. Fu, Y.; Pizzuti, A.; Fenwick, R.; King, J.; Rajnarayan, S.; Dunne, P.; Dubel, J.; Nasser, G.; Ashizawa, T.; Dejong, P.; Wieringa, B.; Korneluk, R.; Perryman, M.; Epstein, H.; Caskey, C., An unstable triplet repeat in a gene related to myotonic muscular-dystrophy. *Science* **1992**, *255* (5049), 1256-1258.
72. Harley, H.; Brook, J.; Rundle, S.; Crow, S.; Reardon, W.; Buckler, A.; Harper, P.; Housman, D.; Shaw, D., Expansion of an unstable DNA region and phenotypic variation in myotonic-dystrophy. *Nature* **1992**, *355* (6360), 545-546.
73. Pizzuti, A.; Fu, Y.; Fenwick, R.; Rajanarayan, P.; Perryman, M.; Epstein, H.; Caskey, C., Identification of an unstable triplet repeat in the myotonic-dystrophy gene, a protein-kinase gene. *Neurology* **1992**, *42* (7), 1426-1426.

74. Groh, W.; Lowe, M.; Zipes, D., Severity of cardiac conduction involvement and arrhythmias in myotonic dystrophy type 1 correlates with age and CTG repeat length. *Journal of Cardiovascular Electrophysiology* **2002**, *13* (5), 444-448.
75. Tsilfidis, C.; Mackenzie, A.; Mettler, G.; Barcelo, J.; Korneluk, R., Correlation between CTG trinucleotide repeat length and frequency of severe congenital myotonic-dystrophy. *Nature Genetics* **1992**, *1* (3), 192-195.
76. Hunter, A.; Tsilfidis, C.; Mettler, G.; Jacob, P.; Mahadevan, M.; Surh, L.; Korneluk, R., The correlation of age of onset with CTG Trinucleotide repeat amplification in myotonic-dystrophy. *Journal of Medical Genetics* **1992**, *29* (11), 774-779.
77. Lavedan, C.; Hofmannradvanyi, H.; Shelbourne, P.; Rabes, J.; Duros, C.; Savoy, D.; Dehaupas, I.; Luce, S.; Johnson, K.; Junien, C., Myotonic-dystrophy - size-dependent and sex-dependent dynamics of CTG meiotic instability, and somatic mosaicism. *American Journal of Human Genetics* **1993**, *52* (5), 875-883.
78. Ricker, K.; Koch, M.; Lehmannhorn, F.; Pongratz, D.; Speich, N.; Reiners, K.; Schneider, C.; Moxley, R., Proximal myotonic myopathy - clinical-features of a multisystem disorder similar to myotonic-dystrophy. *Archives of Neurology* **1995**, *52* (1), 25-31.
79. Day, J.; Ricker, K.; Jacobsen, J.; Rasmussen, L.; Dick, K.; Kress, W.; Schneider, C.; Koch, M.; Beilman, G.; Harrison, A.; Dalton, J.; Ranum, L., Myotonic dystrophy type 2 - Molecular, diagnostic and clinical spectrum. *Neurology* **2003**, *60* (4), 657-664.
80. Taneja, K.; Mccurrach, M.; Schalling, M.; Housman, D.; Singer, R., Foci of trinucleotide repeat transcripts in nuclei of myotonic-dystrophy cells and tissues. *Journal of Cell Biology* **1995**, *128* (6), 995-1002.
81. Taneja, K., Localization of trinucleotide repeat sequences in myotonic dystrophy cells using a single fluorochrome-labeled PNA probe. *Biotechniques* **1998**, *24* (3), 472-476.
82. Hsu, R.; Hsiao, K.; Lin, M.; Li, C.; Wang, L.; Chen, L.; Pan, H., Long Tract of Untranslated CAG Repeats Is Deleterious in Transgenic Mice. *PLOS One* **2011**, *6* (1).

83. He, Y.; Vogelstein, B.; Velculescu, V.; Papadopoulos, N.; Kinzler, K., The Antisense Transcriptomes of Human Cells. *Science* **2008**, *322* (5909), 1855-1857.
84. Zu, T.; Gibbens, B.; Doty, N.; Gomes-Pereira, M.; Huguet, A.; Stone, M.; Margolis, J.; Peterson, M.; Markowski, T.; Ingram, M.; Nan, Z.; Forster, C.; Low, W.; Schoser, B.; Somia, N.; Clark, H.; Schmechel, S.; Bitterman, P.; Gourdon, G.; Swanson, M.; Moseley, M.; Ranum, L., Non-ATG-initiated translation directed by microsatellite expansions. *Proceedings of the National Academy of Sciences of the United States of America* **2011**, *108* (1), 260-265.
85. Michalik, A.; Van Broeckhoven, C., Pathogenesis of polyglutamine disorders: aggregation revisited. *Human Molecular Genetics* **2003**, *12*, R173-R186.
86. Oma, Y.; Kino, Y.; Sasagawa, N.; Ishiura, S., Comparative analysis of the cytotoxicity of homopolymeric amino acids. *Biochimica Et Biophysica Acta-Proteins and Proteomics* **2005**, *1748* (2), 174-179.
87. Tian, B.; White, R.; Xia, T.; Welle, S.; Turner, D.; Mathews, M.; Thornton, C., Expanded CUG repeat RNAs form hairpins that activate the double-stranded RNA-dependent protein kinase PKR. *RNA-A Publication of the RNA Society* **2000**, *6* (1), 79-87.
88. Mooers, B.; Logue, J.; Berglund, J., The structural basis of myotonic dystrophy from the crystal structure of CUG repeats. *Proceedings of the National Academy of Sciences of the United States of America* **2005**, *102* (46), 16626-16631.
89. Mankodi, A.; Urbinati, C.; Yuan, Q.; Moxley, R.; Sansone, V.; Krym, M.; Henderson, D.; Schalling, M.; Swanson, M.; Thornton, C., Muscleblind localizes to nuclear foci of aberrant RNA in myotonic dystrophy types 1 and 2. *Human Molecular Genetics* **2001**, *10* (19), 2165-2170.
90. Yuan, Y.; Compton, S.; Sobczak, K.; Stenberg, M.; Thornton, C.; Griffith, J.; Swanson, M., Muscleblind-like 1 interacts with RNA hairpins in splicing target and pathogenic RNAs. *Nucleic Acids Research* **2007**, *35* (16), 5474-5486.
91. Junghans, R. P., Dystrophia myotonia: why focus on foci? *European Journal of Human Genetics* **2009**, *17* (5), 543-53.

92. Michalowski, S.; Miller, J.; Urbinati, C.; Paliouras, M.; Swanson, M.; Griffith, J., Visualization of double-stranded RNAs from the myotonic dystrophy protein kinase gene and interactions with CUG-binding protein. *Nucleic Acids Research* **1999**, *27* (17), 3534-3542.
93. Timchenko, N.; Cai, Z.; Welm, A.; Reddy, S.; Ashizawa, T.; Timchenko, L., RNA CUG repeats sequester CUGBP1 and alter protein levels and activity of CUGBP1. *Journal of Biological Chemistry* **2001**, *276* (11), 7820-7826.
94. (a) Kuyumcu-Martinez, N. M.; Wang, G. S.; Cooper, T. A., Increased steady-state levels of CUGBP1 in myotonic dystrophy 1 are due to PKC-mediated hyperphosphorylation. *Mol Cell* **2007**, *28* (1), 68-78; (b) Wang, G.; Kuyumcu-Martinez, M.; Sarma, S.; Mathur, N.; Wehrens, X.; Cooper, T., PKC inhibition ameliorates the cardiac phenotype in a mouse model of myotonic dystrophy type 1. *Journal of Clinical Investigation* **2009**, *119* (12), 3797-3806.
95. Wheeler, T., Myotonic dystrophy: Therapeutic strategies for the future. *Neurotherapeutics* **2008**, *5* (4), 592-600.
96. Wheeler, T.; Sobczak, K.; Lueck, J.; Osborne, R.; Lin, X.; Dirksen, R.; Thornton, C., Reversal of Myotonia and Splicing Defects by Antisense Oligomers in a Transgenic Mouse Model of Myotonic Dystrophy Type 1 (DM1). *Neurology* **2009**, *72* (11), A489-A490.
97. Magana, J.; Cisneros, B., Perspectives on Gene Therapy in Myotonic Dystrophy Type 1. *Journal of Neuroscience Research* **2011**, *89* (3), 275-285.
98. Teplova, M.; Patel, D., Structural insights into RNA recognition by the alternative-splicing regulator muscleblind-like MBNL1. *Nature Structural & Molecular Biology* **2008**, *15* (12), 1343-1351.
99. Fu, Y.; Ramisetty, S.; Hussain, N.; Baranger, A., MBNL1-RNA Recognition: Contributions of MBNL1 Sequence and RNA Conformation. *ChemBiochem* **2012**, *13* (1), 112-119.

100. Goers, E.; Purcell, J.; Voelker, R.; Gates, D.; Berglund, J., MBNL1 binds GC motifs embedded in pyrimidines to regulate alternative splicing. *Nucleic Acids Research* **2010**, *38* (7), 2467-2484.
101. Kino, Y.; Mori, D.; Oma, Y.; Takeshita, Y.; Sasagawa, N.; Ishiura, S., Muscleblind protein, MBNL1/EXP, binds specifically to CHHG repeats. *Human Molecular Genetics* **2004**, *13* (5), 495-507.
102. Masuda, A.; Andersen, H.; Doktor, T.; Okamoto, T.; Ito, M.; Andresen, B.; Ohno, K., CUGBP1 and MBNL1 preferentially bind to 3' UTRs and facilitate mRNA decay. *Scientific Reports* **2012**, *2*.
103. Cosson, B.; Gautier-Courteille, C.; Maniey, D.; Ait-Ahmed, O.; Lesimple, M.; Osborne, H.; Paillard, L., Oligomerization of EDEN-BP is required for specific mRNA deadenylation and binding. *Biology of the Cell* **2006**, *98* (11), 653-665.
104. Roberts, R.; Timchenko, N.; Miller, J.; Reddy, S.; Swanson, M.; Timchenko, L., Results of knockout mouse suggest impaired phosphorylation of triplet CUG binding protein pivotal to pathogenesis of cardiac and skeletal muscle dysfunction. *Journal of the American College of Cardiology* **1998**, *31* (2), 422A-422A.
105. Kuyumcu-Martinez, N.; Wang, G.; Cooper, T., Increased steady-state in levels of CUGBP1 in myotonic dystrophy 1 are due to PKC-mediated hyperphosphorylation. *Molecular Cell* **2007**, *28* (1), 68-78.
106. Timchenko, L.; Salisbury, E.; Wang, G.; Nguyen, H.; Albrecht, J.; Hershey, J.; Timchenko, N., Age-specific CUGBP1-eIF2 complex increases translation of CCAAT/enhancer-binding protein beta in old liver. *Journal of Biological Chemistry* **2006**, *281* (43), 32806-32819.
107. Welm, A.; Mackey, S.; Timchenko, L.; Darlington, G.; Timchenko, N., Translational induction of liver-enriched transcriptional inhibitory protein during acute phase response leads to repression of CCAAT/enhancer binding protein alpha mRNA. *Journal of Biological Chemistry* **2000**, *275* (35), 27406-27413.
108. Timchenko, N.; Wang, G.; Timchenko, L., RNA CUG-binding protein 1 increases translation of 20-kDa isoform of CCAAT/enhancer-binding protein beta by interacting

with the alpha and beta subunits of eukaryotic initiation translation factor 2. *Journal of Biological Chemistry* **2005**, *280* (21), 20549-20557.

109. Salisbury, E.; Sakai, K.; Schoser, B.; Huichalaf, C.; Schneider-Gold, C.; Nguyen, H.; Wang, G.; Albrecht, J.; Timchenko, L., Ectopic expression of cyclin D3 corrects differentiation of DM1 myoblasts through activation of RNA CUG-binding protein, CUGBP1. *Experimental Cell Research* **2008**, *314* (11-12), 2266-2278.

110. Nilsson, P.; Virtanen, A., Expression and purification of recombinant poly (A)-specific ribonuclease (PARN). *International Journal of Biological Macromolecules* **2006**, *39* (1-3), 95-99.

111. Wu, M.; Nilsson, P.; Henriksson, N.; Niedzwiecka, A.; Lim, M.; Cheng, Z.; Kokkoris, K.; Virtanen, A.; Song, H., Structural Basis of m(7)GpppG Binding to Poly(A)-Specific Ribonuclease. *Structure* **2009**, *17* (2), 276-286.

112. Nagata, T.; Suzuki, S.; Endo, R.; Shirouzu, M.; Terada, T.; Inoue, M.; Kigawa, T.; Kobayashi, N.; Guntert, P.; Tanaka, A.; Hayashizaki, Y.; Muto, Y.; Yokoyama, S., The RRM domain of poly(A)-specific ribonuclease has a noncanonical binding site for mRNA cap analog recognition. *Nucleic Acids Research* **2008**, *36* (14), 4754-4767.

113. Bertini, I.; Luchinat, C.; Parigi, G., Moving the frontiers in solution and solid-state bioNMR. *Coordination Chemistry Reviews* **2011**, *255* (7-8), 649-663.

114. Banci, L.; Bertini, I.; Luchinat, C.; Mori, M., NMR in structural proteomics and beyond. *Progress in Nuclear Magnetic Resonance Spectroscopy* **2010**, *56* (3), 247-266.

115. Tzakos, A.; Grace, C.; Lukavsky, P.; Riek, R., NMR techniques for very large proteins and RNAs in solution. *Annual Review of Biophysics and Biomolecular Structure* **2006**, *35*, 319-342.

116. Riek, R.; Fiaux, J.; Bertelsen, E.; Horwich, A.; Wuthrich, K., Solution NMR techniques for large molecular and supramolecular structures. *Journal of the American Chemical Society* **2002**, *124* (41), 12144-12153.

117. Fiaux, J.; Bertelsen, E.; Horwich, A.; Wuthrich, K., NMR analysis of a 900K GroEL-GroES complex. *Nature* **2002**, *418* (6894), 207-211.

118. Tugarinov, V.; Muhandiram, R.; Ayed, A.; Kay, L., Four-dimensional NMR spectroscopy of a 723-residue protein: Chemical shift assignments and secondary structure of malate synthase G. *Journal of the American Chemical Society* **2002**, *124* (34), 10025-10035.
119. Cavanagh, J., Protein NMR Spectroscopy - Principles and Practice. 2006.
120. Pervushin, K., Impact of Transverse Relaxation Optimized Spectroscopy (TROSY) on NMR as a technique in structural biology. *Quarterly Reviews of Biophysics* **2000**, *33* (2), 161-197.
121. Pervushin, K.; Riek, R.; Wider, G.; Wuthrich, K., Attenuated T-2 relaxation by mutual cancellation of dipole-dipole coupling and chemical shift anisotropy indicates an avenue to NMR structures of very large biological macromolecules in solution. *Proceedings of the National Academy of Sciences of the United States of America* **1997**, *94* (23), 12366-12371.
122. Weigelt, J., Single scan, sensitivity- and gradient-enhanced TROSY for multidimensional NMR experiments. *Journal of the American Chemical Society* **1998**, *120* (41), 10778-10779.
123. Riek, R.; Pervushin, K.; Wuthrich, K., TROSY and CRINEPT: NMR with large molecular and supramolecular structures in solution. *Trends in Biochemical Sciences* **2000**, *25* (10), 462-468.
124. Wuthrich, K., NMR of Proteins and Nucleic Acids. 1986.
125. Marion, D.; Driscoll, P.; Kay, L.; Wingfield, P.; Bax, A.; Gronenborn, A.; Clore, G., Overcoming the overlap problem in the assignment of H-1-NMR Spectra of larger proteins by use of 3-dimensional heteronuclear H-1-N-15 Hartmann-Hahn multiple quantum coherence and nuclear overhauser multiple quantum coherence spectroscopy - application to interleukin-1-beta. *Biochemistry* **1989**, *28* (15), 6150-6156.
126. (a) Marion, D.; Kay, L.; Sparks, S.; Torchia, D.; Bax, A., 3-dimensional heteronuclear NMR of N-15-labeled proteins. *Journal of the American Chemical Society* **1989**, *111* (4), 1515-1517; (b) Wijmenga, S.; Hallenga, K.; Hilbers, C., A 3-dimensional

heteronuclear multiple-quantum coherence homonuclear Hartmann-Hahn experiment. *Journal of Magnetic Resonance* **1989**, *84* (3), 634-642.

127. Sattler, M.; Schleucher, J.; Griesinger, C., Heteronuclear multidimensional NMR experiments for the structure determination of proteins in solution employing pulsed field gradients. *Progress in Nuclear Magnetic Resonance Spectroscopy* **1999**, *34* (2), 93-158.

128. Wagner, G.; Thanabal, V.; Stockman, B.; Peng, J.; Nirmala, N.; Hyberts, S.; Goldberg, M.; Detlefsen, D.; Clubb, R.; Adler, M., NMR-studies of structure and dynamics of isotope enriched proteins. *Biopolymers* **1992**, *32* (4), 381-390.

129. Wittekind, M.; Mueller, L., HNCACB, a high-sensitivity 3D NMR experiment to correlate amide-proton and nitrogen resonances with the alpha-carbon and beta-carbon resonances in proteins. *Journal of Magnetic Resonance Series B* **1993**, *101* (2), 201-205.

130. Kay, L.; Ikura, M.; Tschudin, R.; Bax, A., 3-dimensional triple-resonance NMR-spectroscopy of isotopically enriched proteins. *Journal of Magnetic Resonance* **1990**, *89* (3), 496-514.

131. Salzmann, M.; Pervushin, K.; Wider, G.; Senn, H.; Wuthrich, K., [C-13]-constant-time [N-15,H-1]-TROSY-HNCA for sequential assignments of large proteins. *Journal of Biomolecular NMR* **1999**, *14* (1), 85-88.

132. Clubb, R.; Thanabal, V.; Wagner, G., A constant-time 3-dimensional triple-resonance pulse scheme to correlate intraresidue H-1(N), N-15, and C-13(') chemical-shifts in N-15-C-13-labeled proteins. *Journal of Magnetic Resonance* **1992**, *97* (1), 213-217.

133. Grzesiek, S.; Bax, A., Improved 3D Triple-resonance NMR Techniques applied to a 31-kDa protein. *Journal of Magnetic Resonance* **1992**, *96* (2), 432-440.

134. Loria, J.; Rance, M.; Palmer, A., Transverse-relaxation-optimized (TROSY) gradient-enhanced triple-resonance NMR spectroscopy. *Journal of Magnetic Resonance* **1999**, *141* (1), 180-184.

135. Salzmann, M.; Wider, G.; Pervushin, K.; Senn, H.; Wuthrich, K., TROSY-type triple-resonance experiments for sequential NMR assignments of large proteins. *Journal of the American Chemical Society* **1999**, *121* (4), 844-848.
136. Grzesiek, S.; Bax, A., An efficient experiment for sequential backbone assignment of medium-sized isotopically enriched proteins. *Journal of Magnetic Resonance* **1992**, *99* (1), 201-207.
137. Vranken, W.; Boucher, W.; Stevens, T.; Fogh, R.; Pajon, A.; Llinas, P.; Ulrich, E.; Markley, J.; Ionides, J.; Laue, E., The CCPN data model for NMR spectroscopy: Development of a software pipeline. *Proteins-Structure Function and Bioinformatics* **2005**, *59* (4), 687-696.
138. Kay, L.; Xu, G.; Singer, A.; Muhandiram, D.; Formankay, J., A gradient-enhanced HCCH TOCSY experiment for recording side-chain H-1 and C-13 correlations in H₂O samples of proteins. *Journal of Magnetic Resonance Series B* **1993**, *101* (3), 333-337.
139. Shuker, S.; Hajduk, P.; Meadows, R.; Fesik, S., Discovering high-affinity ligands for proteins: SAR by NMR. *Science* **1996**, *274* (5292), 1531-1534.
140. Doyle, M., Characterization of binding interactions by isothermal titration calorimetry. *Current Opinion in Biotechnology* **1997**, *8* (1), 31-35.
141. Velaquez-Campoy, A.; Leavitt, S. A.; Freire, E., Characterization of protein-protein interactions by isothermal titration calorimetry. *Methods in molecular biology*: 2004; Vol. 261, pp 35-54.
142. Feig, A., Studying RNA-RNA and RNA-protein interactions by isothermal titration calorimetry. *Methods in Enzymology, Vol 468: Biophysical, Chemical, and Functional Probes of RNA Structure, Interactions and Folding, Pt a* **2009**, *468*, 409-422.
143. Salim, N.; Feig, A., Isothermal titration calorimetry of RNA. *Methods* **2009**, *47* (3), 198-205.
144. Freyer, M.; Lewis, E.; Correia, J.; Detrich, H., Isothermal titration calorimetry: Experimental design, data analysis, and probing Macromolecule/Ligand binding and

kinetic interactions. *Biophysical Tools For Biologists: Vol 1 in Vitro Techniques* **2008**, *84*, 79-113.

145. Ladbury, J.; Chowdhry, B., Sensing the heat: The application of isothermal titration calorimetry to thermodynamic studies of biomolecular interactions. *Chemistry & Biology* **1996**, *3* (10), 791-801.

146. Falconer, R.; Penkova, A.; Jelesarov, I.; Collins, B., Survey of the year 2008: applications of isothermal titration calorimetry. *Journal of Molecular Recognition* **2010**, *23* (5), 395-413.

147. Turnbull, W.; Daranas, A., On the value of c: Can low affinity systems be studied by isothermal titration calorimetry? *Journal of the American Chemical Society* **2003**, *125* (48), 14859-14866.

148. Cliff, M.; Gutierrez, A.; Ladbury, J., A survey of the year 2003 literature on applications of isothermal titration calorimetry. *Journal of Molecular Recognition* **2004**, *17* (6), 513-523.

149. Feigin, L. A.; Svergun, D. I., Structure analysis by small-angle X-ray and neutron scattering. 1987; p 335.

150. Mertens, H.; Svergun, D., Structural characterization of proteins and complexes using small-angle X-ray solution scattering. *Journal of Structural Biology* **2010**, *172* (1), 128-141.

151. Doniach, S., Changes in biomolecular conformation seen by small angle X-ray scattering. *Chemical Reviews* **2001**, *101* (6), 1763-1778.

152. Bernado, P.; Svergun, D., Structural analysis of intrinsically disordered proteins by small-angle X-ray scattering. *Molecular BioSystems*: 2011; Vol. 8, pp 151-167.

153. Koch, M.; Vachette, P.; Svergun, D., Small-angle scattering: a view on the properties, structures and structural changes of biological macromolecules in solution. *Quarterly Reviews of Biophysics* **2003**, *36* (2), 147-227.

154. Aebersold, R.; Mann, M., Mass spectrometry-based proteomics. *Nature* **2003**, *422* (6928), 198-207.

155. Fenn, J.; Mann, M.; Meng, C.; Wong, S.; Whitehouse, C., Electrospray ionization-principles and practice. *Mass Spectrometry Reviews* **1990**, *9* (1), 37-70.
156. Fenn, J.; Mann, M.; Meng, C.; Wong, S.; Whitehouse, C., Electrospray ionization for mass-spectrometry of large biomolecules. *Science* **1989**, *246* (4926), 64-71.
157. Yamashita, M.; Fenn, J., Electrospray ion-source - another variation on the free-jet theme. *Journal of Physical Chemistry* **1984**, *88* (20), 4451-4459.
158. Eyles, S.; Kaltashov, I., Methods to study protein dynamics and folding by mass spectrometry. *Methods* **2004**, *34* (1), 88-99.
159. Kaltashov, I.; Mohimen, A., Estimates of protein surface areas in solution by electrospray ionization mass spectrometry. *Analytical Chemistry* **2005**, *77* (16), 5370-5379.
160. Van Berkel, W.; Van Den Heuvel, R.; Versluis, C.; Heck, A., Detection of intact megaDalton protein assemblies of vanillyl-alcohol oxidase by mass spectrometry. *Protein Science* **2000**, *9* (3), 435-439.
161. Yin, S.; Xie, Y.; Loo, J., Mass spectrometry of protein-ligand complexes: Enhanced gas-phase stability of ribonuclease-nucleotide complexes. *Journal of the American Society For Mass Spectrometry* **2008**, *19* (8), 1199-1208.
162. Hossain, B.; Simmons, D.; Konermann, L., Do electrospray mass spectra reflect the ligand binding state of proteins in solution? *Canadian Journal of Chemistry-Revue Canadienne De Chimie* **2005**, *83* (11), 1953-1960.
163. Studier, F.; Moffatt, B., Use of bacteriophage-T7 RNA-polymerase to direct selective high-level expression of cloned genes. *Journal of Molecular Biology* **1986**, *189* (1), 113-130.
164. Rosenberg, A.; Lade, B.; Chui, D.; Lin, S.; Dunn, J.; Studier, F., Vectors for selective expression of cloned DNAs by T7 RNA-polymerase. *Gene* **1987**, *56* (1), 125-135.
165. Studier, F.; Rosenberg, A.; Dunn, J.; Dubendorff, J., Use of T7 RNA-polymerase to direct expression of cloned genes. *Methods in Enzymology* **1990**, *185*, 60-89.

166. Qi, D.; Scholthof, K., A one-step PCR-based method for rapid and efficient site-directed fragment deletion, insertion, and substitution mutagenesis. *Journal of Virological Methods* **2008**, *149* (1), 85-90.
167. Liu, H.; Naismith, J., An efficient one-step site-directed deletion, insertion, single and multiple-site plasmid mutagenesis protocol. *BMC Biotechnology* **2008**, *8*.
168. Sanger, F.; Nicklen, S.; Coulson, A., DNA sequencing with chain-terminating inhibitors. *Proceedings of the National Academy of Sciences of the United States of America* **1977**, *74* (12), 5463-5467.
169. Hwang, T.; Shaka, A., Water suppression that works - excitation sculpting using arbitrary wave-forms and pulsed-field gradients. *Journal of Magnetic Resonance Series A* **1995**, *112* (2), 275-279.
170. Piotto, M.; Saudek, V.; Sklenar, V., gradient-tailored excitation for single-quantum NMR-spectroscopy of aqueous-solutions. *Journal of Biomolecular NMR* **1992**, *2* (6), 661-665.
171. Liang, B.; Bushweller, J.; Tamm, L., Site-directed parallel spin-labeling and paramagnetic relaxation enhancement in structure determination of membrane proteins by solution NMR spectroscopy. *Journal of the American Chemical Society* **2006**, *128* (13), 4389-4397.
172. Deschamps, M.; Pilka, E.; Potts, J.; Campbell, I.; Boyd, J., Probing protein-peptide binding surfaces using charged stable free radicals and transverse paramagnetic relaxation enhancement (PRE). *Journal of Biomolecular NMR* **2005**, *31* (2), 155-160.
173. Deka, P.; Rajan, P.; Perez-Canadillas, J.; Varani, G., Protein and RNA dynamics play key roles in determining the specific recognition of GU-rich polyadenylation regulatory elements by human Cstf-64 protein. *Journal of Molecular Biology* **2005**, *347* (4), 719-733.
174. Oberstrass, F.; Auweter, S.; Erat, M.; Hargous, Y.; Henning, A.; Wenter, P.; Reymond, L.; Amir-Ahmady, B.; Pitsch, S.; Black, D.; Allain, F., Structure of PTB bound to RNA: Specific binding and implications for splicing regulation. *Science* **2005**, *309* (5743), 2054-2057.

175. Tsuda, K.; Someya, T.; Kuwasako, K.; Takahashi, M.; He, F.; Unzai, S.; Inoue, M.; Harada, T.; Watanabe, S.; Terada, T.; Kobayashi, N.; Shirouzu, M.; Kigawa, T.; Tanaka, A.; Sugano, S.; Guntert, P.; Yokoyama, S.; Muto, Y., Structural basis for the dual RNA-recognition modes of human Tra2-beta RRM. *Nucleic Acids Research* **2011**, *39* (4), 1538-1553.
176. Netter, C.; Weber, G.; Benecke, H.; Wahl, M., Functional stabilization of an RNA recognition motif by a noncanonical N-terminal expansion. *RNA-A Publication of the RNA Society* **2009**, *15* (7), 1305-1313.
177. Clery, A.; Jayne, S.; Benderska, N.; Dominguez, C.; Stamm, S.; Allain, F., Molecular basis of purine-rich RNA recognition by the human SR-like protein Tra2-beta 1. *Nature Structural & Molecular Biology* **2011**, *18* (4), 443-U78.
178. Kleckner, I.; Foster, M., An introduction to NMR-based approaches for measuring protein dynamics. *Biochimica Et Biophysica Acta-Proteins and Proteomics* **2011**, *1814* (8), 942-968.
179. Zuker, M., Mfold web server for nucleic acid folding and hybridization prediction. *Nucleic Acids Research* **2003**, *31* (13), 3406-3415.
180. Clore, G.; Driscoll, P.; Wingfield, P.; Gronenborn, A., Analysis of the backbone dynamics of interleukin-1-beta using 2-dimensional inverse detected heteronuclear N-15-H-1 NMR-spectroscopy. *Biochemistry* **1990**, *29* (32), 7387-7401.
181. Kay, L.; Torchia, D.; Bax, A., Backbone dynamics of proteins as studied by N-15 inverse detected heteronuclear NMR-spectroscopy - application to Staphylococcal nuclease. *Biochemistry* **1989**, *28* (23), 8972-8979.
182. Grasberger, B.; Gronenborn, A.; Clore, G., Analysis of the backbone dynamics of interleukin-8 by N-15 relaxation measurements. *Journal of Molecular Biology* **1993**, *230* (2), 364-372.
183. Mantylahti, S.; Aitio, O.; Hellman, M.; Permi, P., HA-detected experiments for the backbone assignment of intrinsically disordered proteins. *Journal of Biomolecular NMR* **2010**, *47* (3), 171-181.

184. Wen, J.; Wu, J.; Zhou, P., Sparsely sampled high-resolution 4-D experiments for efficient backbone resonance assignment of disordered proteins. *Journal of Magnetic Resonance* **2011**, *209* (1), 94-100.
185. Mantylahti, S.; Hellman, M.; Permi, P., Extension of the HA-detection based approach: (HCA)CON(CA)H and (HCA)NCO(CA)H experiments for the main-chain assignment of intrinsically disordered proteins. *Journal of Biomolecular NMR* **2011**, *49* (2), 99-109.
186. Novacek, J.; Zawadzka-Kazimierczuk, A.; Papouskova, V.; Zidek, L.; Sanderova, H.; Krasny, L.; Kozminski, W.; Sklenar, V., 5D C-13-detected experiments for backbone assignment of unstructured proteins with a very low signal dispersion. *Journal of Biomolecular NMR* **2011**, *50* (1), 1-11.
187. Teplova, M.; Song, J.; Gaw, H. Y.; Teplov, A.; Patel, D. J., Structural insights into RNA recognition by the alternate-splicing regulator CUG-binding protein 1. *Structure* **2010**, *18* (10), 1364-77.
188. Su, X.; Jergic, S.; Ozawa, K.; Burns, N.; Dixon, N.; Otting, G., Measurement of dissociation constants of high-molecular weight protein-protein complexes by transferred N-15-relaxation. *Journal of Biomolecular NMR* **2007**, *38* (1), 65-72.
189. Ryabov, Y.; Geraghty, C.; Varshney, A.; Fushman, D., An efficient computational method for predicting rotational diffusion tensors of globular proteins using an ellipsoid representation. *Journal of the American Chemical Society* **2006**, *128* (48), 15432-15444.
190. Paillard, L.; Legagneux, V.; Maniey, D.; Osborne, H., c-Jun ARE targets mRNA deadenylation by an EDEN-BP (embryo deadenylation element-binding protein)-dependent pathway. *Journal of Biological Chemistry* **2002**, *277* (5), 3232-3235.
191. Sickmier, E.; Frato, K.; Shen, H.; Paranawithana, S.; Green, M.; Kielkopf, C., Structural basis for polypyrimidine tract recognition by the essential pre-mRNA splicing factor U2AF65. *Molecular Cell* **2006**, *23* (1), 49-59.
192. Mackereth, C.; Madl, T.; Bonnal, S.; Simon, B.; Zanier, K.; Gasch, A.; Rybin, V.; Valcarcel, J.; Sattler, M., Multi-domain conformational selection underlies pre-mRNA splicing regulation by U2AF. *Nature* **2011**, *475* (7356), 408-U174.

193. Muto, Y.; Yokoyama, S., Structural insight into RNA recognition motifs: versatile molecular Lego building blocks for biological systems. *Wiley Interdisciplinary Reviews-RNA* **2012**, *3* (2), 229-246.
194. Deo, R.; Bonanno, J.; Sonenberg, N.; Burley, S., Recognition of polyadenylate RNA by the poly(A)-binding protein. *Cell* **1999**, *98* (6), 835-845.
195. Keizers, P.; Ubbink, M., Paramagnetic tagging for protein structure and dynamics analysis. *Progress in Nuclear Magnetic Resonance Spectroscopy* **2011**, *58* (1-2), 88-96.
196. Beattie, J.; Fensom, D.; Freeman, H.; Woodcock, E.; Hill, H.; Stokes, A., NMR investigation of electron-transfer in copper-protein, plastocyanin. *Biochimica Et Biophysica Acta* **1975**, *405* (1), 109-114.
197. Lee, L.; Sykes, B.; Birnbaum, E., Determination of the relative compactness of the Ca²⁺-binding sites of a Ca²⁺-binding fragment of troponin-c and parvalbumin using lanthanide-induced H-1 NMR shifts. *FEBS Letters* **1979**, *98* (1), 169-172.
198. Griffith, O.; McConnel, H., A nitroxide-maleimide spin label. *Proceedings of the National Academy of Sciences of the United States of America* **1966**, *55* (1), 8-&.
199. Anglister, J.; Frey, T.; McConnell, H., NMR technique for assessing contributions of heavy and light-chains to an antibody combining site. *Nature* **1985**, *315* (6014), 65-67.
200. Lee, Y.; Currie, B.; Johnson, M., Interaction of a spin-labeled phenylalanine analog with normal and sickle hemoglobins - detection of site-specific interactions through spin-label-induced H-1-NMR relaxation. *Biochemistry* **1986**, *25* (19), 5647-5654.
201. Cutting, B.; Strauss, A.; Fendrich, G.; Manley, P.; Jahnke, W., NMR resonance assignment of selectively labeled proteins by the use of paramagnetic ligands. *Journal of Biomolecular NMR* **2004**, *30* (2), 205-210.
202. Folkers, P.; Vanduyhoven, J.; Vanlieshout, H.; Harmsen, B.; Vanboom, J.; Tesser, G.; Konings, R.; Hilbers, C., Exploring the DNA-binding domain of gene-V protein

encoded by bacteriophage M13 with the aid of spin-labeled oligonucleotides in combination with H-1-NMR. *Biochemistry* **1993**, *32* (36), 9407-9416.

203. Cai, S.; Zhu, L.; Zhang, Z.; Chen, Y., Determination of the three-dimensional structure of the Mrf2-DNA complex using paramagnetic spin labeling. *Biochemistry* **2007**, *46* (17), 4943-4950.

204. Jin, J.; Wang, G.; Salisbury, E.; Timchenko, L.; Timchenko, N., GSK3 beta-cyclin D3-CUGBP1-eIF2 pathway in aging and in myotonic dystrophy. *Cell Cycle* **2009**, *8* (15), 2356-2359.

205. Maciejewski, P.; Peterson, F.; Anderson, P.; Brooks, C., Mutation of serine-90 to glutamic-acid mimics phosphorylation of bovine prolactin. *Journal of Biological Chemistry* **1995**, *270* (46), 27661-27665.

206. Leger, J.; Kempf, M.; Lee, G.; Brandt, R., Conversion of serine to aspartate imitates phosphorylation-induced changes in the structure and function of microtubule-associated protein tau. *Journal of Biological Chemistry* **1997**, *272* (13), 8441-8446.

207. Korner, C.; Wahle, E., Poly(A) tail shortening by a mammalian poly(A)-specific 3'-exoribonuclease. *Journal of Biological Chemistry* **1997**, *272* (16), 10448-10456.

208. Korner, C.; Wormington, M.; Muckenthaler, M.; Schneider, S.; Dehlin, E.; Wahle, E., The deadenylating nuclease (DAN) is involved in poly(A) tail removal during the meiotic maturation of *Xenopus* oocytes. *EMBO Journal* **1998**, *17* (18), 5427-5437.

209. Copeland, P.; Wormington, M., The mechanism and regulation of deadenylation: Identification and characterization of *Xenopus* PARN. *RNA-A Publication of the RNA Society* **2001**, *7* (6), 875-886.

210. Wu, M.; Reuter, M.; Lilie, H.; Liu, Y.; Wahle, E.; Song, H., Structural insight into poly(A) binding and catalytic mechanism of human PARN. *EMBO Journal* **2005**, *24* (23), 4082-4093.

211. Martinez, J.; Ren, Y.; Thuresson, A.; Hellmann, U.; Astrom, J.; Virtanen, A., A 54-kDa fragment of the poly(A)-specific ribonuclease is an oligomeric, processive, and cap-

interacting poly(A)-specific 3' exonuclease. *Journal of Biological Chemistry* **2000**, 275 (31), 24222-24230.

212. Niedzwiecka, A.; Lekka, M.; Nilsson, P.; Virtanen, A., Global architecture of human poly(A)-specific ribonuclease by atomic force microscopy in liquid and dynamic light scattering. *Biophysical Chemistry* **2011**, 158 (2-3), 141-149.

213. Henriksson, N.; Nilsson, P.; Wu, M.; Song, H.; Virtanen, A., Recognition of Adenosine Residues by the Active Site of Poly(A)-specific Ribonuclease. *Journal of Biological Chemistry* **2010**, 285 (1), 163-170.

214. Nilsson, P.; Henriksson, N.; Niedzwiecka, A.; Balatsos, N.; Kokkoris, K.; Eriksson, J.; Virtanen, A., A multifunctional RNA recognition motif in poly(A)-specific ribonuclease with cap and poly(A) binding properties. *Journal of Biological Chemistry* **2007**, 282 (45), 32902-32911.

215. Henriksson, N.; Nilsson, P.; Mousheng, W.; Song, H.; Virtanen, A., Poly(A)-specific ribonuclease (PARN): Molecular mechanisms of mRNA cap and poly(A) tail recognition. *FEBS Journal* **2010**, 277, 194-194.

216. Liu, W.; Zhang, A.; He, G.; Yan, Y., The R3H domain stabilizes poly(A)-specific ribonuclease by stabilizing the RRM domain. *Biochemical and Biophysical Research Communications* **2007**, 360 (4), 846-851.

217. Ren, Y.; Kirsebom, L.; Virtanen, A., Coordination of divalent metal ions in the active site of poly(A)-specific ribonuclease. *Journal of Biological Chemistry* **2004**, 279 (47), 48702-48706.

218. Selenko, P.; Gregorovic, G.; Sprangers, R.; Stier, G.; Rhani, Z.; Kramer, A.; Sattler, M., Structural basis for the molecular recognition between human splicing factors U2AF(65) and SF1/mBBP. *Molecular Cell* **2003**, 11 (4), 965-976.

219. Kielkopf, C.; Rodionova, N.; Green, M.; Burley, S., A novel peptide recognition mode revealed by the X-ray structure of a core U2AF-(35)/U2AF(65) heterodimer. *Cell* **2001**, 106 (5), 595-605.

220. Elantak, L.; Wagner, S.; Herrmannova, A.; Karaskova, M.; Rutkai, E.; Lukavsky, P.; Valasek, L., The Indispensable N-Terminal Half of eIF3j/HCR1 Cooperates with its Structurally Conserved Binding Partner eIF3b/PRT1-RRM and with eIF1A in Stringent AUG Selection. *Journal of Molecular Biology* **2010**, *396* (4), 1097-1116.
221. Rideau, A.; Gooding, C.; Simpson, P.; Monie, T.; Lorenz, M.; Huttelmaier, S.; Singer, R.; Matthews, S.; Curry, S.; Smith, C., A peptide motif in Raver1 mediates splicing repression by interaction with the PTB RRM2 domain. *Nature Structural & Molecular Biology* **2006**, *13* (9), 839-848.
222. Fribourg, S.; Gatfield, D.; Izaurralde, E.; Conti, E., A novel mode of RBD-protein recognition in the Y14-Mago complex. *Nature Structural Biology* **2003**, *10* (6), 433-439.
223. Kadlec, J.; Izaurralde, E.; Cusack, S., The structural basis for the interaction between nonsense-mediated mRNA decay factors UPF2 and UPF3. *Nature Structural & Molecular Biology* **2004**, *11* (4), 330-337.
224. Wang, Z.; Song, J.; Milne, T.; Wang, G.; Li, H.; Allis, C.; Patel, D., Pro Isomerization in MLL1 PHD3-Bromo Cassette Connects H3K4me Readout to Cyp33 and HDAC-Mediated Repression. *Cell* **2010**, *141* (7), 1183-U151.
225. Zhu, Y.; Chen, G.; Lv, F.; Wang, X.; Ji, X.; Xu, Y.; Sun, J.; Wu, L.; Zheng, Y.; Gao, G., Zinc-finger antiviral protein inhibits HIV-1 infection by selectively targeting multiply spliced viral mRNAs for degradation. *Proceedings of the National Academy of Sciences of the United States of America* **2011**, *108* (38), 15834-15839.

11 Appendix

11.1 Primers

Construct	Primer Sequence
RRM1	GCC GAC AGT GAA AAG TAA AAT GCT GTG GAA G
	C TTC CAC AGC ATT TTA CTT TTC ACT GTC GGC
RRM2	CGTT GCT AGC ATG CGA AAG CTA TTT ATC GGA ATG G
	CGTT AAG CTT TCA GTC TGC GAA CTT TAC CAC TAT TGG
RRM3	GA CAA AAG*GCT AGC CAT ATG GCT GCC GCG
	CAT ATG GCT AGC*CTT TTG TCA CAA CAG GGT TTG
RRM123	G TGA CAA AAG*CCA CAT TGA GGC TGC ATT GAG CTG
	C TCA ATG TGG*CTT TTG TCA CAA CAG GGT TTG GGG GC
S28D	GGT CAG GTT CCT CGA AGC TGG GAC GAG AAA GAG CTA AG
	CT TAG CTC TTT CTC GTC CCA GCT TCG AGG AAC CTG ACC
RRM23	C ATT ATT*GCT AGC CAT ATG GCT GCC GCG
	CAT ATG GCT AGC*AAT AAT GCT GTG GAA GAC CGA AAG

* - Indicates position of the deletion site in the primers used for one-step deletion methods.

11.2 NMR Assignments

11.2.1 RRM1 Wild Type Assignment

Number	Residue	HN Chemical Shift	NH Chemical Shift
1	Met1	-	-
2	Asn2	8.27	119.89
3	Gly3	8.22	110.02
4	Thr4	7.90	114.20
5	Met5	8.24	122.68
6	Asp6	8.08	122.02
7	His7	7.67	116.12
8	Pro8	-	-
9	Asp9	8.51	120.30
10	His10	7.83	118.35
11	Pro11	-	-
12	Asp12	-	-
13	Pro13	-	-
14	Asp14	7.97	114.98
15	Ser15	7.34	114.46
16	Ile16	7.83	121.89
17	Lys17	8.59	129.52
18	Met18	8.67	127.86
19	Phe19	9.60	125.36
20	Val20	8.19	129.28
21	Gly21	9.06	112.78
22	Gln22	8.07	110.05
23	Val23	7.09	115.91
24	Pro24	-	-
25	Arg25	9.02	123.39
26	Ser26	7.63	109.29

27	Trp27	10.16	129.80
	Trp27(E)	7.45	123.75
28	Ser28	9.23	121.80
29	Glu29	9.85	120.49
30	Lys30	7.90	120.06
31	Glu31	7.97	120.12
32	Leu32	7.54	118.80
33	Arg33	8.59	121.93
34	Glu34	7.23	117.20
35	Leu35	7.07	118.88
36	Phe36	8.30	114.83
37	Glu37	8.96	118.85
38	Gln38	7.01	117.19
39	Tyr39	7.90	117.16
40	Gly40	7.30	106.89
41	Ala41	7.94	119.35
42	Val42	9.47	127.28
43	Tyr43	8.21	129.94
44	Glu44	7.34	117.84
45	Ile45	8.44	126.49
46	Asn46	8.80	125.77
47	Val47	8.90	127.59
48	Leu48	7.79	130.62
49	Arg49	8.36	121.74
50	Asp50	8.89	121.30
51	Arg51	8.66	124.92
52	Ser52	8.59	117.08
53	Gln53	6.87	120.25
54	Asn54	8.26	118.54
55	Pro55	-	-
56	Pro56	-	-
57	Gln57	7.38	122.28

58	Ser58	8.03	115.88
59	Lys59	8.88	125.26
60	Gly60	9.47	110.79
61	Cys61	7.08	111.43
62	Cys62	8.86	114.59
63	Phe63	8.43	115.82
64	Ile64	9.18	121.40
65	Thr65	8.66	125.91
66	Phe66	9.76	130.29
67	Tyr67	8.09	119.33
68	Thr68	8.26	104.76
69	Arg69	9.67	126.83
70	Lys70	8.42	117.76
71	Ala71	7.52	121.12
72	Ala72	6.54	118.42
73	Leu73	7.77	116.47
74	Glu74	8.20	122.48
75	Ala75	8.14	123.54
76	Gln76	8.02	118.13
77	Asn77	8.07	115.22
78	Ala78	7.62	119.99
79	Leu79	7.78	114.09
80	His80	8.50	120.17
81	Asn81	9.02	122.28
82	Met82	7.93	116.65
83	Lys83	7.27	121.48
84	Val84	8.52	128.49
85	Leu85	8.91	130.93
86	Pro86	-	-
87	Gly87	8.32	112.12
88	Met88	7.61	118.36
89	His89	8.10	122.06

90	His90	7.39	119.29
91	Pro91	-	-
92	Ile92	8.30	120.28
93	Gln93	7.24	125.58
94	Met94	11.69	130.12
95	Lys95	8.82	123.85
96	Pro96	-	-
97	Ala97	8.86	127.53
98	Asp98	8.58	120.45
99	Ser99	8.06	115.97
100	Glu100	8.36	124.17
101	Lys101	7.68	126.98

11.2.2 RRM1 S28D Assignment

Number	Residue	HN Chemical Shift	NH Chemical Shift
1	Met1	-	-
2	Asn2	8.27	119.91
3	Gly3	8.22	109.99
4	Thr4	7.92	114.14
5	Met5	8.23	122.63
6	Asp6	8.08	122.03
7	His7	7.67	116.18
8	Pro8	-	-
9	Asp9	8.51	120.22
10	His10	7.83	118.52
11	Pro11	-	-
12	Asp12	-	-
13	Pro13	-	-
14	Asp14	7.97	114.88
15	Ser15	7.34	114.37
16	Ile16	7.83	121.81

17	Lys17	8.58	129.47
18	Met18	8.66	127.71
19	Phe19	9.60	125.34
20	Val20	8.20	129.30
21	Gly21	9.06	112.64
22	Gln22	8.05	110.11
23	Val23	7.12	115.77
24	Pro24	-	-
25	Arg25	9.02	123.36
26	Ser26	7.60	109.15
27	Trp27	10.12	129.62
	Trp27(E)	7.42	123.83
28	Asp28	8.94	126.87
29	Glu29	9.86	122.09
30	Lys30	8.31	118.76
31	Glu31	7.96	120.12
32	Leu32	7.76	119.32
33	Arg33	8.89	121.70
34	Glu34	7.26	117.51
35	Leu35	7.04	118.62
36	Phe36	8.34	114.63
37	Glu37	9.02	118.65
38	Gln38	7.00	117.04
39	Tyr39	7.89	117.17
40	Gly40	7.30	106.82
41	Ala41	7.95	119.30
42	Val42	9.51	127.17
43	Tyr43	8.21	130.06
44	Glu44	7.31	117.72
45	Ile45	8.51	126.89
46	Asn46	8.81	125.75
47	Val47	8.96	127.88

48	Leu48	7.78	130.50
49	Arg49	8.38	121.28
50	Asp50	8.91	121.28
51	Arg51	8.70	124.79
52	Ser52	8.58	116.95
53	Gln53	6.88	120.22
54	Asn54	8.25	118.47
55	Pro55	-	-
56	Pro56	-	-
57	Gln57	7.40	122.46
58	Ser58	8.03	115.88
59	Lys59	8.86	125.10
60	Gly60	9.51	110.94
61	Cys61	7.10	111.48
62	Cys62	8.85	114.44
63	Phe63	8.44	115.57
64	Ile64	9.20	121.18
65	Thr65	8.64	125.82
66	Phe66	9.76	130.18
67	Tyr67	8.09	119.21
68	Thr68	8.26	104.72
69	Arg69	9.66	126.72
70	Lys70	8.42	117.60
71	Ala71	7.52	121.07
72	Ala72	6.53	118.35
73	Leu73	7.76	116.34
74	Glu74	8.20	122.44
75	Ala75	8.13	123.45
76	Gln76	8.02	118.05
77	Asn77	8.09	115.27
78	Ala78	7.62	119.90
79	Leu79	7.78	114.04

80	His80	8.49	120.04
81	Asn81	9.03	122.21
82	Met82	7.94	116.61
83	Lys83	7.26	121.42
84	Val84	8.52	128.37
85	Leu85	8.93	130.90
86	Pro86	-	-
87	Gly87	8.32	112.08
88	Met88	7.61	118.29
89	His89	8.10	122.03
90	His90	7.41	118.93
91	Pro91	-	-
92	Ile92	8.30	120.35
93	Gln93	7.29	125.61
94	Met94	11.68	129.92
95	Lys95	8.83	123.85
96	Pro96	-	-
97	Ala97	8.85	127.36
98	Asp98	8.51	120.22
99	Ser99	8.04	116.00
100	Glu100	8.35	123.95
101	Lys101	7.69	127.07

11.2.3 RRM2 Assignment

Number	Residue	HN Chemical Shift	NH Chemical Shift
108	Arg108	7.98	114.72
109	Lys109	7.46	121.78
110	Leu110	9.51	126.92

111	Phe111	9.25	123.34
112	Ile112	8.14	128.04
113	Gly113	9.25	112.16
114	Met114	8.25	114.18
115	Val115	7.26	111.30
116	Ser116	7.04	117.51
117	Lys117	8.98	127.78
118	Asn118	7.99	114.23
119	Cys119	7.05	117.68
120	Asn120	9.34	123.23
121	Glu121	9.40	120.25
122	Asn122	8.20	118.07
123	Asp123	7.88	121.67
124	Ile124	7.48	119.92
125	Arg125	8.60	121.42
126	Ala126	7.88	121.30
127	Met127	7.40	115.75
128	Phe128	7.66	112.71
129	Ser129	8.47	120.76
130	Pro130	-	-
131	Phe131	7.20	112.49
132	Gly132	7.51	104.46
133	Gln133	7.59	120.35
134	Ile134	8.45	127.47
135	Glu135	8.78	129.54
136	Glu136	7.10	116.69
137	Cys137	8.74	126.46
138	Arg138	8.62	126.54
139	Ile139	8.66	125.34
140	Leu140	8.17	129.67
141	Arg141	8.34	123.16
142	Gly142	8.34	108.43
143	Pro143	-	-

144	Asp144	7.80	115.85
145	Gly145	8.16	108.21
146	Met146	7.77	120.80
147	Ser147	8.74	117.21
148	Arg148	9.04	125.08
149	Gly149	9.45	110.44
150	Cys150	6.91	111.11
151	Ala151	8.93	122.37
152	Phe152	8.52	114.78
153	Val153	8.46	121.08
154	Thr154	8.62	123.92
155	Phe155	8.34	126.95
156	The156	8.40	112.16
157	Thr157	7.56	108.68
158	Arg158	9.05	123.34
159	Ser159	8.41	115.88
160	Met160	7.21	121.76
161	Ala161	6.57	119.53
162	Gln162	8.41	115.55
163	Met163	7.66	120.21
164	Ala164	7.57	123.43
165	Ile165	7.60	118.38
166	Lys166	7.46	117.82
167	Ser167	7.46	110.52
168	Met168	7.87	115.61
169	His169	8.09	120.32
170	Gln170	8.45	121.61
171	Ala171	7.75	120.36
172	Gln172	7.07	110.75
173	Thr173	8.54	119.31
174	Met174	9.72	128.23
175	Glu175	8.44	121.92
176	Gly176	8.69	114.34

177	Cys177	7.79	119.11
178	Ser178	-	-
179	Ser179	7.33	117.03
180	Pro180	-	-
181	Ile181	7.96	118.29
182	Val182	8.07	127.84
183	Val183	10.98	129.69
184	Lys184	8.64	122.00
185	Phe185	8.21	120.11
186	Ala186	8.66	125.13
187	Asp187	7.94	125.92

11.2.4 RRM3 Assignment

Number	Residue	HN Chemical Shift	NH Chemical Shift
390	Gly390	8.50	110.75
391	Leu391	8.04	122.22
392	Gly392	8.28	110.18
393	Ala393	8.09	122.80
394	Ala394	-	-
395	Gly395	-	-
396	Ser396	7.75	116.25
397	Gln397	8.21	121.56
398	Lys398	7.98	123.90
399	Glu399	8.27	123.75
400	Gly400	8.93	110.90
401	Pro401	-	-
402	Glu402	8.21	119.96
403	Gly403	8.35	113.21
404	Ala404	8.16	120.49
405	Asn405	7.26	115.95

406	Leu406	9.15	124.22
407	Phe407	8.93	119.35
408	Ile408	8.37	122.39
409	Tyr409	9.25	123.82
410	His410	8.43	112.81
411	Leu411	7.35	115.03
412	Pro412	-	-
413	Gln413	8.91	126.21
414	Glu414	8.95	115.23
415	Phe415	7.44	123.33
416	Gly416	9.40	114.88
417	Asp417	8.48	120.87
418	Gln418	8.70	118.36
419	Asp419	6.90	119.79
420	Leu420	7.52	120.87
421	Leu421	7.57	119.92
422	Gln422	7.81	116.41
423	Met423	7.35	116.47
424	Phe424	7.45	113.61
425	Met425	8.45	128.29
426	Pro426	-	-
427	Phe427	6.43	110.65
428	Gly428	7.50	106.59
429	Asn429	8.84	117.95
430	Val430	8.18	128.72
431	Val431	8.79	130.28
432	Ser432	7.08	114.01
433	Ser433	7.60	116.22
434	Lys434	8.40	125.39
435	Val435	8.43	125.68
436	Phe436	8.09	127.79
437	Ile437	8.13	121.93

438	Asp438	8.55	127.07
439	Lys439	8.74	128.05
440	Gln440	8.51	117.86
441	Thr441	7.63	107.81
442	Asn442	8.32	117.66
443	Leu443	7.48	118.57
444	Ser444	8.59	115.96
445	Lys445	9.12	126.03
446	Cys446	10.02	113.78
447	Phe447	7.54	115.76
448	Gly448	9.11	108.50
449	Phe449	8.64	120.68
450	Val450	7.65	124.26
451	Ser451	8.18	119.96
452	Tyr452	8.25	121.67
453	Asp453	7.73	114.18
454	Asn454	7.07	114.67
455	Pro455	-	-
456	Val456	7.91	121.99
457	Ser457	7.72	118.61
458	Ala458	6.19	120.78
459	Gln459	7.57	116.71
460	Ala460	7.68	123.73
461	Ala461	7.69	122.44
462	Ile462	7.91	119.25
463	Gln463	7.69	117.52
464	Ser464	7.39	111.41
465	Met465	8.17	114.91
466	Asn466	8.23	119.43
467	Gly467	8.83	118.76
468	Phe468	7.78	123.99
469	Gln469	7.88	129.25

470	Ile470	8.32	126.95
471	Gly471	8.80	118.33
472	Met472	8.79	123.74
473	Lys473	7.70	120.26
474	Arg474	7.98	120.18
475	Leu475	8.92	123.33
476	Lys476	7.91	124.23
477	Val477	8.61	127.49
478	Gln478	8.97	124.04
479	Leu479	8.57	123.28
480	Lys480	8.20	124.81
481	Arg481	-	-
482	Ser482	-	-
483	Lys483	-	-
484	Asn484	-	-
485	Asp485	7.96	121.63
486	Ser486	8.03	116.32
487	Lys487	7.95	124.34
488	Pro488	-	-
489	Tyr489	7.30	124.49

